

ResearchOnline@JCU

This file is part of the following reference:

Rackemann, Darryn Wallace (2005) *Evaluation of circulation and heat transfer in calandria tubes of crystallisation vacuum pans*. Masters (Research) thesis, James Cook University.

Access to this file is available from:

<http://eprints.jcu.edu.au/1322/>

The author has certified to JCU that they have made a reasonable effort to gain permission and acknowledge the owner of any third party copyright material included in this document. If you believe that this is not the case, please contact ResearchOnline@jcu.edu.au and quote <http://eprints.jcu.edu.au/1322/>

**‘Evaluation of circulation
and heat transfer in calandria tubes
of crystallisation vacuum pans’**

Thesis submitted by

Darryn Wallace RACKEMANN BE (Hons) Qld

August 2005

**for the degree of Masters of Engineering Science
in the School of Engineering
James Cook University**

STATEMENT OF ACCESS

I, the undersigned, author of this work, understand that James Cook University will make this thesis available for use within the University Library and, via the Australian Digital Theses network, for use elsewhere.

I understand that, as an unpublished work, a thesis has significant protection under the Copyright Act and;

Beyond this, I do not wish to place any further restriction on access to this work.

Signature

18 / 08 / 2005

Date

ABSTRACT

This thesis investigates the importance of circulation and heat transfer in crystallisation vacuum pans that produce raw sugar in the sugar mill. The driving force for circulation and heat transfer occurs in the calandria tubes within vacuum pans.

Numerical and CFD modelling is becoming a cost-effective and reliable way of developing vessel designs especially when there are complex physics and geometries involved, as is the case with vacuum pans. Currently, however, there are no working numerical models of vacuum pans that can be confidently used to design pans with improved circulation and boiling. If the operation of vacuum pans and specifically calandria tubes can be adequately modelled, the design of industrial vacuum pans can be improved to realise the benefits of obtaining more efficient circulation and heat transfer within the pan.

The research aims to provide data on heat transfer and circulation in factory crystallisation vacuum pans and provide data on an experimental rig simulating a single calandria tube for validation of numerical models. Factory trials were conducted to obtain data on heat transfer and circulation in factory pans. A method for measuring circulation speeds in massecuite solutions and vacuum pans was refined as part of this research. The data collected from the factory trials enabled the operating conditions for the single calandria tube boiling rig experimental trials to be determined.

The intention of the experimental rig was to simulate factory conditions to allow detailed examinations of the heat transfer process and vapour volume fraction profiles to be obtained. Natural and forced circulation conditions were investigated as both types of circulation are present in factory vacuum pans. The data gathered from these experiments were preliminary in nature as the rig did not adequately represent factory equipment.

The research highlights problems associated with the boiling of viscous fluids, such as molasses on a laboratory scale. Strategies and recommendations are provided to enable a more adequate representation of factory conditions in the experimental rig. These

improvements will allow more accurate data to be obtained that can be used to develop improved models of calandria tubes and vacuum pans.

The experiments conducted on the single calandria tube detailed the physical changes and heat transfer characteristics for boiling in calandria tubes with changing material properties and heat input conditions. The experiments allowed fluid specific correlations to be obtained for heat transfer coefficients and vapour distribution during boiling in the calandria tubes. These correlations were used to develop numerical models of the boiling that occurs in calandria tubes. The numerical models provided a better understanding of the flow characteristics in the vessel and can facilitate the development of improved engineering designs.

The project shows the applicability of a pilot scale rig to provide data that can be used to improve the understanding and modelling of flow and heat transfer in the calandria tubes of crystallisation vacuum pans.

STATEMENT OF SOURCES

DECLARATION

I declare that this thesis is my own work and has not been submitted in any form for another degree or diploma at any university or other institution of tertiary education. Information derived from the published or unpublished work of others has been acknowledged in the text and a list of references is given.

Signature

18 / 08 / 2005

Date

ELECTRONIC COPY

I, the undersigned, the author of this work, declare that the electronic copy of this thesis provided to the James Cook University Library is an accurate copy of the print thesis submitted, within the limits of the technology available.

Signature

18 / 08 / 2005

Date

ACKNOWLEDGEMENTS

The author wishes to thank the following people for their valuable contributions:

Dr Phil Schneider, my principal supervisor at James Cook University (JCU), for his enthusiasm and motivation, which were one of the major driving forces in the completion of this thesis.

Dr Ross Broadfoot from Sugar Research Institute (SRI) for his wisdom and information relating to the operation and control of vacuum pans.

Dr Bill Doherty also from SRI is acknowledged for his editing contributions.

A number of undergraduate students and staff at JCU assisted in the construction, installation and commissioning of the experimental rig at JCU. In particular the contributions of Mr Dave Kauppila, JCU workshop and electrical staff, Mr Drew Penny, Mr Jarrod Giese and Mr Geoff Devin are acknowledged.

Dr Darrin Stephens for his friendship, understanding and especially advice early in the research program.

My parents and friends especially my partner, Kylie for their support and encouragement throughout the duration of this thesis.

The valuable assistance of the staff from Macknade Mill in the planning and conduct of the factory trials test program.

The financial support of the Department of State Development and Innovation, Sugar Research Development Corporation and SRI, for the funding of this thesis should also be acknowledged. In particular SRI provided a lot of the required infrastructure as a large portion of the research was not conducted at JCU.

Contents

STATEMENT OF ACCESS	i
ABSTRACT	ii
STATEMENT OF SOURCES	iv
ACKNOWLEDGEMENTS	vi
LIST OF FIGURES.....	x
LIST OF TABLES.....	xii
LIST OF SYMBOLS.....	xiii
1 INTRODUCTION	1
1.1 Crystallisation vacuum pans	3
1.2 Crystallisation vacuum pan design	4
1.3 CFD modelling	6
1.4 Problem statement.....	7
2 CIRCULATION AND HEAT TRANSFER MEASUREMENTS.....	9
2.1 Circulation theory	9
2.2 Circulation measurements	11
2.2.1 <i>Measurement method</i>	13
2.2.2 <i>Measurement results</i>	14
2.2.3 <i>Summary</i>	15
2.3 Heat transfer	15
2.4 Fluid properties.....	17
2.4.1 <i>Liquid density</i>	18
2.4.2 <i>Specific heat capacity</i>	19
2.4.3 <i>Enthalpy</i>	20
2.4.4 <i>Rheological properties</i>	20
2.4.5 <i>Thermal conductivity</i>	23
2.4.6 <i>Surface tension</i>	24
2.4.7 <i>Vapour properties</i>	24
2.4.8 <i>Boiling point elevation</i>	25
2.4.9 <i>Impurities</i>	26
2.5 Summary	26
3 FACTORY TRIALS.....	28

3.1	Introduction	28
3.2	Hot film anemometers.....	28
3.3	Anemometer calibrations	31
3.4	Anemometer error sources	33
3.5	Overview of the factory trials.....	34
3.6	Sample analysis	36
3.7	Circulation results.....	39
3.7.1	<i>Measurement issues</i>	45
3.8	Heat transfer	49
3.9	Heat transfer results	50
3.10	Summary	53
4	NUMERICAL MODELLING.....	55
4.1	Introduction	55
4.2	Modelling of circulation in vacuum pans.....	56
4.3	Boiling in calandria tubes.....	59
4.4	Modelling calandria tubes	60
4.5	Empirical correlations	63
4.5.1	<i>Heat transfer</i>	64
4.5.2	<i>Vapour distribution within the calandria tube</i>	68
4.6	Summary	72
5	EXPERIMENTAL RIG	74
5.1	Introduction	74
5.2	Single calandria tube boiling rig.....	74
5.2.1	<i>Configuration 1</i>	75
5.2.2	<i>Configuration 2</i>	76
5.2.3	<i>Configuration 3</i>	77
5.3	Instrumentation.....	80
5.3.1	<i>Instrumentation errors</i>	83
5.4	Control software and instrumentation.....	84
5.5	Commissioning of rig.....	86
5.5.1	<i>Densitometer positioning and calibration</i>	86
5.5.2	<i>Densitometer results</i>	90
5.5.3	<i>Pressure control</i>	91
5.5.4	<i>Flow circulation control</i>	93
5.5.5	<i>Temperature effects</i>	95
5.5.6	<i>Heat flux control</i>	97
5.6	Experimental work program.....	100
6	EXPERIMENTAL RESULTS	103
6.1	Introduction	103

6.2	Experimental trials.....	103
6.2.1	<i>Natural circulation</i>	103
6.2.2	<i>Forced circulation</i>	104
6.3	Sample analysis	106
6.4	Summary of results	107
6.5	Empirical correlations	110
6.5.1	<i>Heat transfer</i>	110
6.5.2	<i>Vapour distribution</i>	115
6.6	Summary	117
7	MODELLING RESULTS	119
7.1	Background.....	119
7.2	Validation against experimental data.....	121
7.2.1	<i>Slip ratio for the determination of vapour distribution</i>	124
7.3	Tube performance curves	126
7.4	Summary	134
8	CONCLUSIONS AND RECOMMENDATIONS	135
8.1	Conclusions	135
8.2	Recommendations.....	137
8.2.1	<i>Modification of experimental rig</i>	137
8.2.2	<i>Other experimentation</i>	139
8.2.3	<i>Numerical modelling</i>	141
	BIBLIOGRAPHY	143
	APPENDIX A – Glossary of terms	153
	APPENDIX B – Calibration constants for the anemometer probes.....	156
	APPENDIX C – MTL8000 I/O wiring information	157
	APPENDIX D – ProcessACT schematics	160
	APPENDIX E – Citect schematics	166
	APPENDIX F – SEW Motor and Inverter wiring information.....	174
	APPENDIX G – Summary of JCU experimental data	177
	APPENDIX H – One dimensional Visual Basic tube model.....	207

LIST OF FIGURES

Figure 1-1	Sectioned view of a batch fixed calandria pan, from Stephens (2001).	3
Figure 1-2	Circulation pattern in a fixed calandria batch pan.	5
Figure 2-1	Circulation patterns in a vacuum pan due to eruptive boiling, from Wright (1966).....	10
Figure 3-1	Diagram of Turck insertion flow sensor.....	29
Figure 3-2	Schematic of calibration rig.....	32
Figure 3-3	Orientations of the anemometer tip to the cross-flow profile, adaptation from Incropera and DeWitt (1996).	33
Figure 3-4	Socket locations for the anemometer probes and general pan dimensions (in mm) of Macknade No. 6 pan.....	35
Figure 3-5	Anemometer probe housing and gland arrangement for insertion into vacuum pans.....	36
Figure 3-6	Average velocity trends at socket location ‘A’ for various insertion depths on No. 6 pan at Macknade Mill during the A massecuite strike.	40
Figure 3-7	Average velocity trends at socket location ‘B’ for various insertion depths on No. 6 pan at Macknade Mill during the A massecuite strike.	41
Figure 3-8	Average velocity trends at socket location ‘C’ for various insertion depths on No. 6 pan at Macknade Mill during the A massecuite strike.	41
Figure 3-9	Average velocity trends at socket location ‘D’ for various insertion depths on No. 6 pan at Macknade Mill during the A massecuite strike.	42
Figure 3-10	Average velocity trends at socket location ‘E’ for various insertion depths on No. 6 pan at Macknade Mill during the A massecuite strike.	42
Figure 3-11	Comparison of the circulation results between the 2001 and 2002 factory trials measured at location ‘B’ at an insertion depth of 300-330 mm for the seed preparation step on Macknade No. 6 pan.....	44
Figure 3-12	Comparison of the circulation results between the 2001 and 2002 factory trials measured at location ‘B’ at an insertion depth of 300-330 mm for the A massecuite strike on Macknade No. 6 pan.....	44
Figure 3-13	Effect of probe insertion depth versus probe orientation to the expected main direction for massecuite flow.	45
Figure 3-14	Velocity trends of different production runs for probe 1 inserted to a depth of 100 mm at location ‘C’ and probe 2 inserted to a depth of	

	600 mm at location ‘A’ for the seed preparation step on Macknade No. 6 pan during trials in the 2002 season.	46
Figure 3-15	Velocity trends of different strikes for probe 1 inserted to a depth of 100 mm at location ‘C’ and probe 2 inserted to a depth of 600 mm at location ‘A’ for the A massecuite strike on Macknade No. 6 pan during trials in the 2002 season.	47
Figure 3-16	Velocity trends of different production runs for probe 3 inserted to a depth of 1000 mm at locations ‘D’ and ‘E’ for the seed preparation step on Macknade No. 6 pan during trials in the 2002 season.....	48
Figure 3-17	Velocity trends of different strikes for probe 3 inserted to a depth of 1000 mm at locations ‘D’ and ‘E’ for the A massecuite strike on Macknade No. 6 pan during trials in the 2002 season.	49
Figure 3-18	HTC values plotted against operating level for Macknade No. 6 pan during trials in the 2001 season.	51
Figure 3-19	HTC values and operating level plotted against time for Macknade No. 6 pan during trials in the 2001 season.	52
Figure 4-1	Diagram of temperatures and void fractions when boiling in a vertical tube, from Rouillard (1985).	59
Figure 4-2	Illustration of the thermal boundary layer.	63
Figure 5-1	Schematic of the single calandria tube boiling rig at JCU.	76
Figure 5-2	Photo of the electrical heating bands.....	77
Figure 5-3	Photo of the internal gear pump.....	78
Figure 5-4	Schematic of the single calandria boiling tube rig located at JCU.	79
Figure 5-5	Photo of the modified pipe work and insulated header tank.	80
Figure 5-6	Experimental calandria boiling tube instrumentation.	82
Figure 5-7	Photo of the instrumentation installed on the single calandria boiling tube rig.....	82
Figure 5-8	Schematic of SCADA system hierarchy.	85
Figure 5-9	Citect overview of boiling circuit controller.	86
Figure 5-10	Densitometer positioning system layout.	87
Figure 5-11	Data obtained from the densitometer.	90
Figure 5-12	Operating pressure in the headspace for various experimental trials.....	92
Figure 5-13	Operating pressure in the headspace for leak test trials.	93
Figure 5-14	Operating level in the header tank for various experimental trials.	94
Figure 5-15	Temperature profiles along the tube length during an experimental trial.	96
Figure 5-16	Temperature profiles and heat transfer data for the vapour heat exchanger during an experimental trial.	99
Figure 6-1	Heat transfer correlation for the natural circulation trials.	113
Figure 6-2	Heat transfer correlation for the forced circulation trials.	114
Figure 6-3	Vapour volume fraction correlation for the experimental trials.....	117

Figure 7-1	Performance curve showing the pressure driving force as a function of mass flow rate through the calandria tube.....	128
Figure 7-2	Performance curve showing a zoomed section of figure 7-1.	129
Figure 7-3	Performance curve showing the heat flux as a function of mass flow rate through the calandria tube.....	130
Figure 7-4	Performance curve showing the pressure driving force as a function of average circulation velocity through the calandria tube.....	131
Figure 7-5	Performance curve showing a zoomed section of figure 7-4.	131
Figure 8-1	Suggested positioning of instrumentation for the additional factory-based trials in one calandria tube of a vacuum pan.....	140

LIST OF TABLES

Table 2-1	List of velocity measurements in industrial vacuum pans.....	12
Table 3-1	List of analyses conducted on massecuite and molasses samples.	37
Table 3-2	Summary of sample analyses for Macknade No. 6 pan.	38
Table 4-1	Summary of numerical modelling attempts of vacuum pan operation.....	57
Table 6-1	Summary of average operating conditions for the natural circulation trials (configurations 1 and 2).....	104
Table 6-2	Summary of operating conditions for the forced circulation trials (configuration 3).....	105
Table 6-3	Analyses of the sample mixtures used in the experimental boiling trials.....	107
Table 6-4	Summary of the results and average operating conditions for the natural circulation trials (configurations 1 and 2).....	108
Table 6-5	Summary of the results and operating conditions for the forced circulation trials (configuration 3).	108
Table 7-1	Comparisons between the experimental data and predicted values for the single calandria tube boiling trials.	122
Table 7-2	Typical average fluid properties and operating conditions for high-grade massecuite strikes.	127

LIST OF SYMBOLS

A_{film}	Heat transfer area of metal film	m^2
A_{HT}	Heat transfer area	m^2
A_{tube}	Surface area of the calandria tube	m^2
A_R	Entrained air constant for viscosity calculations	-
Bo	Non-dimensional Bond number	-
BPE	Boiling point elevation of the massecuite	$^{\circ}C$
BPE_S	Boiling point elevation of the sugar solution	$^{\circ}C$
Bx_{liq}	Brix of the sugar solution	%
Bx_{mass}	Brix of the massecuite	%
Bx_{mol}	Brix of the molasses	%
C_Y, C_X, n_K	King's law constants	-
C_0	Flow distribution parameter	-
CC_{mass}	Crystal content by weight of massecuite	%
CC_{vol}	Volume ratio of crystal to molasses in the solution	%
$C_{p,liq}$	Specific heat of the sugar solution	$J.kg^{-1}.K^{-1}$
$C_{p,mass}$	Specific heat of the liquid	$J.kg^{-1}.K^{-1}$
$C_{p,sug}$	Specific heat of the sugar	$J.kg^{-1}.K^{-1}$
C_N	Count rate for the process fluid in the heated tube	$counts.s^{-1}$
CV	Coefficient of variation in the crystal size distribution	%
C_W	Count rate for a fluid with specific gravity of unity	$counts.s^{-1}$
d_{bub}	Diameter of the bubble	m
dP_{grav}	Pressure loss due to elevation	$N.m^{-2}$
dP_{acc}	Pressure loss due to acceleration	$N.m^{-2}$
dP_{frict}	Pressure loss due to friction	$N.m^{-2}$
D	Internal diameter of the heated tube	m
DS_{liq}	Dry substance of the solution	%
DS_{mass}	Dry substance of the massecuite	%
DS_{mol}	Dry substance of the mother molasses	%
E	Voltage output of the anemometer	Volt
F_R	Crystal property constant for viscosity calculations	-
f_f	Fanning friction factor	-
f_{liq}	Fanning friction factor evaluated for the liquid velocity	-
f_{vap}	Fanning friction factor evaluated for the vapour velocity	-
g	Gravitational acceleration constant	$m.s^{-2}$

G	Mass flow rate in the tube	kg.s^{-1}
h_{boil}	Boiling heat transfer coefficient	$\text{W.m}^{-2}.\text{K}^{-1}$
h_{cond}	Condensation heat transfer coefficient	$\text{W.m}^{-2}.\text{K}^{-1}$
h_{conv}	Convection heat transfer coefficient	$\text{W.m}^{-2}.\text{K}^{-1}$
h_{FC}	Forced convection heat transfer coefficient	$\text{W.m}^{-2}.\text{K}^{-1}$
h_{NB}	Nucleate boiling heat transfer coefficient	$\text{W.m}^{-2}.\text{K}^{-1}$
h_{SP}	Single phase transfer coefficient	$\text{W.m}^{-2}.\text{K}^{-1}$
h_{TP}	Boiling or two-phase heat transfer coefficient	$\text{W.m}^{-2}.\text{K}^{-1}$
I	Current in the heating element	A
Ja	Non-dimensional Jacob number	-
k_{liq}	Thermal conductivity of the sugar solution	$\text{W.m}^{-1}.\text{K}^{-1}$
k_{mass}	Thermal conductivity of massecuite	$\text{W.m}^{-1}.\text{K}^{-1}$
K_{liq}	Consistency of the liquid	$\text{N.m}^{-2}.\text{s}^n$
L_{xal}	Mean crystal size	mm
L_D	Path length of the process fluid	m
L	Length scale for heat transfer	m
L_T	Length of the heated tube	m
M_{AC}	Mass absorption coefficient	$\text{m}^2.\text{kg}^{-1}$
M_{CW}	Mass flow rate of the cooling water stream	kg.s^{-1}
M_{leak}	Leakage mass flow rate of air	kg.h^{-1}
M_{steam}	Mass flow rate of the steam	kg.s^{-1}
MW	Molecular weight	kg.kmol^{-1}
n_{flow}	Viscosity flow behaviour index	-
N_{bub}	Experimentally determined constant (Equation 4.22)	-
Nu_L	Non-dimensional Nusselt number	-
Nu_{TP}	Non-dimensional two-phase Nusselt number	-
p	Static pressure in the heated tube	kPa
P_{liq}	True purity of the solution	%
P_{mass}	True purity of the massecuite	%
P_{mol}	True purity of the mother molasses	%
Pr	Non-dimensional Prandtl number	-
Q	Heat flux	W
Q_{cond}	Heat flux in the heat exchanger	W
Q_{leak}	Air leakage rate in the rig	$\text{m}^3.\text{Pa.s}^{-1}$
Q_{liq}	Volumetric flow rate of liquid in the tube	$\text{m}^3.\text{s}^{-1}$
Q_{tube}	Heat flow rate to the calandria tube	W
Q_{vap}	Volumetric flow rate of vapour in the tube	$\text{m}^3.\text{s}^{-1}$

r	Internal radius of the heated tube	m
R	Gas constant	$8.314 \text{ m}^3 \cdot \text{Pa} \cdot \text{mol}^{-1} \cdot \text{K}^{-1}$
Re_{TP}	Non-dimensional two-phase Reynolds number	-
R_m	Metal heating element resistance	Ω
R_{SW}	Heating resistance from the condensing steam to the tube	$\text{W}^{-1} \cdot ^\circ\text{C}$
R_{WM}	Heating resistance from the tube wall to the massecuite	$\text{W}^{-1} \cdot ^\circ\text{C}$
S	Liquid – vapour slip ratio	-
suc_{liq}	Sucrose content of the solution	%
T_a	Ambient fluid temperature	$^\circ\text{C}$
T_{air}	Temperature of the air leaking into the system	$^\circ\text{C}$
$T_{CW\text{in}}$	Inlet cooling water temperature	$^\circ\text{C}$
$T_{CW\text{out}}$	Outlet cooling water temperature	$^\circ\text{C}$
T_f	Film temperature	$^\circ\text{C}$
T_{liq}	Temperature of the liquid	$^\circ\text{C}$
T_{mass}	Temperature of the massecuite	$^\circ\text{C}$
T_{mol}	Temperature of the molasses	$^\circ\text{C}$
T_{steam}	Temperature of the condensing steam	$^\circ\text{C}$
T_{sat}	Temperature of the saturated vapour produced by boiling	$^\circ\text{C}$
T_{sug}	Temperature of sugar	$^\circ\text{C}$
T_{wall}	Temperature of the tube wall	$^\circ\text{C}$
u_{liq}	Superficial liquid phase velocity	$\text{m} \cdot \text{s}^{-1}$
\bar{u}_{liq}	Average liquid phase velocity	$\text{m} \cdot \text{s}^{-1}$
u_{TP}	Two-phase velocity of the liquid-vapour mixture	$\text{m} \cdot \text{s}^{-1}$
u_{vap}	Superficial vapour phase velocity	$\text{m} \cdot \text{s}^{-1}$
\bar{u}_{vap}	Average vapour phase velocity	$\text{m} \cdot \text{s}^{-1}$
U	Overall heat transfer coefficient	$\text{W} \cdot \text{m}^{-2} \cdot \text{K}^{-1}$
V_{fluid}	Velocity of the fluid perpendicular to the probe	$\text{m} \cdot \text{s}^{-1}$
V_{liq}	Mean velocity of the fluid entering the tube	$\text{m} \cdot \text{s}^{-1}$
V_r	Mean bubble rising velocity	$\text{m} \cdot \text{s}^{-1}$
x	Mixture quality	-
z	Length along the heated tube	m

Greek letters

α	Vapour volume fraction	-
α_{dif}	Thermal diffusivity	$\text{m}^2 \cdot \text{s}^{-1}$
∂_t	Thermal boundary layer thickness	m
ΔT	Temperature difference between the tube wall and liquid	$^\circ\text{C}$

ΔT_{eff}	Effective temperature difference	K
γ	Shear rate	s^{-1}
γ_{corr}	Corrected shear rate	s^{-1}
λ_{fg}	Latent heat of condensation of the steam	$J.kg^{-1}$
$\lambda_{fg,liq}$	Latent heat of the sugar solution	$J.kg^{-1}$
ρ_{liq}	Density of the liquid	$kg.m^{-3}$
ρ_{mass}	Density of the massecuite	$kg.m^{-3}$
ρ_{mol}	Density of the molasses	$kg.m^{-3}$
ρ_{mix}	Density of the process fluid in the heated tube	$kg.m^{-3}$
ρ_{vap}	Density of saturated water vapour	$kg.m^{-3}$
ρ_{xal}	Density of the crystal	$kg.m^{-3}$
μ_{liq}	Dynamic viscosity of the liquid	Pa.s
μ_{mass}	Dynamic viscosity of the massecuite	Pa.s
μ_{mol}	Dynamic viscosity of the mother molasses	Pa.s
σ_{liq}	Surface tension of sugar solution	$N.m^{-2}$
σ_{mol}	Surface tension of mother molasses	$N.m^{-2}$
τ	True shear stress	$N.m^{-2}$

Subscripts

liq	Liquid component of solution
vap	Vapour component of solution
mass	Massecuite
mol	Molasses
sug	Sugar

1 INTRODUCTION

Sugar is a major contributor to the Australian economy. It is Queensland's largest agricultural crop and is the second largest export crop in Australia (Queensland Sugar Corporation, 1997). Appendix A provides a glossary of some of the specific terms used in the sugar industry.

The sugar manufacturing process involves harvesting the sugarcane as billets and transporting to the sugar mill where the cane is processed. The billets pass through a series of milling stages that crush the cane through grooved rollers extracting the juice containing the sugar from the fibrous material, which is called bagasse. The juice is pumped away for processing and the bagasse is stored and used as fuel for combustion in the mill boilers.

The juice extracted from the milling train is passed through a clarification stage that involves heating the juice and adjusting the pH with lime saccharate. The added lime neutralises the acids and promotes the formation of precipitates. Heating the juice increases the reactivity of the non-sucrose impurities and also helps to prevent bacterial decomposition. The insoluble impurities, soil particles and precipitates are separated from the juice in vessels called sedimentation clarifiers. The separated mud mixture is used as soil conditioner in cane farms or gardens.

The clarified juice from the clarifiers is sent to the evaporator station. The evaporator station, which usually comprises of five effects connected in series, concentrates the juice by boiling off the excess water. The effects operate under progressively higher vacuum levels to minimise the temperature of the final juice boiling step. The first effect is normally heated using low-pressure exhaust steam from the mill turbines. The boilers create steam that runs turbo-alternators to produce electricity for the factory. Subsequent effects are heated using the vapour that is boiled off from the previous effect. The concentrated juice produced by the evaporator station is called final liquor or syrup.

The syrup is then concentrated further and crystallised into sugar by boiling in large vessels called vacuum pans. The vacuum pans are seeded with small sugar crystals and the sugar solution is kept supersaturated to encourage the seed crystals to grow to a desired size by adding more syrup while controlling the boiling conditions. This process is called crystallisation. When the crystals reach the required size, the mixture is discharged from the pan. This mixture of molasses and crystals is called massecuite.

There are two modes of operation of crystallisation vacuum pans, namely batch and continuous. Continuous pans introduce seed crystal and feed liquor on a continuous basis and at the same time discharge the product massecuite at a relatively constant and continuous rate. Batch vacuum pans initially take in a footing of syrup with seed crystals, and then feed on a supply of liquor or molasses until the sugar crystals are grown to the desired size and properties. The product massecuite is then discharged at the end of this process. The pan then needs to be cleaned out, usually through the use of steam, before the next batch of massecuite is started. These batch cycles are commonly referred to as strikes.

Most Australian factories operate under a three-massecuite boiling formula, which is described in more detail later. The first or 'A' pan produces a mixture of sugar crystals and molasses called 'A' massecuite. The molasses separated from 'A' massecuite is called 'A' molasses. The 'A' molasses is boiled again in the second or 'B' pan to recover and produce more sugar crystals. Similarly 'B' molasses is separated from the 'B' massecuite and is boiled again in the third or 'C' pan to recover more sugar. The purity of the massecuite decreases for each successive boiling. Generally 'A' and 'B' pans are considered high-grade and produce the raw sugar from the factory available for export or consumption. The sugar crystals produced from the 'C' massecuite in 'C' or low-grade pans are retained for use as seed crystals for the high-grade pans or can be remelted.

Molasses is separated from the massecuite in centrifugals, which consist of perforated baskets that spin at high speeds. The mother molasses solution surrounding the crystals is spun off due to the centrifugal forces and passes through the perforated basket. The final molasses is the molasses stream produced during the centrifuging of the 'C' massecuite and this is normally used as feedstock for animals or fermentation.

Sugar driers are used to dry the raw sugar crystals produced from centrifuging the high-grade massecuites. The dried raw sugar is stored in bulk bins at the mills to await transport or shipment.

This project investigates the operation of high-grade batch vacuum pans. Batch pans represent a major capital asset in many mills, with each pan representing a capital value in excess of one million dollars. Many good performing pans can last over 30 years. It is important that vacuum pans operate efficiently and productively to justify their high capital investment and this can be achieved through a well-designed pan. Due to the large capital investment it is also preferable to

some factories to retrofit modifications to their current batch pans in order to achieve improvements in steam efficiency and productivity rather than install new pans.

1.1 Crystallisation vacuum pans

Surveys of Australian sugar mills conducted by Stephens (2001) and Briody (2001) found batch pans were more predominant than continuous pans. Furthermore, the surveys showed that more than 90% of the batch pans found in the Australian sugar industry are of fixed calandria design making them the most common type of batch pan used in the industry. For this reason, this project concentrates on the operation of batch fixed calandria pans.

Figure 1-1 shows a sectioned view of a fixed calandria batch vacuum pan illustrating the key design components. The tubes in the calandria are heated externally by condensing steam, which causes the massecuite inside the tubes to boil and evaporate water concentrating the sugar solution. Each sugar factory typically uses eight vacuum pans, which range in volume from 40 m³ to 160 m³.

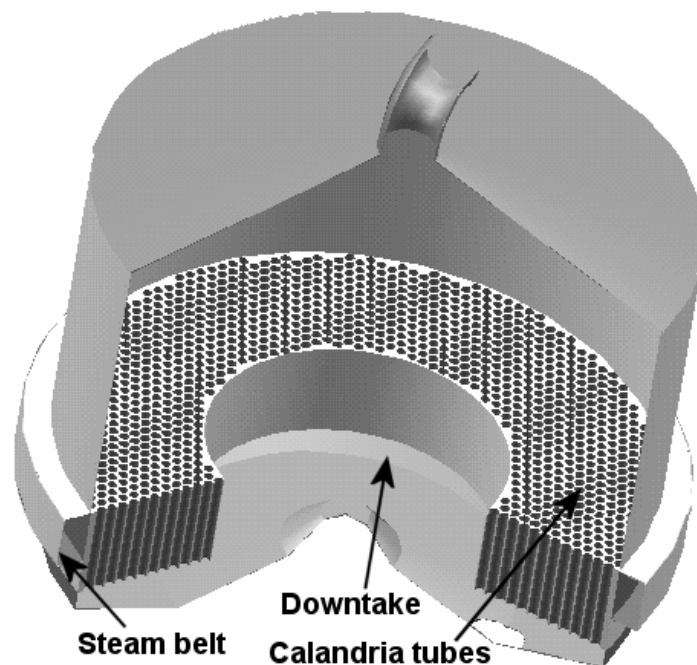


Figure 1-1 Sectioned view of a batch fixed calandria pan, from Stephens (2001).

Strong circulation movement of the massecuite is required to provide adequate mixing of the contents in the pan and create uniform conditions for crystallisation. As well, a strong circulation flow enhances the heat transfer from the condensing steam to the massecuite.

The evaporation of water from the sugar syrup occurs by boiling the solution under vacuum (typical pressure in the head space is 10 kPa (absolute) to 15 kPa (absolute)). Pans are operated under high vacuum to decrease the temperature at which the sugar solution will boil. Generally, lower temperature boiling produces better circulation through the increased volume of vapour due to the increase in specific volume. At lower temperature there is also less colour formation and degradation of sucrose, which are important quality issues of the final product sugar. For a given sugar solution, lower temperatures will increase the level of supersaturation, which is the driving force for crystal growth. Lower temperatures will also increase the viscosity of the solution, which will impact on heat transfer, circulation and crystal growth rates. The operating temperature is a compromise between the quality advantages of lower temperatures and the faster crystal growth rates (provided supersaturation levels are maintained) and lower viscosities at higher temperatures.

The steam supply to vacuum pans is normally the exhaust steam from turbines, which drive the milling train and the turbo-alternators. This steam (called process steam) is typically at 200 kPa (absolute) with a saturation temperature of approximately 120 °C.

1.2 Crystallisation vacuum pan design

The ideal crystallisation vacuum pan has been described as a pan designed to boil a given volume of syrup in the least amount of time, with the least heat input to give the highest yield of maximum quality sugar crystals (Skyring, 1965). Performance indicators of vacuum pans include the circulation speed, sugar quality, boiling time or even heat transmission.

Circulation as a performance indicator warrants extra attention as factors like sugar quality, length of pan strikes and heat transmission can all be linked to good circulation. Circulation relates to the movement of massecuite in a pan. Good circulation within pans is important to provide adequate mixing of the contents in the pan to provide uniform conditions. The provision of uniform conditions leads to the production of high quality sugar as consistent crystal growth is maintained throughout the pan. Uniform conditions in the pan also allow a higher level of supersaturation to be utilised, without nucleation, and so increases the average crystal growth rate. This results in reduced cycle times for the pan and increased productivity.

High average velocities in the tubes across the full width of the calandria and an absence of recirculating zones and slow moving regions where crystals will settle are also indicative of a good circulating pan, although these factors are difficult to assess. Figure 1-2 illustrates the ideal circulation patterns found in a fixed calandria batch pan.

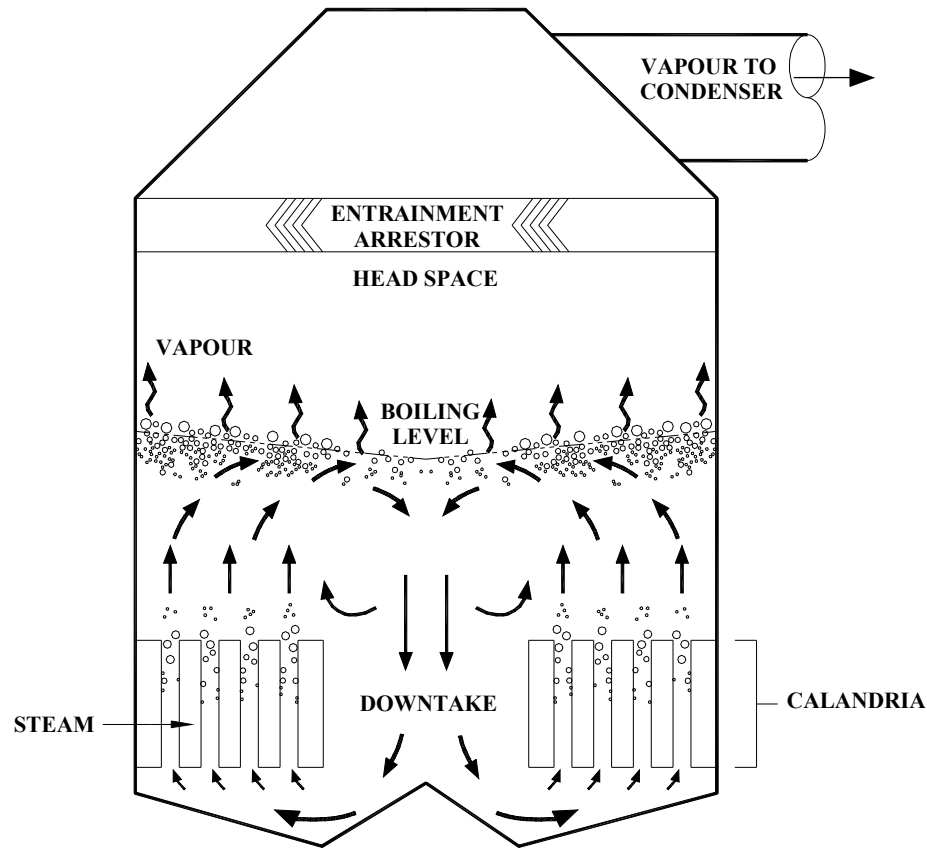


Figure 1-2 Circulation pattern in a fixed calandria batch pan.

While it is difficult to adequately characterise the circulation, it is important to look at the factors that promote or restrict circulation. According to Behne (1938), there are two factors that govern the speed of circulation within pans, viz. those resulting from the design of the pan, and those due to the characteristics of the boiling liquid. While the characteristics of the boiling fluid (viscosity, density, crystal content and the size and shape of crystals) are normally set by production requirements, the design of vacuum pans can be varied to realise the benefits of obtaining more efficient circulation and heat transfer within the pan.

Heat transfer to the massecuite results from the steam condensing on the outside of the calandria tubes, supplying latent heat to the massecuite flowing up through the inside of the calandria tubes. The massecuite in the calandria tubes is heated until boiling occurs producing vapour. The vapour flows up through the tubes, lifting the massecuite to the surface where the vapour disengages from the liquid. Higher density massecuite then flows back down the downtake. The density difference between the higher and lower density massecuite and the drag induced by the vapour bubbles rising through the viscous liquid towards the surface, provides the driving force for natural circulation. It is important that the heat transfer in vacuum pans is able to provide sufficient driving force to sustain natural circulation.

Sugar mills produce electricity by passing steam through turbo-alternators for internal consumption as well as exporting to the state grid in a process commonly known as co-generation. Maximising the co-generation ability is an opportunity to gain extra revenue and maintain economic viability for a sugar factory. Any large-scale co-generation scheme implemented by sugar factories will need to reduce the steam consumption used for sugar manufacture (Broadfoot, 2001) to increase the steam available for co-generation.

More efficient operation of the crystallisation and evaporation stations is one way to reduce this steam consumption. Another promising option for steam reduction is the use of vapour bleeding¹ from the evaporator station for heating duties in other areas of the factory such as that supplied to the crystallisation station. The ability of vacuum pans to operate on lower pressure vapours (vapour bleeds) can be realised through better and more efficient design and represents enormous potential for raw sugar factories to reduce their steam consumption and increase their revenue through co-generation.

1.3 CFD modelling

The emergence of computational fluid dynamics (CFD) modelling as a tool for equipment design has contributed towards more effective designs and modifications in many industries including the sugar industry. Steindl (1995) of Sugar Research Institute (SRI) outlines the general use and potential of CFD modelling to improve the performance in processes involving heat transfer and fluid flow. Previous SRI studies of flow patterns inside vessels used tracer tests and residence time distribution analyses to determine velocities, but these do not show the flow patterns at specific locations within vessels. In comparison, CFD modelling can give

¹ Vapour bleeding refers to the process of using the exhaust vapour collected from an evaporator for other operations other than heating in the subsequent evaporator vessel.

localised flow patterns. Within the sugar industry there has been a recent resurgence in the use of CFD modelling, which has been used to give insight into the design of clarifiers (Steindl, 1995), vertical cooling crystallisers (Harris *et al.*, 1995), evaporators (Steindl and Ingram, 1999; Pennisi *et al.*, 2004), steam boilers (Luo *et al.*, 1997; Mann *et al.*, 2001), combustion furnaces (Woodfield *et al.*, 1998) and effluent flows in ponds (Wood *et al.*, 1997). Some of these studies have led to the development of new or modified vessel designs (Steindl *et al.*, 1998; Sima and Harris, 1999). Other studies have highlighted the need for better quality factory data for validation of the CFD models (Stephens, 2001).

Many CFD software packages use finite volume methods to solve the flow patterns. The finite volume technique is a well-established and thoroughly validated numerical algorithm suitable for many general purpose problems (Versteeg and Malalasekera, 1995). For many projects, to obtain the maximum amount of information for complex problems and geometries, while utilising maximum functionality, the use of a commercial CFD package is preferred over developing a new code. The advantage of using a commercial CFD package includes robustness, solution convergence, user interface capabilities and pre-processing and post-processing visualisation options that come from thousands of man-hours of development.

The design of vacuum pans has been based on ‘rules of thumb’ developed over more than 50 years experience within the sugar industry, partly based on science and partly based on the empiricism of trends. In order to improve vacuum pan designs, new techniques such as CFD modelling, coupled with current measurements of pan operation, need to be utilised. This project provides the data that can be used to develop CFD models and improve the design of vacuum pans.

1.4 Problem statement

Numerical and CFD modelling is becoming a cost-effective and reliable way of developing vessel designs especially when there are complex physics and geometries involved, as is the case with vacuum pans. Currently, however, there are no working numerical models of vacuum pans that can be confidently used to design pans with improved circulation and boiling.

There is also a limited availability of experimental (and suitable factory) measurements for the validation and calibration of numerical models as chapters 2 and 4 will show. This research project aims to provide data on heat transfer and circulation in industrial crystallisation vacuum pans and provide data on an experimental rig simulating a single calandria tube. These

experiments will detail the physical changes and heat transfer characteristics for boiling in calandria tubes with changing material properties and heat input conditions.

The experiments will allow fluid specific correlations to be obtained for heat transfer and flow in calandria tubes that will, in turn, be used to develop numerical models of boiling in calandria tubes. The numerical models will provide a better understanding of the flow characteristics in the vessel, enabling improved engineering design.

2 CIRCULATION AND HEAT TRANSFER MEASUREMENTS

This chapter outlines the theory of circulation and heat transfer that occurs in vacuum pans. A review of the measurements made by previous investigators of circulation and heat transfer is also provided and discussed. The chapter also presents relevant fluid properties that are important in the analysis of heat transfer and circulation.

2.1 Circulation theory

It has long been recognised that the majority of the resistance to circulation occurs within the tubes (Waddell, 1939; Austmeyer, 1986) that can account for more than 90% of the total resistance to circulation. This is especially important under conditions towards the end of a pan strike where lower velocities and higher viscosities enlarge this resistance. The design of new vacuum pans is based on limiting these resistances to flow.

Honig (1951) postulates that the massecuite leaving the calandria tubes in the upward direction is not uniformly heated. There are many tiny areas where massecuite is flashing to produce vapour where localised hot spots are above the local boiling point and then condense as the heated vapour comes in contact with areas of cooler massecuite. The flashing and condensing of these vapours are small in volume and duration but are multiple in number and extend from the tube to the massecuite surface. This explains the periodic boiling nature on the massecuite surface that can be observed through sight glasses, located on vacuum pan vessels.

Allan (1962) believed, through visual observation of pan behaviour, that large amounts of energy are dissipated during the pan's circulation path as vapour is flashed off at the massecuite surface. This is especially so if the boiling is vigorous and, due to high vertical liquid velocities, material is projected substantially into the vapour disengagement space above the boiling level. This energy loss should also be considered along with the frictional resistances experienced in the tubes and downtake when calculating the forces involved in causing circulation within vacuum pans.

Based on observations and experience within the sugar industry Wright (1966) presents a similar view of the mechanism for circulation as Honig (1951), where vapour is formed discontinuously in the calandria tubes driving circulation. This leads to spasmodic or eruptive boiling on the massecuite surface. This erratic heating may lead to short-circuiting through the

creation of circulation loops above the calandria. These circulation loops prevent the masecuite from travelling along its desired path as illustrated in figure 2-1.

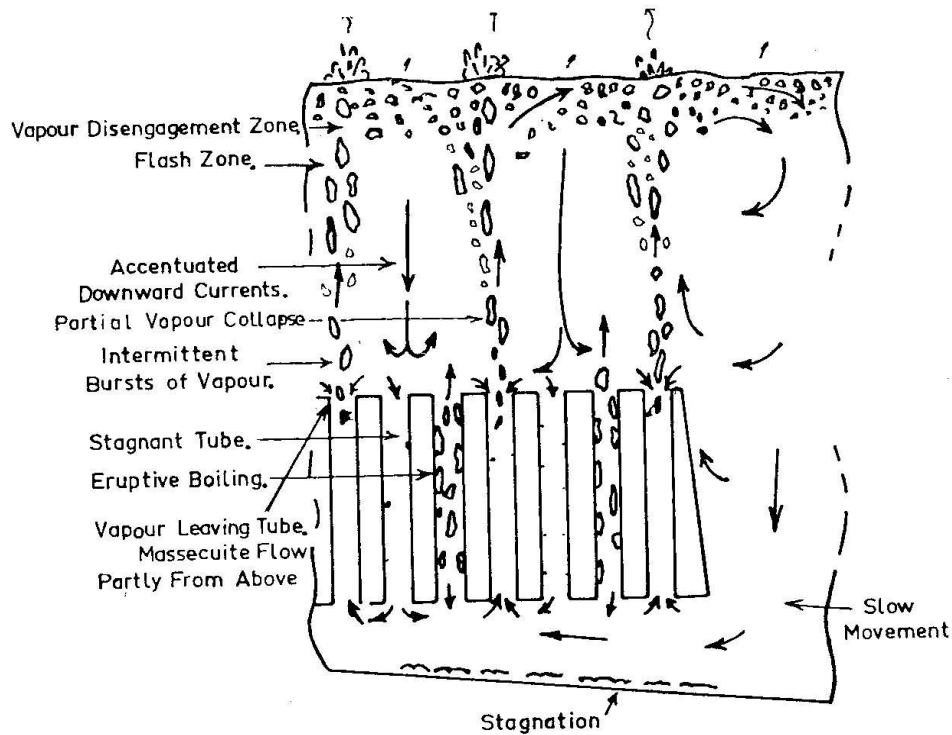


Figure 2-1 Circulation patterns in a vacuum pan due to eruptive boiling, from Wright (1966).

Tait *et al.* (1995) simplified a more idealised interpretation of the mechanisms of circulation. As masecuite flows up through the calandria tubes, boiling is first suppressed due to the hydrostatic head. Boiling then commences and progresses until the bubbles formed approach the size of the tube and slug flow results. This is believed to be closer to the top of the tube. After leaving the tube the bubbles rise and expand due to the reduction in hydrostatic head. The temperature of the bubbles also decreases, as vapour is lost to equilibrate at the lower static pressure. Tait *et al.* (1995) believe the large bubbles rise quickly but contribute little to circulation due to the small residence time. They believe that the effect of the volume fraction on circulation is more important than its residence time. The bubbles will ultimately affect the pressure driving force that determines the circulation. The viscous drag of the bubbles would help to promote circulation, but a larger number of smaller bubbles with overall higher surface area will promote greater circulation.

2.2 Circulation measurements

In order to characterise circulation flows and velocities in vacuum pans an instrument or device, capable of measuring this parameter, is required. For effective measurements, the characteristics of operation of such a device would include:

- Responsive and sensitive to variations in flow velocity;
- Ability to detect localised flows;
- Rugged, robust and operable over a wide range of operating conditions;
- Ability to give repeatable, accurate and reliable results;
- Low cost, easy to use and maintain; and
- Low obstruction/interference with the flow fields.

There are basically two measurement principles for determining circulation velocity in vacuum pans. They are single-point or ensemble measurements. Single-point measuring techniques determine the velocity or one vector component of the velocity at a specific point within the vessel. Ensemble measuring techniques such as laser Doppler and particle imaging velocimetry can simultaneously determine the flow pattern over a wider region or cross-section of the vessel (Mavros, 2001).

There are a number of different techniques and instruments available for measuring the circulation velocities in vacuum pans. These techniques range in complexity and some require special sensors and software that add to the cost of the method. The presence of bulky probes will disrupt flow patterns and can result in false or inaccurate results. Non-intrusive techniques such as particle tracking and tomography have the advantage of not disrupting flow, but these methods also have their drawbacks and obtain limited velocity data. Tracer methods (radioactive, conductivity) under favourable conditions are able to obtain velocities in calandria tubes but are not suitable to obtaining results elsewhere in pans. Imagery techniques are also able to obtain qualitative data on surface circulation (Mavros, 2001) although due to the low optical clarity of typical pan materials, optical imagery methods are not favoured. Prandtl probes and anemometers have also shown potential as a simple and low cost method of obtaining localised flow velocities. Smaller and more robust probes have been developed to minimise interference effects on the flow patterns and anemometers have also been successfully used in applications in the sugar industry (Miller and Muddle, 2000).

It is difficult to characterise the circulation in a vacuum pan during operation due to the lack of optical clarity and the difficulty in accessing the velocity field. Nevertheless, some progress has been made albeit to varying degrees of success, often in specific portions of the pan. Table 2-1 lists some of the velocities obtained for different pans and the methods used.

Table 2-1 List of velocity measurements in industrial vacuum pans.

Pan type	Velocity range, m.s ⁻¹	Velocity location	Method used	Source	Comment
Fixed calandria pan, 'A' duty	0.08-0.23 0.08-0.66	Tubes Entire pan	Conductivity Radioactive	Behne (1938) Wright (1966)	
Fixed calandria pan, 'B' duty	0.03-0.17	Tubes	Conductivity	Behne (1938)	
Floating calandria pan, 'A' duty	0.01-0.07 0.06-0.29	Tubes Entire pan	Conductivity Radioactive	Behne (1938) Wright (1966)	
Floating calandria pan, 'B' duty	0.01-0.07	Tubes	Conductivity	Behne (1938)	
Floating calandria pan, 'C' duty	0.085 0.01-0.47	Entire pan Tubes	Radioactive Evaporation rate	Wright (1966) Webre (1933)	The circulation fell with time to 0.004 mm.s ⁻¹ after 6 h.
Webre calandria pan, 'B' duty	0.03-0.26	Tubes	Conductivity	Behne (1938)	
Webre calandria pan, 'C' duty	0.01-0.18 0.085 0.15-0.38	Tubes Entire pan Tubes	Conductivity Radioactive Conductivity	Behne (1938) Wright (1966) Nicklin and Beale (1960)	Measurements taken near and midway between steam inlets
Coil pan, 'A' duty	0.1	See comment	Hot wire anemometer	Bosworth and Dulo (1950)	Averaged values from a number of positions in pan
Coil pan, 'B' duty	0.04	See comment	Hot wire anemometer	Bosworth and Dulo (1950)	Averaged values from a number of positions in pan
Coil pan, 'C' duty	0.02 0.03-0.05	See comment	Hot wire anemometer Radioactive	Bosworth and Dulo (1950) Wright (1966)	Averaged values from a number of positions in pan
Continuous pan, 'C' duty	0.01-0.07	Entire pan	Radio transmitter	Broadfoot and Steindl (1974)	
Continuous pan, 'A' duty	0.075-0.17	Annular downtake	Conductivity	Broadfoot <i>et al.</i> (1991)	

Fixed calandria pans consist of the calandria fixed to the outer shell of the vessel with a downtake in the middle as shown in figure 1-1. The calandria adds to the rigid support of the pan making larger sized pans possible. This design is in contrast to floating calandria pans where the calandria is placed on the inside of the vessel and an annular downcomer is positioned adjacent to the outer wall. While the project concentrates on the operation of fixed calandria pans, circulation results are presented in table 2-1 for other types of batch vacuum pans. Other pan designs mentioned include coil pans that operate with the heating source for evaporation coming from steam forced through a number of coils in the bottom half of the vessel normally made of copper held together and in place by clips or brackets. The Webre pans mentioned in table 2-1 refer to fixed calandria vacuum pans that have a mechanical stirrer installed in the downtake to aid circulation.

2.2.1 Measurement method

A number of methods have been used to measure the velocities in vacuum pans for a wide variety of conditions. They include:

- Evaporation rates;
- Conductivity;
- Radioactive isotope;
- Radio transmitter; and
- Hot wire anemometers.

These methods are discussed below:

Evaporation rates: The average rate at which water is evaporated is related to the average mass velocity flowing through the calandria tubes (Webre, 1933). The assumption of even flows, especially in vacuum pans 70 years ago before the advent of evenly distributed feed and steam systems, is erroneous and would result in inaccurate predictions of velocities. Webre also based his estimations of circulation velocities using evaporation rates on the assumption that no boiling was taking place within the calandria tubes, which was incorrect.

Conductivity: An electrolyte tracer is introduced into the pan and the average velocity in the calandria tubes obtained from the timed response of electrodes placed above and below the calandria (Nicklin and Beale, 1960; Broadfoot *et al.*, 1991). Alternatively, water can be used as the tracer by increasing the conductivity of the mass (Behne, 1938). These methods rely

on the fact that the tracer is not dissipated during travel between the measuring electrodes, especially by substantial radial flows. The repeatability of this method was poor.

Radioactive isotope: The isotope is placed in a sealed container and its position is monitored externally. Tracking the isotope position is complicated by path size restrictions, presence of metal when the isotope is travelling up the tubes, the radioactive signal being dependent on the path between the isotope and detector, and the buoyancy of the container (Wright, 1966). It poses a health and environmental concern and is not an acceptable method.

Radio transmitter: A radio transmitter encased in a Teflon ball is suspended in the massecuite and the transmitter detected externally (Broadfoot and Steindl, 1974). The method and its shortcomings are similar to the radioactive isotope method except for the health and environmental concerns.

Hot wire anemometry: The rate of heat removal from a heated wire is a function of the local velocity at the probe (Bosworth and Duloy, 1950). Anemometers are susceptible to scaling and are affected by the presence of vapour. Robust anemometers also have substantial thermal lag and deliver slower responses. However, anemometers emerge as a potential and easy operational method of gathering accurate and reliable results within vacuum pans at a low cost.

A number of instrument options were explored for measuring circulation in vacuum pans. Due to the recent success in using anemometers in the sugar industry (Miller and Muddle, 2000) as well as their low cost and easy operational method, anemometers were utilised to determine circulation in vacuum pans in this research. The anemometers have the ability to obtain localised flow measurements over different cross-sections of vacuum pans under a wide range of operating conditions and can be designed to give relatively low interference to the flow fields. Anemometer probes typically have no moving parts which also results in increased reliability and reduced maintenance.

2.2.2 Measurement results

There is a vast range of velocities present in the pans as shown in Table 2-1. The velocities measured in the pans range from 0.03 m.s⁻¹ to 0.47 m.s⁻¹ in calandria tubes to 0.05 m.s⁻¹ to 0.66 m.s⁻¹ in other parts of the pan. Lower velocities were measured when the massecuites were at high concentration due to the high viscosity (Broadfoot and Steindl, 1974). The corresponding boiling level increase with time increases the suppression of boiling and is

expected to contribute to a decrease in measured velocity. However, in spite of these reasons, there is a wide range of velocities between the different studies.

Older pan designs showed a larger decrease in velocity over the course of a strike compared to newer pan designs (Bosworth and Duloy, 1950). The improved result for the newer designs has been attributed to better circulation. The removal of circulation obstructions such as internal baffles has been found to improve pan performance (Bosworth and Duloy, 1950). Nicklin and Beale (1960) found that velocities near the steam inlet were slightly higher than for other parts of the pan, and the velocities measured radially across the calandria width were uniform. The condensate rate as a measure of the heat transfer occurring in the calandria was found to increase with increasing circulation velocity. The use of higher steam flow rates also was found to improve the circulation rate (Broadfoot and Steindl, 1974).

The circulation in the pans is affected by the production of vapour while flow restrictions act to reduce the circulation velocities. Vacuum pan designs have focussed on improving circulation by reducing flow restrictions (Bosworth and Duloy, 1950; Wright, 1966).

2.2.3 Summary

The methods for measuring masscuite velocities, and hence circulation, in vacuum pans do not provide accurate quantitative results due to the difficulty in gaining access to suitable measuring points during pan operation. The literature survey has indicated that the anemometry approach, which gives local velocity data, is a promising method if it can be made robust and calibrated for masscuite properties. The overall trend in flow circulation is that it decreases with time during a strike, but there is little agreement on the actual velocities between different workers. A robust measurement technique should provide more reliable velocity values that can be used to validate numerical models of pans, as well as provide insight into the flow characteristics of the pan and its operation.

2.3 Heat transfer

The overall heat transfer coefficient (HTC) for a pan gives an indication of the effectiveness of heat transfer and can also be used to measure the performance of pans. Efficient utilisation of the heating surface area is important to provide good heat transfer to the contents of a vacuum pan. Heat transfer from the calandria to the boiling masscuite is a critical aspect for the development of circulation patterns within the pan.

To develop HTC correlations for calandria tubes, the overall heat transfer can be estimated using knowledge of the steam consumption over the heating surface area. The overall HTC (Austmeyer, 1986) can then be defined as,

$$U = \frac{Q}{A_{HT} \Delta T_{eff}} \quad (2.1)$$

where U is the overall HTC ($W.m^{-2}.K^{-1}$),
 Q is the heat flux (W),
 A_{HT} is the area available for heat transfer (m^2), and
 ΔT_{eff} is the effective temperature difference (K) between the massecuite (measured as the boiling temperature at the headspace pressure) and the condensing steam in the calandria. The ΔT_{eff} is sometimes referred to as the temperature driving force.

Continuous pans are believed to be able to give better heat transfer performance than batch pans as they operate at lower hydrostatic levels than their batch counterparts. Broadfoot (1992) gives typical values for the HTC in SRI type continuous pans as:

	<i>HTC ($W.m^{-2}.K^{-1}$)</i>
A massecuite	380-475
B massecuite	210-335

There are limited reports of HTC values for batch pans in recent times. Hugot (1972) gives typical HTC values for batch vacuum pans in beet and cane sugar factories with and without a mechanical circulator over a pan strike as:

		<i>HTC ($W.m^{-2}.K^{-1}$)</i>		
	<i>Purity</i>	<i>At start</i>	<i>At finish</i>	
A massecuite (beet)	96	315-350	70	(No stirrer)
B massecuite (beet)	82	70-105	15-35	(No stirrer)
B massecuite (cane)	72	175	10	(No stirrer)
B massecuite (cane)	72	180	70	(Stirrer)

Similarly, Allan (1963) also gives estimates of HTC values for batch vacuum pans in a cane sugar factory over a pan strike as:

	<i>HTC (W.m⁻².K⁻¹)</i>	
	<i>At start</i>	<i>At finish</i>
A massecuite (cane)	165-185	90-110
C massecuite (cane)	110	20

The HTC values for vacuum pans of modern design in cane sugar factories are expected to be higher than these reported values. The HTC is sensitive to the boiling height of massecuite above the tube plate and the purity of the mother molasses (Tippens, 1972). In vacuum pans of modern design, changes to the operating conditions (*i.e.*, increased purity) and utilisation of the total heating surface area will improve the heat transfer performance in pans. Present day pans nominally operate at lower boiling heights compared to earlier practice. This reduction in boiling height significantly increases the HTC that can be obtained at the end of a pan strike.

To correlate the heat transfer in the tubes to the overall heat transfer of the pan relies on the assumption of uniform steam distribution in the calandria and uniform massecuite distribution to the inlets of all the calandria tubes. Malcomson (2000) shows that provided uniform steam flow through steam belts can be accomplished, uniform steam distribution in the calandria is achievable. While Malcomson uses CFD models to investigate the steam distribution, earlier methods have been reported which show the variation of steam flow in the calandria can be minimised through appropriate design of steam distribution (Hill, 1969; Tromp, 1966).

2.4 Fluid properties

Massecuite is a mixture of molasses, syrup and sugar crystals. In general terms massecuite consists of water and soluble and insoluble solids, which are made up of impurities and sucrose. The amount of each of these constituents in the cane supply will vary throughout the season, from year to year and from location to location within a cane growing district or country and will also depend on climate, soil types and harvesting procedure. The main non-sucrose constituents in the massecuite are the reducing sugars glucose and fructose. Other impurities include waxes, high molecular weight molecules, polysaccharides, gums, inorganic salts, and organic acids. These impurities and the variation of their composition can affect the properties of molasses and massecuites and make empirical correlations of high accuracy for fluid properties difficult to determine.

The constituents of massecuite and sugar solutions are typically characterised by the concentration of sucrose, soluble solids, impurities and crystal content. Parameters such as brix,

dry substance, purity and crystal content are typically used to define massecuite mixtures. More information on these parameters is available in Appendix A. The solution brix is defined as the percentage weight of soluble solids in the solution, with the soluble solids comprising sucrose and impurities. The brix is typically determined by measuring the refractive index of the material. Dry substance is a measurement of the total solids in the solution, both soluble and insoluble. Purity is the percentage of sucrose by weight contained within the total solids of the solution. In this research, the true purity, as described in Appendix A, is used, unless specified otherwise. Crystal content is the percentage by weight of sugar crystals present in the massecuite.

The transport and thermodynamic properties of liquids are important in the analysis of heat transfer and circulation. These properties include:

- Density;
- Specific heat capacity;
- Enthalpy;
- Rheological properties such as viscosity;
- Thermal conductivity; and
- Surface tension.

Empirical correlations and descriptions of these properties are detailed in sections 2.4.1 to 2.4.9. Empirical correlations for most of these properties are normally functions of the constituents of the massecuite material and temperature.

2.4.1 Liquid density

From the early processing stages of sugar production the sugar juice comprises predominantly water and the quantity of water has a large impact on the juice density. As the water is evaporated the predominant constituent becomes sucrose. Then, during crystallisation sugar crystals are formed changing the impact of these components on the solution density. Sugar crystals in pure form have a density of approximately 1580 kg.m⁻³.

The density of pure sucrose solutions has been correlated by Rouillard (1985) as,

$$\rho_{liq} = 938.8 + 6.298 Bx_{liq} - 0.8365 T_{liq} \quad (2.2)$$

where ρ_{liq} is the liquid density (kg.m^{-3}),
 Bx_{liq} is the brix of the sugar solution (%), and
 T_{liq} is the temperature of the liquid ($^{\circ}\text{C}$).

The density of molasses solutions can be evaluated using equation 2.2. The density of massecuite solutions can be evaluated based on the volume-weighted fraction of crystal and molasses in the solution by,

$$\frac{1}{\rho_{mass}} = \left(\frac{CC_{mass}}{100} \right) \frac{1}{\rho_{sug}} + \left(\frac{100 - CC_{mass}}{100} \right) \frac{1}{\rho_{mol}} \quad (2.3)$$

where ρ_{mass} is the massecuite density (kg.m^{-3}),
 ρ_{sug} is the sugar crystal density (typically, 1580 kg.m^{-3}),
 ρ_{mol} is the molasses density (kg.m^{-3}), and
 CC_{mass} is the crystal content of massecuite on a mass basis (%).

2.4.2 Specific heat capacity

The specific heat capacity of sucrose solutions was proposed by Janovskii and Archangelskii (1928) which was then modified and reported by Rouillard (1985) for molasses as,

$$C_{p,liq} = a_{JA} + b_{JA} T_{liq} \quad (2.4)$$

where $C_{p,liq}$ is the specific heat of the sugar solution ($\text{J.kg}^{-1}.\text{K}^{-1}$),
 $a_{JA} = 4186.8 - DS_{liq} (0.0297 - 4.6 \times 10^{-5} P_{liq})$,
 $b_{JA} = 7.5 \times 10^{-5} DS_{liq}$,
 P_{liq} is the true purity of the sugar solution (%), and
 DS_{liq} is the dry substance of the sugar solution (%).

The specific heat capacity of massecuites is different to molasses due to the effect of sugar crystals and has been estimated by Hugot (1972) as,

$$C_{p,mass} = 4186.8 \left(1 - 0.001 \left(6 + \frac{CC_{mass}}{60} \right) Bx_{mass} \right) \quad (2.5)$$

where $C_{p, mass}$ is the specific heat of the massecuite ($J.kg^{-1}.K^{-1}$), and
 Bx_{mass} is the brix of the massecuite (%).

The specific heat capacity for crystallised sugar was also reported by Hugot (1972) as,

$$C_{p, sug} = 4186.8(0.2775 + 0.000085 T_{sug}) \quad (2.6)$$

where $C_{p, sug}$ is the specific heat of sugar ($J.kg^{-1}.K^{-1}$), and
 T_{sug} is the temperature of sugar ($^{\circ}C$).

2.4.3 Enthalpy

Peacock (1995) reports a correlation for enthalpy of sucrose solutions based on data supplied by Lyle (1950) as,

$$\lambda_{fg, liq} = 2326 \left(\frac{Bx_{liq}}{10} \left(\frac{100 + Bx_{liq}}{900 - 8 Bx_{liq}} \right) + 1.8 T_{liq} \left(1 - \frac{Bx_{liq}}{100} (0.6 - 0.0009 T_{liq}) \right) \right) \quad (2.7)$$

where $\lambda_{fg, liq}$ is the enthalpy of the sugar solution ($J.kg^{-1}$).

The correlation gives a good fit to the experimental data for solutions ranging from 0 to 90% brix and temperatures of up to 100 $^{\circ}C$.

2.4.4 Rheological properties

Viscosity is the measurement of the resistance to the flow of the fluid under specific conditions of shear. Consistency is an intrinsic fluid characteristic, which is independent of the shearing strain applied during the measurement period. If the shear stress of a fluid is proportional to the flow velocity gradient or strain then the fluid is considered to be Newtonian. Newtonian fluids can be shear independent and temperature dependent.

Masseccutes have been generally described as exhibiting pseudo plastic and shear thinning behaviour (Adkins, 1951; Rouillard and Koenig, 1980; Broadfoot and Miller, 1990; Broadfoot *et al.*, 1998). Masseccutes are also thixotropic² (Rouillard and Koenig, 1980). Molasses or the mother solution has sometimes been considered Newtonian (Thiele and Langen, 1974) or

² Becoming fluid when disturbed but settling to a gel when allowed to stand.

approaching Newtonian especially at high shear rates (Ness, 1984) but usually is considered slightly pseudo plastic.

Masseccutes and molasses are known to exhibit pseudo plastic behaviour as the viscosity of these materials decrease with higher applied shear rates. As the viscosity depends on the shear rate, to enable a classification of the viscosity, a correction is required for the change in shear rate such that,

$$\mu_{liq} = \frac{\tau}{\gamma_{corr}} \quad (2.8)$$

where μ_{liq} is the dynamic viscosity of the liquid (Pa.s),
 τ is the true shear stress (N.m⁻²),
 γ_{corr} is the corrected shear rate (s⁻¹).

The ‘Power Law’ model is generally used to describe the non-Newtonian behaviour of these materials and can be stated as,

$$\tau = K_{liq} \gamma_{corr}^{n_{flow}} \quad (2.9)$$

where K_{liq} is the consistency of the liquid (N.m⁻².sⁿ)
 n_{flow} is the viscosity flow behaviour index for the liquid.

Higher values of K_{liq} indicate a more viscous material whereas the deviation from unity of n_{flow} can be used as a measure of the degree of non-Newtonian behaviour. A value of n_{flow} less than unity indicates a shear-thinning substance, which is consistent with pseudo plastic behaviour, exhibited by masseccutes and molasses. It has been shown that the power law model does give a good fit to experimental data (Ness, 1984; Broadfoot and Miller, 1990; Broadfoot *et al.*, 1998).

Temperature has also been shown to affect viscosity through changing the values of K_{liq} and n_{flow} (Thiele and Langen, 1974; Awang and White, 1976; Ness, 1984; Broadfoot and Miller, 1990; Broadfoot *et al.*, 1998).

Entrained air has also been known to cause problems and increase viscosity (Black and White, 1977; Rouillard and Koenig, 1980; Rouillard, 1984; Ness, 1984; Broadfoot and Miller, 1990; Broadfoot *et al.*, 1998). Entrained air causes molasses to deviate from Newtonian behaviour. Black and White (1977) theorised that the bubbles behaved similar to rigid particles (like crystals) and that 10% entrained air could increase the apparent viscosity by 20% to 30%. The presence of entrained air, while important in the determination of viscosity, is less relevant in vacuum pans where air is removed due to the contents of the pan being under vacuum.

Many authors (Awang and White, 1976; Broadfoot and Steindl, 1980; Steindl, 1981) have looked at the effect of other variables such as dry substance, purity, crystal content and crystal size, and produced expressions based on these variables. One such equation (Broadfoot and Steindl, 1980) gives the viscosity for molasses over typical operating ranges in factory situations as,

$$\mu_{mol} = A_R P_{mol}^{-1.3} \gamma^{-0.16} \exp\left(\frac{3.7 DS^*}{113.5 - DS^*}\right) \quad (2.10)$$

where μ_{mol} is the dynamic viscosity of the mother molasses (Pa.s),

$$DS^* = DS_{mol} - 0.19 (T_{mol} - 50),$$

DS_{mol} is the dry substance of the molasses (%),

T_{mol} is the temperature of the molasses (°C), and

P_{mol} is the true purity of the molasses (%),

γ is the shear rate (s⁻¹), and

A_R is a constant that depends on the amount of entrained air. Typically this value is 0.111 where there is no entrained air as would be the case within vacuum pans.

Massecuite viscosity at the same temperature and shear conditions of the molasses can be expressed according to Steindl (1981) as,

$$\mu_{mass} = \mu_{mol} e^{\left[F_R \rho_{mol} \left(\frac{CC_{mass}}{1 - CC_{mass}} \right) \right]} \quad (2.11)$$

where μ_{mass} is the dynamic viscosity of the massecuite (Pa.s),

ρ_{mol} is the density of the molasses (kg.m⁻³), and

F_R is a constant that depends on the crystal size and coefficient of variation (for typical high-grade massecuite strikes, F_R is 0.002265).

Generally the crystal content has a significant effect on the viscosity (Thiele and Langen, 1974; Rouillard and Koenig, 1980; Broadfoot and Miller, 1990; Broadfoot *et al.*, 1998) Massecuite viscosities are generally 3 to 6 times the magnitude of their mother molasses (Awang and White, 1976). Awang and White (1976) present a correlation between the viscosity of massecuite and its mother molasses based on crystal content and crystal properties such that,

$$\log_{10} \frac{\mu_{mass}}{\mu_{mol}} = 1.65 CC_{vol} L_{xal}^{0.5} \left(1 - \frac{CV}{12}\right) \quad (2.12)$$

where CC_{vol} is the volume ratio of crystal to molasses in the solution (%),
 CV is the coefficient of variation in the crystal size distribution (%), and
 L_{xal} is the mean crystal size (mm).

The CV in the crystal size distribution is calculated by the ratio of the standard deviation of the crystal size to the mean crystal size, as determined by a sieve test. The volume ratio of crystal to molasses can be calculated by,

$$CC_{vol} = \left(\frac{CC_{mass}}{100 - CC_{mass}} \right) \left(\frac{\rho_{mol}}{\rho_{sug}} \right) \quad (2.13)$$

2.4.5 Thermal conductivity

Watson (1986) used data from Lyle (1950) to develop a correlation for the thermal conductivity of typical sugar solutions. The correlation is,

$$k_{liq} = 0.574 + 1.699 \times 10^{-3} (T_{liq}) - 6.308 \times 10^{-6} (T_{liq})^2 - 3.528 \times 10^{-3} Bx_{liq} \quad (2.14)$$

where k_{liq} is the thermal conductivity of the sugar solution ($W \cdot m^{-1} \cdot K^{-1}$).

Rouillard (1985) presents a correlation developed by Bosworth (1941) for the thermal conductivity of massecuite solutions and can be stated as,

$$k_{mass} = A_B DS_{mass} + B_B \quad (2.15)$$

and

$$A_B = T_{mass} \left[5.466 \times 10^{-8} T_{mass} - 1.176 \times 10^{-5} \right] - 3.024 \times 10^{-3} \quad (2.16)$$

$$B_B = T_{mass} \left[1.196 \times 10^{-3} - 7.847 \times 10^{-6} T_{mass} \right] + 0.563 \quad (2.17)$$

where k_{mass} is the thermal conductivity of the massecuite ($\text{W.m}^{-1}.\text{K}^{-1}$), and T_{mass} is the temperature of the massecuite ($^{\circ}\text{C}$).

2.4.6 Surface tension

Surface tension is caused by the imbalance of forces at the surface due to the net attractive forces from neighbouring molecules. The overall net force tends to pull the surface molecules into the bulk of the liquid (Miller and Pike, 1993). The surface tension of a solution decreases with increasing temperature due to the increased kinetic energy of the molecules that allow the surface attraction forces to be overcome. Surface tension also increases with increasing purity and decreasing dry substance of the sugar solution. The concentration of pure sucrose on the surface of sugar solutions is also lower than the bulk of the solution as it is negatively adsorbed at the interface. This indicates the presence of naturally occurring surface-active agents present in the impurities in factory sugar solutions and reduces the surface tension (Miller and Pike, 1993).

Measurements of the surface tension of cane molasses are generally lower than the surface tension of distilled water (Miller and Pike, 1993) due to the impurities present in solution. Watson (1986) used data from Berger (1975) to develop a correlation for surface tension of sugar solutions,

$$\sigma_{mol} = 0.07575 - 1.4518 \times 10^{-4} T_{mol} - 2.3922 \times 10^{-7} T_{mol}^2 + 1.10 \times 10^{-4} Bx_{mol} \quad (2.18)$$

where σ_{mol} is the surface tension of the mother molasses (N.m^{-2}), and Bx_{mol} is the molasses brix (%).

2.4.7 Vapour properties

During the boiling process in vacuum pans, water is evaporated from the liquid. The properties of the vapour may be required for heat transfer calculations. Data is readily available from steam tables in Thermodynamics textbooks and other literature such as the American Society of

Mechanical Engineers (1967). Polynomial correlations were used in this research to interpolate the steam properties of density, viscosity, enthalpy and latent heat of vaporisation. These properties are evaluated at the saturation temperature of the liquid. The saturation temperature is determined using the assumption that the vapour is saturated and not superheated or sub-cooled. The saturation temperature is evaluated at the vapour pressure.

2.4.8 Boiling point elevation

Boiling point elevation is the increase in the boiling point temperature of a liquid due to a substance being dissolved in the solution. The magnitude of the boiling point elevation is proportional to the amount of substance dissolved. The boiling point elevation is not influenced by the crystal content. The boiling point of the liquid is defined as the temperature at which the vapour pressure is equal to the external pressure. If the vapour pressure exceeds the external pressure, the vapour is said to be superheated. Boiling point elevation data gathered from pure sucrose solutions has been fitted to the integrated form of the Clausius-Clapeyron equation by Saska (2002).

$$BPE_S = 0.166 \left(\frac{DS_{mol}}{100 - DS_{mol}} \right)^{1.1394} \left(\frac{273.15 + T_{sat}}{100} \right)^{1.9735} \left(\frac{P_{mol}}{100} \right)^{0.1237} \quad (2.19)$$

where BPE_S is the boiling point elevation of the sugar solution (Δ °C), and

T_{sat} is the temperature of the saturated vapour produced by boiling (°C).

Batterham and Norgate (1975) defined a correlation for boiling point elevation for impure sucrose solutions based on the dry substance, purity and operating pressure,

$$BPE = A_{BPE} T_{sat} + B_{BPE} + C_{BPE} \quad (2.20)$$

and

$$A_{BPE} = 0.3604 - 2.5681 \times 10^{-2} DS_{mass} + 6.8488 \times 10^{-4} DS_{mass}^2 - 8.0158 \times 10^{-6} DS_{mass}^3 + 3.5601 \times 10^{-8} DS_{mass}^4 \quad (2.21)$$

$$B_{BPE} = 50.84 - 3.516 DS_{mass} + 9.122 \times 10^{-2} DS_{mass}^2 - 8.0158 \times 10^{-6} DS_{mass}^3 + 3.5601 \times 10^{-8} DS_{mass}^4 \quad (2.22)$$

$$C_{BPE} = -0.272 - 2.27 \times 10^{-2} P_{mass} + 2.542 \times 10^{-2} P_{mass}^2 + 5.311 \times 10^{-4} DS_{mass} (100 - P_{mass}) \quad (2.23)$$

where BPE is the boiling point elevation of the massecuite (Δ °C),
 DS_{mass} is the dry substance of the massecuite (%), and
 P_{mass} is the purity of the massecuite (%).

2.4.9 Impurities

In vacuum pans, the addition of crystals and vapour bubbles can cause localised variations in the bulk fluid properties which often make the massecuite properties difficult to determine or measure. The accuracy of many engineering calculations is dependent on the accuracy of the correlations for the physical properties.

The presence of impurities in massecuites will often lead to inaccuracies in the empirical correlations for fluid properties. The influence of impurities can lead to significant differences between the actual physical value and the value calculated using the empirical correlation. However, these correlations can provide an estimation of the fluid properties if the properties are not directly measured.

2.5 Summary

Circulation measurements recorded in pans tested by Webre (1933), Behne (1938), Bosworth and Duloy (1950), Nicklin and Beale (1960) and Wright (1966) do not represent pans of modern design used in the Australian sugar industry today. Limited data exist on circulation velocities within vacuum pans of modern design. Previous circulation measurements do however give an indication of the expected velocity ranges and may be used to help identify aspects of pan design that contributes to poor circulation.

The overall HTC for a pan can be used as a secondary measure to circulation, to gauge the performance of a pan. Efficient heat transfer will produce vapour, which drives circulation within the vacuum pan and so heat transfer performance can be closely linked to circulation. The heat transfer performance can be estimated using knowledge of the steam consumption, the heating surface area and temperature driving force.

The constituents of massecuite and sugar solutions are typically characterised by parameters such as brix, dry substance, purity and crystal content that can be easily determined using analytical methods. Transport and thermodynamic properties of liquids are important in the analysis of heat transfer and circulation. Some of these fluid properties are easy to measure, while others are quite difficult, especially if they are also dependent on operating parameters such as shear and temperature. Empirical correlations are available for fluid properties of sugar solutions that are too difficult or tedious to measure individually for factory investigations.

3 FACTORY TRIALS

This chapter provides details and results of the factory trials. Factory trials were undertaken on vacuum pans to determine typical operating conditions. These operating conditions were used for the experimental trials as discussed in chapter 5. Circulation, heat transfer and fluid conditions were measured during the factory trials.

3.1 Introduction

Proven methods and techniques are available for the measurement of heat transfer and fluid conditions within factory vacuum pans. There are a number of techniques available to measure the circulation within vacuum pans; however, in order to obtain more accurate measurements, one of the available techniques had to be improved. A summary of the various techniques and measuring instruments utilised by previous investigators to characterise circulation within vacuum pans was presented in section 2.2.

The option of using a number of different instruments for measuring circulation in vacuum pans was explored. The use of anemometers emerged as a potential and easy operational method for gathering accurate and reliable results at a low cost. Anemometers have the ability to obtain localised flow measurements over different cross-sections of vacuum pans under a wide range of operating conditions. Small anemometer probes can be designed to give relatively low interference to the flow fields and can be rugged and robust under typical operating conditions in a factory pan. Anemometer probes typically have no moving parts, resulting in increased reliability and reduced maintenance. Due to these features, and recent success in using anemometers in the sugar industry (Miller and Muddle, 2000), anemometers were utilised as the measurement technique for determining circulation in factory vacuum pans.

3.2 Hot film anemometers

The anemometers used in this study are a constant-temperature mode hot film anemometer constructed from stainless steel. It is a Turck insertion flow sensor (Turck, 2001) for high temperatures as shown in figure 3-1. Hot film anemometry relies on the heat transfer process through a metal film rather than an exposed wire such as the hot-wire anemometers used by Bosworth and Duloy (1950). This makes the probes more rugged and robust but introduces a degree of lag in the measurement process. The fluid patterns within vacuum pans are expected

to be relatively stable over small periods of time, so the disadvantages of the slower response of the instrument are expected to be unimportant.

The hot film anemometer consists of two temperature detectors encased in a metal cylindrical tip that can be immersed into fluid flow paths. One of the detectors measures the temperature of the surrounding fluid or film around the cylindrical metal tip while the other is connected to a heating element. The power applied to the heating element is varied in order to maintain the second detector in the anemometer tip at a constant temperature slightly above the temperature of the flowing fluid. The power to the heating element will vary depending on the heat transfer rate between the probe and the surrounding fluid. The heat transfer rate from the hot film anemometer to the surrounding fluid will depend on the fluid velocity and properties of the fluid. Outputs from the hot film anemometer can therefore be correlated to the flow velocity of the fluid provided the properties of the fluid are known.

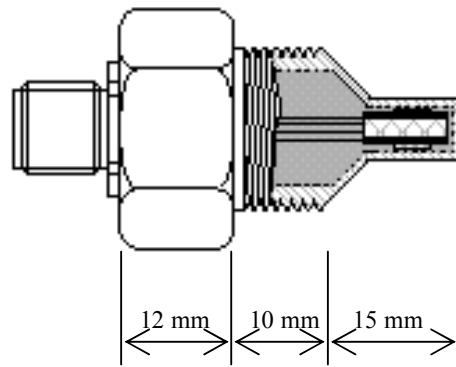


Figure 3-1 Diagram of Turck insertion flow sensor.

For flow around the anemometer probe, it is assumed that the major heat transfer mechanism is convection, with radiation and conduction heat transfer being insignificant in comparison. From an energy balance, the power output from the anemometer is related by,

$$I^2 R_m = h_{conv} A_{film} (T_f - T_a) \quad (3.1)$$

where I is the current in the heating element (A),
 R_m is the metal heating element resistance (Ω),
 h_{conv} is the convection HTC ($W.m^{-2}.K^{-1}$),
 A_{film} is the heat transfer area (m^2),

T_f is the film temperature (°C), and

T_a is the ambient fluid temperature (°C).

Based on empirical evidence, King's law (1914) was developed for thin films around constant temperature anemometers to relate the instantaneous convection velocity (V_{fluid}) to the voltage required to maintain the anemometer tip at the required temperature. The output of the anemometer probe is proportional to this voltage. King's law states,

$$E^2 = I^2 R_m^2 = (C_Y + C_X \cdot V_{fluid}^{n_K}) (T_f - T_a) \quad (3.2)$$

where E is the voltage output of the anemometer (Volt),

V_{fluid} is the velocity of the fluid perpendicular to the probe ($m \cdot s^{-1}$), and

C_Y, C_X, n_K are constants and depend on the fluid properties.

For the calibrations and the factory vacuum pan tests, dry substance and purity were the properties used to characterise the massecuites. For constant temperature anemometers like the ones used in this study, the heat transfer area and the temperature difference between the fluid and the anemometer probe are constant. Provided the temperature is relatively constant, the metal heating element resistance can also be assumed to be constant. Thus from equations 3.1 and 3.2,

$$h_{conv} \propto C_Y + C_X \cdot V_{fluid}^{n_K} \quad (3.3)$$

The probes were calibrated to give a sensor output reading of zero for zero flow, which allows the removal of the intercept C_Y from the calibration curve. Four anemometer probes were used in this study and were labelled probe 1 to probe 4. All probes required separate calibration. For the calibrations, the output signal from the anemometer probe is proportional to the output voltage of the circuit. Thus for the calibration data for probe 1,

$$(\text{Probe 1 reading})^2 = C_{1A} (V_{fluid})^{n1} \quad (3.4)$$

and for probe 2,

$$(\text{Probe 2 reading})^2 = C_{2A} (V_{fluid})^{n2} \quad (3.5)$$

and so forth,

where $C_{1A}, C_{2A}, C_{3A}, C_{4A}, n_1, n_2, n_3, n_4$ are functions of the fluid composition and are detailed in Appendix B.

In sugar solutions, the fluid composition can generally be described by the dry substance and purity. For this exercise the dry substance and purity values were taken to be representative of the fluid composition. Similarly the Nusselt number, which can be related to the HTC, is also typically a function of density, viscosity, velocity, specific heat, and thermal conductivity. All these parameters except velocity are normally also functions of the temperature and solids content of the fluid giving confidence to using dry substance and purity to describe the fluid composition in this situation. The Nusselt number (Nu_L) can be defined as,

$$Nu_L = \frac{h_{conv} L}{k_{liq}} \quad (3.6)$$

where L is a length scale for heat transfer (m).

3.3 Anemometer calibrations

Calibration is required for all fluids and is generally performed using water before and after each set of experiments to determine if the probe has suffered any effects of drift. Prior to any calibrations, the hot film anemometers were modelled using CFD software for a number of situations including insertion into pipes as well as vacuum pans. Due to the high viscosity and relatively low flows (small Reynolds numbers) eddy shedding was not observed in the simulations.

The hot film anemometers were calibrated using a circulation rig, which consisted of a buffer tank (25 L) from which a Mono pump transports the fluid around the loop at controlled speeds, using a variable speed drive. The Mono pump was operated with the discharge on the gland side so that the gland packing was under positive pressure and would leak slightly. This mode of operation prevented air from being sucked in through the gland when pumping the viscous masecutes, as air entrainment into the masecuite would alter the properties of the material. The fluid flowed past the hot film anemometer positioned in the middle of the pipe and then recirculated back into the buffer tank. A resistive temperature device (RTD) and a magnetic flowmeter were also positioned on the rig as shown in figure 3-2.

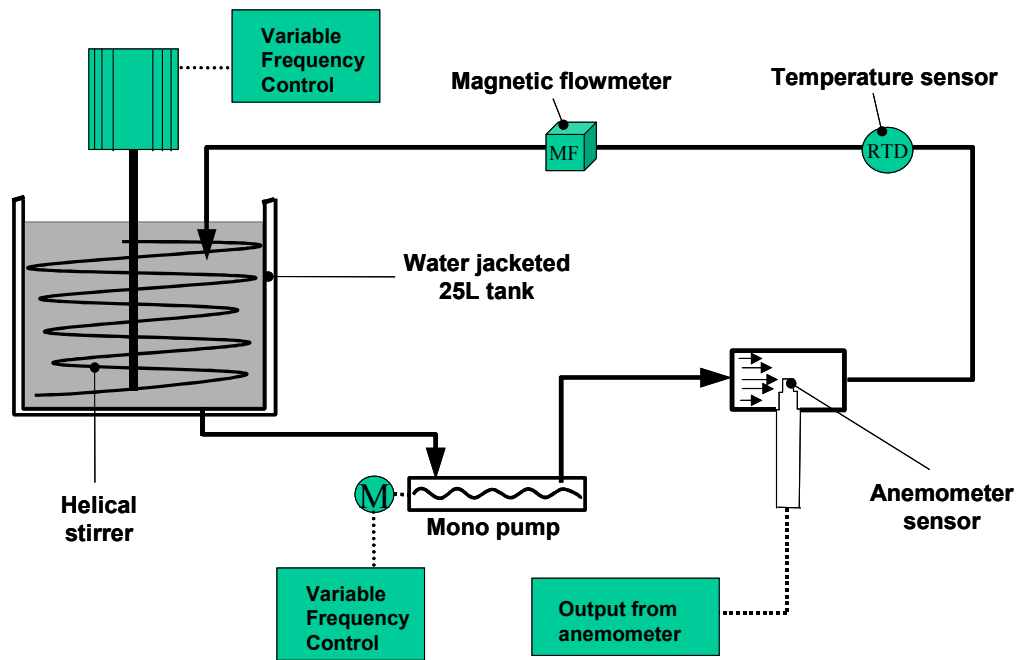


Figure 3-2 Schematic of calibration rig.

The buffer tank was water jacketed for better temperature control and had a helical stirrer that contacted the tank sides and bottom to prevent crystals from settling in the tank. Helical ribbon stirrers have been considered satisfactory for mixing viscous fluids (White and Hertle, 1984). Some heating of the system also occurred from energy absorbed during pumping.

Various fluid velocities, as measured by the magnetic flow meter, could be selected by varying the pump speed. The output from the anemometer was measured when the performance of the rig was stable in terms of steady flow rate and minimal temperature variations.

Readings from the probe could then be taken for a range of speeds and used to determine a correlation for converting the output signal to an actual velocity past the probe tip. Different fluid mixtures were tested in this calibration rig to gather data on anemometer outputs at different flow velocities for a range of fluid mixtures and properties. These fluid mixtures and fluid properties need to be analogous to those in factory pans so that readings from the anemometer obtained in the factory trials can be related to actual flow velocities. The fluid properties of the calibration mixtures were adjusted by mixing samples from typical factory streams to reflect the properties experienced during operation of vacuum pans. The errors in dry substance and purity determinations were approximately ± 0.3 units and ± 0.8 units, respectively.

3.4 Anemometer error sources

The orientation of the probe and any variations in temperature of the fluid impact on the output of the hot film anemometer. The manufacturer (Turck, 2001) claims that measurements of fluid flow are independent of the orientation of the tip provided it is still perpendicular to the flow; however the following theory shows that this may not be the case. Figure 3-3 shows variations to the orientation of the heating and sensing temperature detectors within the anemometer probe tip relative to the fluid flow. It is also noted that the obstruction caused by the insertion of the tip will slightly alter the flow pattern. From figure 3-3 it can be seen that the velocity adjacent to the sensing detectors within the tip are dependent on how the temperature detectors within the tip are orientated towards the flow profile and stagnation layer.

During the calibration of the instrument, the tip was rotated to the position where a maximum signal reading was identified. The tip was also perpendicular to the flow path. This orientation was noted and used for subsequent trials. The velocity calculated using King's Law would thus give the velocity of fluid flow perpendicular to the probe tip.

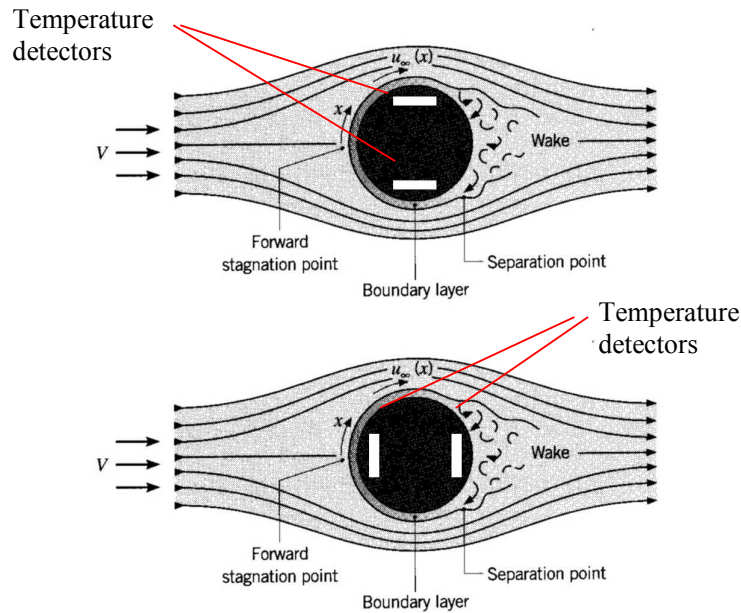


Figure 3-3 Orientations of the anemometer tip to the cross-flow profile, adaptation from Incropera and DeWitt (1996).

The effect of variations in temperature is expected to be minimal over the temperature ranges encountered in vacuum pan operation (65 °C to 73 °C). The sensor also has the ability to compensate for sudden temperature changes at a temperature gradient less than 250 °C.min⁻¹ or 4.2 °C.s⁻¹ (Turck, 2001). This is 10 to 15 times higher than standard flow devices and makes the

sensor very stable under the imposed conditions experienced during the calibrations and factory trials.

Some typical problems or sources of error in using and calibrating anemometers include (Liow, 2001):

- Contamination and scale build up on the probe tip leading to a drift in sensor outputs;
- Probe vibrations or eddy shedding caused by probe or flow proximity to solids or walls and the insulating effects of low velocity flows in viscous media;
- Ambient temperature changes leading to changes in fluid properties; and
- Fluid flow is not perpendicular to the probe tip and the orientation of the probe tip to the main flow direction is not well defined.

3.5 Overview of the factory trials

Factory trials were conducted on a number of batch pans in 2001 and 2002. The factory trials involved circulation measurements taken with the anemometer probes at key positions and at varying depths within the pan, and heat transfer measurements taken during the tests. Although numerous vacuum pans were studied, this project focuses on one vacuum pan located at Macknade Mill, Queensland, Australia. The vacuum pan was chosen for the investigations as it has shown reasonably strong performance in the past. The pan is considered to be a good example of a strongly performing modern pan. The attributes of the pan are as follows;

- No. 6 vacuum pan at Macknade Mill.
- Capacity of 105 t (or 75 m³ volume) when full.
- Overall vessel diameter of 5800 mm.
- Fixed calandria design with 1250 calandria tubes.
- Calandria tubes have an outside diameter of 114.3 mm and are 1180 mm long.

Figure 3-4 shows the probe locations and the general dimensions of the No. 6 pan at Macknade Mill. Sockets at locations ‘A’ and ‘E’ were installed to allow additional measurements to be made during the 2002 season. Sockets at locations ‘B’, ‘C’ and ‘D’ were installed prior to the 2001 season.

An extensive amount of data was gathered from factory trials during the 2001 and 2002 cane crushing seasons on the pan. Twenty one measurement trials were conducted during the 2001

crushing season and twenty measurement trials were conducted during the 2002 crushing season. The results over the two seasons' trials showed reasonable agreement at similar probe locations and insertion depths. Heat transfer measurements were only obtained during the 2001 season.

The circulation and heat transfer measurements obtained through the factory trials concluded that the pan does perform well, in agreement with past observations (Stephens, 2001). A brief assessment of the factory trials are reported in this section.

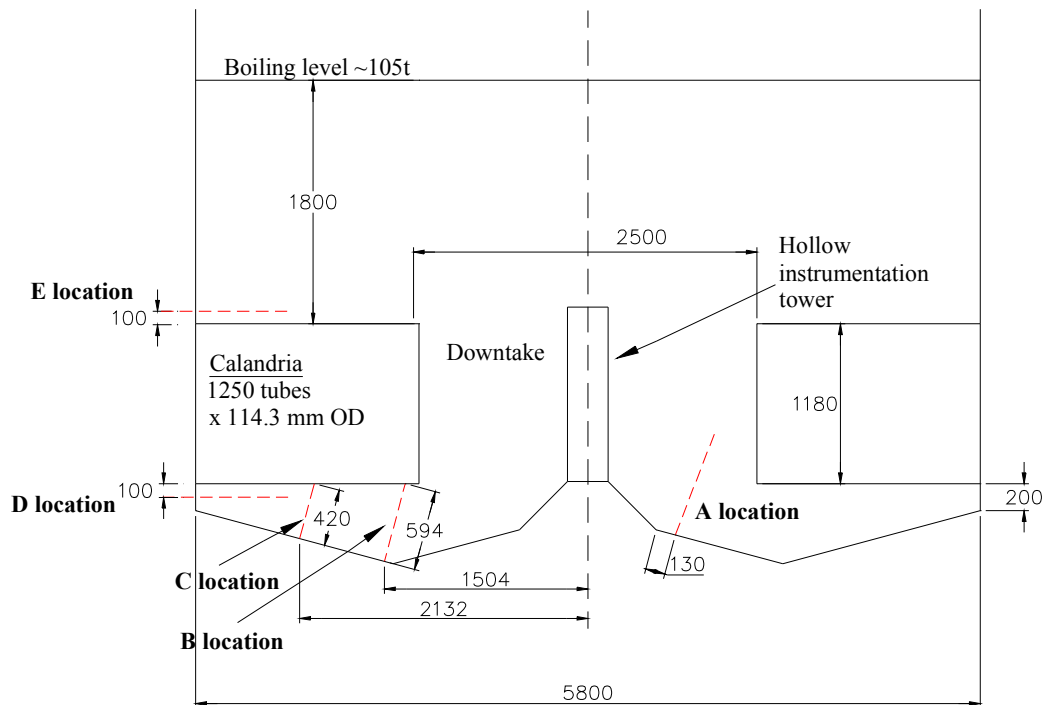


Figure 3-4 Socket locations for the anemometer probes and general pan dimensions (in mm) of Macknade No. 6 pan.

The hollow instrumentation tower (in figure 3-4) originally held instruments such as conductivity probes that could measure fluid properties within the downtake.

The operating parameters such as calandria pressure and steam flow rates were used to determine heat transfer data for the pan during operation. The circulation and heat transfer measurements obtained from the factory trials were used to define the operating conditions for the experimental trials on the single calandria tube boiling rig (as discussed in chapter 5).

Another objective of the factory trials was to collect localised flow circulation data that could be used to validate and calibrate numerical models of circulation within vacuum pans. The gathered data also provides confidence and validates the method of using anemometers to obtain accurate circulation data inside vacuum pans.

The hot film anemometers were inserted into the vacuum pans using a special housing and gland arrangement. The smaller end of the probe housing being inserted into the pan, as shown in figure 3-5, was made of brass for pragmatic manufacturing reasons. The use of a tip of smaller diameter than the main shaft was employed in order to reduce the intrusive effect of the probe on the flow pattern within the pan in the region of velocity measurement.

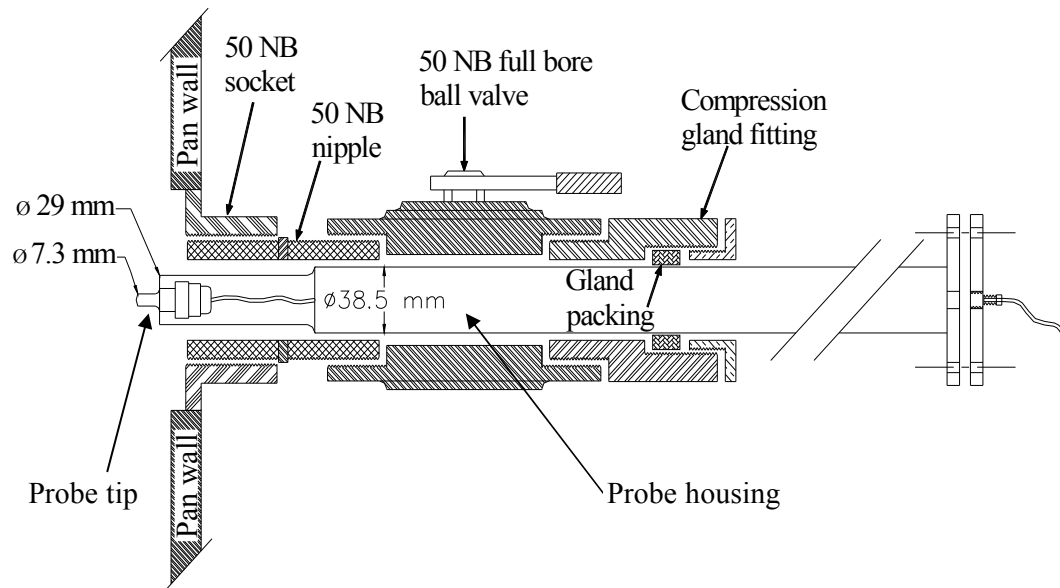


Figure 3-5 Anemometer probe housing and gland arrangement for insertion into vacuum pans.

The technique and procedure for using hot film anemometers to measure circulation velocities in vacuum pans have also been reported by Rackemann and Stephens (2002).

3.6 Sample analysis

Massecuite samples were obtained during pan strikes at Macknade Mill. The massecuite samples were pressure filtered to give samples of the mother molasses that, along with the samples of massecuite, were used for analysis and viscosity determination. The analyses performed on the massecuite and mother molasses samples are summarised in table 3-1.

Table 3-1 List of analyses conducted on massecuite and molasses samples.

Sample	Parameter	Method of Analysis
Massecuite	Dry substance	Vacuum oven drying (Method 19#)
	Sucrose	Double polarisation (Method 18#)
	Crystal content	Purity difference between massecuite and mother molasses sample
	Temperature	Digital thermometer
	Viscosity	Brookfield RVT viscometer with disc spindles
Molasses from pressure filtered massecuite sample	Dry substance	Vacuum oven drying (Method 19#)
	Sucrose	Double polarisation (Method 18#)
	Temperature	Digital thermometer
	Viscosity	Brookfield RVTD viscometer with small sample adapter.

Methods nominated by BSES (1991).

Dry substance was determined by oven drying at 65 °C for 16 h following Method 19 (BSES, 1991). Sucrose was measured using the double polarisation method following Method 18 (BSES, 1991). The purity of the sample is calculated by,

$$P_{liq} = \frac{suc_{liq}}{DS_{liq}} \times 100 \quad (3.7)$$

where P_{liq} is the true purity of the solution (%),
 suc_{liq} is the sucrose content of the solution (%), and
 DS_{liq} is the dry substance of the solution (%).

The crystal content, defined as a mass percentage by weight of the massecuite, is calculated from the difference in purity of the massecuite sample and its corresponding mother molasses sample as follows,

$$CC_{mass} = \frac{(P_{mass} - P_{mol})}{(100 - P_{mol})} \times DS_{mass} \quad (3.8)$$

where CC_{mass} is the crystal content of the massecuite (%),

DS_{mass} is the dry substance of the massecuite (%), and

P_{mass} and P_{mol} are the true purity of the massecuite and mother molasses respectively (%).

Determining the rheological behaviour of high purity massecuites is very difficult owing to the settling of crystals during measurement and the crystal migration away from the wall or surface of the viscometer where the shear is imposed (Broadfoot *et al.*, 1998). There appears to be no satisfactory procedure for measuring the rheological behaviour of high-grade massecuites due to the effects of crystal settling and migration (ICUMSA, 1994). However, for factory rheological measurements, using the Brookfield viscometer with disc spindles is the preferred method owing to the substantially reduced time required for measurements (Broadfoot *et al.*, 1998).

The viscosity of the massecuite was measured with a Brookfield Synchro-lectric viscometer Model RVT using a RVT No. 4 disc spindle. The viscosity of the mother molasses was measured using the same Brookfield viscometer fitted with a small sample adapter and SC4 27/13 spindle. All viscometer measurements of massecuite and molasses samples follow the procedure outlined in Method 24 (BSES, 1991) and SPS-5 (ICUMSA, 1994).

The viscosity was measured at several speed settings so that the effect of shear rate on the viscosity could be quantified. A computer program was used to calculate the rheological properties from the measured data, which are specified as the K_{liq} (the corrected viscosity for a shear rate of 1 s^{-1}) and n_{flow} instead of defining a single viscosity value. Table 3-2 summarises the properties of the massecuite samples taken during the factory trials.

Table 3-2 Summary of sample analyses for Macknade No. 6 pan.

Sample	Dry substance, % (<i>i.e.</i> , solids content)	Purity, %	Crystal content, % of massecuite	Viscosity at a shear rate of 1 s^{-1} , Pa.s (measured at $65 \text{ }^\circ\text{C}$)
Massecuite				
Start of pan cycle	85-87	91-92	25-30	1.5-4.0
End of pan cycle	89-90	88-90	40-45	15.0-30.0
Molasses				
Start of pan cycle	77-79	83-85	-	0.3-1.0
End of pan cycle	80-82	78-81	-	1.0-5.0

The massecuite dry substance and purity were analysed from spot samples obtained throughout the pan cycle. Simple linear relationships for the fluid properties were correlated to the operating level in the pan to allow dry substance and purity values to be interpolated at different stages through the pan cycle. These values are used to calculate circulation speeds using the calibration equations (equations 3.4 and 3.5) for each of the anemometer probes. The

relationships for dry substance and purity are assumed to be reasonably linear over short periods of the pan cycle but ideally the full time-dependent characterisation of the pan properties is required to provide accurate correlations to the anemometer reading output.

3.7 Circulation results

Under general operation at Macknade, No. 6 pan would take in a charge of 40 t to 45 t of prepared magma from No. 3 pan and then increase the level to approximately 105 t, feeding on liquor over a period of approximately 1 h. This initial part of the pan cycle is to provide the footing for both the A massecuite strike in No. 6 pan and an A massecuite strike in another pan. Once No. 6 pan is full, approximately half the contents of the pan are transferred to No. 2 pan. No. 6 pan is then run back up to 105 t to 108 t feeding on liquor, with the final 10 t feeding on A molasses, which is the boil back period. This second stage of the pan cycle takes approximately 80 min to 90 min. The pan is then heavied up for a further 15 min. When the pan's contents are ready to be discharged, 4 t of molasses are added for lubrication to assist with fuggalling. The terminology used to define these two phases of the operation of No. 6 pan are the seed preparation step and the A massecuite strike.

The operating levels in the pan have been broken down into 5 stages for the A massecuite strike from where the level changes from pre-determined values. These 5 stages include:

- 55 t to 70 t operating level in the pan;
- 70 t to 85 t operating level in the pan;
- 85 t to 95 t operating level in the pan;
- 95 t to the end of the feed stage; and
- During the heavy up stage³.

The first stage begins once the operating level in the pan reaches 55 t. Initially the pan is given a footing volume of approximately 40 t to 45 t. The data taken during the time where the massecuite quantity in the pan increases to 55 t is disregarded to account for the vacuum and steam rate being ramped to their operating set points during this period.

³ The heavy up stage occurs after the pan has finished feeding with liquor or molasses.

Average velocities were calculated during these stages for the five socket locations on the pan at a number of different insertion depths. The results are shown for both the 2001 and 2002 crushing seasons in figures 3-6, 3-7, 3-8, 3-9 and 3-10 for only the A massecuite strike.

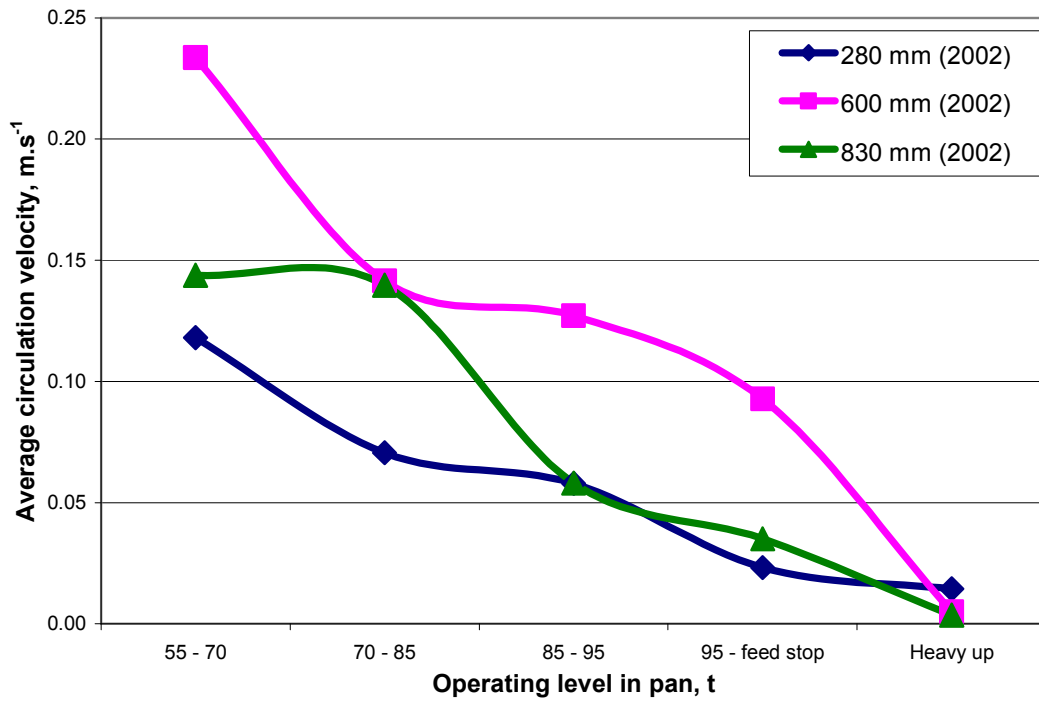


Figure 3-6 Average velocity trends at socket location ‘A’ for various insertion depths on No. 6 pan at Macknade Mill during the A massecuite strike.

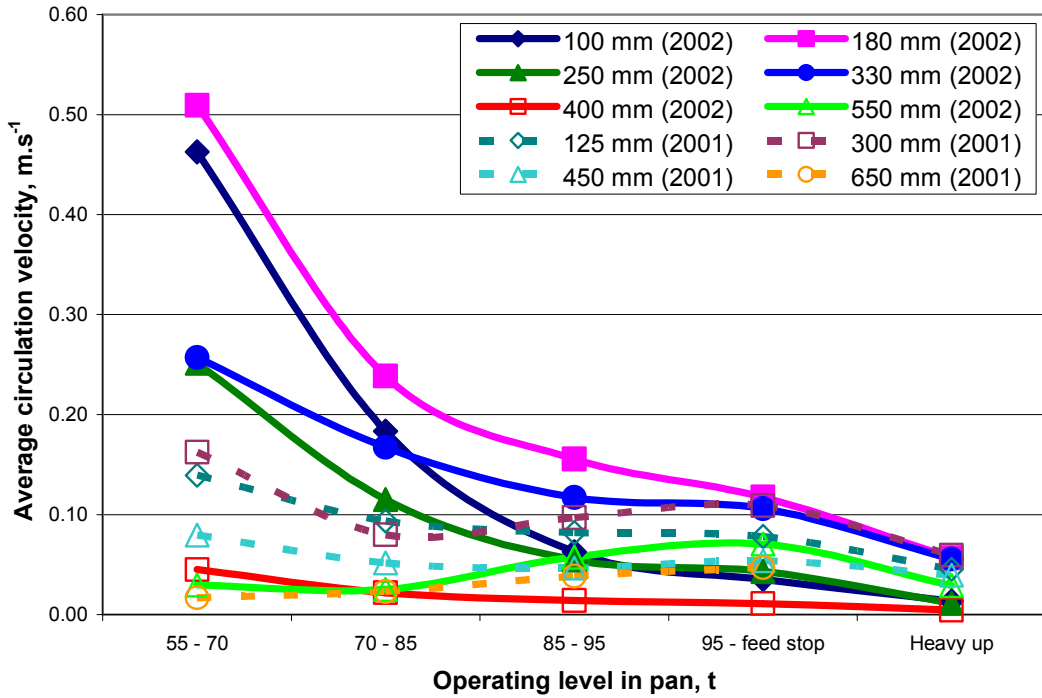


Figure 3-7 Average velocity trends at socket location ‘B’ for various insertion depths on No. 6 pan at Macknade Mill during the A massecuite strike.

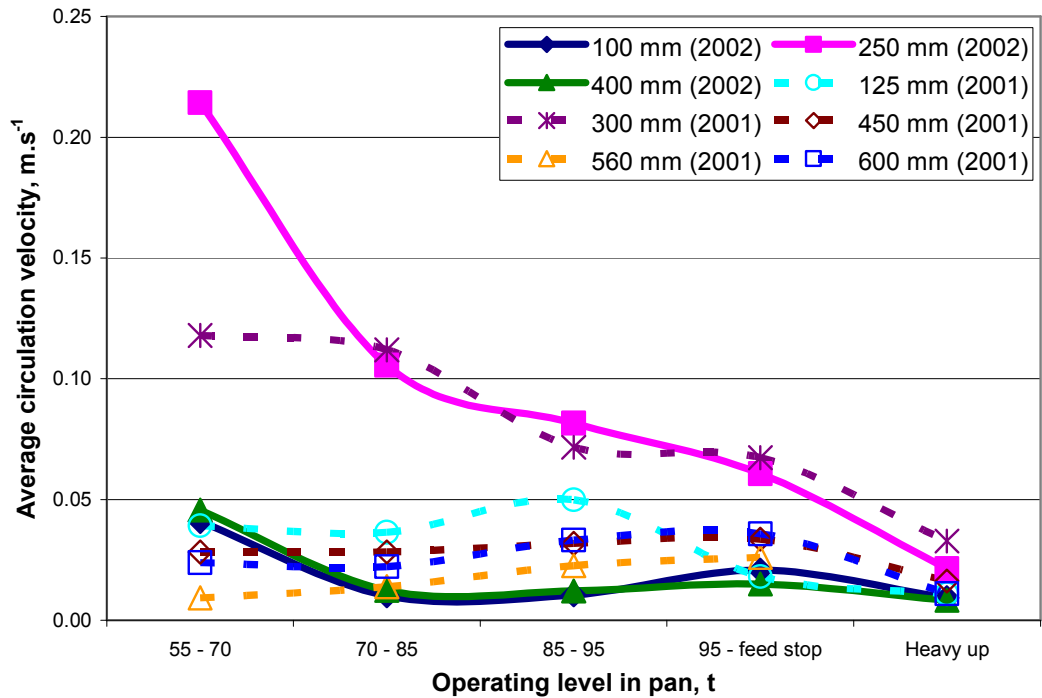


Figure 3-8 Average velocity trends at socket location ‘C’ for various insertion depths on No. 6 pan at Macknade Mill during the A massecuite strike.

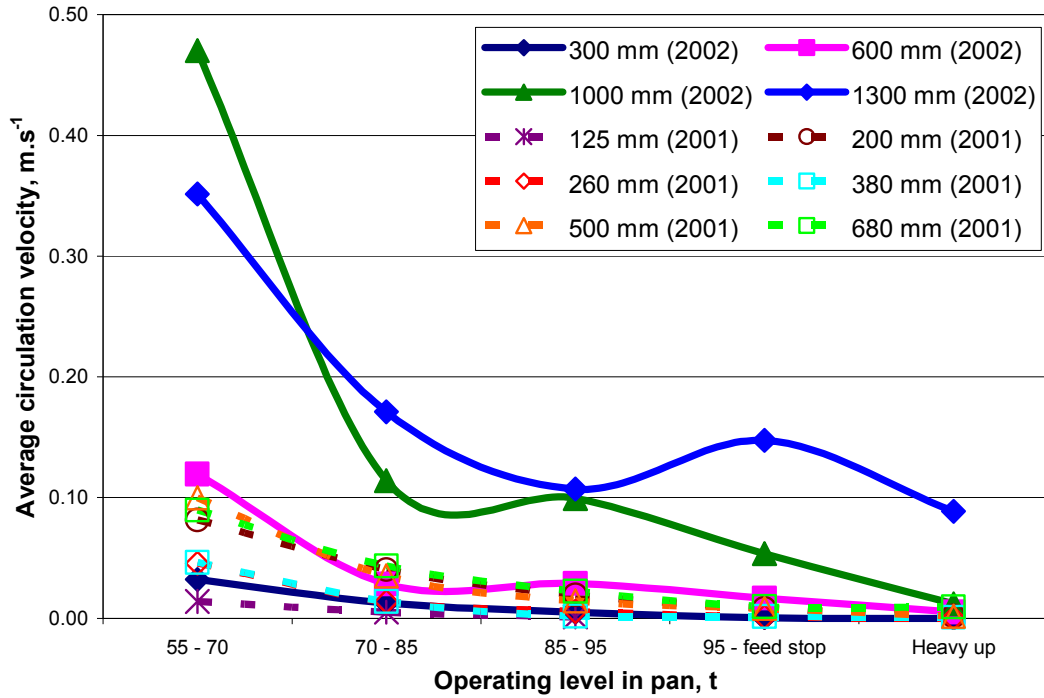


Figure 3-9 Average velocity trends at socket location ‘D’ for various insertion depths on No. 6 pan at Macknade Mill during the A massecuite strike.

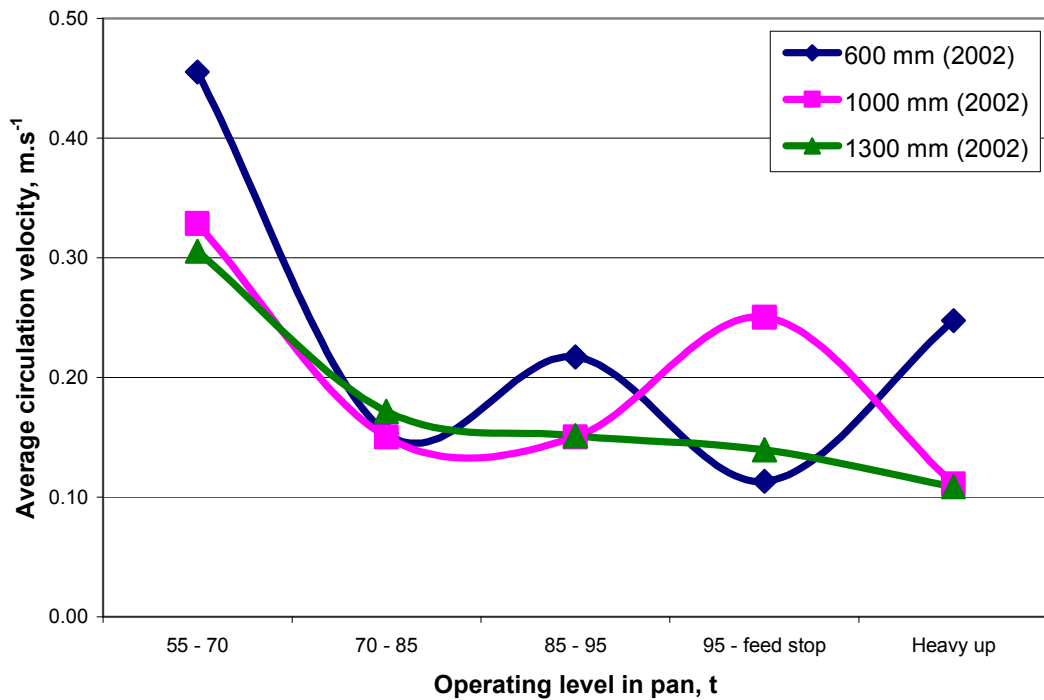


Figure 3-10 Average velocity trends at socket location ‘E’ for various insertion depths on No. 6 pan at Macknade Mill during the A massecuite strike.

Figures 3-6 and 3-7 indicate greater velocities were measured at locations 'B' compared to location 'A'. The volumetric flow in the downtake (measurable at location 'A') should be equal to the volumetric flow at location 'B', which aligns with the first row of tubes of the calandria. The cross-sectional area is 15% less at location 'B' compared to the downtake (location 'A') and it would be expected that the average velocity would thus be greater across this position than across the downtake.

Other significant results include:

- Very low velocities were recorded at location 'C' at an insertion depth of 100 mm from the pan base. This indicates the presence of a slow moving region in this area close to the pan floor, even at low boiling levels;
- The highest velocities at location 'B' were measured at a position 100 mm to 200 mm from the pan floor. It appears that there is a strong flow pattern occurring at this location, which is the lowest position in the pan;
- Locations 'D' and 'E' also showed strong velocities;
- Towards the end of the strike the velocities measured at all locations were low, as expected; and
- Similar trends were observed for both the 2001 and 2002 seasons.

The results measured for the 2002 season were compared to those obtained from the 2001 season trials for the same socket locations and similar insertion depths. These comparisons at location 'B' have been plotted in figures 3-11 and 3-12 for both the seed preparation step and A massecuite strike respectively.

In figure 3-11, the circulation velocities measured at an insertion depth of 330 mm for the 2001 factory trials and 300 mm for the 2002 factory trials at location 'B' are plotted for the seed preparation step. Figure 3-12 displays the data of the A massecuite strike for the same probe positions.

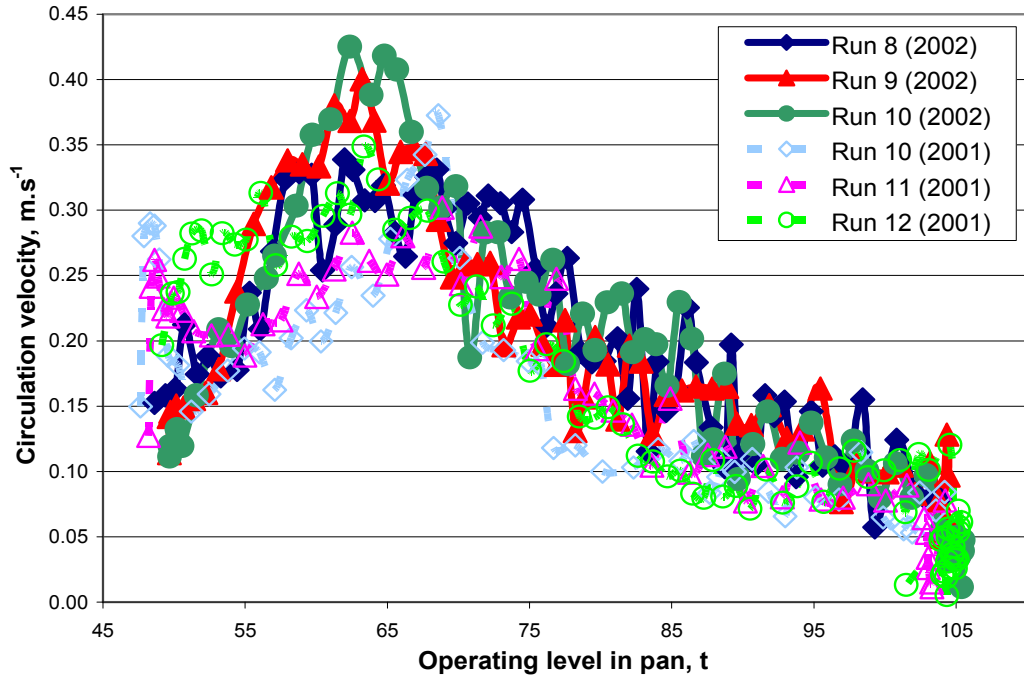


Figure 3-11 Comparison of the circulation results between the 2001 and 2002 factory trials measured at location ‘B’ at an insertion depth of 300-330 mm for the seed preparation step on Macknade No. 6 pan.

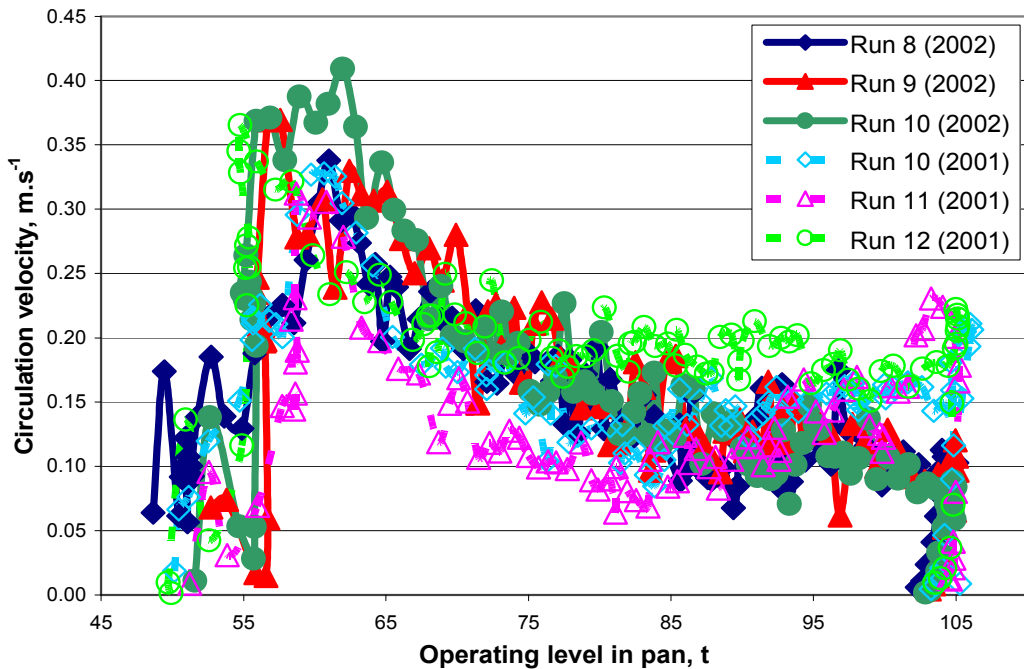


Figure 3-12 Comparison of the circulation results between the 2001 and 2002 factory trials measured at location ‘B’ at an insertion depth of 300-330 mm for the A masseuite strike on Macknade No. 6 pan.

The results shown in figures 3-11 and 3-12 show reasonable agreement in the magnitude and trends of the measured velocities at similar probe locations and insertion depths over the two seasons. The similarities over the two seasons add confidence to the anemometer technique, especially as the anemometer probes were recalibrated at the start of the 2002 season. Comparisons at other probe locations were limited, as similar insertion depths were not used during both seasons' trials.

3.7.1 Measurement issues

Lower magnitude velocities were measured at locations 'B' and 'C' when the probe was inserted close to the bottom of the calandria. These lower velocities can be explained by considering how the anemometer probes function. When the probe is located close to the calandria the flow path is closer to parallel rather than perpendicular past the probe tip as the massecuite is directed up the calandria tubes. This is illustrated in figure 3-13. The large angle away from perpendicular will reduce the reading of the probe.

Similarly for flow in the downtake region (location 'A') of the pan, the glancing flow direction relative to the probe tip may have reduced the measured circulation velocities by as much as 20% to 30%.

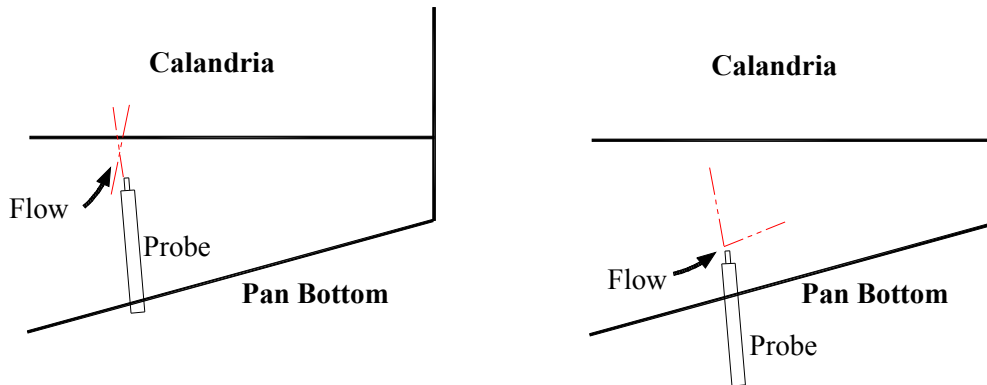


Figure 3-13 Effect of probe insertion depth versus probe orientation to the expected main direction for massecuite flow.

The data obtained from the anemometer probes used during the factory trials are considered to be reasonably consistent and reproducible, as shown by figures 3-14 and 3-15. Figure 3-14 shows the velocity trends of four separate seed preparation steps in which probe 1 is inserted to a depth of 100 mm at location 'C' and probe 2 is inserted to a depth of 600 mm at location 'A'. The applied steam rate during the seed preparation step is held at 20 t.h⁻¹ for run 13 and 22 t.h⁻¹

for runs 14, 15 and 16 during the 2002 season. The lower set point for steam flow used in run 13 can explain the slightly lower circulation velocity measured during that seed preparation step. Figure 3.15 displays the data for the A massecuite strike for the same probe positions and runs as displayed in figure 3-14. The steam rate is held constant at 16 t.h^{-1} for all the A massecuite strikes. The similar trends seen in figures 3-14 and 3-15 across the four production runs indicate consistent and steadily controlled operation of the pan by the boilers as well as the repeatability of the anemometer technique.

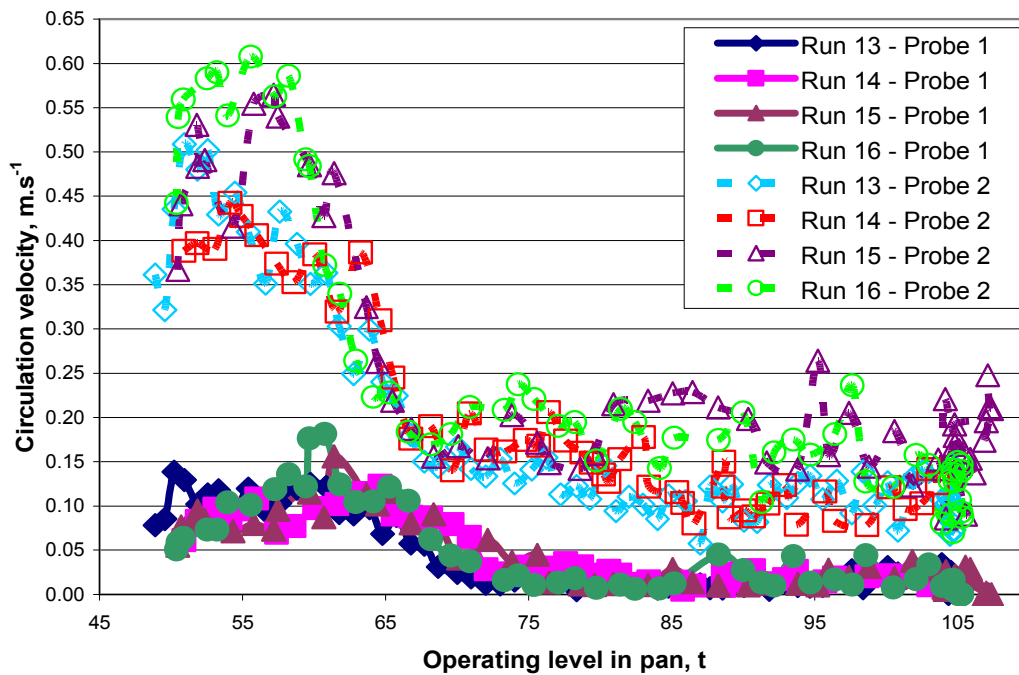


Figure 3-14 Velocity trends of different production runs for probe 1 inserted to a depth of 100 mm at location ‘C’ and probe 2 inserted to a depth of 600 mm at location ‘A’ for the seed preparation step on Macknade No. 6 pan during trials in the 2002 season.

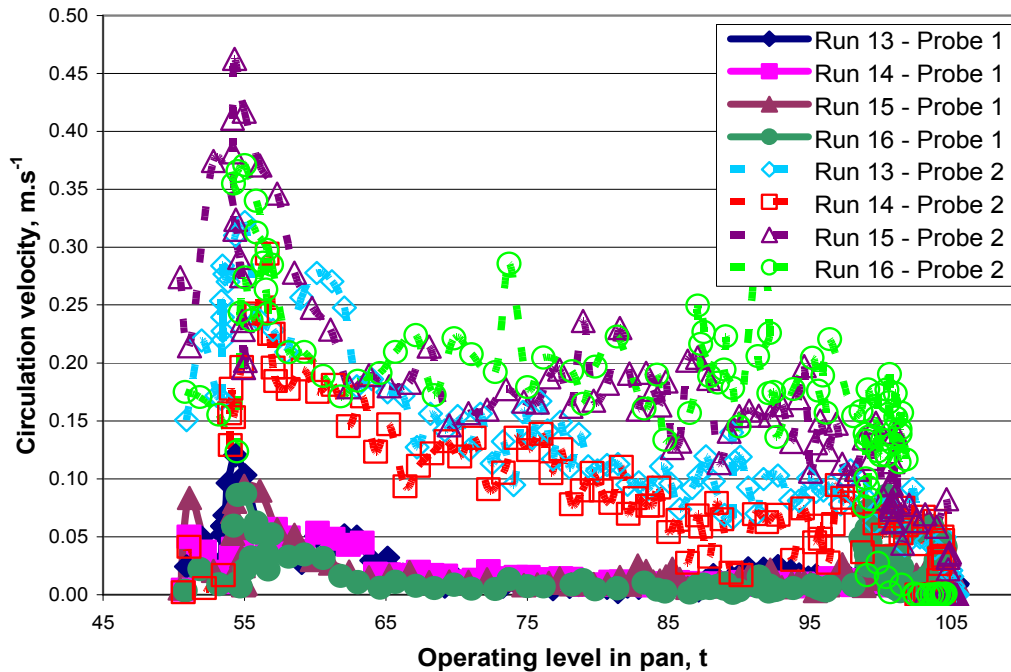


Figure 3-15 Velocity trends of different strikes for probe 1 inserted to a depth of 100 mm at location ‘C’ and probe 2 inserted to a depth of 600 mm at location ‘A’ for the A massecuite strike on Macknade No. 6 pan during trials in the 2002 season.

An additional socket was installed above the calandria to measure the velocity of the massecuite exiting the calandria tubes and to compare this with the massecuite velocity entering the calandria tubes. The tips of the anemometer probes inserted at this position are expected to be perpendicular to the flow path. Figures 3-16 and 3-17 compare the velocities measured by probe 3 inserted to a depth of 1000 mm both above and below the calandria for both the seed preparation step and A massecuite strike respectively during selected pan strikes over the 2002 season.

As seen in figures 3-16 and 3-17 very high velocities (0.4 m.s^{-1} to 0.75 m.s^{-1}) were measured both above and below the calandria, especially at the start of each production run when the massecuite was at a low level. The measured velocities below the calandria are slightly greater in magnitude than the measured velocities above the calandria. The results suggest that minimal vapour exists at the specific location of the probes (100 mm above the calandria) or the vapour produced in the calandria tube does not affect the velocity measurements at the start of the production run as much as first thought as the presence of vapour will change the thermal conductivity properties of the fluid.

Towards the end of both the seed preparation step and A massecuite strike it is expected that due to suppression caused by the high static head of the boiling massecuite, no vapour is present at the position 100 mm above the calandria. Vapour bubbles will only be produced once the boiling point elevation is overcome as the heated liquid rises to the surface of the massecuite. It is noted the velocities measured above and below the calandria at the high boiling level are comparable.

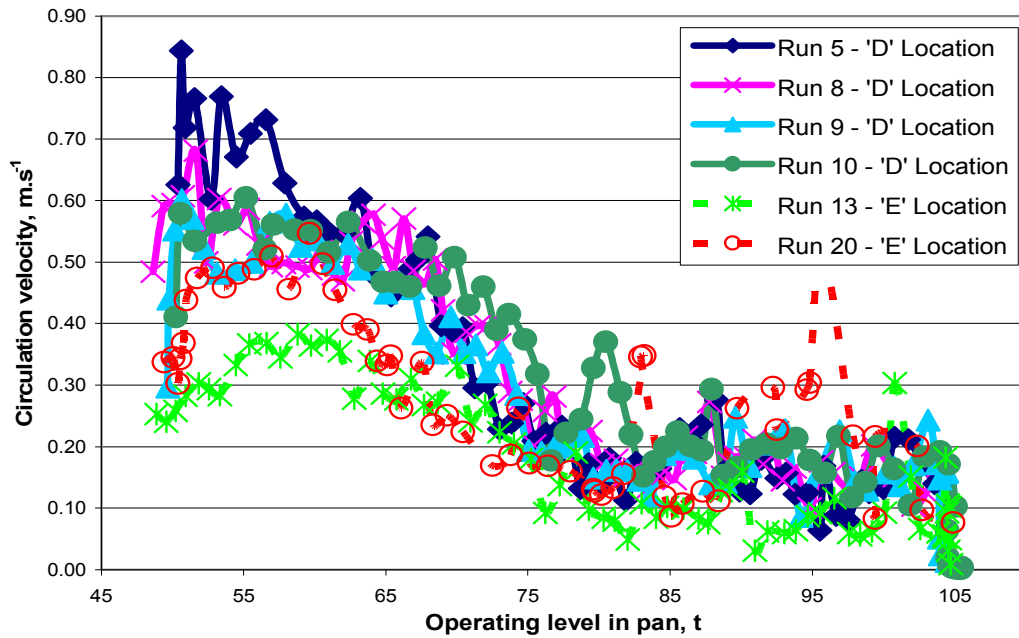


Figure 3-16 Velocity trends of different production runs for probe 3 inserted to a depth of 1000 mm at locations ‘D’ and ‘E’ for the seed preparation step on Macknade No. 6 pan during trials in the 2002 season.

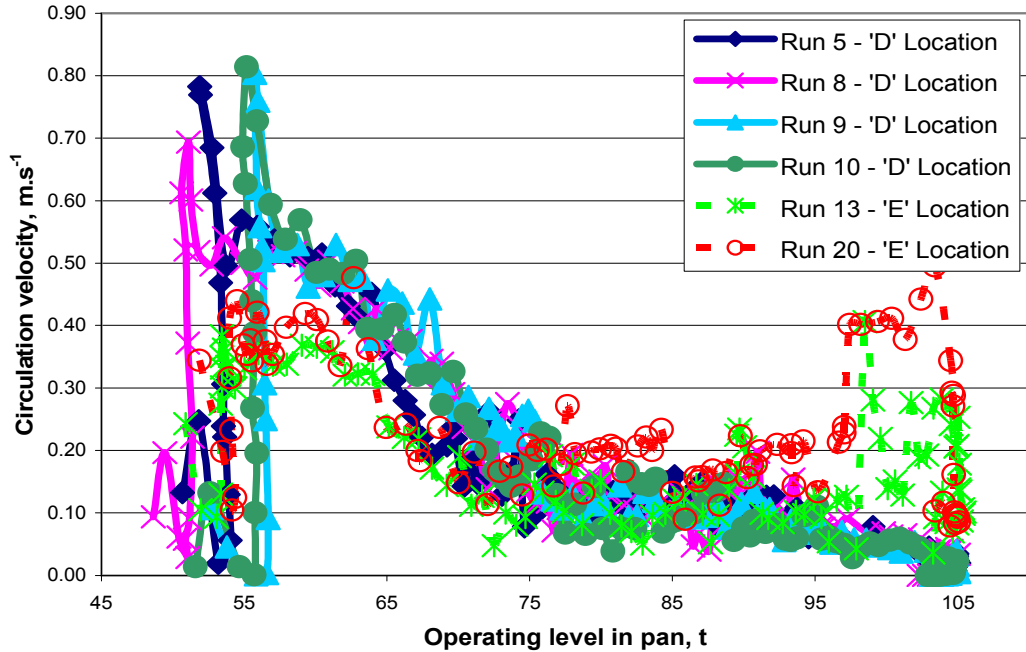


Figure 3-17 Velocity trends of different strikes for probe 3 inserted to a depth of 1000 mm at locations ‘D’ and ‘E’ for the A massecuite strike on Macknade No. 6 pan during trials in the 2002 season.

However, during each production run, large pulses of circulation were measured at the probe location above the calandria towards the end of the run as illustrated in figures 3-16 and 3-17. The effect is more pronounced during the A massecuite strike during the boil back period and could not be adequately explained.

3.8 Heat transfer

The overall HTC for a pan gives an indication of the effectiveness of heat transfer and can also be used to measure the performance of the pan.

The overall HTC can be calculated using equation 2.1 as follows,

$$U = \frac{Q}{A_{HT} \Delta T_{eff}}$$

Heat transfer data that were gathered on No. 6 pan at Macknade included the steam pressure in the calandria, steam flow rate, condensate flow rate, massecuite temperature and massecuite level in the pan for numerous strikes. The latent heat and temperature of the steam were

calculated using the measured calandria pressure based on the assumption that the supply steam is saturated within the calandria. Measurements of the condensate flow rates using a magnetic flowmeter were taken to check the accuracy of steam rate measurements. Both flow rate measurements were similar. The heat flux (Q) is then determined by,

$$Q = \lambda_{fg} M_{steam} \quad (3.9)$$

where λ_{fg} is the latent heat of condensation of the steam (J.kg^{-1}) and M_{steam} is the mass flow rate of the steam (kg.s^{-1}).

To accurately calculate the correct heating surface area (A_{HT}) for each vessel according to the BSES (1984) method, the heating surface area should be calculated as follows;

- Based on the outside surface area of the tubes, over the distance between the outer surfaces of the tube plates,
- Inclusive of the top and bottom tube plate area, less the area occupied by the tubes, downtakes and any condensate drains, and
- Inclusive of the outside surface area of any downtakes.

3.9 Heat transfer results

Data from five runs chosen out of the 21 total production runs logged at Macknade Mill on No. 6 pan during the 2001 season were used to calculate average HTCs.

Figure 3-18 shows the calculated HTC values plotted against the operating level in No. 6 pan. The plots show similar trends between the different runs. The HTCs were higher for similar operating levels during the initial seed preparation step of the pan cycle compared to the A massecuite strike. This was primarily due to the steam rate, set at 24 t.h^{-1} during the initial seed preparation step and at 16 t.h^{-1} for the A massecuite strike. The change in the steam rate alters the circulation velocity in the pan and thus indirectly influences the HTC. The higher HTC calculated during the seed preparation step also reflects the lower crystal content and lower viscosity of the massecuite during these periods. These parameters affect the ability of the massecuite in the calandria to transfer heat from the tube surface. The reduction in HTC with level is also more pronounced during the seed preparation step.

Figure 3-19 shows a comparison of the HTC and operating level when plotted against time for each pan cycle, both for the seed preparation step and A massecuite strike. Observations suggest that the change in the HTC over time is negatively proportional to the change in operating level over time during the run up phase. The HTC drops off more rapidly when the massecuite undergoes heavy up, which occurs during the A massecuite strike. This is due to the decrease in steam flow caused by the more viscous material, which slows the circulation, and indirectly affects the heat transfer. The reduction in heat transfer occurs even though the steam control valve is fully open and the steam pressure (and hence temperature) is increased to the maximum to provide the greatest effective temperature difference (heat transfer driving force) between the massecuite and steam.

The HTCs at the end of the seed preparation step and at the beginning of the A massecuite strike are virtually identical, despite major changes in massecuite level, steam temperature, steam flow, vacuum and massecuite temperature. The similarities are assumed to be coincidental, with the change in steam flow and temperature causing a change in the circulation velocity of the pan at the start of the A massecuite strike.

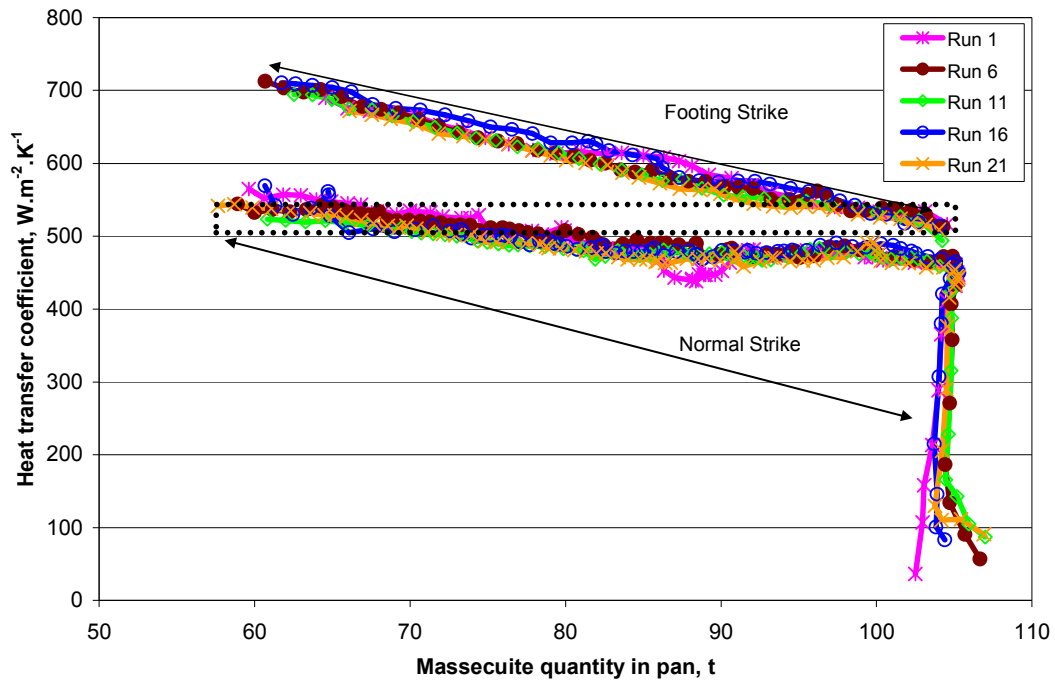


Figure 3-18 HTC values plotted against operating level for Macknade No. 6 pan during trials in the 2001 season.

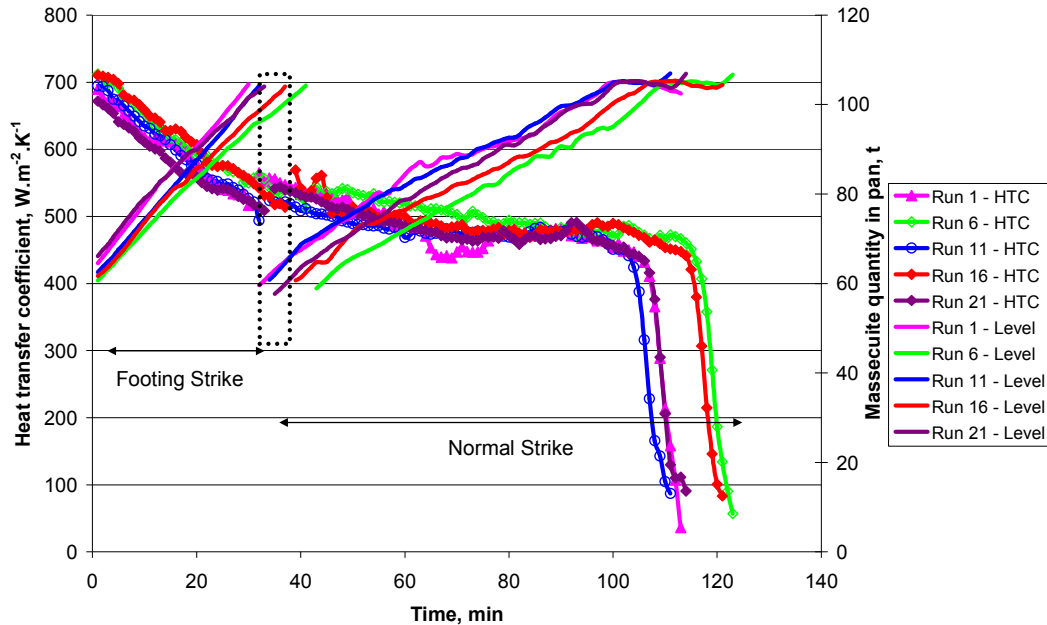


Figure 3-19 HTC values and operating level plotted against time for Macknade No. 6 pan during trials in the 2001 season.

The average HTC values for No. 6 pan are summarised as follows;

- Over the entire seed preparation step	600 W.m ⁻² .K ⁻¹
- Over the entire A massecuite strike	465 W.m ⁻² .K ⁻¹
- At the start of the A massecuite strikes	550 W.m ⁻² .K ⁻¹
- At the start of heavy up on the A massecuite strikes	415 W.m ⁻² .K ⁻¹
- During heavy up on the A massecuite strikes	280 W.m ⁻² .K ⁻¹
- End of heavy up on the A massecuite strikes	<100 W.m ⁻² .K ⁻¹

The initial HTC value at the start of the A massecuite strike is the calculated average of the HTC values obtained after the pan is ramped to the operating vacuum and steam rate. The ‘During heavy up’ value is taken as the average HTC calculated from when the level reaches its maximum to the final level in the pan before the steam and vacuum are reduced to drop the pan’s contents. The ‘start of heavy up’ value is the HTC value obtained at the start of the heavy up phase in the pan cycle.

For vacuum pans producing A massecuite, the average calculated HTCs over the pan strikes for No. 6 pan are comparable to those quoted by Broadfoot (1992) for continuous pans of 380 W.m⁻².K⁻¹ to 475 W.m⁻².K⁻¹. Continuous pans nominally operate on heating surface to volume ratios

of approximately 10 m^{-1} , which is much greater than the heating surface to volume ratio 7.42 m^{-1} of the No. 6 pan at Macknade. The average results obtained at Macknade of $465 \text{ W.m}^{-2}.\text{K}^{-1}$ falls at the high end of the range reported by Broadfoot (1992). This indicates that quite good heat transfer performance occurs in the Macknade No. 6 pan.

3.10 Summary

A method for measuring circulation speeds in massecuite solutions and vacuum pans has been refined as part of this research. The method, which uses anemometer probes, has been effective in measuring velocity profiles at selected positions within vacuum pans. The method is considered to give reproducible results based on repeat tests undertaken both within and over successive seasons. The circulation results can be summarised as follows:

- The measured circulation velocities fall to low levels at all positions once the boiling level in the pan increases above 85 t for the test pan. This corresponds to a height of approximately 1.25 m above the top tube plate of the calandria. This pattern has been consistently observed in circulation measurements in several vacuum pans (Rackemann, 2004);
- The highest circulation velocity was measured in the region under the calandria next to the downtake in the lowest region of the pan (location 'B'). Velocities measured in this region ranged from 0.05 m.s^{-1} to 0.5 m.s^{-1} during the pan cycle;
- The velocities measured 100 mm from the pan bottom at a position about half way under the calandria (location 'C') were very slow ($<0.05 \text{ m.s}^{-1}$) for the entire pan cycle;
- Measurements made at positions 100 mm above and below the calandria showed strong and comparable circulation patterns at similar insertion depths from the side wall of the pan. At this position the flow path is perpendicular to the probe tip;
- The velocities measured in the lower section of the downtake were affected by the orientation of the probe tip to the direction of flow which deviated from perpendicular. Velocities measured in this region ranged from 0.05 m.s^{-1} to 0.25 m.s^{-1} during the pan cycle;
- Some flow spiking was observed at the location immediately above the calandria towards the end of some strikes, which could not be adequately explained; and
- The recorded average velocity ranges encountered during the factory trials (0.01 m.s^{-1} to 0.5 m.s^{-1}) for the pan cycle are indicative of strong circulation patterns within the pan. This range of values is consistent with measured values of circulation velocities in vacuum pans reported by other investigators (Stephens, 2001).

The high HTC's indicate that adequate heat transfer is occurring within the calandria, which is further evidence that satisfactory circulation is present in the pan. Overall, the high heat transfer and adequate circulation patterns observed and measured during the factory trials indicate that No. 6 pan is a well-designed pan for the high-grade seed preparation step and A massecuite duty.

The circulation and heat transfer measurements collected from the factory trials enable the operating conditions for the single calandria tube boiling rig experimental trials to be determined. The operating conditions that can be related to various times throughout an A massecuite strike includes:

- Tube circulation velocity ranging from 0.01 m.s^{-1} to 0.5 m.s^{-1} ;
- Static pressure at the top of the calandria tube, which accounts for the head space pressure and the massecuite operating level, ranging from 15 kPa to 35 kPa;
- Tube wall temperature ranging from $96 \text{ }^{\circ}\text{C}$ to $120 \text{ }^{\circ}\text{C}$;
- Heat transfer rate ranging from $280 \text{ W.m}^{-2}.\text{K}^{-1}$ to $600 \text{ W.m}^{-2}.\text{K}^{-1}$; and
- Solution properties that include viscosity ranging from 0.5 Pa.s to 20 Pa.s (at $65 \text{ }^{\circ}\text{C}$) and crystal content ranging from 25% to 45% on massecuite. These properties exclude pan drop conditions.

4 NUMERICAL MODELLING

This chapter outlines some of the concepts involved in modelling the operation of calandria tubes and vacuum pans. A summary of the attempts to model vacuum pans by previous investigators is included. The chapter also presents a number of empirical correlations for heat transfer and vapour distribution within the calandria tubes.

4.1 Introduction

A comprehensive multi-dimensional vacuum pan model capable of predicting circulation, heat transfer, crystal growth and the distribution of other parameters over the course of a pan strike is not considered feasible (Stephens, 2001). This is mainly due to the complex geometries to model the pan arrangement and the complex physics involved in modelling the heat transfer and circulation mechanisms that would require large computational time and space. Numerical modelling approaches such as CFD can handle the complex geometries but the complicated physics has relatively only recently been introduced into many commercial codes.

This research aims to provide factory and practical data that can be used to validate and evaluate developed numerical models of calandria tubes and vacuum pan operation. The modelling of vacuum pans has been divided into two main parts, namely the calandria tube segment and the main pan body segment. The calandria tube segment dictates the driving mechanisms for circulation and heat transfer while the main pan body segment deals with the complex geometries of the pan structure. This approach complements the previous work of Stephens (2001).

An important aspect in the modelling of vacuum pans is the flow and heat transfer phenomena occurring in the calandria tubes. The heat transfer which dictates the formation of vapour is the driving force for circulation in the vacuum pan and originates inside the calandria tubes.

The complex flows and heat transfer phenomena occurring in calandria tubes represent a three-dimensional transient problem involving two phases. These types of problems are extremely difficult to solve quickly and accurately with current available technology. Although giving rise to various inaccuracies, often the problem is simplified to a one-dimensional model. The two phases can then be solved using either a homogeneous or a separated flow model (Butterworth and Hewitt, 1977). Generally, the theoretical one-dimensional models are not capable of predicting two-phase flow behaviour unless they are supplemented by methods based on

experimental measurements rather than on the complex fluid dynamics relations such as the Navier-Stokes equations.

For the purpose of this project, the errors of simplified models based on fluid specific correlations are considered satisfactory, as the purpose of this type of model is to estimate rather than implicitly model the boiling heat transfer phenomena. The developed models will only be required to simulate and predict the conditions and general characteristics of flow.

4.2 Modelling of circulation in vacuum pans

The distinction should be made between circulation and convection. Convection is the cause and circulation is the effect. In vacuum pans, circulation refers to the flow that is caused by energy transfer processes such as convection, which includes boiling. Both natural and forced circulation conditions exist in factory vacuum pans. Forced circulation conditions occur where mechanical stirrers are installed (typically at the bottom of the downtake) albeit to aid circulation by pushing material outwards from the downtake and up the calandria tubes. In stirred pans there is a combination of both forced and natural convection processes. Natural circulation is caused by natural convection processes where energy is transferred by sensible heating by both conduction and bulk fluid motion (*i.e.*, buoyancy driven flows). Additional circulation is caused by latent heating and occurs in vacuum pans from the heat transfer caused by boiling. The ebullition resulting from the boiling process also adds to the natural circulation.

While there have been a number of efforts to model in vacuum pans (Smythe, 1971; Wright, 1971; Wright and White, 1974; Broadfoot, 1980; Garside, 1985; and Dittl *et al.*, 1990), there have been few attempts at modelling the circulation in vacuum pans (Stephens, 2001). Early models of circulation involved simplified expressions of Poiseuille's law to determine velocities in the calandria tubes (Jenkins, 1958; Hugot, 1972). These expressions were based on conditions of laminar flow and assumed the driving force was balanced against the resistances to flow. The driving forces were calculated by the evaporation rate or the temperature difference between the steam and massecuite and the pressure losses caused by the flow of massecuite in the tubes and massecuite flow circuit. These simplified expressions take no account of energy losses associated with the flashing process at the boiling surface that has been observed in vacuum pans as discussed in section 2.1.

Table 4-1 summarises some of the attempts to model the operation of vacuum pans by previous investigators.

Table 4-1 Summary of numerical modelling attempts of vacuum pan operation.

Investigator	Software	Modelling approach	Assumptions	Comments
Bunton (1981)	Developed own CFD code	Lumped equations representing calandria and downtake. 2D finite difference scheme representing the rest of the pan (simplified to neglect complex shape of pan bottom)	Crystallisation not modelled. Crystal content fraction used in fluid properties. Newtonian liquid but viscosity a function of temperature and crystal content. Constant and evenly distributed heat transfer in calandria. Homogeneous flow. No slip conditions between phases. No boiling or heat losses.	Distribution of velocity, growth and supersaturation levels. Adequate circulation patterns developed if heat transfer area is sufficient. Calculated velocity ranges from model - 0.03 m.s^{-1} to 0.3 m.s^{-1} . Values consistent with those reported by Webre (1933) and Behne (1938).
Rouillard (1985)	Iterative method written in Basic.	1D tube model to represent calandria and lumped equations to represent rest of pan.	Frictional losses were lumped together in pan to determine the circulation. (Circulation defined as average tube velocity.) Liquid non-Newtonian Even distribution of material to all tubes.	Boiling code in 1D tube model contains estimated parameters and fluid specific correlations determined from experiments.
Brown <i>et al.</i> (1991)	Fluent software package	Calandria modelled as a series of concentric channels rather than as a tube bundle. 2D finite volume scheme representing the rest of the pan	Adiabatic conditions No vapour production or boiling in tubes. Newtonian liquid.	Only looked at stirred pans. Model showed downward fluid flow through innermost tubes and regions of slow circulation above the calandria and on the pan bottom.
Stephens (2001)	CFX software for pan model and user fortran for calandria model.	Segmented approach. 1D tube model similar to Rouillard (1985). Tubes represented as concentric channels for boundary conditions. Pan model uses a 2D axisymmetric finite volume scheme.	Uniform distribution of steam in calandria. Sugar crystals or crystallisation not accounted for in model. Newtonian liquid. Isothermal conditions. Mono-dispersed bubble size (only option in CFX) Fluid properties based on pure sucrose solutions.	Used Rouillard's data to develop tube model. Free surface modelled as a rigid boundary with slip conditions. Model predicts recirculating region above calandria, which increases in magnitude with increasing boiling level.

Bunton (1981) concluded that factors such as crystal content, operating pressure (vacuum) in the headspace of the pan, evaporation rates, massecuite boiling heights and pan body flared

regions showed significant effects on the crystal size distribution and hence performance of vacuum pans due to their effect on circulation patterns. Interestingly, some simulations that exhibited higher circulation rates did not necessarily give adequate conditions throughout the vacuum pan. This observation highlights the importance of the pan geometry. Similarly, Stephens (2001) showed the importance of pan geometry in providing an even distribution of heat transfer and flow in the calandria of vacuum pans.

Numerical stability problems were experienced by previous investigators using CFD software when trying to model vigorous boiling and so in most cases the models had to be simplified (Bunton, 1981; Brown *et al.*, 1991). The large grid size and simplistic structure representation needed to reduce computational run times in the models developed by Bunton (1981), Brown *et al.* (1991) and Stephens (2001) lead to poor resolution of important flow features according to best practice guidelines (Casey and Wintergerste, 2000). The models, though, have been able to highlight such problems in vacuum pans such as dead spots and recirculating eddy flows that have been measured and proven experimentally using circulation instruments. Brown's model also showed the effects on circulation patterns caused by the stirrer and allows further confidence in the use of CFD modelling as a tool to simulate vacuum pan operation.

Regardless of the simplifications, the CFD models developed by Bunton (1981), Brown *et al.* (1991) and Stephens (2001) showed that CFD can be used as a valuable tool in simulating the circulation and heat transfer mechanisms to analyse pan designs. The CFD models have been shown to calibrate reasonably well to the factory operation. With the advancements in computer software, more complex geometries are able to be modelled without requiring excessive run times so that the geometry aspect of design analysis can be evaluated.

In general though, the CFD models developed by Bunton (1981), Brown *et al.* (1991) and Stephens (2001) were too simplified to adequately capture the boiling nature of the flow in vacuum pans. To make improvements to the modelling of vacuum pans the models need to capture the complex physics of the non-adiabatic conditions that exist in the pans as well as the production of vapour and boiling within the calandria tubes and in the upper regions of the pan.

The most important aspect of the modelling of vacuum pans is the flow and heat transfer phenomena occurring in the calandria tubes. Any improvements in the modelling of the calandria tubes will thus have the greatest impact on improving CFD models of vacuum pans. This research concentrates on the development of the one-dimensional tube models developed by both Rouillard (1985) and Stephens (2001) in order to create a better understanding of the

flow and heat transfer mechanisms occurring within the tubes. This will lead to further improvements to be made to CFD models of the rest of the vacuum pan.

4.3 Boiling in calandria tubes

The mechanisms of boiling and the different flow regimes that exist in calandria tubes heated by steam were examined by Rouillard (1985). As massecuite flows up the calandria tubes, vapour is formed through ebullition. Figure 4-1 indicates the expected changes in temperature and vapour volume fraction (void fraction) that occur due to boiling (Rouillard, 1985).

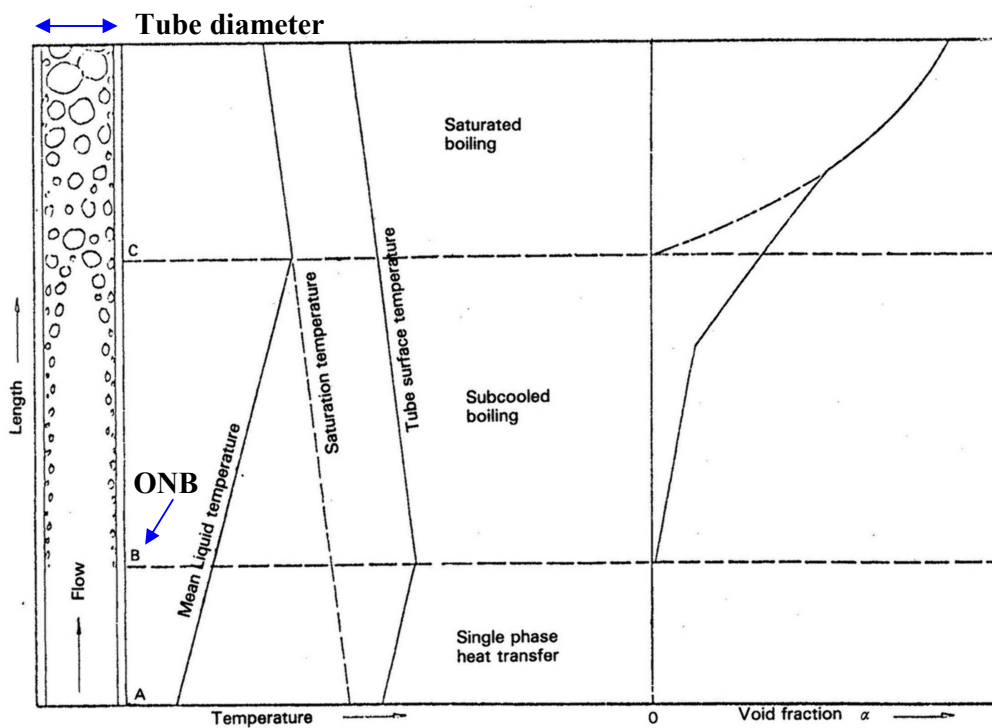


Figure 4-1 Diagram of temperatures and void fractions when boiling in a vertical tube, from Rouillard (1985).

As liquid enters the tube from below the calandria it is sub-cooled in that the mean liquid temperature is below the saturation temperature for boiling. While the massecuite is sub-cooled, heat is transferred through the walls of the calandria tube to the liquid entirely by single phase forced convection. Austmeyer (1986) proposes that the viscosity of the solution is the major factor determining the length of the sub-cooled region before boiling commences. At point B in figure 4-1, which is referred to as the onset of nucleate boiling (ONB), the temperature of the

liquid adjacent to the calandria tube reaches the boiling temperature and ebullition begins. At this stage between B and C the bulk of the liquid is still sub-cooled and the boiling heat transfer that results is called sub-cooled boiling.

Within the sub-cooled boiling region the vapour bubbles grow due to the heat from the steam heated tube and due to the decrease in static head as the bubbles rise up the tube. The bubbles also start to detach from the tube wall, once the forces resulting from buoyancy and flow overcome the forces of adhesion, so that heat is transferred radially through the tube. At point C the bulk liquid temperature reaches the saturation temperature where the average of the combined enthalpy of the liquid and vapour equal the saturation enthalpy of the liquid. Boiling will then extend across the sectional area of the tube. This point marks the start of bulk boiling. This type of boiling heat transfer is called saturated or fully developed nucleate boiling. The vapour volume fraction increases slightly in the sub-cooled region, but then a rapid increase is observed once saturated boiling commences (Rouillard, 1985).

Under large hydrostatic pressures, which are similar to conditions in vacuum pans towards the end of a strike, the transition to saturated boiling does not occur and the sub-cooled boiling region extends to the top of the calandria tubes (Rouillard, 1985).

The ONB can be determined using an approach by Hsu (1962) whereby bubbles are formed where the embryo of the bubble is completely surrounded by superheated liquid such as in the region close to the wall. An alternative approach determines the ONB as corresponding to the critical point of instability of the vapour-liquid interface (Dhir, 1998).

4.4 Modelling calandria tubes

In previous reviews of the literature by Rouillard (1985) and Stephens (2001) it was found that a lack of data exist on boiling heat transfer data for calculating HTCs of non-Newtonian fluids and two-phase viscous mixtures under vacuum, and especially for sugar solutions.

Rouillard (1985) developed a one-dimensional model of a calandria tube based on experimental data obtained from a single tube boiling rig. The boiling rig could be operated under forced or natural circulation conditions. Rouillard's one-dimensional model predicted the driving force for circulation produced by the tube as a function of heat transfer and massecuite flow rate. Rouillard developed HTC correlations for the separate sub-cooled and saturated boiling regions using empirical data based on sugar solutions obtained from South African factories.

The vapour effects on circulation and HTC's measured by Rouillard were determined for a situation where no additional hydrostatic head above the top of the calandria tube was present during the boiling process. Essentially in Rouillard's experimental work, no build up of level was allowed to occur in the header tank. This significantly changes the boiling characteristics within the tube (and expected vapour fraction exiting the tube, which was up to 80% in Rouillard's experimental work) and the empirical correlations used in Rouillard's model.

Stephens (2001) used the HTC correlations developed by Rouillard and calibrated the results of his model against the experimental data gathered by Rouillard. Stephens also used modified empirical correlations from water/air systems for the thermal boundary layer thickness, vapour rise velocity, vapour bubble characteristics and the radial distribution of vapour as empirical data for sugar solutions were not available. Stephens' one-dimensional model predicted reasonably well the evaporation rate, pressure drop and vapour fraction at the exit of the tube measured by Rouillard for a limited number of experiments. The model, however, is based quite heavily on the data reported by Rouillard.

Stephens' model assumes the majority of the driving force for circulation comes from the formation of bubbles within the calandria tubes. Stephens calculates that approximately 20% to 25% of the vapour is generated above the calandria tube as the hotter liquid rises to the surface and the boiling level suppression is relaxed. Another significant contribution to the circulation forces is the expansion of the bubbles as they rise to the surface if the vapour does not condense when coming in contact with cooler liquid. However, some of the energy caused by the expansion of vapour is removed as the vapour is flashed at the free surface through kinetic losses.

The agglomeration of smaller bubbles may also occur above the calandria that may reduce the contribution to circulation as larger bubbles have less surface area per volume than smaller vapour bubbles. However, there is limited literature on the multi-phase bubble effects in viscous non-Newtonian fluids such as massecuite solutions.

The vapour volume fraction and flashing that occurs at the boiling surface in factory pans gives rise to a sloping boiling level that is higher above the calandria than above the downtake. This change in level helps promote circulation by producing a flow pattern from the regions above the calandria towards the downtake.

Stephens (2001) details several important two-dimensional hydrodynamic concepts in the modelling of boiling in pans such as the hydrodynamic and thermal entrance lengths. Stephens calculated the hydrodynamic length to be less than one tube diameter under conditions representative of flow in factory vacuum pans. This implies that the flow in the heated tube becomes fully developed relatively quickly by the time the fluid travels past the entrance of the tube and hence the modelling assumes the flow is hydraulically fully developed.

The thermal entrance length however is much greater. The thermal boundary layer is important as the initiation of boiling occurs in the region close to the surface of the tube (see section 4.3). The heat flux and temperature and flow profiles were used by Stephens (2001) to give the solution of the thermal boundary layer thickness as a function of position along the tube such that,

$$200 \partial_t^3 R^2 - 135 \partial_t^4 R + 200 \partial_t^5 = \frac{3600 r^3 \alpha_{dif} z}{V_{liq}} \quad (4.1)$$

where ∂_t is the thermal boundary layer thickness (m),
 r is the internal radius of the heated tube (m),
 z is the length along the heated tube (m), and
 V_{liq} is the mean velocity of the fluid entering the tube (m.s⁻¹), and
 α_{dif} is the thermal diffusivity (m².s⁻¹).

The thermal diffusivity can be calculated by,

$$\alpha_{dif} = \frac{k_{liq}}{C_{p,liq} \rho_{liq}} \quad (4.2)$$

Increasing the static head (*i.e.*, raising the boiling level above the calandria tube) or increasing the operating pressure has the effect of increasing the saturation temperature within the tube and shifting the radial position where, according to Hsu (1962), the bubble embryo is surrounded by superheated fluid, to a location closer to the wall. The thermal boundary layer concept is illustrated in figure 4-2. If the same embryo bubble size is used then this moves the onset of boiling to further along the length of the tube as the thermal boundary layer increases along the length of the tube.

The superheat required to initiate boiling has also been shown to be dependent on the viscosity of the solution and sugar concentration (Grimsey and Brown, 1994). Hence at a lower operating

pressure, the superheat required to instigate boiling will increase as the viscosity is greater at lower temperatures.

The void volume per unit surface area is postulated by Rouillard (1983) to be proportional to the ratio of the boiling HTC to the single-phase HTC, which is expected to be a function of the pressure and hydrodynamic and thermal boundary layers.

To provide accurate calibrations of a one-dimensional model simulating the behaviour in calandria tubes, factory or pilot scale data using Australian sugar solutions is required.

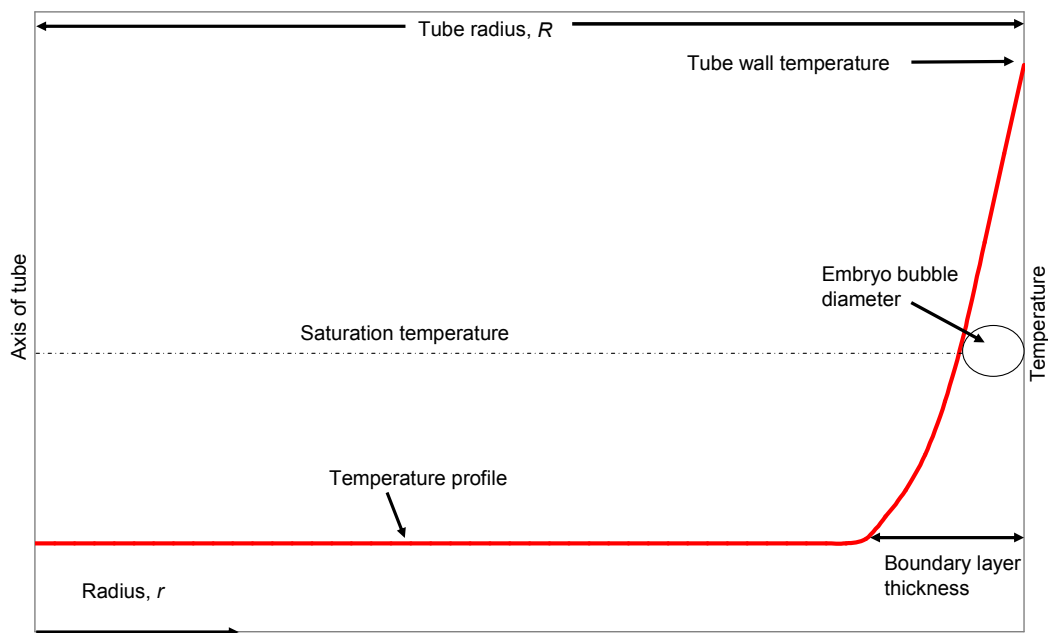


Figure 4-2 Illustration of the thermal boundary layer.

4.5 Empirical correlations

In many complex cases, empirical data correlations are used to predict the two-phase flow behaviour of boiling solutions. These data correlations often are reduced to dimensionless groups. Specific empirical correlations are presented for heat transfer and vapour volume fraction in the calandria tubes of vacuum pans. These correlations are only applicable to the test fluid studied.

4.5.1 Heat transfer

Rouillard (1985) presented two main approaches to determine correlation equations for HTC. The first involves an interpolation/superposition technique where a correlation to pool boiling is added to a single-phase forced convection component. This method has been proven adequate to use in turbulent regions but can be erroneous when predicting sub-cooled boiling flows. Most correlations have significant deviations, in the order of 40%, when applied to test data.

The second method involves the use of dimensionless groups. Correlations using this second method are only applicable to the test liquid studied, but due to its simple and direct nature, this method is more widely used. These HTC correlations can be expressed with or without a distinction between the partly, or fully, developed boiling regimes. Rouillard (1985) found the form of the correlation to be;

$$Nu_{TP} = \frac{h_{TP}D}{k_{liq}} = f \left\{ [Re_{TP}], [Pr], \left[\frac{\rho_{liq}}{\rho_{vap}} \right], \left[\frac{D}{L_T} \right] \right\} \quad (4.3)$$

where

Nu_{TP} is the boiling or two-phase Nusselt number,

h_{TP} is the boiling HTC ($W.m^{-2}.K^{-1}$),

D is the internal diameter of the heated tube (m),

k_{liq} is the thermal conductivity of the sugar solution ($W.m^{-1}.K^{-1}$),

Re_{TP} is the two-phase Reynolds number, and

Pr is the Prandtl number.

ρ_{liq} is the liquid density ($kg.m^{-3}$),

ρ_{vap} is the density of saturated water vapour ($kg.m^{-3}$), and

L_T is the length of the heated tube (m).

and

$$Re_{TP} = \left[\frac{D u_{TP} \rho_{liq}}{\mu_{liq}} \right] \quad (4.4)$$

$$Pr = \left[\frac{C_{p,liq} \mu_{liq}}{k_{liq}} \right] \quad (4.5)$$

where u_{TP} is the two-phase velocity of the liquid-vapour mixture ($\text{m}\cdot\text{s}^{-1}$),
 μ_{liq} is the dynamic viscosity of the liquid ($\text{Pa}\cdot\text{s}$), and
 $C_{p,liq}$ is the specific heat of the sugar solution ($\text{J}\cdot\text{kg}^{-1}\cdot\text{K}^{-1}$).

The Nusselt number is commonly used in heat transfer applications to describe the convective heat transfer occurring at the heating surface (Incropera and DeWitt, 1996). The Reynolds number is used to describe the ratio of the inertia to viscous forces where as the Prandtl number is used to describe the ratio of the momentum and thermal diffusivities.

The two-phase velocity of the liquid-vapour mixture is calculated by the following,

$$u_{TP} = \frac{4 (Q_{liq} + Q_{vap})}{\pi D^2} \quad (4.6)$$

where Q_{liq} is the volumetric flow rate of liquid in the tube ($\text{m}^3\cdot\text{s}^{-1}$), and
 Q_{vap} is the volumetric flow rate of vapour in the tube ($\text{m}^3\cdot\text{s}^{-1}$).

For Rouillard's (1985) experimental trials, the boiling heat transfer was expressed more specifically by,

$$Nu_{TP} = 4.48 Re_{TP}^{0.386} \left[\frac{\rho_{liq}}{\rho_{vap}} \right]^{0.202} \left[\frac{D}{L_T} \right]^{\frac{1}{3}} \quad (4.7)$$

From equation 4.7 increasing the tube diameter and reducing the tube length will increase the boiling HTC. The experiments conducted by Rouillard (1985) were conducted on a tube of only a single length, which would make it difficult to experimentally determine the effect of this variable. Accordingly the exponent of the last term of equation 4.7 was arbitrarily assigned a value of 1/3 as it was felt that the effect would be similar to that for single phase transfer in laminar flow due to the low vapour volume fractions expected when boiling viscous sugar solutions. Rouillard abandoned this last term in subsequent calculations.

For typical tube and fluid conditions in the operation of vacuum pans that include;

- Tube diameters of 101.3 mm to 127 mm,
- Tube lengths of 0.8 m to 1.2 m,
- Tube velocities of $0.1 \text{ m}\cdot\text{s}^{-1}$ to $0.5 \text{ m}\cdot\text{s}^{-1}$,

- Massecuite densities of 1450 kg.m⁻³ to 1480 kg.m⁻³,
- Vapour densities of 0.1 kg.m⁻³ to 0.15 kg.m⁻³,
- Massecuite viscosities of 1 Pa.s to 15 Pa.s,
- Constant thermal conductivity of the massecuite of 0.4 W.m⁻¹.K⁻¹, and
- Constant specific heat capacity of the massecuite of 1950 J.kg⁻¹.K⁻¹,

the predicted Nusselt number (Nu_{TP}) calculated from equation 4.7 ranges from 10 to 75 and the boiling HTC (h_{TP}) ranges between 50 W.m⁻².K⁻¹ to 240 W.m⁻².K⁻¹. These HTCs are substantially lower than the HTCs measured in factory applications for high-grade massecuites that ranged from 200 W.m⁻².K⁻¹ to 550 W.m⁻².K⁻¹ as detailed in section 3.9.

In calculating the HTC for typical vacuum pan applications, the abandonment of the last term has the effect of approximately doubling the HTC over the range of variables mentioned above. Stephens (2001) also observed that equation 4.7 seriously under-predicts the Nusselt number when applied to single phase flow. Both these observations create serious doubt on the applicability of equation 4.7 in predicting the HTC in calandria tubes of vacuum pans.

It was also shown by Tailby *et al.* (1976) that the surface tension influences the boiling heat transfer due to its effect on bubble formation and removal from the tube wall surface. The static pressure has also been shown to affect the boiling due to suppression at higher pressures. In other reports, Rouillard (1983) proposed an alternative expression for the boiling heat transfer with the following form,

$$Nu_{TP} = f \left\{ [Re_{TP}], [Pr], \left[\frac{\rho_{liq}}{\rho_{vap}} \right], \left[\frac{\sigma_{liq}}{p D} \right] \right\} \quad (4.8)$$

where σ_{liq} is the surface tension of the sugar solution (N.m⁻²), and
 p is the static pressure in the heated tube (kPa).

In the research conducted by Rouillard (1983), HTCs were determined specifically for the different boiling regions along the length of the heated tube. The HTC in the sub-cooled boiling region was expressed by,

$$Nu_{TP} = 0.0105 Re_{TP}^{0.456} [Pr]^{0.282} \left[\frac{\rho_{liq}}{\rho_{vap}} \right]^{0.498} \left[\frac{\sigma_{liq}}{p D} \right]^{-0.374} \quad (4.9)$$

And the HTC in the saturated boiling region by,

$$Nu_{TP} = 0.029 Re_{TP}^{0.247} [Pr]^{0.11} \left[\frac{\rho_{liq}}{\rho_{vap}} \right]^{0.664} \left[\frac{\sigma_{liq}}{p D} \right]^{-0.484} \quad (4.10)$$

Using the same tube and fluid conditions mentioned previously to assess the Nusselt number predicted by equation 4.7 as well as the following typical values;

- Operating pressure of 15 kPa to 30 kPa, and
- Massecuite surface tension of 0.4 N.m⁻²,

the predicted Nusselt number (Nu_{TP}) in equation 4.9 ranges from 60 to 420 and for equation 4.10 ranges from 160 to 780. The corresponding boiling HTC (h_{TP}) in equation 4.9 ranges between 250 W.m⁻².K⁻¹ to 1330 W.m⁻².K⁻¹ and for equation 4.10 ranges between 630 W.m⁻².K⁻¹ to 2460 W.m⁻².K⁻¹. These HTCs are significantly higher than the HTCs predicted by equation 4.7 and the HTCs measured for factory applications as detailed in section 3.9. The high HTCs can also be attributed to the various feed materials (syrup) used during some of the boiling trials. In these experiments the operating conditions are representative of evaporators rather than crystallisation pans. The HTCs in sugar factory evaporators typically range from 600 W.m⁻².K⁻¹ to 3000 W.m⁻².K⁻¹ (Watson, 1986). It should be noted that the range of evaporation rates per unit heat transfer area of the trials conducted by Rouillard (1983, 1985) cover the range of evaporation rates measured during the factory trials reported in section 3.9, viz. 11 kg.h⁻¹.m⁻² to 45 kg.h⁻¹.m⁻².

In the development of separate HTCs for different boiling regions, Rouillard assumed there was constant heat transfer along the length of the tube and accurate measurements could be made of this heat transfer. Both these assumptions contain errors that reduce the reliability of using Rouillard’s predicted correlations. The heat transfer along the tube varies depending on the boiling regime inside the tube. Heat transfer measurements were made with a “bucket and stopwatch” approach inherent with small errors that would also propagate errors in the HTC correlations.

Both heat transfer functional expressions, equations 4.3 and 4.8, used by Rouillard (1983, 1985) were evaluated in this research.

4.5.2 Vapour distribution within the calandria tube

In the development of a one-dimensional model, Rouillard (1985) also used correlations for two-phase pressure drop, vapour hold up and the radial distribution of vapour. The pressure change of two-phase flow within the calandria tube can be calculated using the momentum equation and consists of a gravitational term (static head), a frictional loss term and an acceleration term to account for the acceleration of flow caused by the vapour. The pressure change within a calandria tube can be expressed simply by,

$$\Sigma \frac{dP}{dz} = \frac{dP_{grav}}{dz} + \frac{dP_{acc}}{dz} + \frac{dP_{frict}}{dz} \quad (4.11)$$

where dz is the length along the calandria tube (m),
 dP_{grav} is the pressure loss due to elevation (N.m⁻²),
 dP_{acc} is the pressure loss due to acceleration (N.m⁻²), and
 dP_{frict} is the pressure loss due to friction (N.m⁻²).

The pressure loss due to elevation can be expressed as,

$$\frac{dP_{grav}}{dz} = [\alpha \rho_{vap} + (1 - \alpha) \rho_{liq}] g \quad (4.12)$$

where α is the vapour volume fraction, and
 g is the gravitational acceleration constant (m.s⁻²).

The pressure loss due to acceleration (Butterworth and Hewitt, 1977) can be expressed as,

$$\frac{dP_{acc}}{dz} = G^2 \left[\frac{x^2}{\alpha \rho_{vap}} + \frac{(1-x)^2}{\rho_{liq} (1-\alpha)} \right] \quad (4.13)$$

where G is the mass flow rate through the tube (kg.s⁻¹), and
 x is the mixture quality (mass fraction of vapour).

A number of theories are presented to determine the frictional loss. Rouillard (1985) concluded that the Griffith and Wallis (1961) method was most suited for calculating pressure drop in his experimental work. The Griffith and Wallis (1961) method was developed for oil-gas mixtures

in the bubbly flow regime and related to a modified (weighted) Fanning friction factor and can be expressed as,

$$\frac{dP_{frict}}{dz} = \frac{2 f_f u_{liq}^2 \rho_{liq}}{D (1 - \alpha)^2} \quad (4.14)$$

where f_f is the Fanning friction factor, and
 u_{liq} is the superficial liquid phase velocity (m.s⁻¹).

The Fanning friction factor is obtained from a conventional Reynolds number – Fanning friction factor plot using the superficial liquid phase velocity (u_{liq}) defined as,

$$u_{liq} = \frac{4 G}{\pi D^2 (1 - \alpha)} \quad (4.15)$$

Additionally the superficial vapour phase velocity (u_{vap}) is defined as,

$$u_{vap} = \frac{4 G}{\pi D^2 \alpha} \quad (4.16)$$

Other correlations for frictional loss are available such as those reported by Sieder and Tate (1936), Martinelli and Nelson (1948), Lockhart and Martinelli (1949) and Oliver and Young Hoon (1968). Collier and Thome (1996), however, conclude that there is no definitive result for the two-phase friction loss but commonly uses a weighted two-phase friction factor. Stephens (2001) uses a weighted volume fraction approach to express the pressure loss due to friction as,

$$\frac{dP_{frict}}{dz} = \frac{2 (1 - \alpha) f_{liq} G^2}{\rho_{liq} D} + \frac{2 \alpha f_{vap} G^2}{\rho_{vap} D} \quad (4.17)$$

where f_{liq} is the Fanning friction factor evaluated for the liquid velocity, and
 f_{vap} is the Fanning friction factor evaluated for the vapour velocity.

Correlations for vapour volume fraction are dependent on the characteristics of the bubble, such as its size and requirements for departure, dependency on heat flux, superheat, pressure, velocity or boundary layer thickness *etc.* Obviously obtaining data on these parameters for sugar solutions is crucial to determining an accurate correlation for vapour volume fraction. Empirical

data specific for sugar solutions were not available to correlate these bubble characteristics, so empirical correlations based on other systems such as water / air or water / steam were modified and substituted. The values substituted into the various correlations are at best only an estimate. This introduces a large degree of uncertainty and inaccuracy in the developed one-dimensional models of Rouillard (1985) and Stephens (2001).

Rouillard (1985) used dimensional analysis to determine a correlation for the local vapour volume fraction in the sub-cooled boiling region as,

$$\alpha = f \left\{ c \left[\frac{h_{TP} k_{liq}}{h_{SP}^2 D} \right], [\text{Pr}], \left[\frac{\rho_{liq}}{\rho_{vap}} \right] \right\} \quad (4.18)$$

where h_{SP} is the single phase HTC ($\text{W.m}^{-2}.\text{K}^{-1}$), and

h_{TP} is the sub-cooled boiling HTC calculated in equation 4.3.

For Rouillard's (1985) experimental trials, the correlation for the local vapour volume fraction was expressed more specifically by,

$$\alpha = 0.00649 \frac{h_{TP} k_{liq}}{h_{SP}^2 D} [\text{Pr}]^{0.351} \left[\frac{\rho_{liq}}{\rho_{vap}} \right]^{0.414} \quad (4.19)$$

Equation 4.19 relates to the vapour volume fraction exiting the heated tube. However, the correlation was determined for a single length and diameter tube. Caution should be used in applying this equation to different tube geometries. The single phase HTC was calculated according to Rouillard using the Dittus-Boelter (1930) equation, which is stated as follows,

$$h_{SP} = \frac{0.023 k_{liq} [\text{Re}]^{0.8} [\text{Pr}]^{0.4}}{D} \quad (4.20)$$

According to Incropera and DeWitt (1996), the Dittus-Boelter equation was derived for turbulent flow conditions. Turbulent flow conditions may have been present in the syrup boiling trials conducted by Rouillard (1985) but are not expected for typical conditions in vacuum pans. An alternative equation for calculating the average convection for laminar flow conditions was presented by Incropera and DeWitt (1996) as follows,

$$h_{SP} = \left(\frac{k_{liq}}{D} \right) \left[3.66 + \frac{0.0668 \left(\frac{D}{L_T} \right) \text{Re Pr}}{1 + 0.04 \left[\left(\frac{D}{L_T} \right) \text{Re Pr} \right]^{\frac{2}{3}}} \right] \quad (4.21)$$

The vapour volume fraction is not only dependent on the amount of vapour produced in the tube but also on the rate at which it is rising, which is dependent on the position of the vapour flow relative to the tube wall. The rising vapour velocity of bubbles in concurrent flow in vertical tubes has been shown to consist of two components, viz. a basic rising velocity (drift seen in still liquid) and a contribution due to the non-uniform distribution of the vapour in the liquid. Nicklin *et al.* (1962) derived an equation for the non-uniform distribution of vapour as,

$$\frac{Q_{vap}}{\alpha A} = \frac{C_0 (Q_{vap} + Q_{liq})}{A} + V_r \quad (4.22)$$

where C_0 is the flow distribution parameter, and

V_r is the mean bubble rising velocity (m.s⁻¹).

The value of C_0 decreases towards unity with increasing pressure, with a value of 1.0 common for isolated small vapour bubbles. The value of C_0 was calculated at the tube outlet by Rouillard (1985), for trials where saturated boiling took place, to be on average approximately 1.13 (average value of C_0 was 1.3 in Rouillard, 1983). The C_0 value is close to 1.0 and suggests the flow of vapour takes place close to the wall. A value close to 2.0 would indicate conditions similar to laminar flow where the maximum velocity at the centreline is twice the average velocity. The flow distribution parameter accounts for the effect that non-uniform radial vapour volume fraction profiles have on the velocities of both the liquid and vapour phases. The flow distribution parameter is used to take a two-dimensional effect and lump it into a one-dimensional model.

Rouillard (1983) states that values for C_0 could not be determined in the sub-cooled boiling region. Typically, the method used by many investigators (Rouillard, 1983) is to use a constant value of C_0 equal to the value of C_0 for the saturated boiling region.

The bubble rise velocity is dependent on the drag forces acting on the individual bubbles, which in turn are dependent on the vapour volume fraction. Zuber (1964) provides an expression for the bubble rise velocity based on vapour volume fraction as,

$$V_r = \frac{g d_{bub}^2 (\rho_{liq} - \rho_{vap})}{18 \mu_{liq}} (1 - \alpha)^{N_{bub}} \quad (4.23)$$

where d_{bub} is the diameter of the bubble (m), and
 N_{bub} is an experimentally determined constant.

Zuber and Findlay (1965) proposed the following equation for estimating the rising velocity that is independent of the bubble diameter and vapour volume fraction. This allows the bubble rise velocity to be calculated independently of experimentally determined parameters.

$$V_r = 1.53 \left[\frac{\sigma g (\rho_{liq} - \rho_{vap})}{\rho_{liq}^2} \right]^{\frac{1}{4}} \quad (4.24)$$

This is similar to the expression given by Kroeger and Zuber (1968) for the mean bubble rising velocity; however, the constant changes from 1.53 to 1.41. These equations show decreasing the vapour volume fraction or surface tension will predict a decrease in the bubble rise velocity. The distribution parameter expressed in equation 4.22 was evaluated in this research using vapour rise velocity calculated using equation 4.24.

4.6 Summary

The design of vacuum pans has changed little over the past 30 years and substantial increases in productivity are sought as mills expect to expand their throughput. The use of more sophisticated computational models opens a new avenue for characterising the circulation movements throughout the entire pan. CFD modelling has emerged as a powerful tool for the design and improvement of the performance of process equipment that involves heat transfer and fluid flows. Previous vacuum pan modelling attempts have required large computer capacity and run times.

The modelling of vacuum pans has been divided into two main parts, namely the calandria tube segment and the main pan body segment. The calandria tube segment dictates the driving

mechanisms for circulation and heat transfer while the main pan body segment deals with the complex geometries of the pan structure.

The results obtained using CFD modelling (Bunton, 1981; Brown *et al.*, 1991; and Stephens, 2001) have demonstrated the usefulness and potential of CFD as a tool to provide insight into the design process to improve the performance characteristics of process vessel designs. However these models were too simple to adequately capture the boiling nature of the flow in vacuum pans. To make improvements to the modelling of vacuum pans the models need to be able to capture the complex physics of boiling conditions that exist within the calandria tubes and in the upper regions of the pan.

Modelling of flow and heat transfer behaviour within the calandria tubes has often been simplified to a one-dimensional problem. The one-dimensional models are not capable of predicting the two-phase flow behaviour without empirical data correlations. This research aims to provide factory and practical data that can be used to develop empirical data correlations as well as validate and evaluate developed numerical models of calandria tubes and vacuum pan operation.

5 EXPERIMENTAL RIG

This chapter provides a description of the single calandria tube boiling rig and modifications made during the commissioning of the rig. An experimental plan is presented and the results of the commissioning of the rig are detailed.

5.1 Introduction

Experimental trials were conducted on a single calandria tube boiling rig located at James Cook University (JCU) to determine the circulation and heat transfer characteristics for boiling in calandria tubes with changing material properties and heat input conditions. In addition, the aim of these trials was to obtain fundamental data for boiling in tubes and to determine voidage or vapour volume fraction changes due to evaporation. These data enabled empirical correlations to be determined and were used to develop numerical models of boiling and heat transfer occurring in calandria tubes. These models can then be applied to factory pans and will provide a better understanding of the flow characteristics within pans to facilitate improved engineering designs.

Acknowledgements are given to the undergraduate students and JCU staff who assisted in the construction and partial commissioning of the experimental rig. Substantial contributions were made to the following;

- Installation of the majority of process sensors and instrumentation,
- Installation and connection of all electrical equipment and utility services,
- Wiring of the data transfer system between the instrumentation and control system, and
- Development of the computer controller system and user interface.

5.2 Single calandria tube boiling rig

The single boiling tube rig consists of a single calandria tube, recirculation leg and a large header tank as shown in figure 5-1. The calandria tube was made from a 100 NB mild steel tube which is similar to the size used in factory pans. The calandria tube is 1300 mm in length. Five separate ceramic, electrical heating bands (shown in figure 5-2) provide heat to the contents within the calandria tube. The heating bands are controlled by varying the power input.

Vapour exiting the header tank is cooled in a heat exchanger (not shown in figure 5-1) and returned to the bottom of the header tank as condensate to enable quasi-equilibrium conditions to be obtained. The header tank is comprised of a 350 NB mild steel tube, 2000 mm in length which provides ample room for the vapour to disengage from the boiling level. Extensive instrumentation has been installed on the rig to measure temperature and pressure profiles, heat flux, circulation flows and material density within the calandria tube. Control and monitoring equipment has also been installed to control the operating conditions and allow easy acquisition of data.

Experimental trials were conducted on the single boiling tube rig under three configurations. These configurations are described in no particular order (of importance or chronologically in reference to when the experimental trials were conducted) in sections 5.2.1, 5.2.2 and 5.2.3.

5.2.1 Configuration 1

Configuration 1 is shown in figure 5-1, where the single boiling tube rig is only capable of simulating natural circulation conditions. Due to the flow restrictions caused by the recirculation leg, the circulation obtained in the rig was minimal and not indicative of factory conditions. The majority of the restrictions in the recirculation leg are caused by pipe reductions required for the installation of the magnetic flow meter. The smaller diameter magnetic flow meter was used to enable more accurate measurements of circulation rates.

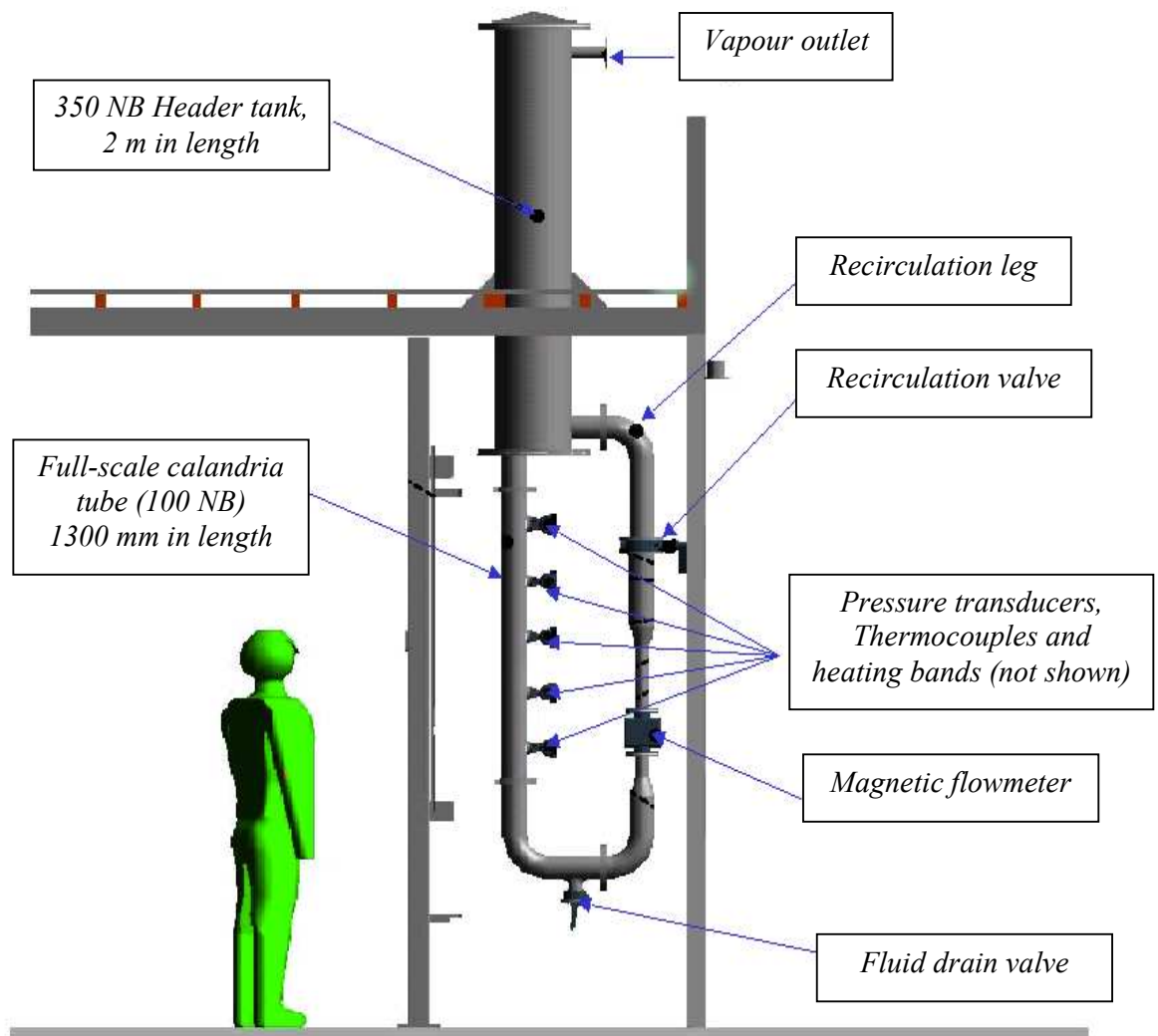


Figure 5-1 Schematic of the single calandria tube boiling rig at JCU.

5.2.2 Configuration 2

A second configuration of the boiling rig was constructed with the magnetic flow meter and associated restriction removed. Instead, allowance was made on the recirculation leg to insert a hot film anemometer to measure the circulation velocity. The technique and procedure for using hot film anemometers to measure circulation velocities in vacuum pans and mixtures of massecuite and molasses have been reported by Rackemann and Stephens (2002).

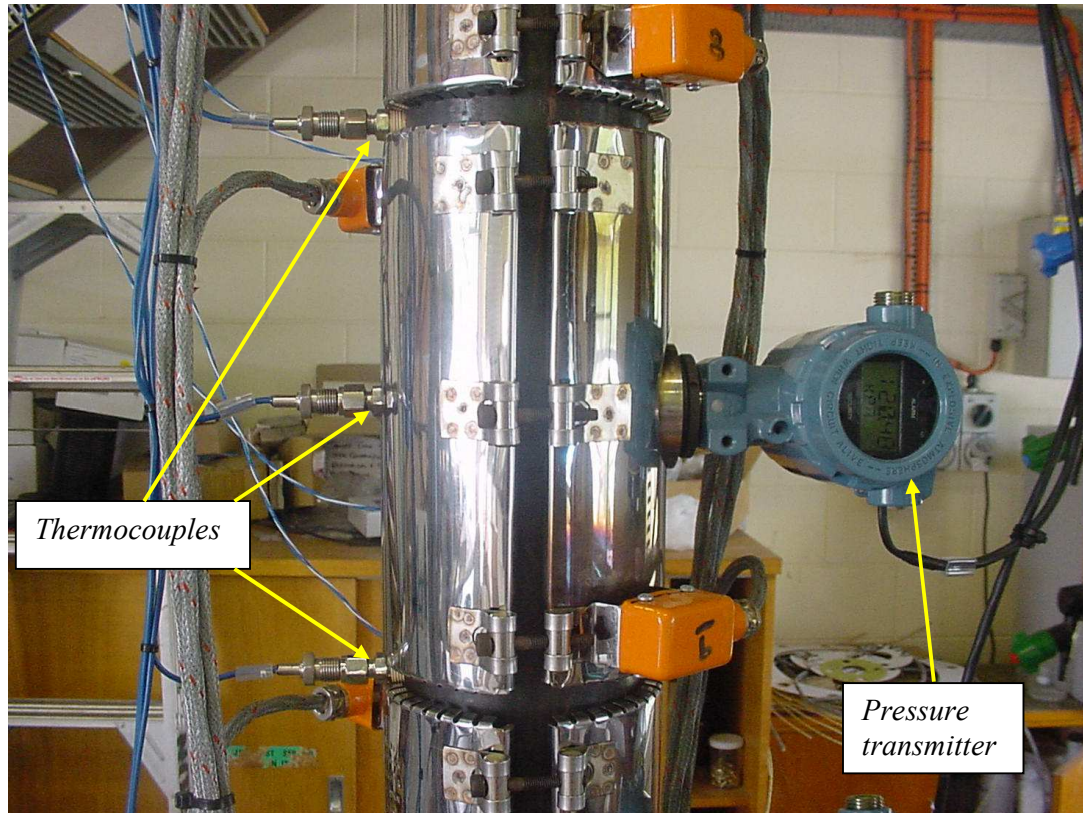


Figure 5-2 Photo of the electrical heating bands.

5.2.3 Configuration 3

To overcome the flow restrictions and frictional resistance in the recirculation leg a positive displacement, internal gear pump (Ebsray MD300) was installed at the bottom of the recirculation leg to achieve adequate and controllable circulation rates. The pump uses a gearbox to operate at speeds of 30 r.min^{-1} to 130 r.min^{-1} or provide flow rates of 80 L.min^{-1} to 300 L.min^{-1} . The installation of a pump enabled the rig to simulate a wider range of circulation conditions. The majority of the trials were conducted under forced circulation conditions using the third boiling rig configuration, which is illustrated in figures 5-3 and 5-4.

Low pump speeds were used to prevent excessive shear leading to viscous heating effects of the material as well as breakage of sugar crystals. Crystal size distributions of the material were not analysed before and after boiling trials to determine the level of crystal breakage. Only visual observations of the material before and after boiling trials confirmed crystal breakage occurred. Internal gear pumps claim to produce smooth even flow with minimal pulsation or surging, which is beneficial if the experimental rig is to simulate and maintain the same flow hydrodynamics of the circulation conditions that prevail in factory pans. For this reason the

internal gear pump was favoured over positive displacement pumps such as Mono pumps for this application. Forced circulation caused by the inclusion of a pump in a boiling circuit was shown by Austmeyer and Schliephake (1983) to have negligible effect on the fluid with respect to heat transfer in contrast to the effect of micro-pulsations produced by the vapour bubbles.

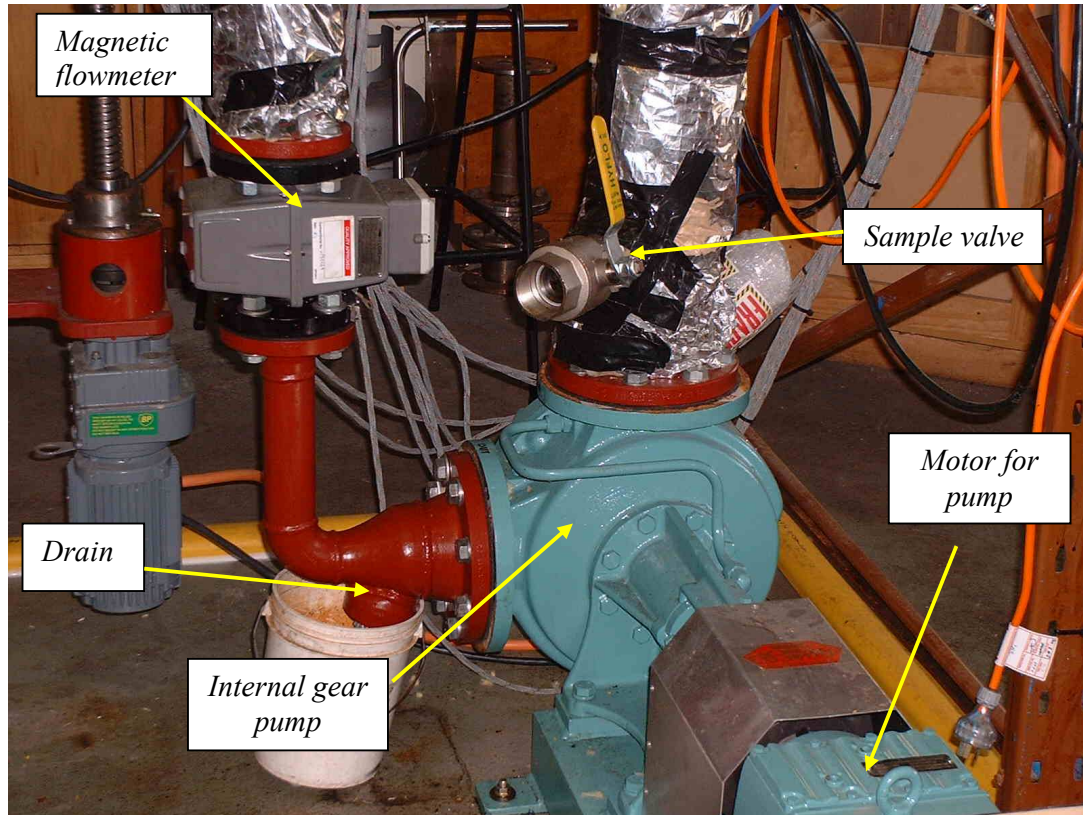


Figure 5-3 Photo of the internal gear pump.

The following modifications were completed to enable the rig to handle the viscous molasses material and increase the flexibility of the rig to boil a variety of mixtures;

- Installation of a liquid separator on the vapour line from the header tank to the heat exchanger to ensure entrained sugar did not foul the heat exchanger plates,
- Installation of hot water connections to the heat exchanger for cleaning,
- Installation of a needle valve for manual vacuum control and a vacuum break valve on the header tank,
- Electrical heat tracing and insulation of the recirculation leg, header tank and rest of the rig to reduce the heat loss to the surrounding environment,

- Installation of a graduated cylinder to measure condensate rates from the heat exchanger, and
- Installation of a condensate take off vessel to enable dilute solutions to be concentrated.

As well, the entire pipe work connected to the header tank was reconstructed for ease of maintenance and insulation purposes. The modified pipe work arrangement is illustrated in figures 5-4 and 5-5.

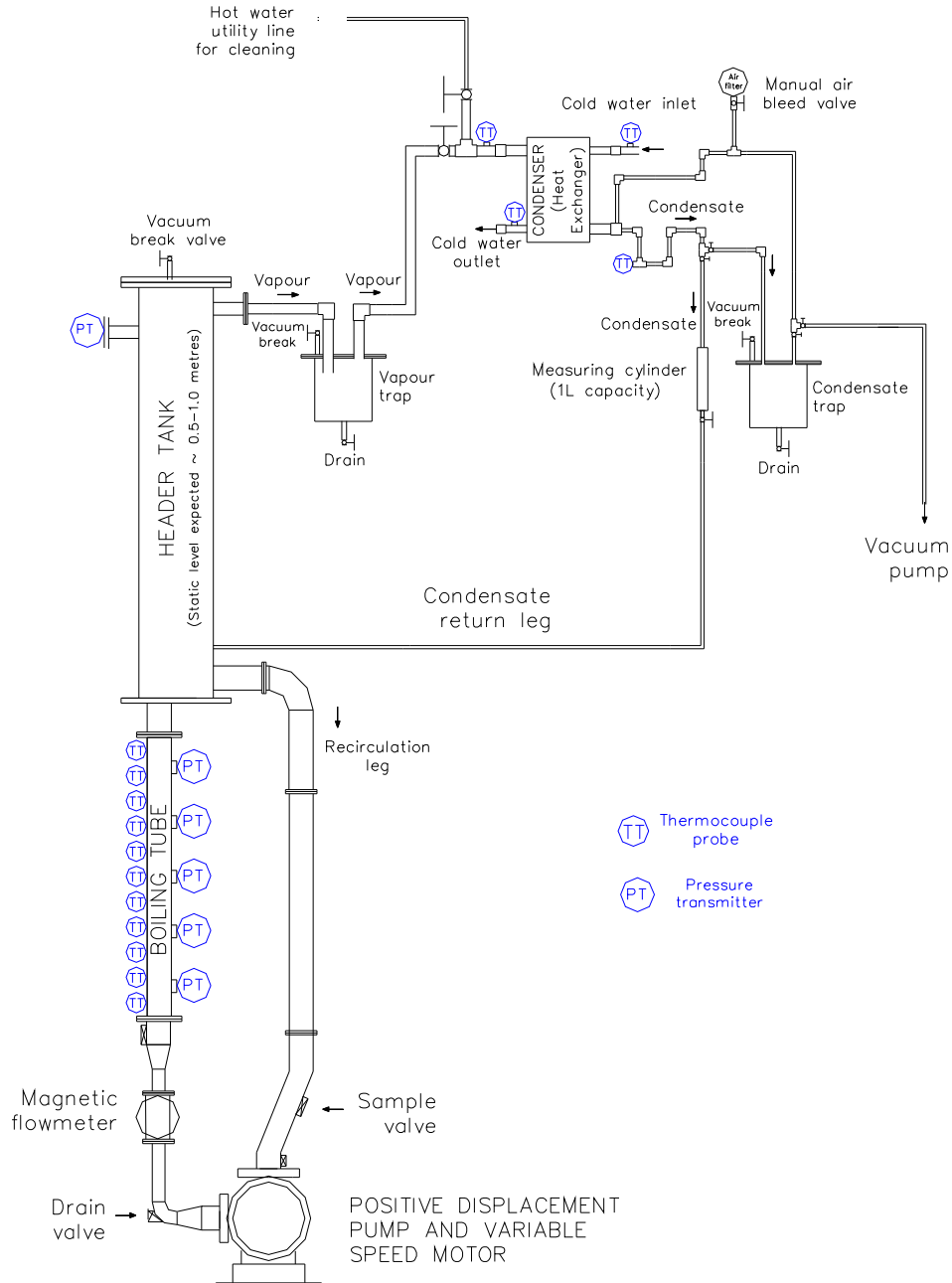


Figure 5-4 Schematic of the single calandria boiling tube rig located at JCU.

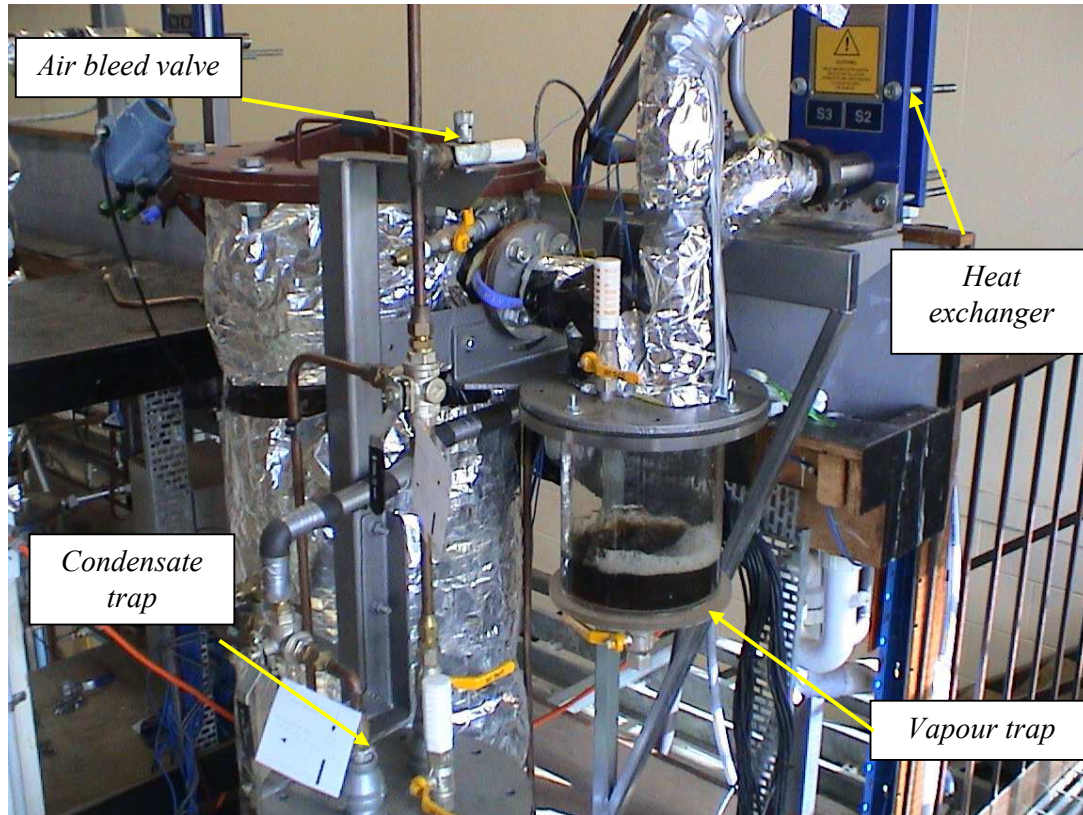


Figure 5-5 Photo of the modified pipe work and insulated header tank.

5.3 Instrumentation

The following instrumentation was installed on the boiling rig and includes:

- Five segmented electrical heating bands with individual power transmitters (Helios, 2000). The heating bands are flexible, ceramic half bands that clamp together to form one band. As the bands cover most of the calandria tube, access holes were incorporated to allow the insertion of instrumentation, such as pressure transducers and thermocouples. Each heating band (made up of two half bands) can supply a maximum of 4000 Watts. The heating bands can be controlled to a set heat input (pulse width modulated control) or alternatively can control the temperature of the calandria tube wall (PID control);
- Eleven temperature transmitters (type T thermocouples) equally spaced along the length of the heated calandria tube to measure the process temperature of the fluid. The thermocouples were inserted through compression fittings so that the end of the probe

was aligned with the centre of the calandria tube. The location of the thermocouples is shown in figure 5-6;

- Four temperature transmitters (RTDs) positioned between the five electrical heating bands in the tube wall to measure the wall temperature. A 2.5 mm hole was drilled tangentially in the tube wall between heating bands to insert the RTDs. The position of the RTDs along the calandria tube is also shown in figure 5-6. The temperature of the tube wall can also be used as one method to control the heat input to the calandria tube;
- Six pressure transducers, five spaced along the length of the calandria tube as illustrated in figures 5-2 and 5-6 and one positioned on the header tank to determine operating pressure profiles in the rig;
- Two magnetic flow meters; one on the recirculation leg measuring the volumetric flow rate through the calandria tube and the other on the inlet line measuring the cooling water flow to the heat exchanger;
- Four temperature transmitters (type T thermocouples) on the inlet and outlet streams of the heat exchanger. Along with the magnetic flowmeter these thermocouples can be used to calculate heat fluxes in the heat exchanger;
- Densitometer (or density gauge detector) for measuring the specific gravity of fluids in the calandria tube (shown in figure 5-7) to enable calculation of the amount of vapour produced by the boiling process. The vertical position of the densitometer is controlled by a movable yoke which is motorised using a power screw linked to the control system. The control system provides either manual or automatic control of the vertical position of the densitometer; and
- A conductivity probe was inserted on the recirculation leg of the rig to enable an indication of concentration (brix) to be determined. This measurement was required in order to gauge the dilution or concentration when mixing and preparing solutions for a set of experimental trials. The conductivity meter provided a visual assessment and was not linked to the data acquisition system.

All sensors were calibrated and/or processes have been developed to enable their calibration, in order to monitor the process as accurately as possible. For more detail on the commissioning of the instrumentation refer to Penny (2001).

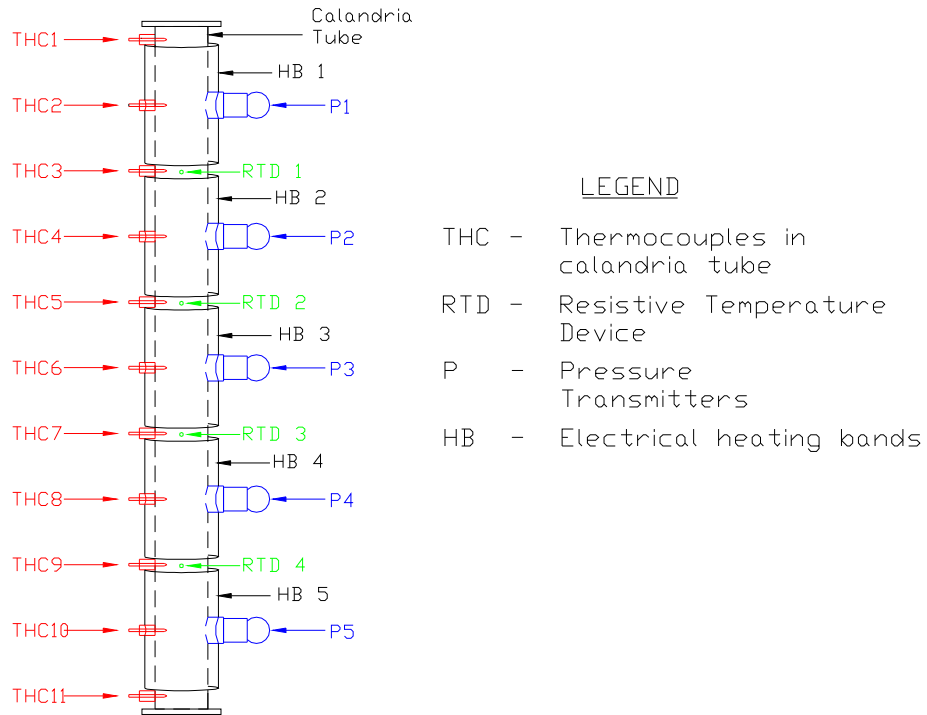


Figure 5-6 Experimental calandria boiling tube instrumentation.

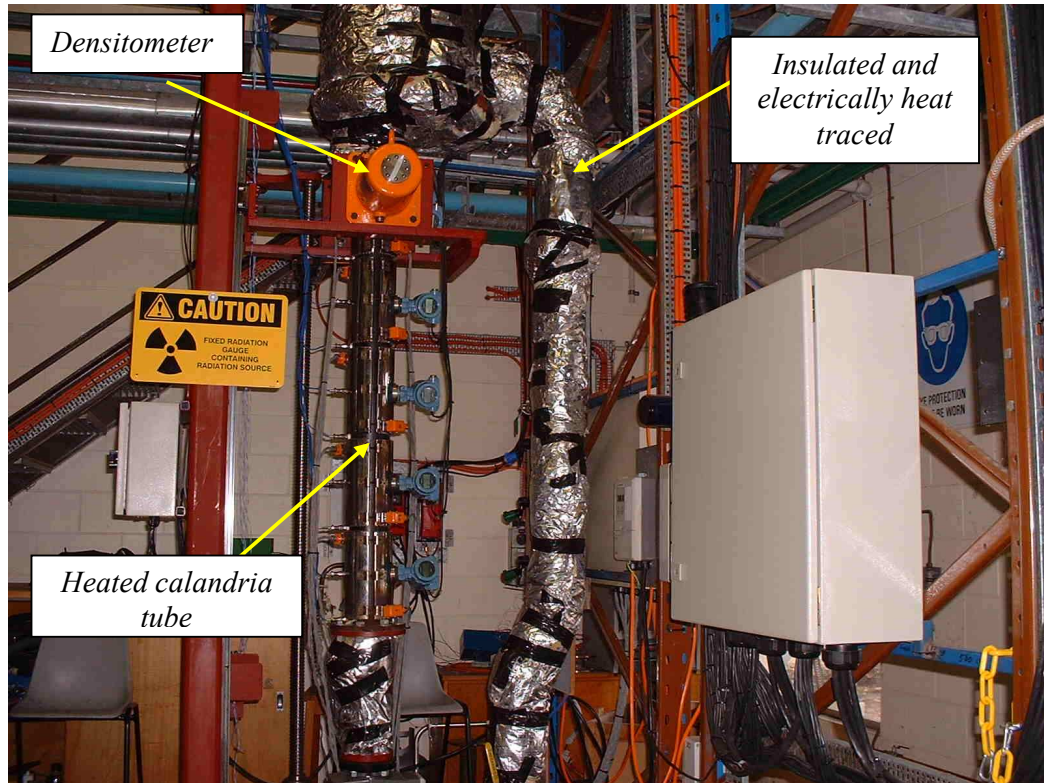


Figure 5-7 Photo of the instrumentation installed on the single calandria boiling tube rig.

5.3.1 Instrumentation errors

The following errors were associated with the instrumentation used to take measurements on the boiling rig:

- The power transmitters for the five segmented electrical heating bands had a noted error of $\pm 0.2\%$ of the range (4 kW) plus $\sim 0.02\%$ error for temperature effects and an additional error of $\sim 0.2\%$ for ripple and load change effects;
- The fifteen temperature transmitters (type T thermocouples) spaced along the heated calandria tube and on the inlet and outlet streams of the heat exchanger have an accuracy $\pm 0.1\%$ of the range (0 °C to 150 °C) and a repeatability of $\pm 0.05\%$ of the span. The thermocouple wiring accounts for the largest source of error at $\sim 0.75\%$ of the reading;
- The four RTDs measuring the wall temperature in the tube wall have an accuracy of $\pm 0.2\%$ of the range (0 °C to 150 °C);
- For the six pressure transducers, the manufacturer provides a reference accuracy (accounts for hysteresis, linearity, repeatability) of $\pm 0.2\%$ of the range (150 kPa) for the pressure transducers. Extra vibrational and stability errors up to $\pm 0.1\%$ of the range and an ambient temperature effect of $\pm 0.6\%$ over the range of 0 °C and 85 °C is also given;
- The two magnetic flow meters have a rated error of $\sim \pm 0.5\%$ of the rate over the specified operating range (i.e. for the 50 mm magnetic flowmeter the specified operating range is 0.053 m³.h⁻¹ to 71 m³.h⁻¹). This error takes into account pressure effects ($< 0.15\%$), sensor measurement ($\sim 0.03\%$) and transmitter error ($\sim 0.08\%$); and
- The densitometer has an error of 0.1% resolution on the current input, a repeatability error of $\pm 0.01\%$ S.G. units and a temperature drift error of ± 0.003 S.G units per °C.

The flow and temperature measurements on the indirect heat exchanger were used to calculate the evaporation rate based on a heat balance. These temperature measurements are critical, because of the small temperature rise over the heat exchanger on the cooling water side. Based on the measurement errors detailed above (0.8 °C for the two thermocouples and 0.1 L.min⁻¹ for the magnetic flowmeter), the maximum error in the calculation of evaporation rates can be up to approximately 16%. This also does not account for the heat loss from the exchanger to the atmosphere, which is estimated at approximately 5%. A limited amount of insulation was provided on the heat exchanger as well as the inlet and outlet pipes.

The high amount of steel work associated with the boiling rig coupled with the 3 phase motors for the pump and power screw connected to the densitometer introduced a small amount of electrical noise in the measurements from time to time. Provisions were made and additional earthing used to reduce the electrical noise influences so that during the majority of the experimental trials, fluctuations in the measurements induced by noise were not apparent.

5.4 Control software and instrumentation

All process sensors were connected to a supervisory control and data acquisition (SCADA) system, located close to the experimental rig. The SCADA system is a key component of the experimental rig. The SCADA system is a hierarchy of integrated subsystems, designed to carry out specific tasks, pictured in figure 5-8.

At the level immediately above the boiling rig is the MTL8000 plant input/output system. This system handles data transfer between the boiling circuit sensors and actuators and the computer controller system, located above it. The wiring connections for the MTL8000 system are shown in Appendix C

The control system, designed using the software-based system ProcessACT⁴, is a function block driven, real time software package capable of controlling various aspects of the boiling rig' operation, such as wall temperatures of the calandria tube. ProcessACT was chosen because of its power and flexibility, enabling rapid prototyping of a control system for the boiling rig. It was also possible to custom design blocks for tasks specific to the boiling rig such as controlling the position of the density gauge according to commands issued by the operator. In this case ProcessACT controlled the position through a sub-software package that controlled the revolutions of the power screw through the SEW MOVIDRIVE drive inverter.

⁴ ProcessACT previously known as UNAC was donated by Matrikon Australia for this project.

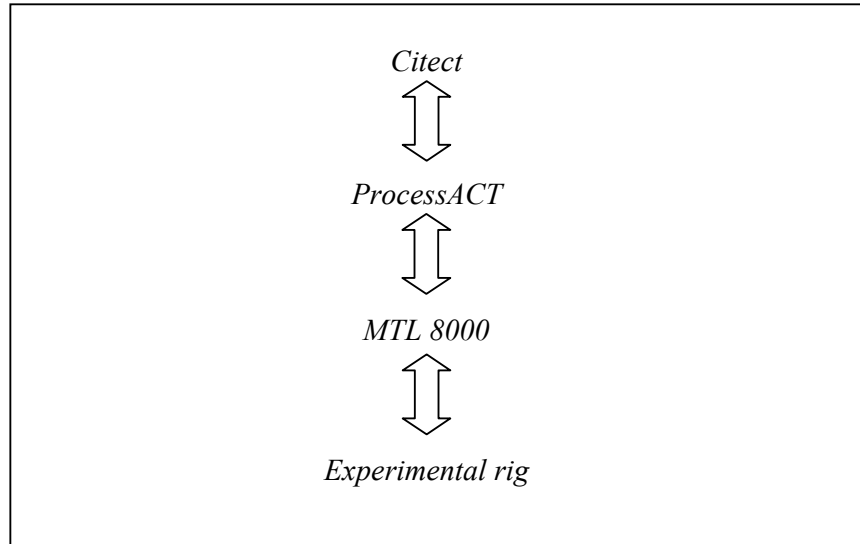


Figure 5-8 Schematic of SCADA system hierarchy.

Schematics were designed using the ProcessACT software for both data acquisition and control of the boiling rig. Super blocks and parameter files have been used extensively in the design to provide a simple interface for the user and to hide the size and complexity of the control and data acquisition system. Penny (2001) and Giese (2002) provide details on the development and user accessibility of the ProcessACT schematics and software. The ProcessACT schematics used in this project are reproduced in Appendix D.

While ProcessACT has the ability to trend and log data, it has a relatively poor man-machine interface. For this reason a Citect interface was developed to give operators better control of the boiling rig and easier access to process data. Citect is a graphical system that allows a user to indirectly interact with the ProcessACT control configuration. A TCP/IP protocol developed by ProcessACT allowed the interfacing of Citect and ProcessACT. A typical Citect display is shown in figure 5-9, showing the system overview of the boiling circuit and its ancillary components. In most cases, the operator can simply “point and click” in order to interact with the boiling rig.

Devin (2002) provides details and guides for the Citect software and development of user interfaces. A basic outline and the displays of the interface pages utilised in this project are reproduced in Appendix E.

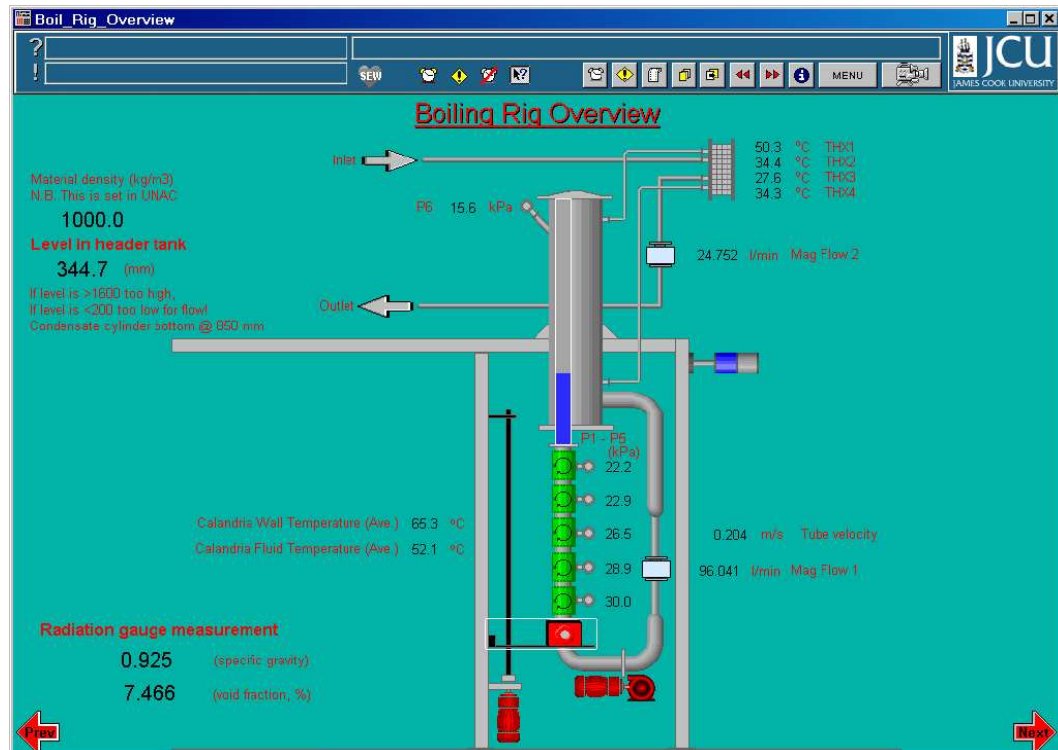


Figure 5-9 Citect overview of boiling circuit controller.

5.5 Commissioning of rig

5.5.1 Densitometer positioning and calibration

The densitometer positioning system uses a vertically traversing mechanism to allow the accurate positioning of the density gauge along the calandria tube. The system consists of a carrier, power screw, two linear bearings and SEW servo motor driven by a SEW MOVIDRIVE drive inverter. The drive inverter is programmed using propriety programming tools. However, it still requires control information from ProcessACT through the MTL8000. The wiring connections for the SEW motor and inverter are shown in Appendix F. The layout of the densitometer positioning system is shown in figure 5-10. Two limit switches were installed on the rig to limit the distance the densitometer travels restricting the damage that can be caused by the densitometer. Once a limit switch is tripped by the yoke, it causes the movement of the yoke to instantly halt until the control software is manually reset and the yoke is moved off the hardware limit switch.

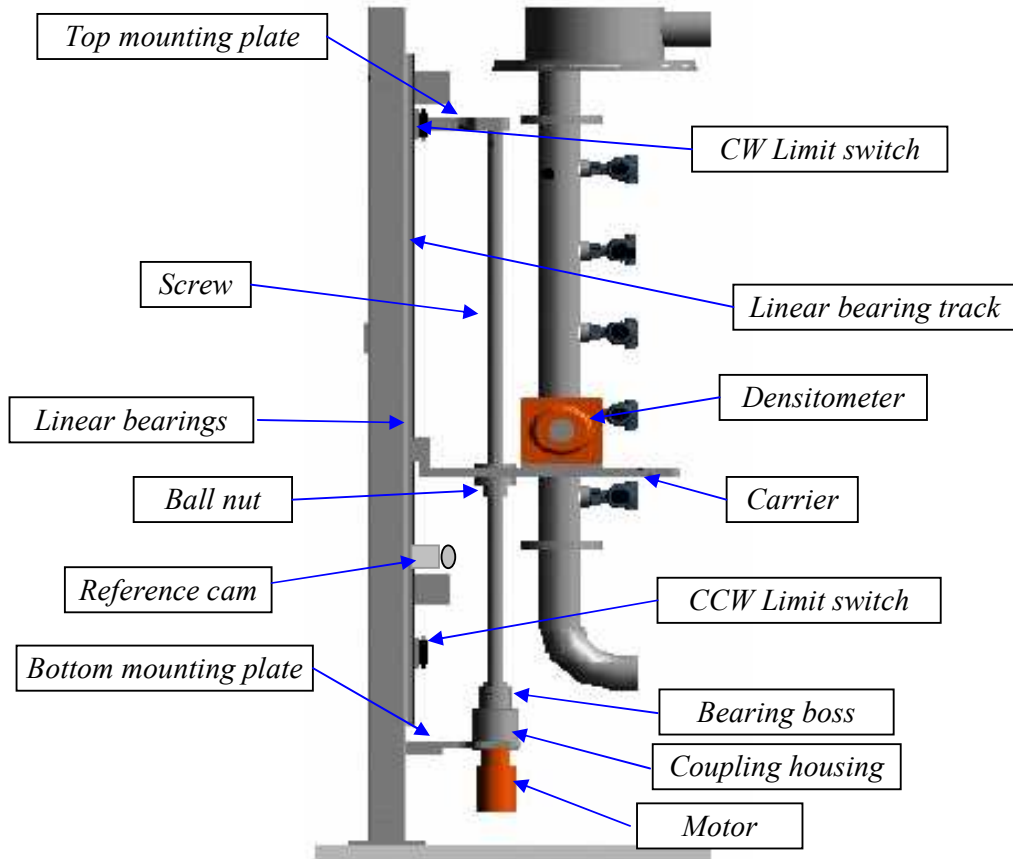


Figure 5-10 Densitometer positioning system layout.

A reference cam was also installed to provide the yoke with a machine-zero location for positioning. On start up the control software forces the yoke to perform a ‘reference travel’ down the calandria tube until it trips the reference cam. Once the reference cam has been found, the control software will move the yoke to a reference offset from this position (*i.e.*, 50 mm above) to designate a machine-zero location. The control software will remember this location as the reference position until the power is turned off or the program is reset. The machine-zero position was designated to correspond to the bottom of the heated calandria tube. The positioning system for the yoke is based on the distance from the machine-zero location.

A control tower stack light and two tone buzzer were installed to allow a visual and audible indication of when the positioning system is operational, satisfying safety requirements.

The movement of the yoke along the length of the calandria tube is controlled by the drive inverter that controls the functionality of a variable frequency (VF) synchronous motor. The VF motor unit turns the power screw a set number of revolutions, corresponding to a millimetre

increment sent by the drive inverter. The motor unit can turn the power screw at speeds ranging from 0 to 3000 r.min⁻¹. Included in the inverter is the IPOS Sequence and Positioning Control System software which allows the inverter to be controlled via signals from the MTL8000 and ProcessACT software.

Giese (2002) provides details on the development and functionality of the densitometer positioning system.

The digital density gauge (SIStec Model SS200) is manufactured by Specialised Industrial Systems and employs a sodium iodide scintillation detector which enables much greater count rates to be achieved compared to ion chamber techniques and hence provides greater accuracy. The densitometer uses a Cs-137 source rated at 20 mCi. The nucleonic density gauge has a number of built in functions to improve the accuracy of measurement. These include:

- Decay compensation to allow for the decay of the radioactive source over time;
- Gain stabilisation that automatically adjusts the gain (conversion of the gamma ray into an electrical pulse to be analysed) using a control technique that compares a statistical model of the radiation to the count rate; and
- Dead-time correction which corrects the number of counts using a well known statistical formula.

The narrow beam geometry theory employed by the density meter relates the density of the process fluid to the change in absorption of the gamma rays by the following simplified equation,

$$\log\left(\frac{C_N}{C_W}\right) = -M_{AC} L_D \rho_{mix} \quad (5.1)$$

where C_N is the count rate for the process fluid in the heated tube (counts.s⁻¹),
 C_W is the count rate for a fluid with specific gravity of unity (counts.s⁻¹),
 M_{AC} is the mass absorption coefficient (m².kg⁻¹),
 L_D is the path length through the process fluid (x10⁻² m), and
 ρ_{mix} is the density of the process fluid in the heated tube (kg.m⁻³).

The small gap between the two halves of the heating bands, as shown in figure 5-2, allowed absorption measurements to be taken where the gamma rays do not pass through the ceramic bands. No measurements were taken corresponding to positions where instrumentation was installed on the heated tube. This was because the metal in the probes of the instrumentation would affect the count rates measured by the densitometer.

Calibrations of the density gauge are routinely required to correct for pipe wear and long term drift in detector efficiency. Calibrations were carried out by measuring the count rates for the heated tube both completely empty and full of pure water. The mass absorption coefficient is calculated from this data and is specific to the tube material, diameter and wall thickness.

Additional standardisation was carried out when using different mixtures during experimentation to provide a base value for comparison along the entire length of the tube that was independent of tube wall thickness. This allowed the amount of vapour to be determined during the boiling trials. This was performed by measuring the specific gravity of the mixture using the density gauge before the commencement of an experimental trial. During the experimental trials the deviation from the base values of specific gravity along the tube length allows the mixture quality (x) to be determined from the following formula,

$$\left(\frac{1}{\rho_{mix}} \right) = \left(\frac{x}{\rho_{vap}} \right) + \left(\frac{1-x}{\rho_{liq}} \right) \quad (5.2)$$

The vapour volume fraction (α) can then be determined by,

$$\alpha = x \frac{\rho_{mix}}{\rho_{vap}} \quad (5.3)$$

As the mixture quality is very small and the density of the vapour phase is significantly smaller by orders of magnitude than the density of the liquid phase, the vapour volume fraction can be estimated by solving the following equation,

$$\rho_{mix} = \alpha \rho_{vap} + (1-\alpha)\rho_{liq} \quad (5.4)$$

As the tube wall thickness varied along the length of the heated tube (due to internal corrosion and instrumentation) the standardisation was carried out along the length of the heated tube. A tube with consistent wall thickness would make the technique much more accurate. The disadvantage of this method was that when no boiling was occurring and hence no flow through

the tube circuit, the solids in the sugar solutions would settle hence affecting the comparison reading. Alternatively, samples can be obtained and analysed for density but the disadvantage of this method is the inherent entrainment of air that occurs when a sample is taken under non-vacuum conditions.

5.5.2 Densitometer results

Results of measurements obtained by the densitometer and the calculations of average vapour volume fractions are shown in figure 5-11 for molasses boiled in the experimental rig operating with a level of approximately 1200 mm in the header tank. The results are more consistent in the lower part of the calandria tube where no boiling is occurring. The measured densities in the upper parts of the tube vary considerably and may indicate the presence of an eruptive or cyclical boiling process.

The results obtained by the radiation gauge have been averaged over the time (~3 min to 5 min) the densitometer was measuring absorption at each individual location to remove any oscillating behaviour.

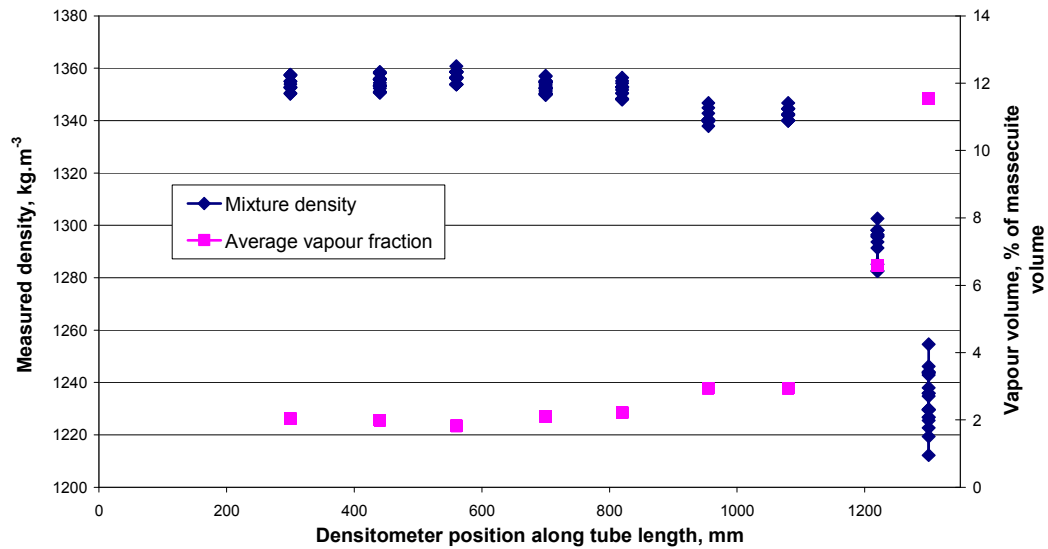


Figure 5-11 Data obtained from the densitometer.

The results measured from 300 mm to 1080 mm along the tube show vapour volume fractions of approximately 2%. In sub-cooled boiling conditions it is common to see low vapour volume fractions before the onset of bulk boiling (refer section 4.3). After this point, the vapour volume fraction increases substantially with increasing elevation in the tube. Prior to bulk boiling, the

bubbles are attached to the heated wall with the bulk liquid at high sub-cooling (Unal, 1975). The ceramic heating bands are approximately 250 mm in length with a gap of approximately 10 mm to 12 mm between bands. There are also circles of 80 mm diameter for the location of the pressure transducers and 20 mm diameter for the location of the thermocouples where the heating band is not in contact with the outer tube surface. This will lead to localised non-heating although the non-uniform heating effects are expected to be minimal.

The small vapour volume fractions measured for a large proportion of the lower section of the tube may have been caused by rapid condensation of the formed vapour bubbles through heat diffusion effects where the superheating is not sufficient to allow the vapour to progress up the tube. This is prevalent in sub-cooled boiling conditions. Alternatively the small amount of vapour volume could be attributed to the ingress of air through the pump, although this could not be confirmed (see section 5.5.3 and 5.5.4), or small discrepancies between the measured and calibration data. In the operation of the rig under forced circulation, the pump was turned off during the calibration to ensure the ingress of air did not affect the calibrations. Discrepancies could occur between the measured and calibration data by the fact that the suspended solids in the sugar solution can settle when no flow is present in the tube circuit, producing lower base readings for comparison.

5.5.3 Pressure control

The pressure in the headspace above the boiling level in the header tank gives an indication of the nature of the boiling process and also highlights the limited capacity and performance of the liquid ring vacuum pump. The maximum vacuum achieved by the vacuum pump is dependent on the temperature of the pump sealing water and varies throughout the day as the ambient water source increases in temperature. Limited vacuum control instrumentation exists on the experimental rig. A small needle valve air bleed on the vacuum source line to the header tank allows the operating pressure in the head space to be adjusted away from the minimum pressure provided by the vacuum pump. This is achieved manually and has no feedback control to adjust to variations. A buffer tank installed in-line from the vacuum source would help to minimise fluctuations from the vacuum pump.

Figure 5-12 shows the pressure in the headspace for various operating conditions of several experimental trials, but with the same fluid conditions. In these experiments the rig is operating under forced circulation conditions (configuration 3). Small fluctuations in the operating pressure can be observed throughout the experimental trials that are caused by the boiling

within the rig. The fluctuations could be caused by the slight cyclical or pulsing nature of the pump. However, during the boiling process, as the vapour travels to the surface of the boiling level there is an expansion of the vapour that is eruptive in nature and sporadic within the single tube. This eruptive expansion of vapour is likely to cause micro-pulsations observed by Austmeyer and Schliephake (1983) that have a dominant effect on the heat transfer to the fluid and mask any cycling or pulsing caused by the recirculation pump.

The minimum operating pressure in the header tank throughout each experimental trial is related to the flow rate circulating within the experimental rig as well as the amount of heat input or boiling that is occurring within the calandria tube. A higher operating pressure can be observed when the heat input to the heating bands is set at 90% which produces more boiling within the rig. For the same power input, higher operating pressures can be observed when the speed of the recirculation pump is increased so that the flow rate circulating within the rig increases.

The greater operating pressure at higher flow rates is likely to also be effected by the increase in air ingress through the pump at increased pump speeds as detailed in section 5.5.4.

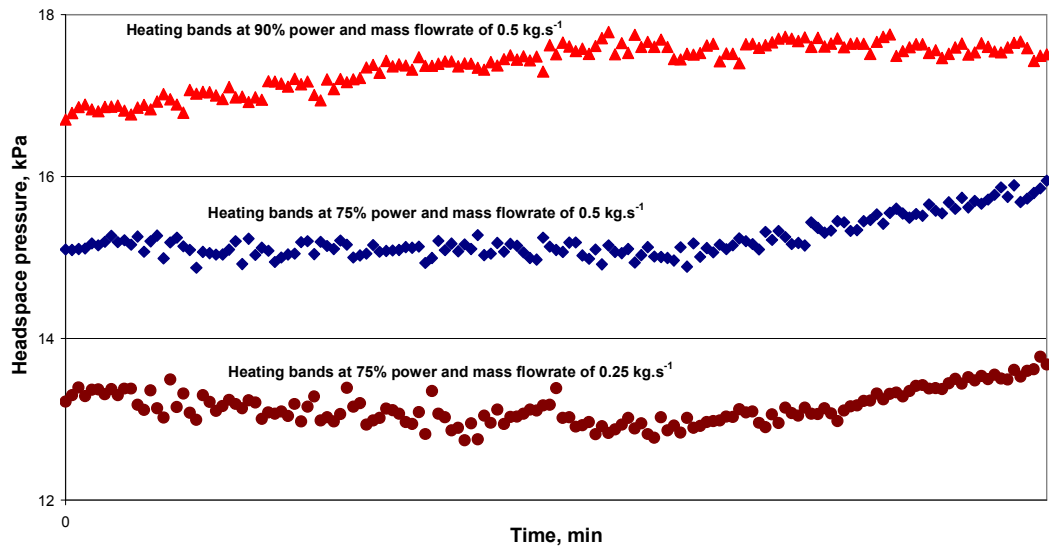


Figure 5-12 Operating pressure in the headspace for various experimental trials.

The rate of air leakage was also measured in the experimental rig by isolating the vacuum source for two cases. The results of these two cases are illustrated in figure 5-13 where the leakage rate was evaluated under forced circulation conditions with boiling and ambient conditions with no forced circulation or boiling. The air leakage rates were measured at approximately $2.4 \text{ m}^3 \cdot \text{Pa} \cdot \text{s}^{-1}$ for the case with no circulation or boiling and up to $18.4 \text{ m}^3 \cdot \text{Pa} \cdot \text{s}^{-1}$

for the case with forced circulation and boiling. Using ideal gas properties⁵, this corresponds to an air leakage mass flow rate of 0.1 kg.h⁻¹ with no circulation or boiling to 0.63 kg.h⁻¹ with forced circulation and boiling. The high leakage rates place extra importance on the fittings used in the experimental rig and the care required when making modifications to the pipe work. In general, flared vacuum fittings were used rather than standard compression fittings to reduce the air leakage rates.

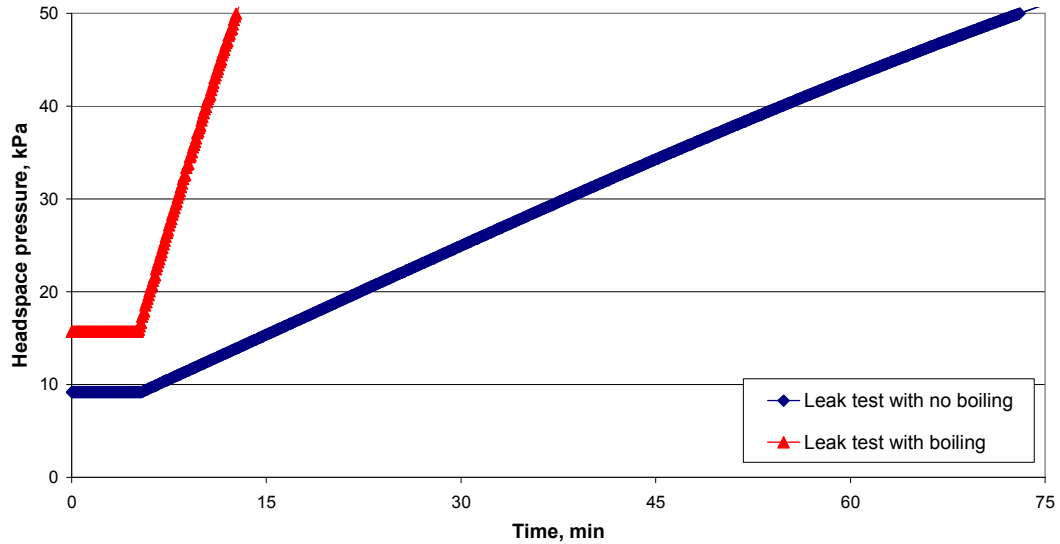


Figure 5-13 Operating pressure in the headspace for leak test trials.

5.5.4 Flow circulation control

The level in the header tank was calculated by the pressure difference between the lowest pressure transducer (130 mm from the bottom of the tube in the middle of the first heating band) and the head space pressure transducer and multiplied by the density measured by the radiation gauge to determine a static height. This assumes there is no vapour fraction but the presence of vapour would change the actual boiling level. The influence of the vapour produced in the

$$^5 \quad Q_{leak} = M_{leak} R \frac{273.15 + T_{air}}{MW} \quad (5.5)$$

where Q_{leak} is the air leakage rate in the apparatus which has an internal volume of 240 L (m³.Pa.s⁻¹),
 M_{leak} is the leakage mass flow rate of air (kg.h⁻¹),
 R is the gas constant (8.314 m³.Pa.mol⁻¹.K⁻¹),
 T_{air} is the temperature of the air leaking into the system (°C), and
 MW is the molecular weight of air (29 kg.kmol⁻¹).

calandria tube would be diluted by the increase in cross-sectional area as the vapour leaves the tube which is 100 mm in diameter and travels up the header tank which is 350 mm in diameter.

The incorporation of a pump in the recirculation leg of the boiling rig represents a significant source of air leakage into the rig. The air is incondensable and so is transported to the vacuum pump. Along the way, however, vapour humidifies the air and so part of the vapour produced in the rig exits the system through the vacuum source. The humidification is shown through the loss of static level in header tank and has been measured and is shown in figure 5-14.

The data in figure 5-14 are for a power input to the heating bands of 15 kW. The leakage rate measured in the header tank when the pump was providing an average flow rate in the heated tube of approximately $0.1 \text{ m}\cdot\text{s}^{-1}$ was approximately $0.77 \text{ mm}\cdot\text{min}^{-1}$ or $69 \text{ mL}\cdot\text{min}^{-1}$. These rates were determined by the loss of static level in header tank. Similarly for an average flow rate of approximately $0.4 \text{ m}\cdot\text{s}^{-1}$, the leakage rate was approximately $1.54 \text{ mm}\cdot\text{min}^{-1}$ or $137 \text{ mL}\cdot\text{min}^{-1}$. Typically each trial would last about 45 min which would produce a loss of 3 L to 6 L of condensed vapour over the length of the trial. Overall the total amount of fluid in the experimental rig for a level of 500 mm in the header tank with the configuration set up with the pump is approximately 90 L making the loss equal to approximately 3% to 6% over the course of a trial. This loss of vapour causes the concentration of the sugar solution to increase and hence change the properties of the fluid throughout the experimental trials.

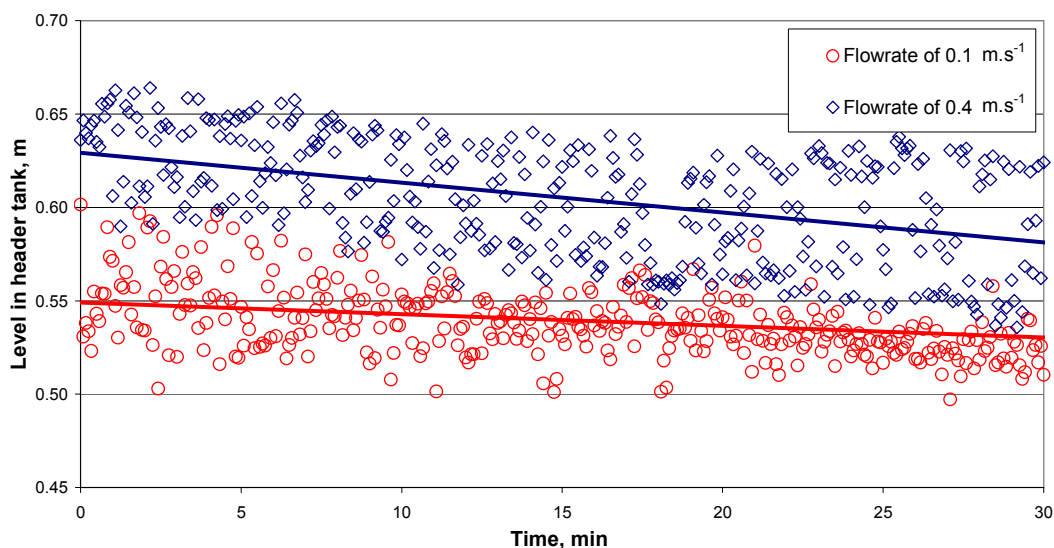


Figure 5-14 Operating level in the header tank for various experimental trials.

The humidification of the air leaking into the rig can not explain the overall drop in level (as measured by the pressure transducers) within the header tank. The air leakage is of the order of $<1 \text{ kg}\cdot\text{h}^{-1}$ (section 5.5.3) whereas the drop in level measured in the header tank is approximately $4 \text{ kg}\cdot\text{h}^{-1}$ to $8 \text{ kg}\cdot\text{h}^{-1}$. The air transported to the vacuum pump would have to have a moisture level of over 400% to reconcile the drop in level measured in the header tank. It is likely that some of the vapour is not fully condensed in the heat exchanger (inefficient operation) and is also transported to the vacuum pump with the air. Another explanation would be a small rise in pressure measured by the transducer in the head space due to a temperature increase during the boiling process or a small air leak around the diaphragm of the pressure transducer. This would give the impression that the level in the header tank is decreasing even though no loss of vapour may be occurring. Visual observation of the level in the header tank was not possible to confirm this theory.

The conductivity probe inserted on the recirculation leg of the rig also measured a decrease in reading over the course of an experimental trial. To control the loss of vapour and to enable the concentration of the process fluid in the experimental rig to be controlled, water was added periodically throughout a trial. The conductivity measurement was also required in order to gauge the dilution or concentration when mixing and to prepare solutions for a set of experimental trials. The conductivity meter provided a visual assessment and was not linked to the data acquisition system.

5.5.5 Temperature effects

The temperature profiles measured for one particular experimental trial under natural circulation conditions are illustrated in figure 5-15. The temperature profiles show that the axial temperature measurements made along the centreline of the tube are sub-cooled for the entire length of the tube as they fall below the boiling point temperature profile, which is also shown in figure 5-15. The axial temperature measurements are based on average temperature values of each of the eleven thermocouples spaced evenly along the length of the heated tube. The boiling point temperature is calculated by the saturation temperature evaluated at the static pressure for a given vertical location plus the boiling point elevation calculated using equation 2.20. Typically in sub-cooled boiling conditions the radial temperature profile is non-uniform as the hot vapour produced at the tube wall has not transferred heat to the fluid in the centre of the tube. Radial temperatures were not measured during the experimental trials.

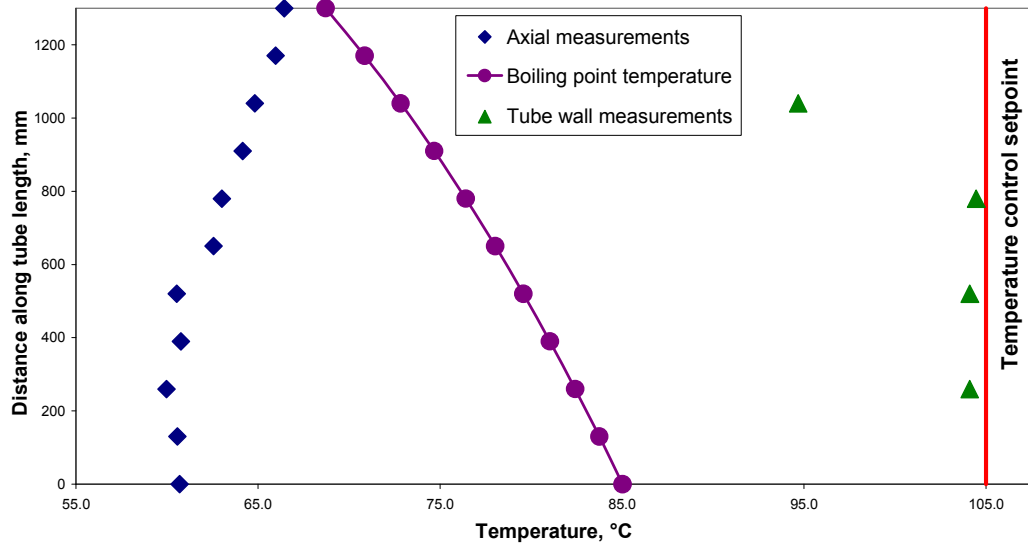


Figure 5-15 Temperature profiles along the tube length during an experimental trial.

The axial temperature profile indicates a reasonably constant temperature is maintained along the first 600 mm of heated tube length. After this point the axial temperature gradually increases to the end of the heated tube. This increase in temperature is caused by the transfer of heat from the bubbles and hotter liquid located close to the tube wall migrating towards the centre of the tube heating the bulk of the fluid. Factors that influence the heat transfer to the fluid in the centre of the heated tube include the vapour volume fraction, viscosity and mass flow rate of liquid. Increasing the mass flow rate (forced circulation conditions using the pump) had the effect of increasing the temperature difference (amount of sub-cooling) between the axial temperature profile and the boiling point temperature profile.

Temperature measurements made by Webre (1933) along the axial location within calandria tubes in factory pans during operation also showed non-superheated conditions when compared to the corresponding boiling point temperature. Webre thus concluded that no ebullition was occurring within the calandria tubes in factory pans. This observation really meant that the tube was actually sub-cooled. If Webre had been able to use a fast response temperature measuring device positioned close to the tube wall he would have measured superheated temperatures. Superheated vapour temperatures (up to 4 °C above the boiling temperature) were measured in the head space of factory pans (Webre, 1962). Similarly the temperature of the vapour being condensed in the heat exchanger during the experimental trials on the single calandria tube was measured with up to 5 °C superheat above the saturation temperature.

The temperature of the heated tube wall was measured by four RTDs positioned in the middle of the tube wall, which is 6 mm thick. The tube wall temperature is not constant as it is limited by the resistance from the heated tube to the boiling massécuite. The heating resistance is non uniform along the length of the tube especially within the uppermost region where more vapour is produced. The vapour forms and moves away from the heating surface in the upper tube section allowing more heat to be transferred from the wall to the fluid. Austmeyer and Schliephake (1983) state that the increase in heat transfer is created by the turbulent flow of vapour bubbles. This is shown in figure 5-15 for an experimental trial where the tube wall temperature was controlled to a set point of 105 °C. Under this control set up, the top ceramic heating band was operating at 100% but was unable to heat the temperature of the tube wall to the required set point.

Due to this effect, tuning of the heating band PID algorithms was not intensively employed. There were also a lot of interacting factors and the RTD measurements influenced the control of more than one heating bands. Some of the heat is also transferred within the tube wall to adjacent sections. Similar trends were also found when the electrical heating bands were controlled by a power set point. However, in this case the bottom RTD or the temperature of tube wall at the bottom of the tube also showed slightly lower temperatures. The fluid entering the bottom of the tube would also be at the lowest temperature (averaged across the cross-sectional area) and thermal boundary layers would be developing close to the tube wall (see section 4.4).

5.5.6 Heat flux control

The control of the heating bands is physically achieved by switching the power to the heating bands using solid-state relays. The software programming for the switching is based on two methods of control; temperature and power control. Temperature control involves the system being given a tube wall temperature set point and the control software aims to adjust the power input to each of the heating band pairs to maintain the tube wall at that temperature. Control by power input requires a set point for the power level. The control system uses a pulse width modulation (PWM) sequence to provide the power level required. The PWM sequence was set over a period of 20 s (*i.e.*, if the power input set point was 75% then the PWM block would turn the heating bands on for 75% and off for 25% of the time period, or on for 15 s and off for 5 s).

Control using the temperature method requires automation and is accomplished by a (PID) controller in the ProcessACT interface for each of the heating bands. The process involves

calculating the difference between the set point for the tube wall temperature and the process variable (tube wall temperature measured by the RTDs). This value, called the error signal, is fed into the PID controller. The values for the proportional gain, the integral time and the derivative time are set by the operator. The output from the PID controller block is limited to a value between 0 and 100% and this value is pulse width modulated to switch the solid-state relay for the heating band.

There are only four RTDs measuring the tube wall temperature between the five heating band pairs as pictured in figure 5-6. The temperature control of each of the heating bands (except the top and bottom heating bands) takes the average value of the temperatures measured by the RTDs in the tube wall both above and below the corresponding heating band. The output of a heating band thus affects the tube wall temperature in two locations and vice versa. As mentioned previously, intensive tuning of the heating band PID algorithms was not employed due to the interactions of the tube wall temperature measurements and the power outputs to the heating bands.

Control using the power input method is accomplished manually by inputting a set point for the power level, as a percentage. This value bypasses the PID controller block and passes through the PWM block.

Heat flux measurements on the single boiling tube rig were taken by two separate means; viz. from the active power transducers on each of the individual heating band pairs as well as temperature and flow measurements on the heat exchanger cooling the vapour produced by the boiling process and returning it to the rig.

The heat flux to the heating bands is obtained by summing the averaged power readings from the transducers on each of the heating band pairs. For the power control method the heat flux is just the power percentage set point multiplied by the maximum power of each heating band pair (4 kW) multiplied by the number of heating bands switched on.

Using the temperature and flow measurements through the heat exchanger the heat flux of the condenser can be determined by,

$$Q_{cond} = M_{CW} C_{p,liq} (T_{CWout} - T_{CWin}) \quad (5.10)$$

where Q_{cond} is the heat flow rate in the heat exchanger (W),

M_{CW} is the mass flow rate of the cooling water stream ($\text{kg}\cdot\text{s}^{-1}$),

$C_{p,liq}$ is the specific heat of the cooling water ($\text{J}\cdot\text{kg}^{-1}\cdot\text{K}^{-1}$),

T_{CWout} is the outlet cooling water temperature ($^{\circ}\text{C}$), and

T_{CWin} is the inlet cooling water temperature ($^{\circ}\text{C}$).

The thermocouples in the lines to and from the heat exchanger measuring the temperature of the vapour, the condensate and the cooling water were orientated so that the probes were completely immersed by the fluid even if the pipe work is not full of liquid.

Temperature measurements of the vapour and condensed vapour (condensate return) through the heat exchanger over the course of an experimental trial are shown in figure 5-16. Both the set point of the heating bands and the heat flux calculated using equation 5.10 are also shown in figure 5-16. For this experimental trial, all five heating bands were set at 75% power giving a total heat input of 15 kW. However, the heat removed through the heat exchanger was calculated to be 12.7 kW (average). This represents a significant heat loss and was partly caused by a lack of insulation around the electrical heating bands. The entire rig and pipe work apart from the heated tube section was insulated, however, a cost-effective and pragmatic method of insulating the heating bands could not be found.

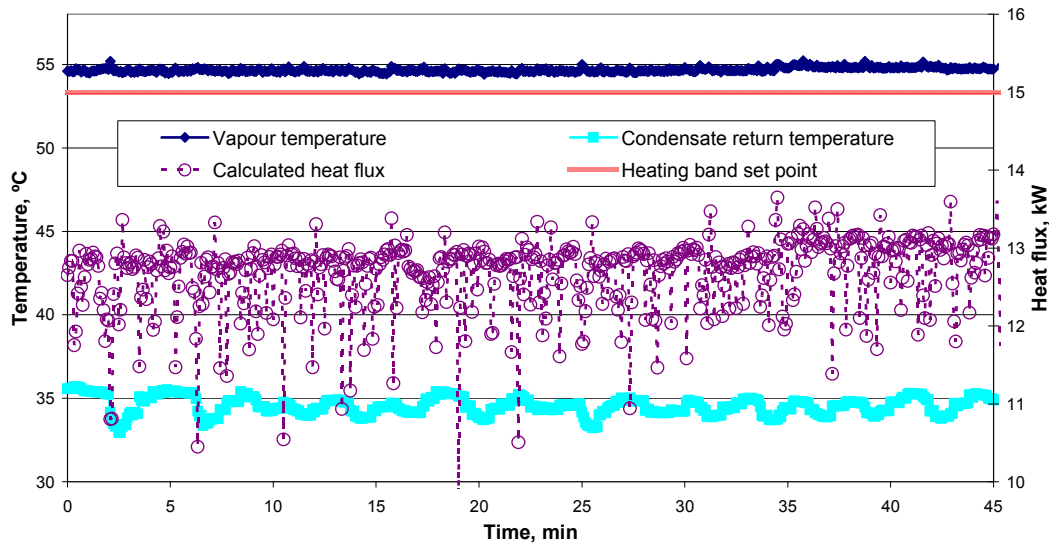


Figure 5-16 Temperature profiles and heat transfer data for the vapour heat exchanger during an experimental trial.

Figure 5-16 shows oscillations in the temperature measurements of the condensate return, which is a further indication of the cyclical boiling nature mentioned in sections 2.1, 5.5.2 and 5.5.3.

For the analysis of the experimental trials the measured heat fluxes from the heating bands on the boiling rig were adjusted to approximately 85% of their values to account for the non-insulating effects and heat losses to the atmosphere. This adjustment also reflects the heat flux calculated in the heat exchanger. The electrical heating of the single calandria boiling tube represents one of the major differences between steam heating of the calandria tubes in factory pans.

5.6 Experimental work program

The experimental plan for the trials conducted on the single calandria tube boiling rig was as follows;

- Samples of different molasses were collected from local sugar mills and transported to JCU for storage.
- Sugar solutions of varying fluid properties were prepared using raw sugar crystals and the molasses samples and added to the experimental rig.
- The sugar solutions were boiled under various operating conditions.
- Measurements were taken during the experimental trials to calculate and determine specific fluid correlations. The measurements included tube wall temperature, head space pressure, heating band power, heat flux, circulating flow rate, and temperature, pressure and vapour volume fraction along the tube length.
- The specific fluid correlations (detailed in section 4.5) were used to develop numerical models of boiling within calandria tubes.

To avoid problems occurring with the degradation of factory samples the molasses samples were stored in a refrigerated cold room located at JCU. A limited number of molasses samples were also stored in a refrigerated unit at SRI. Unfortunately the cold room at JCU failed numerous times over the course of the research and this resulted in the degradation of many molasses samples. Conducting boiling experiments on the degraded molasses samples required numerous hours of boiling and the addition of a defoaming agent to remove the dissolved gases and froth that was entrained in the molasses. The level of degradation of the molasses samples significantly affects the properties of the boiling fluid.

The experimental solutions were prepared by combining the various molasses samples and adding sugar crystals to replicate factory massecurites as close as possible. Sodium azide was added (~ 5 ppm) in most cases to retard microbial degradation. The molasses samples that had

sodium azide added, experienced less degradation when the cold room failed. These samples also created less foaming problems when boiled.

The experimental rig was intended to simulate the conditions present in factory pans to allow detailed examinations of the heat transfer process and vapour volume fraction profiles to be obtained. The data gathered on the experimental rig were preliminary in nature as the rig did not adequately represent factory equipment. The main differences between the experimental rig and the conditions in factory vessels include:

- The differences between steam heating and electrical heating of the calandria tube. In steam heated tubes, the steam flow rate and heat flux is limited by the heat transfer through the tube wall to the circulating fluid in order to condense the steam. The tube in the experimental rig is heated electrically and is not restricted by some of the issues associated with steam heating. In factory steam heated calandria tubes, there are minimal heat losses as the calandria section is adequately insulated whereas the experimental rig has limited insulation. The measured heat fluxes from the heating bands on the boiling rig were adjusted to approximately 85% of their values to account for the heat losses to the atmosphere (see section 5.5.6). Steam heating also provides more consistent heating of the calandria tube as the steam makes contact with the entire outer tube surface. Steam heating is also a direct replication of the conditions in factory vessels. In the experimental boiling rig, there are gaps where the ceramic heating bands are not in contact with the outer tube surface;
- The incorporation of a pump in the boiling rig. In the forced circulation boiling trials, the pump creates a source of air leakage into the rig. The incondensable air is humidified as it is transported to the vacuum source removing vapour from the system (see section 5.5.4). The removal of a small amount of vapour causes the concentration of the sugar solution to increase slightly. Hence, changes to the properties of the sugar solution occur throughout the boiling trials;
- Material composition of the molasses samples. The molasses samples were stored for a number of months before boiling trials were conducted allowing the molasses to degrade. The level of degradation of the molasses samples significantly affects the properties of the boiling fluid;
- Calandria tube and recirculation leg geometry. In the experimental boiling rig, part of the recirculation leg is the same diameter both prior and immediately exiting the heated calandria tube. This reduces the entrance and exit effects of the flow in the heated tube section as the flow is fully developed before entering the heated tube. However, the

flow will still develop thermally in the heated tube section. The size of the recirculation leg and header tank is also significantly smaller and more restrictive in comparison to the downtake and upper pan region of factory vessels. The smaller area in the experimental boiling rig affects the flow by generating relatively greater amounts of frictional resistance. The effects of multiple neighbouring calandria tubes on the flow in the upper pan region can not be investigated in the experimental boiling rig; and

- Insulation of the boiling rig. In factory vessels the entire vessel is typically well insulated including the heated calandria tubes. The large volume of massecuite flowing within the pan also helps insulate the massecuite inside the vessel. The provision of insulation on the experimental rig was not as comprehensive as the insulation in factory vessels. The measured heat fluxes in the experimental trials had to be adjusted to account for this fact.

6 EXPERIMENTAL RESULTS

This chapter provides details and results of the experimental trials conducted as part of the research. Experimental boiling trials were undertaken on a single calandria tube boiling rig to enable boiling characteristics to be determined in calandria tubes with changing material properties and heat input conditions. The experimental data provides results that are used to develop empirical correlations and validate numerical tube models in chapter 7.

6.1 Introduction

Numerous boiling trials were conducted on the single boiling tube rig at JCU using molasses and sugar solutions obtained from local mills over a six month period. The results and operating parameters of these trials are presented in this section.

The main operating conditions tested in the experimental investigation other than the solution properties include:

- Operating pressure in the head space (12 kPa to 24 kPa);
- Static boiling level in the header tank (300 mm to 1200 mm);
- Tube wall temperature (90 °C to 115 °C);
- Circulation speed in the calandria tube (0.01 m.s⁻¹ to 0.43 m.s⁻¹);
- Length of heated tube section (780 mm to 1300 mm); and
- Power input to heating bands (9 kW to 18 kW).

6.2 Experimental trials

6.2.1 Natural circulation

A total of 15 experimental runs were conducted under the two natural circulation rig configurations. These trials were restricted due to the limited circulation rates possible under the rig configurations and the limited availability of adequate molasses samples. The operating conditions for the trials are summarised in table 6-1. Trials 1n to 8n were conducted with the experimental rig in configuration 2 (see section 5.2.2) whereby the circulation of material in the heated tube was measured using a hot film anemometer inserted in the recirculation leg. Trials 9n to 15n were conducted with the experimental rig in configuration 1 (see section 5.2.2) whereby the circulation of material in the heated tube was measured using the magnetic

flowmeter on the recirculation leg. A summary of operating parameters and measured values averaged over each of the natural circulation trials are included in Appendix G.

Table 6-1 Summary of average operating conditions for the natural circulation trials (configurations 1 and 2).

Date	Trial	Wall temperature, °C	Heat flux, kW	Average circulation, m.s ⁻¹	Tube length, mm	Headspace pressure, kPa	Boiling level above tube, mm
Circulation measured by hot film anemometer (configuration 2)							
29/04/04	1n	92.2	15.0	0.038	1300	15.5	750
29/04/04	2n	98.2	18.0	0.045	1300	17.5	720
29/04/04	3n	93.7	14.4	0.004	1040	15.2	960
29/04/04	4n	99.2	15.0	0.015	1300	14.7	590
29/04/04	5n	104.7	18.0	0.029	1300	16.9	585
29/04/04	6n	109.3	18.0	0.044	1300	22.7	620
29/04/04	7n	109.5	18.0	0.045	1300	16.6	370
29/04/04	8n	101.1	15.0	0.020	1300	13.2	360
Circulation measured by magnetic flowmeter (configuration 1)							
26/05/04	9n	91.4	12.0	0.026	1040	15.0	1180
26/05/04	10n	97.4	18.0	0.053	1300	18.8	880
26/05/04	11n	103.4	14.4	0.032	1040	16.5	1050
27/05/04	12n	91.2	15.0	0.032	1300	15.5	810
27/05/04	13n	100.2	18.0	0.048	1300	14.0	1050
27/05/04	14n	105.7	9.0	0.013	780	12.0	930
27/05/04	15n	106.3	10.7	0.011	1040	13.0	900

6.2.2 Forced circulation

A total of 75 experimental runs were conducted under forced circulation conditions prior to the start of March 2004. These tests were completed under a variety of operating pressures, boiling levels, circulation speeds, heat fluxes or tube wall temperatures and tube lengths. The operating conditions are summarised in table 6-2. A summary of operating parameters and measured values averaged over each of the forced circulation trials are included in Appendix G.

Table 6-2 Summary of operating conditions for the forced circulation trials (configuration 3).

Date	Trial	Wall temperature, °C	Heat flux, kW	Average circulation, m.s ⁻¹	Tube length, mm	Headspace pressure, kPa	Boiling level above tube, mm
11/11/03	1	90.0	15.0	0.07	1300	17.0	580
11/11/03	2	90.3	15.0	0.14	1300	16.8	585
11/11/03	3	91.5	15.0	0.29	1300	16.9	585
11/11/03	4	97.1	18.0	0.29	1300	18.6	550
11/11/03	5	97.4	18.0	0.14	1300	18.7	530
11/11/03	6	98.1	18.0	0.07	1300	19.1	490
12/11/03	7	103.7	14.4	0.07	1040	18.2	560
12/11/03	8	103.2	14.4	0.14	1040	18.4	560
12/11/03	9	102.9	14.4	0.29	1040	19.1	575
12/11/03	10	102.4	15.0	0.29	1300	23.2	575
12/11/03	11	101.9	15.0	0.14	1300	23.1	565
12/11/03	12	102.3	15.0	0.07	1300	23.2	520
12/11/03	13	105.1	18.0	0.07	1300	24.1	500
12/11/03	14	105.1	18.0	0.14	1300	24.3	525
12/11/03	15	105.0	18.0	0.29	1300	24.1	535
12/11/03	16	105.1	18.0	0.43	1300	24.2	540
04/02/04	17	96.9	15.0	0.39	1300	16.4	600
04/02/04	18	102.0	15.0	0.09	1300	16.8	550
04/02/04	19	104.1	15.0	0.19	1300	14.5	550
04/02/04	20	103.8	15.0	0.10	1300	16.9	540
04/02/04	21	108.4	18.0	0.10	1300	18.8	525
04/02/04	22	110.2	18.0	0.19	1300	19.2	550
04/02/04	23	97.2	18.0	0.39	1300	19.2	620
04/02/04	24	101.2	12.0	0.20	1040	15.7	820
04/02/04	25	103.9	12.0	0.10	1040	15.6	790
04/02/04	26	101.3	12.0	0.10	1040	15.5	550
04/02/04	27	100.5	12.0	0.20	1040	15.4	580
05/02/04	28	105.9	15.0	0.10	1300	15.5	500
05/02/04	29	106.4	15.0	0.16	1300	15.3	560
05/02/04	30	115.2	15.0	0.05	1300	15.2	320
05/02/04	31	107.2	15.0	0.35	1300	16.2	1050
05/02/04	32	105.4	17.0	0.19	1300	17.3	580
17/02/04	33	92.1	15.1	0.15	1300	15.2	610
17/02/04	34	91.9	15.1	0.30	1300	15.4	620
17/02/04	35	97.8	18.0	0.30	1300	16.7	620
17/02/04	36	98.8	18.0	0.15	1300	16.6	590
17/02/04	37	97.5	14.4	0.15	1040	14.5	610
17/02/04	38	94.7	14.4	0.30	1040	14.1	630
17/02/04	39	92.2	10.8	0.30	780	12.2	630
17/02/04	40	93.1	10.6	0.15	780	12.1	630
17/02/04	41	98.4	15.0	0.15	1300	13.9	520
17/02/04	42	97.6	15.0	0.30	1300	14.9	510
18/02/04	43	102.1	18.0	0.30	1300	16.8	390
18/02/04	44	103.4	18.0	0.20	1300	16.8	360
18/02/04	45	103.4	18.0	0.10	1300	16.8	330

18/02/04	46	100.7	14.4	0.10	1040	14.7	370
18/02/04	47	97.0	14.4	0.20	1040	15.0	450
18/02/04	48	99.7	15.0	0.20	1300	14.8	350
18/02/04	49	98.3	15.0	0.10	1300	14.6	290
18/02/04	50	99.5	15.0	0.30	1300	14.9	380
19/02/04	51	96.9	15.0	0.10	1300	15.3	640
19/02/04	52	96.7	15.0	0.20	1300	15.5	745
24/02/04	53	99.8	15.0	0.20	1300	14.2	550
24/02/04	54	99.1	15.0	0.10	1300	14.4	540
24/02/04	55	97.0	15.0	0.30	1300	14.6	560
25/02/04	56	102.0	15.8	0.10	1300	15.9	500
25/02/04	57	101.8	15.5	0.30	1300	15.9	510
25/02/04	58	101.4	14.7	0.20	1300	15.6	480
25/02/04	59	105.0	15.2	0.20	1300	16.0	450
25/02/04	60	107.7	18.0	0.20	1300	16.3	480
25/02/04	61	108.8	18.0	0.30	1300	16.6	500
25/02/04	62	104.2	14.4	0.30	1040	14.5	550
25/02/04	63	103.9	14.4	0.20	1040	14.3	535
25/02/04	64	101.8	10.8	0.20	780	12.6	540
26/02/04	65	100.0	15.0	0.20	1300	14.8	500
26/02/04	66	99.9	15.0	0.30	1300	14.8	515
26/02/04	67	100.6	15.0	0.10	1300	14.7	495
26/02/04	68	105.5	18.0	0.10	1300	16.2	480
26/02/04	69	105.0	18.0	0.30	1300	16.6	490
26/02/04	70	104.7	18.0	0.30	1300	16.8	580
26/02/04	71	105.1	18.0	0.20	1300	16.6	540
26/02/04	72	101.3	15.0	0.20	1300	14.7	530
26/02/04	73	101.5	15.0	0.30	1300	14.9	560
26/02/04	74	102.8	12.0	0.30	1040	13.4	840
26/02/04	75	103.0	12.0	0.20	1040	13.1	805

6.3 Sample analysis

Sample mixtures were analysed for dry substance, purity, brix and viscosity using similar methods to the factory trials, as reported in section 3.6. A summary of the sample analyses are reported in table 6-3. Other fluid properties such as density, surface tension, latent heat, specific heat capacity and thermal conductivity were calculated based on the correlation equations detailed in section 2.4. Properties of the vapour produced during the boiling process were also evaluated at the operating pressure in the headspace of the header tank. The properties of the mixtures are required as inputs for the numerical models.

Table 6-3 Analyses of the sample mixtures used in the experimental boiling trials.

Sample	Date	Dry substance, %	Purity, %	Brix, %	Viscosity measured at a shear rate of 1 s^{-1} , Pa.s	Boiling rig configuration
1	11/11/03	72.5	79.2	72.8	0.38	3
2	12/11/03	73.9	77.4	73.8	1.55	3
3	12/11/03	72.4	78.5	74.6	0.31	3
4	04/02/04	79.6	68.2	81.7	1.01	3
5	05/02/04	86.2	77.3	79.9	4.02	3
6	17/02/04	75.8	73.5	78.2	0.37	3
7	17/02/04	71.1	73.7	73.0	0.09	3
8	18/02/04	79.7	80.4	80.7	4.46	3
9	18/02/04	78.5	78.2	79.7	1.24	3
10	19/02/04	74.2	80.5	74.0	-	3
11	19/02/04	71.7	66.2	73.6	0.16	3
12	24/02/04	73.9	66.8	75.8	0.43	3
13	25/02/04	79.5	66.6	81.6	0.76	3
14	25/02/04	79.1	66.3	81.2	0.66	3
15	26/02/04	77.4	71.9	79.9	0.13	3
16	26/02/04	84.1	76.3	83.2	2.13	3
17	26/02/04	81.5	71.7	83.5	0.50	3
18	26/02/04	82.0	76.5	-	-	3
19	29/04/04	75.5	72.2	77.1	-	2
20	29/04/04	80.3	72.8	82.1	1.22	2
21	29/04/04	84.1	72.4	86.0	2.91	2
22	26/05/04	67.4	75.9	70.2	-	1
23	26/05/04	80.1	76.2	82.6	1.87	1
24	27/05/04	75.2	76.2	-	-	1
25	27/05/04	77.7	76.7	79.9	0.30	1
26	27/05/04	82.2	76.8	85.4	1.90	1

6.4 Summary of results

Selected results of the boiling trials are summarised in tables 6-4 and 6-5 for the natural and forced circulation trials respectively.

Table 6-4 Summary of the results and average operating conditions for the natural circulation trials (configurations 1 and 2).

Trial	Average mass flow, kg.s ⁻¹	Boiling level above tube, mm	Headspace pressure, kPa	Heat flux in heating bands, kW	Heat flux in heat exchanger, kW	Vapour volume fraction at tube outlet, %	Pressure difference over heated tube, kPa
Circulation measured by hot film anemometer (configuration 2)							
1n	0.42	750	15.5	15.0	14.0	5.0	13.6
2n	0.50	720	17.5	18.0	15.1	4.2	13.8
3n	0.05	960	15.2	14.4	12.9	4.1	10.4
4n	0.17	590	14.7	15.0	12.5	4.8	14.1
5n	0.33	585	16.9	18.0	15.2	6.1	14.1
6n	0.50	620	22.7	18.0	15.3	7.4	14.5
7n	0.52	370	16.6	18.0	15.0	53.1	14.0
8n	0.23	360	13.2	15.0	11.2	27.3	13.7
Circulation measured by magnetic flowmeter (configuration 1)							
9n	0.30	1180	15.0	12.0	11.3	7.6	10.2
10n	0.60	880	18.8	18.0	15.3	9.4	13.8
11n	0.37	1050	16.5	14.4	13.0	13.0	10.5
12n	0.36	810	15.5	15.0	12.4	5.7	13.6
13n	0.54	1050	14.0	18.0	15.5	12.1	13.7
14n	0.15	930	12.0	9.0	9.0	11.2	6.9
15n	0.13	900	13.0	10.66	9.3	9.9	10.5

Table 6-5 Summary of the results and operating conditions for the forced circulation trials (configuration 3).

Trial	Average mass flow, kg.s ⁻¹	Boiling level above tube, mm	Headspace pressure, kPa	Heat flux in heating bands, kW	Heat flux * in heat exchanger, kW	Vapour volume fraction at tube outlet, %	Pressure difference over heated tube, kPa
1	0.80	580	17.0	15.0	12.0	4.1	10.8
2	1.58	580	17.0	15.0	12.2	3.1	11.0
3	3.18	585	16.8	15.0	12.7	2.5	11.2
4	3.18	585	16.9	18.0	14.5	2.4	11.3
5	1.59	550	18.6	18.0	14.5	-	11.0
6	0.79	530	18.7	18.0	14.3	6.2	10.9
7	0.79	490	19.1	14.4	12.3	2.3	7.8
8	1.59	560	18.2	14.4	12.7	2.4	7.8
9	3.20	560	18.4	14.4	12.5	1.6	7.9
10	3.18	575	19.1	15.0	13.0	2.3	11.6
11	1.58	575	23.2	15.0	12.9	2.2	11.4
12	0.81	565	23.1	15.0	13.0	3.6	11.4
13	0.81	520	23.2	18.0	15.3	12.5	11.4
14	1.60	500	24.1	18.0	15.6	3.1	11.3
15	3.20	525	24.3	18.0	15.3	2.3	11.4
16	4.80	535	24.1	18.0	15.5	1.8	11.6
17	4.41	540	24.2	15.0	12.2	-	13.5
18	1.02	600	16.4	15.0	12.7	3.1	13.8
19	2.21	550	16.8	15.0	13.0	1.8	14.1
20	1.10	550	14.5	15.0	12.9	3.4	13.9
21	1.10	540	16.9	18.0	15.0	7.5	13.9

22	2.20	525	18.8	18.0	15.3	4.9	14.1
23	4.42	550	19.2	18.0	15.2	1.6	14.7
24	2.23	620	19.2	12.0	10.9	2.0	10.6
25	1.10	820	15.7	12.0	10.6	4.9	10.4
26	1.10	790	15.6	12.0	10.6	2.6	10.2
27	2.22	550	15.5	12.0	10.6	2.1	10.4
28	1.13	580	15.4	15.0	12.5	26.0	14.1
29	2.29	500	15.5	15.0	12.1	33.3	14.6
30	0.60	560	15.3	15.0	12.1	53.4	13.3
31	4.13	320	15.2	15.0	13.2	27.5	18.9
32	2.28	1050	16.2	17.0	13.5	6.7	14.4
33	1.64	580	17.3	15.1	-	0.2	13.5
34	3.28	610	15.2	15.1	-	-	13.7
35	3.28	620	15.4	18.0	-	0.5	13.8
36	1.64	620	16.7	18.0	-	-	13.6
37	1.64	590	16.6	14.4	-	-	10.2
38	3.28	610	14.5	14.4	-	-	10.3
39	3.28	630	14.1	10.8	-	-	6.8
40	1.64	630	12.2	10.6	-	-	6.7
41	1.64	630	12.1	15.0	-	2.0	13.5
42	3.36	520	13.9	15.0	-	1.6	13.5
43	3.42	510	14.9	18.0	-	5.9	14.4
44	2.28	390	16.8	18.0	-	19.5	14.2
45	1.14	360	16.8	18.0	-	16.7	13.9
46	1.14	330	16.8	14.4	-	16.7	10.5
47	2.28	370	14.7	14.4	-	4.7	10.6
48	2.28	450	15.0	15.0	-	4.5	14.2
49	1.14	350	14.8	15.0	-	28.0	13.9
50	3.43	290	14.6	15.0	-	2.8	14.4
51	1.10	380	14.9	15.0	-	-	13.5
52	2.20	640	15.3	15.0	-	-	13.7
53	2.22	745	15.5	15.0	-	0.1	13.7
54	1.11	550	14.2	15.0	-	1.2	13.5
55	3.33	540	14.4	15.0	-	0.9	13.4
56	1.14	560	14.6	15.8	-	-	12.7
57	3.42	500	15.9	15.5	-	-	12.9
58	2.28	510	15.9	14.7	-	4.9	13.2
59	2.28	480	15.6	15.2	-	12.1	10.3
60	2.27	450	16.0	18.0	-	7.2	10.2
61	3.41	480	16.3	18.0	-	6.0	6.5
62	3.41	500	16.6	14.4	-	1.6	12.8
63	2.27	550	14.5	14.4	-	1.8	12.7
64	2.27	535	14.3	10.8	-	-	12.6
65	2.26	540	12.6	15.0	-	1.3	12.6
66	3.38	500	14.8	15.0	-	0.9	12.7
67	1.13	515	14.8	15.0	-	3.4	13.4
68	2.26	495	14.7	18.0	-	3.5	13.1
69	3.38	480	16.2	18.0	-	4.1	13.2
70	3.49	490	16.6	18.0	-	7.6	13.4
71	2.32	580	16.8	18.0	-	5.3	13.1
72	2.32	540	16.6	15.0	-	3.2	13.2
73	3.49	530	14.7	15.0	-	3.1	13.4
74	3.49	560	14.9	12.0	-	2.0	10.2
75	2.32	840	13.4	12.0	-	1.9	9.9

* The acquisition of data for the heat flux in the heat exchanger failed for runs 33 to 75.

6.5 Empirical correlations

In this study the modelling of flow and heat transfer behaviour within the calandria tubes has been simplified to a one-dimensional problem. The one-dimensional model requires empirical data correlations to predict the two-phase flow behaviour of boiling solutions. The data obtained in the boiling trials conducted on the single tube rig have been reduced to dimensionless groups in order to produce empirical correlations for heat transfer and vapour volume fraction. These correlations are only applicable to molasses solutions obtained from Australian sugar factories. Deviations are expected for molasses of differing properties.

6.5.1 Heat transfer

Rouillard (1983, 1985) developed HTC correlations in which the vapour volume fraction data was determined for a situation where the boiling level in the rig was kept level with the top of the calandria tube that were expressed with distinction to the boiling regime within particular regions of a heated tube (equations 4.9 and 4.10). In Rouillard's experimental work the fluid was drained from the header tank to a positive displacement pump and no build up of fluid was allowed to occur in the header tank. These conditions do not mimic factory pans.

For the trials conducted on the single boiling tube rig at JCU, the level in the header tank was kept between 300 mm and 1200 mm above the top of the calandria tube. This significantly changes the boiling characteristics within the tube (and expected vapour volume fraction exiting the tube, which was up to 80% in Rouillard's experimental work) and the empirical correlations used to describe the heat transfer in the heated tube. As such the data for all the boiling trials conducted at JCU were evaluated under sub-cooled conditions only, which is in contrast to Rouillard's experiments where the majority of the trials were conducted under saturated boiling conditions. Measurements of the temperature of the molasses exiting the calandria confirm that the heat transfer occurring within the heated tube was sub-cooled for all the boiling trials conducted at JCU.

HTC correlations were developed for the data obtained from the single calandria tube rig using equations 4.3 and 4.8. Regression was performed on grouped data from the boiling trials for the three different boiling rig configurations to determine empirical correlations for HTCs. Correlations were determined for both rig configurations allowing natural circulation as well as a combined correlation for both configuration 1 and 2.

The temperature and pressure used to calculate dimensionless parameters were based on the average temperature of the liquid in the heated tube. The vapour properties were calculated at the saturation temperature of the liquid in the heated tube. For all the natural circulation trials, the form of equation 4.3 was found to be,

$$Nu_{TP} = 4404.2 [Re_{TP}]^{0.018} [Pr]^{-0.026} \left[\frac{\rho_{liq}}{\rho_{vap}} \right]^{-0.203} \left[\frac{D}{L_T} \right]^{0.56} \quad (6.1)$$

A coefficient of determination (R-squared value) of 0.78 was obtained for equation 6.1 from the 15 sets of data. In most cases, a strong interaction was found between the Prandtl and Reynolds numbers due to the dominant effect of viscosity. Unfortunately experiments were only conducted on a heated tube of single diameter.

Determination of the F-statistic test for the data above at a confidence level of 95% found the correlation equation 6.1 to be statistically insignificant, however at the 90% confidence level the correlation becomes significant.

For all the natural circulation trials, the form of equation 4.8 was also found to be,

$$Nu_{TP} = 248.7 [Re_{TP}]^{-0.038} [Pr]^{-0.036} \left[\frac{\rho_{liq}}{\rho_{vap}} \right]^{-0.064} \left[\frac{\sigma_{liq}}{p D} \right]^{-0.310} \quad (6.2)$$

An R-squared value of 0.52 was obtained for equation 6.2 for the 15 sets of data. The F-statistic test found the correlation for the all the natural circulation data used to determine equation 6.2 to be statistically insignificant at a 90% confidence level.

For the natural circulation trials where the anemometer was used to measure circulation within the rig (configuration 2), the form of equation 4.3 was found to be,

$$Nu_{TP} = 1914.3 [Re_{TP}]^{0.096} [Pr]^{0.082} \left[\frac{\rho_{liq}}{\rho_{vap}} \right]^{0.026} \left[\frac{D}{L_T} \right]^{1.453} \quad (6.3)$$

An R-squared value of 0.80 was obtained for equation 6.3 for the 8 sets of data. The F-statistic test found the correlation for equation 6.3 to be statistically insignificant at a 90% confidence level. For these natural circulation trials, the form of equation 4.8 was also found to be,

$$Nu_{TP} = 698875.8 [Re_{TP}]^{-0.079} [Pr]^{-0.235} \left[\frac{\rho_{liq}}{\rho_{vap}} \right]^{-0.596} \left[\frac{\sigma_{liq}}{p D} \right]^{0.827} \quad (6.4)$$

An R-squared value of 0.72 was obtained for equation 6.4 for the 8 sets of data. The F-statistic test found the correlation for equation 6.4 to be statistically insignificant at a 90% confidence level.

For the natural circulation trials where the magnetic flowmeter was used to measure circulation within the rig (configuration 1), the form of equation 4.3 was found to be,

$$Nu_{TP} = 2837.9 [Re_{TP}]^{0.163} [Pr]^{0.160} \left[\frac{\rho_{liq}}{\rho_{vap}} \right]^{-0.274} \left[\frac{D}{L_T} \right]^{0.841} \quad (6.5)$$

An R-squared value of 0.99 was obtained for equation 6.5 for the 7 sets of data. The F-statistic test found the correlation for equation 6.5 to be statistically significant at a 95% confidence level. For these natural circulation trials, the form of equation 4.8 was also found to be,

$$Nu_{TP} = 337.3 [Re_{TP}]^{0.056} [Pr]^{0.173} \left[\frac{\rho_{liq}}{\rho_{vap}} \right]^{-0.295} \left[\frac{\sigma_{liq}}{p D} \right]^{-0.253} \quad (6.6)$$

An R-squared value of 0.56 was obtained for equation 6.6 for the 7 sets of data. The F-statistic test found the correlation for equation 6.6 to be statistically insignificant at a 90% confidence level.

The correlations determined in equations 6.1 to 6.6 are shown graphically in figure 6-1 against the measured data for the natural circulation trials. The average error is $\pm 4.5\%$ with the maximum error of 13.2%.

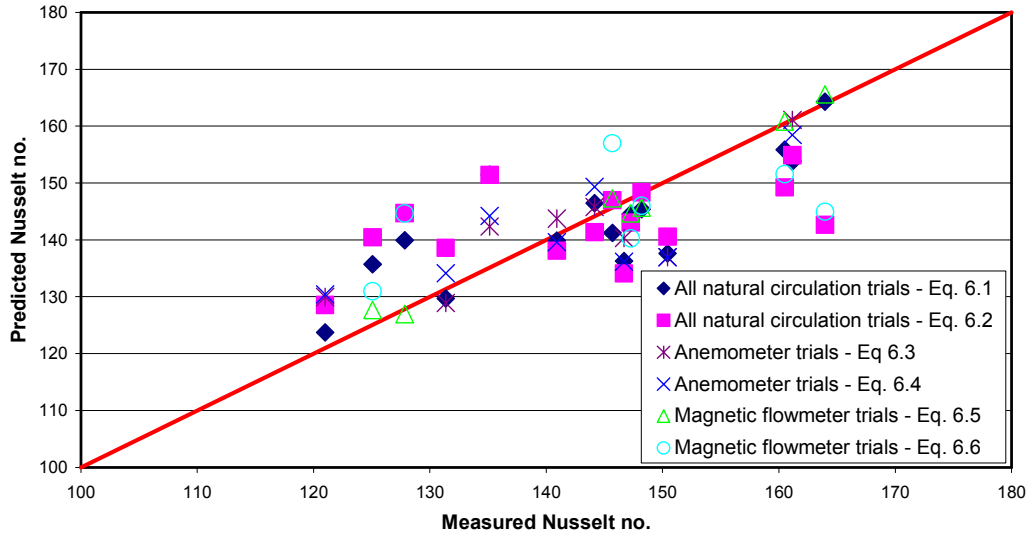


Figure 6-1 Heat transfer correlation for the natural circulation trials.

For the entire forced circulation trials, the form of equation 4.3 was found to be,

$$Nu_{TP} = 8.56 [Re_{TP}]^{0.0534} [Pr]^{0.0573} \left[\frac{\rho_{liq}}{\rho_{vap}} \right]^{0.475} \left[\frac{D}{L_T} \right]^{0.514} \quad (6.7)$$

An R-squared value of 0.60 was obtained for equation 6.7 for the 62 sets of data (13 sets of data were not used due to a lack of vapour volume fraction data). Even though the R-squared value is reasonably low, the F-statistic test found the correlation for the all the forced circulation data used to determine equation 6.7 to be statistically significant at a 95% confidence level.

For the forced circulation trials, the form of equation 4.8 was found to be,

$$Nu_{TP} = [Re_{TP}]^{0.0512} [Pr]^{0.054} \left[\frac{\rho_{liq}}{\rho_{vap}} \right]^{0.610} \left[\frac{\sigma_{liq}}{p D} \right]^{0.0608} \quad (6.8)$$

An R-squared value of 0.47 was obtained for equation 6.8 for the 62 sets of data (13 sets of data were not used due to a lack of vapour volume fraction data). The F-statistic test found the correlation for the all the forced circulation data used to determine equation 6.8 to be statistically significant at a 95% confidence level.

The correlations determined in equations 6.7 and 6.8 are shown graphically in figure 6-2 against the measured data for the forced circulation trials. The average error is $\pm 6.8\%$ with the maximum error of 20.8%. The data illustrated in figure 6-2 show that the empirical correlations over-predict the HTC at lower values and under-predict at higher values. This general trend is also evident in figure 6-1 for the natural circulation trials. However, a smaller range of HTCs were obtained due to the restricted number of trials conducted using the rig configured for only natural circulation.

Other than the extended range of HTC values obtained in the forced circulation boiling trials there were limited differences to the correlations determined for the natural circulation boiling trials.

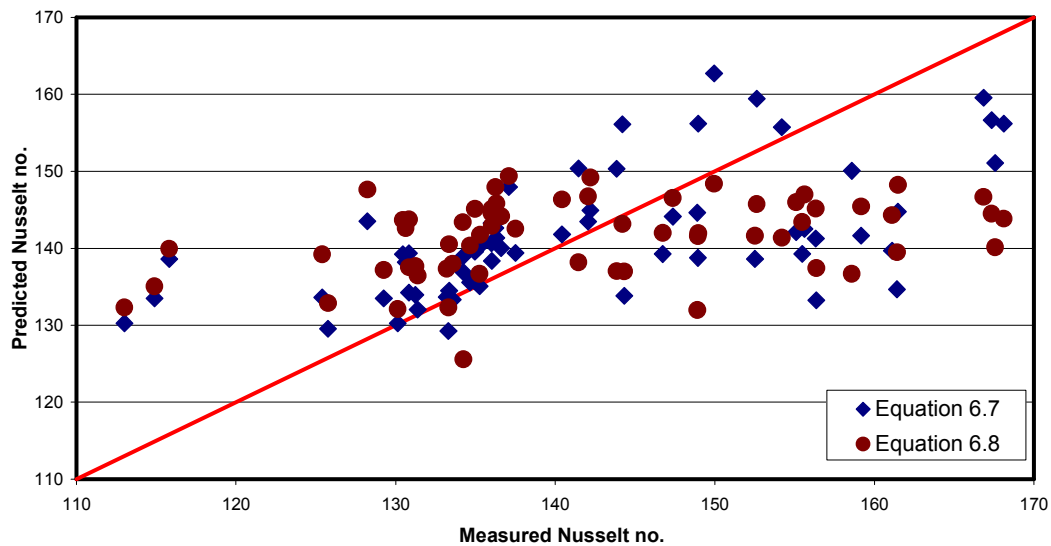


Figure 6-2 Heat transfer correlation for the forced circulation trials.

Caution should be used in applying equations 6.1 to 6.8 to different tube geometries (*i.e.*, tube diameter) as data only for a single tube diameter were used to develop the correlations. The low R-squared values and lack of statistical significance shown by the F-statistic test for the determination of equations 6.1 to 6.8 highlight the deficiencies in these correlation equations. Further work is required to improve the applicability of such empirical correlations to laboratory and factory data. Care should also be exercised applying the HTC correlations to alternative tube surfaces because different liquid-tube surface combinations have different nucleation properties and hence will produce different HTCs (Incropera and DeWitt, 1996). The empirical correlations are also specific to the molasses samples taken from Australian Sugar factories so these correlations will probably not produce accurate predictions for other test liquids.

As an alternative to Rouillards's representation of Nu_{TP} , Incropera and DeWitt (1996) expressed Nu_{TP} in the form;

$$Nu_{TP} = f \left\{ \left[\frac{g (\rho_{liq} - \rho_{vap}) D^3}{\mu_{liq}^2} \right], [Ja], [Pr], [Bo] \right\} \quad (6.9)$$

where Ja is the non-dimensional Jacob number, and
 Bo is the non-dimensional Bond number.

and

$$Ja = \frac{C_{p,liq} \Delta T}{\lambda_{liq}} \quad (6.10)$$

$$Bo = \frac{g (\rho_{liq} - \rho_{vap}) D^2}{\sigma_{liq}} \quad (6.11)$$

where ΔT is the temperature difference between the tube wall and liquid (°C).

The Jacob number is used to describe the ratio of sensible to latent energy absorbed during liquid-vapour phase change and the Bond number is used to describe the ratio of gravitational and surface tension forces (Incropera and DeWitt, 1996).

Fitting regressions to the experimental data came up with excessively large or small values for the coefficient (*i.e.*, 10^{44} or 10^{-41}) and so this form of correlation was disregarded.

6.5.2 Vapour distribution

The vapour rise velocity was evaluated according to Zuber and Findlay (1965) from equation 4.24 and found to be approximately 0.4 m.s^{-1} for all the boiling trials, with limited variation under the different conditions. This equation was developed for the up flow of small vapour bubbles and does not account for coalescence and other multi-bubble effects or the constraining effects of the tube wall. The rise time and flow patterns of bubbles with diameters greater than 12.5% of the tube diameter (*i.e.*, $>12.5 \text{ mm}$) can be hindered by the wall effects (Krishna *et al.*, 1999). However, neither visual observations nor instrument measurements were able to validate the hydrodynamic effects on the bubbles that occur within the heated tube.

The bubble rise velocity is dependent on the drag forces acting on the individual bubbles, which in turn are dependent on the size of the actual bubbles. The calculation of the vapour rise velocity in equation 4.24 is independent of the bubble size. While the independence of bubble diameter makes the calculation of vapour rise velocity simpler, it may not reflect the hydrodynamic effects existing in the heated tube. Additionally, the bubble rise velocity calculated in equation 4.24 has no dependence on viscosity which has a strong influence on the drag forces. This also suggests that equation 4.24 will not capture the hydrodynamic effects existing in the heated tube.

For this work, the flow distribution parameter, based on the bubble rise velocity (Nicklin *et al.*, 1962), was calculated at the exit of the heated tube using the correlation equation 4.22. For the natural circulation trials the flow distribution parameter varied from 0.5 to 110 and for the forced circulation trials the flow distribution parameter varied from -15 to 15. The work conducted by Rouillard (1985) assumes the distribution flow parameter remains constant along the length of the sub-cooled boiling region to allow the mass vapour quality to be calculated along the heated tube. This assumption provides the simplification to allow the evaporation to be considered as a steady state phenomenon or as constant along the length of the heated tube. In reality, though, boiling heat transfer is intrinsically unsteady and difficult to characterise, making simplifications necessary for modelling the heat transfer in calandria tubes.

Further examination of Rouillard's (1983, 1985) calculations found that some values were in error by an order of magnitude leading to significant differences in the stated average value for the flow distribution parameter of 1.13 (or 1.3 stated by Rouillard, 1983) in his experimental trials. It is plausible that the air leakage problems experienced in this research may have been inherent and not noticed in Rouillard's experiments with the same detrimental effects on the results produced.

Another approach to determine the vapour distribution in the tube is using the correlation developed by Rouillard (1985) in section 4.5.2. Figure 6-3 shows the prediction for vapour volume fraction exiting the heated tube based on equation 4.18. For the natural circulation trials, the average error is $\pm 25.7\%$ with the maximum error of 87% although an average error of $\pm 11.2\%$ is obtained for the natural circulation trials operating under configuration 1 (magnetic flowmeter used to measure circulation). For the forced circulation trials, the average error is $\pm 92.4\%$ with the maximum error of 710%. The lesser fit of the correlation to the forced circulation data may also be caused or affected by the air leakage problems detailed in sections 5.5.3 and 5.5.4.

These errors and the deviations shown in figure 6-3 show that equation 4.18 was inadequate for predicting the vapour volume fraction in the boiling trials at JCU especially for high vapour volume fraction, as measured at the exit of the calandria tube. Equation 4.18 also does not consider the effect of tube length on the vapour volume fraction which may influence the results. This correlation was disregarded in the numerical modelling of calandria tubes undertaken in this research.

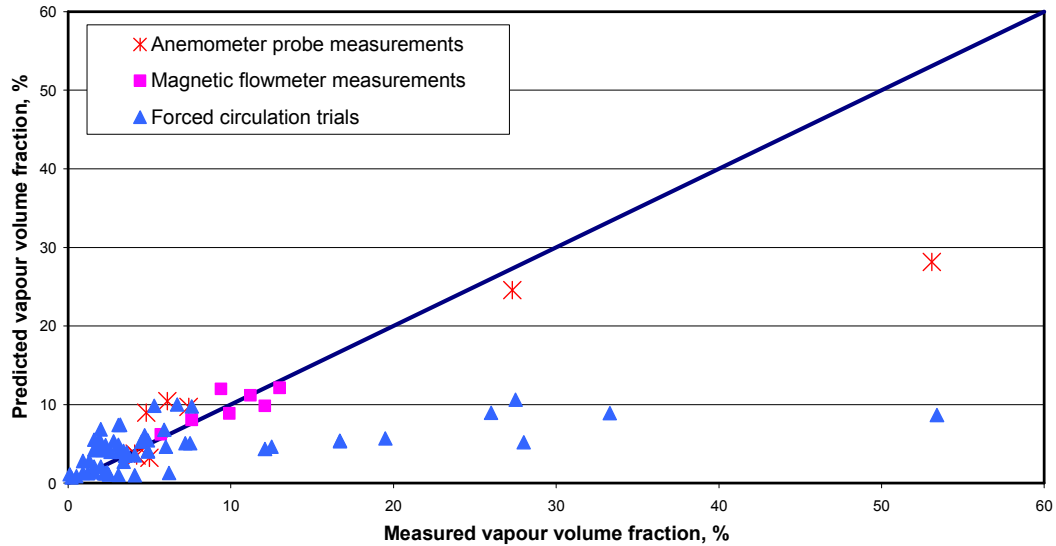


Figure 6-3 Vapour volume fraction correlation for the experimental trials.

6.6 Summary

The experiments conducted on the single calandria tube detailed the physical changes and heat transfer characteristics for boiling in calandria tubes with changing material properties and heat input conditions. Natural and forced circulation conditions were investigated in the experimental trials as both types of circulation are present in factory vacuum pans. The experiments allowed values to be calculated for the flow distribution parameter and allowed fluid specific correlations to be obtained for boiling HTCs and vapour volume fraction in the calandria tubes. The correlations for vapour volume fraction were disregarded due to the large errors in predicting the measured data. The flow distribution parameter was shown to vary significantly for sub-cooled boiling conditions. Significant errors were obtained using correlations for vapour volume fraction based on functional equations reported by Rouillard (1985) when compared to the measured data.

The results achieved with the experimental rig show that with improvements to the apparatus the applicability of a pilot scale rig to provide data can be used to improve the understanding and modelling of flow and heat transfer in the calandria tubes of vacuum pans.

7 MODELLING RESULTS

This chapter compares the experimental data and the predictions produced by one-dimensional tube models. A discussion of the results is provided and the application of numerical modelling to improve the design of vacuum pans is presented.

7.1 Background

Rouillard (1985) developed a numerical model of pan circulation, written in the programming language, Basic. This model simulated the boiling process taking into account the heat transfer, vapour distribution and hydraulic pressure losses. The model calculates the circulation velocity produced in the calandria tubes based on the frictional losses associated with the pan geometry, measured steam flow rates, operating pressure and boiling level. The model also uses a boiling subroutine to calculate the vapour volume fraction, two-phase frictional losses and heat transfer occurring within the calandria tubes. The frictional losses associated with the pan geometry were simplified and lumped into the one-dimensional model. The model is unable to calculate the circulation within the rest of the pan. CFD models are much better adapted to determining circulation patterns within vessels especially when investigating changes to the vessel geometry to analyse pan designs.

Rouillard's model assumes that the energy produced through the boiling process in the tubes is used to overcome the acceleration and frictional losses in the circulation path of the whole vessel. This assumption does not take into account the energy lost in the vapour disengagement of vigorous boiling (see sections 2.1 and 4.2) and so overestimates the circulation velocity produced. Other factors not considered by Rouillard (1985) in his model include the additional driving force caused by the thermal expansion of both the liquid and vapour phases and the condensation of vapour that may occur after the liquid leaves the calandria tubes.

Stephens (2001) also developed a one-dimensional numerical model of calandria tubes using a similar methodology to Rouillard, but in the programming language, Fortran. He coupled the one-dimensional tube model with a CFD model of the rest of the vacuum pan. CFD models are able to account for the additional energy losses and driving forces that were not considered in Rouillard's modelling. The Fortran programming language was compatible with the CFD software used by Stephens. Stephens' CFD models were unable to determine the transient and

non-isothermal effects, but showed that CFD can be used as an alternative tool in simulating the circulation and heat transfer mechanisms to analyse pan geometries.

Stephens' (2001) also investigated using two-dimensional CFD models to predict the boiling behaviour in calandria tubes. Stephens found that the CFD models were unable to adequately model the boiling process, as the boiling subroutines could not model the departure of vapour from the heating surface. Stephens concluded that more knowledge was required on the bubble formation and migration physics and their incorporation into the boiling subroutines as well as the interphase slip between the vapour and liquid phases before two-dimensional tube models could be sufficiently used to model calandria tubes.

The one-dimensional tube model developed by Stephens (2001) was used as the basis for the evaluation and development of numerical models of calandria tubes investigated in this research. Stephens' tube model was preferred over Rouillard's pan circulation model due to its flexibility of application to CFD software and direct simulation of only the calandria tube with no dependence on pan geometry. The numerical tube model was used to predict the characteristics of calandria tube operation that could be compared to the experimental data obtained from the single calandria tube boiling rig.

For added flexibility the Fortran tube model developed by Stephens (2001) was converted to Microsoft Excel Visual Basic to allow implementation in a spreadsheet environment. This allows easier and more transparent processing of the model to enable quicker feedback for development. The new tube model has a more user friendly interface, allowing inputs to be viewed directly and easily changed on a single worksheet. The model processes these inputs to deliver outputs and predictions of the calandria tube behaviour on a separate worksheet. The main Visual Basic code of the one-dimensional tube model is included in Appendix H.

The numerical tube model modified in this research solves only the pressure distribution and energy balance equations for the liquid phase. The flow distribution parameter is used to account for the non-uniform vapour distribution. This allows interfacial transfer equations (lift, drag and other forces) to be disregarded. Superheating (diffusion, viscous heating) effects are also disregarded based on the premise of thermodynamic equilibrium.

The model procedure is iterative and is summarised as follows;

1. Initially set the fluid properties (density and viscosity of the fluid and vapour phases, surface tension, heat capacity, thermal conductivity of the fluid and wall). These properties have been detailed in Chapter 2 and also require measurements of dry substance, purity and brix as well as the operating pressure and temperature which were measured during the experimental trials.
2. Set the operating conditions (operating pressure and static level in the header tank, mass flow rate circulating through the calandria tube and inlet temperature of the fluid) and tube geometry (tube diameter and length). These independent variables are based on measured parameters from the experimental data.
3. Determine a pressure distribution profile based on no boiling (*i.e.*, hydrostatic pressure only) and the corresponding saturation temperature profile.
4. Calculate heat transfer parameters based on the empirical correlations determined from experimental boiling trials. The HTC correlations in section 6.5.1 were used (namely equation 6.1, 6.3 and 6.5 depending on the rig configuration).
5. Determine the point of nucleation/boiling or amount of sub-cooling from the average radial temperature, based on boundary layer thickness, bubble dynamics and mass flow rate (using equation 4.1).
6. After the initiation of boiling, the pressure distribution will change and the heat transfer is broken into sensible heating and evaporation to determine a temperature distribution along the length of the tube. A heat balance is used to determine the vapour quality. Using a correlation for the flow distribution parameter (Equation 4.22) the vapour volume fraction profile can then be calculated.
7. The contributions to the pressure distribution are then determined. This involves calculating the pressure change due to gravity, acceleration (accounts for both phases) and friction (based on a weighted combination of the liquid and vapour phases).
8. Calculate the new pressure distribution. The pressure distribution is then refined (iterated until a specified tolerance is satisfied) before the model is solved for saturation temperature distribution due to its dependence on the pressure distribution.

7.2 Validation against experimental data

The numerical tube model was assessed by making comparisons between the measured experimental data and the predicted values calculated by the model of the boiling behaviour in a calandria tube. Comparisons between the predicted values and experimental data were made for the vapour volume fraction profile at the exit of the heated calandria tube, the net pressure driving force and the total heat transferred to the solution. The net pressure driving force is the

measured pressure difference across the calandria tube relative to the hydrostatic pressure in the calandria tube evaluated for liquid only. A summary of the comparison of specific parameters for arbitrarily selected trials are detailed in table 7-1.

Table 7-1 Comparisons between the experimental data and predicted values for the single calandria tube boiling trials.

Trial	Mass flow rate, kg.s ⁻¹	Measured net pressure driving force, kPa	Predicted net pressure driving force, kPa	Measured heat flux, kW	Predicted heat flux, kW	Measured vapour volume fraction, %	Predicted vapour volume fraction, %
Natural circulation trials							
3n	0.05	0.01	0.48	12.9	12.6	4.1	7.2
7n	0.52	0.90	1.22	11.2	11.8	32.5	34.3
12n	0.36	0.41	1.40	12.4	12.1	5.7	15.4
Forced circulation trials							
13	0.81	2.51	2.40	15.3	16.5	12.5	19.4
29	2.29	-0.03	-3.33	12.1	12.8	33.3	62.4
45	1.14	0.26	0.38	15.3	15.3	16.7	17.6
73	3.49	1.01	1.44	12.8	13.3	3.1	67.5

The comparisons between the predicted values and measured experimental data highlight the difficulties in depicting the two or three-dimensional mechanisms in a one-dimensional model. The numerical tube model reasonably predicts the heat transfer for both the natural and forced circulation trials. This is expected as the HTC correlations were determined from the experimental data and showed reasonable agreement to the measured values (see section 6.5.1). The numerical tube model had less success predicting the net pressure driving force. This is compounded by the fact that the numerical tube model predicts excess vapour volume fraction at the exit of the calandria tube. The increase in vapour volume fraction strongly influences the predicted pressure driving force as the additional vapour produced at the start of the tube produces a greater net pressure driving force.

The measured net pressure driving force ranges from -4 kPa to 3 kPa for all the boiling trials conducted in this research. This is substantially less than the net pressure driving force measured by Rouillard (1985). Rouillard (1985) measured net pressure driving forces of greater than 10 kPa for some of his boiling trials. The large pressure driving forces in Rouillard’s trials result from operation with no static level above the calandria tube, which are not representative of the conditions found in factory pans. The boiling trials in this research were conducted with a

static level of 300 mm to 1200 mm. The static boiling level suppresses the boiling within the tube and thus reduces the pressure driving force.

The flow distribution parameter has a large influence on the vapour volume fraction exiting the calandria tube and a lesser influence on the predicted heat transfer. Rouillard used a constant value for the flow distribution parameter in his modelling simulations. In this research, the flow distribution parameter varied between trials and the value calculated for the specific boiling run was used in these simulations

The largest factor influencing the heat transfer is the point at which boiling is initiated. In the simulations, the model uses an estimated bubble size of 2 mm to determine the point of nucleation (using equation 4.1). Prior to the onset of boiling, the HTC is calculated based on correlations given by Stephens (2001) for single-phase heat convection developing flows rather than the fully developed single-phase heat transfer coefficients given in equation 4.21 by Incropera and DeWitt (1996).

Further development of the numerical tube model is required to more accurately predict the boiling characteristics occurring within the calandria tube. The one-dimensional model had difficulty predicting the measured vapour volume fraction exiting the heated tube due to the following reasons;

- The vapour distribution effects occurring within the tube were evaluated using the heat flux and flow distribution parameter. While the tube model predicted the heat flux reasonably well, the flow distribution parameter is prone to errors as it uses a correlation for the bubble rise velocity. Reducing the solution viscosity should allow the vapour bubbles to rise more rapidly as lower drag is experienced by the bubbles, however this is not reflected in the vapour rise velocity correlation (equation 4.24) or in the flow distribution parameter. Due to these reasons, the correlation for bubble rise velocity may be unsuitable for the determination of the flow distribution parameter.
- The incorporation of a pump in the recirculation leg of the boiling rig represents a source of air leakage into the rig, which was not taken into account. The problem results from the fact that the air is humidified by the vapour produced by boiling in the rig and transported to the vacuum source. Possibly additional vapour also exits the system through the vacuum pump as discussed in section 5.5.4. This represents a loss from the system and causes the concentration of the sugar solution to increase slightly. Hence, changes to the physical properties of the fluid occur throughout the trials. The physical

properties were averaged from data collected experimentally and used in the numerical tube model.

- The numerical tube model was developed for the situation where the applied heat flux is calculated from the local heat transfer coefficient and temperature difference along the length of the tube. The average tube wall temperature is used by the numerical tube model to determine the heat flux. The experimental results (section 5.5.5) show that the tube wall temperature is non-uniform along the length of the tube. A significant drop in temperature is observed towards the top of the tube due to the production of vapour within the tube. The non-uniform tube wall temperature will lead to non-uniform heat flux and influence the production of vapour.
- The liquid and vapour properties also change along the vertical length of the heated tube as the temperature and static pressure change and the amount of vapour increases. The average liquid and vapour properties are used as inputs in the numerical tube model with no dependence on the vertical level within the tube.
- The model disregards superheating effects (other than the boiling point elevation) for the sake of simplification. The amount of heat taken up as superheat is expected to be minimal as the single phase heating component is significantly lower than the heat required for evaporation. If some of the heating is required to superheat the liquid or vapour it would slightly reduce the overall amount of vapour generated.

Overall the numerical tube model is capable of predicting the boiling characteristics in calandria tube in terms of heat transfer. The prediction of vapour volume fraction profiles is poor, and the vapour volume fraction has a strong influence on the net pressure driving force. Even though the numerical tube model can not accurately predict the vapour volume fraction exiting the tube, the model can be used to evaluate trends in modelling the calandria tube behaviour under varying operating conditions.

7.2.1 Slip ratio for the determination of vapour distribution

The difference in velocity of the liquid and vapour phases is often called the slip velocity. The distinguishing factor between the natural circulation and forced circulation trials is the much lower mass flow rates in the calandria tube for the natural circulation trials. The mass flow rate influences the relative motion of the vapour to the liquid phase especially if the rise velocity of vapour bubbles is much greater than the liquid velocity, which is the case in the natural circulation trials. The average liquid velocity ranged from 0.011 m.s⁻¹ to 0.045 m.s⁻¹ for the natural circulation trials and from 0.051 m.s⁻¹ to 0.388 m.s⁻¹ for the forced circulation trials. The

vapour rise velocity evaluated using equation 4.24 was found to be approximately 0.4 m.s^{-1} for all the boiling trials, with limited variation under the different conditions.

In the development of numerical models of calandria tube behaviour, Stephens (2001) introduces a slip ratio rather than the flow distribution parameter as an alternative means to account for the uneven radial distribution of vapour in the tube. The slip ratio is defined by Stephens (2001) as the ratio of the liquid to vapour phase velocities such that,

$$S = \frac{\bar{u}_{vap}}{\bar{u}_{liq}} = \left(\frac{x}{1-x} \right) \left(\frac{1-\alpha}{\alpha} \right) \left(\frac{\rho_{liq}}{\rho_{vap}} \right) \quad (7.1)$$

where S is the slip ratio,

\bar{u}_{vap} is the average vapour phase velocity (m.s^{-1}),

\bar{u}_{liq} is the average liquid phase velocity (m.s^{-1}),

x is the mixture quality (mass fraction of vapour, See section 4.5.2),

α is the vapour volume fraction,

ρ_{liq} is the liquid density (kg.m^{-3}), and

ρ_{vap} is the density of saturated water vapour (kg.m^{-3}).

The volume fraction equation can then be defined to allow for different average phase velocities (Stephens 2001) to give,

$$\alpha = \frac{1}{\left(1 + S \left(\frac{1-x}{x} \right) \frac{\rho_{vap}}{\rho_{liq}} \right)} \quad (7.2)$$

The slip ratio is not caused by the relative motion between the phases but rather by the non-uniform radial vapour volume fraction profile across the tube. The slip ratio was used by Stephens (2001) to tune his numerical models of calandria tubes to the experimental data provided by Rouillard. The method of using a slip ratio to tune numerical models does not provide additional understanding of the flow characteristics occurring within the heated tube. An empirical correlation for predicting the slip ratio would be an ideal way to model the non-uniform radial distribution of vapour in the tube for sub-cooled boiling conditions, however none exist at present.

The ability to predict the slip ratio or improvements to be able to use a flow distribution parameter are required to determine the non-uniform distribution of vapour effect on the vapour volume fraction exiting the calandria tube. More detailed experiments and numerical modelling on the bubble dynamics and drag effects are required to improve the handling of vapour distribution along the tube length in a numerical tube model.

7.3 Tube performance curves

While the numerical tube model may not accurately predict the vapour volume fraction exiting the tube, the model can be used to determine trends for the performance characteristics of specific tube geometries. Keeping constant fluid properties and operating conditions, the effect of tube geometry can be investigated.

Typically, vacuum pans are designed to provide optimum performance under the worst case operating conditions to ensure productivity is maintained at the highest possible levels. The worst case conditions occur towards the end of the strike when the operating level is highest suppressing the boiling within the calandria tubes and the viscosity of the massecuite increases restricting the circulation in the vessel. As a high-grade massecuite strike progresses, a number of things can be observed that include:

- The hydrostatic boiling level above the calandria tubes increases as does the temperature of the massecuite entering the calandria tubes and the calandria tube wall temperature (higher temperatures are required to provide the temperature driving force for heat transfer). The tube wall temperature increases to a larger extent than the massecuite entering the calandria tubes;
- The viscosity, dry substance, crystal content and crystal size increase;
- A purity decrease may be observed depending on the relative purity of the feed to the seed material;
- The liquid and vapour density increase slightly due to the increase in dry substance and crystal content. The vapour density increases with elevated temperature; and
- The specific heat capacity and latent heat of vaporisation decrease slightly at higher temperatures.

The performance of calandria tubes operating under high-grade massecuite conditions was evaluated with the numerical tube model. Performance curves were generated for typical calandria tube geometries that include:

- Tubes with outside pipe diameters of 101.6 mm, 114.3 mm and 127.0 mm. These diameters correspond to the three main tube sizes (100 NB, 115 NB and 125 NB) used in industry; and
- Tubes lengths of 800 mm, 1000 mm and 1200 mm.

The development of tube performance curves enables a better understanding of the effects of circulation and heat transfer in calandria tubes to be obtained. Table 7-2 shows the average fluid conditions used to represent the end point conditions of a typical high-grade massecuite strike. The numerical tube model was used to predict the net pressure driving force and predicted heat flux for a range of mass flow rates through the single calandria tube for the given fluid properties and operating conditions summarised in table 7-2. These predictions allowed performance curves to be determined for the various tube geometries investigated.

Table 7-2 Typical average fluid properties and operating conditions for high-grade massecuite strikes.

Parameter	End of strike conditions
Boiling level (static height) above tubes, m	1.5
Inlet temperature, °C	68.0
Tube wall temperature, °C	115.0
Liquid density, kg.m ⁻³	1420.0
Liquid viscosity, Pa.s	15.0
Vapour density, kg.m ⁻³	0.189
Dry substance, %	89.0
Purity, %	89.0
Crystal content, % of massecuite	45.0
Crystal size, mm	0.8
Specific heat capacity, J.kg ⁻¹ .K ⁻¹	1643.3
Latent heat of vaporisation, kJ.kg ⁻¹	2338.0

Figures 7-1 to 7-5 show the performance curves for the three tube diameters and tube lengths investigated. The performance curves neglect the effects on circulation caused by flow in the vacuum pan external to the tubes. They do not take into account the negative pressure driving forces caused by the frictional resistance to the flow in the vessel external to the tubes and the

energy losses associated with the vapour disengagement at the free surface nor the positive pressure force gains due to buoyancy caused by thermal density changes in the fluid.

Figures 7-1 and 7-2 show the predicted net pressure driving force plotted against the mass flow rate in the tube. In the experimental trials the average liquid velocity in the calandria tube ranged from 0.011 m.s^{-1} to 0.388 m.s^{-1} which was equivalent to a mass flow rate of 0.05 kg.s^{-1} to 4.42 kg.s^{-1} respectively. At high mass flow rates the plots show that tubes with larger diameters and shorter lengths produce a greater net pressure driving force (lower negative driving force) due to a reduction in the frictional losses within the tube. At a mass flow rate of approximately 0.5 kg.s^{-1} to 1.0 kg.s^{-1} the net pressure driving force reduces to zero. For smaller diameter tubes (*i.e.*, 100 NB) and longer length tubes there is a reduction in the mass flow rate where the net pressure driving force is equal to zero.

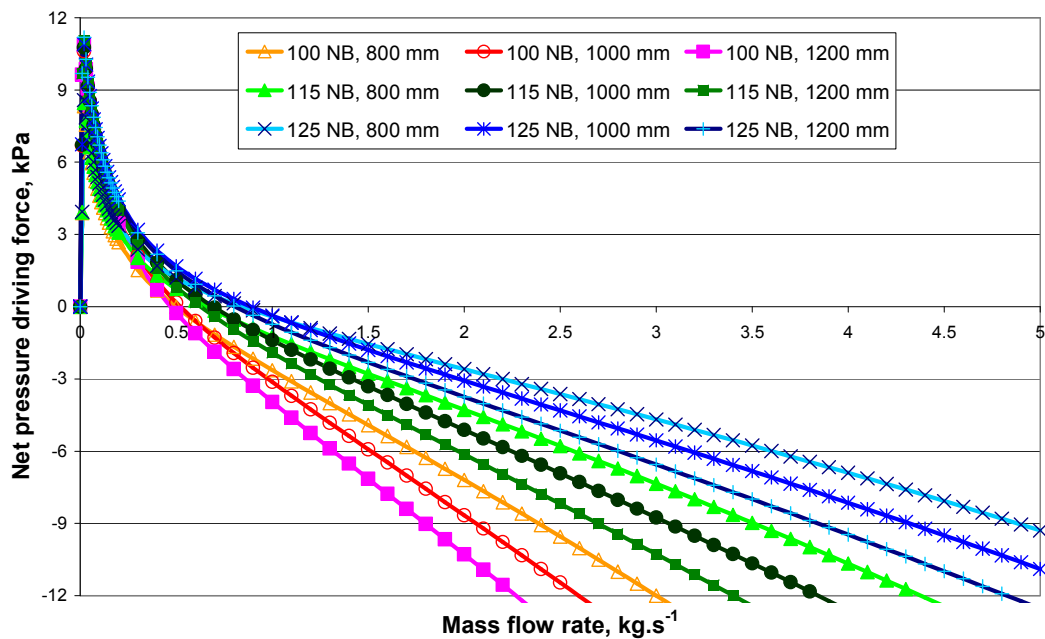


Figure 7-1 Performance curve showing the pressure driving force as a function of mass flow rate through the calandria tube.

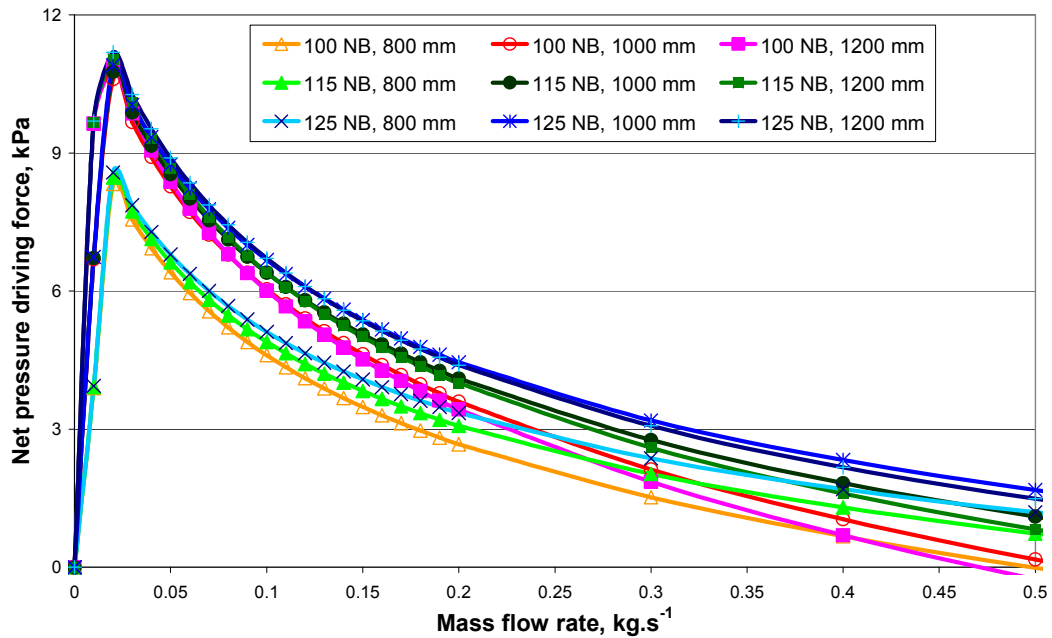


Figure 7-2 Performance curve showing a zoomed section of figure 7-1.

At low mass flow rates ($<0.2 \text{ kg.s}^{-1}$), as depicted more clearly in figure 7-2, the tube performance curves predict greater net pressure driving force is produced by the longer length tubes. There are marginal differences in the 1000 mm and 1200 mm tubes for the various tube diameters. However, the largest net pressure driving force is predicted for the largest tube diameter investigated (125 NB) at low mass flow rates.

The corresponding heat flux provided by the various tube geometries for the conditions summarised in table 7-2 is shown in figure 7-3. For similar length tubes, greater heat flux is produced by tubes of larger diameter. For tubes of similar diameter, greater heat flux is produced by 1000 mm long tubes followed by 1200 mm and then 800 mm long tubes. As only three tube lengths were studied, the optimum tube length may actually be between 800 mm and 1000 mm or 1000 mm and 1200 mm for the given set of fluid properties and operating conditions evaluated. More simulations would be required to determine the optimum tube length.

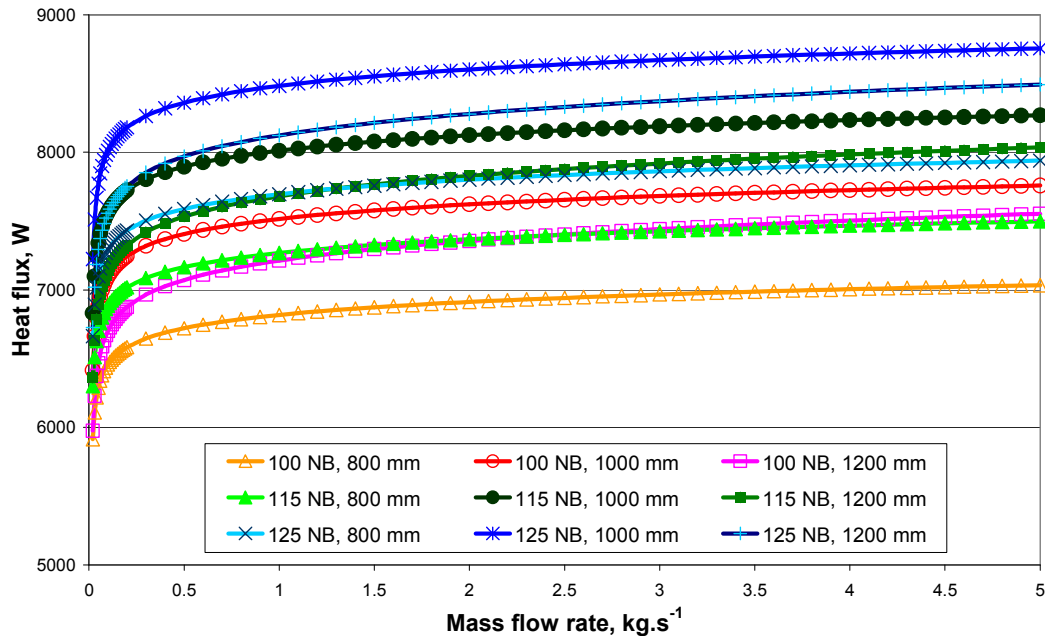


Figure 7-3 Performance curve showing the heat flux as a function of mass flow rate through the calandria tube.

Additional tube lengths could be evaluated using the numerical tube model to determine the optimum length. However, the optimum tube length will change depending on the pan duty and operating conditions. The purpose of using the tube performance curves was to show that a method was available that can be used to determine the optimum tube geometry specification for a given set of operating conditions.

For the same mass flow rate, the average velocity in the tube reduces with increasing tube diameter due to the increase in cross-sectional area. Figures 7-4 and 7-5 show the predicted net pressure driving force plotted against the average circulation velocity in the tube. At high circulation velocities the plots show that tubes with larger diameters and shorter lengths produce a greater net pressure driving force (lower negative driving force) due to a reduction in the frictional losses within the tube. This is similar to the trends shown in figures 7-1 and 7-2. However, figure 7-4 shows that the length of the tube has a greater influence than the diameter on the predicted pressure driving force. This is shown for the case where the tube geometry with a diameter of 114.3 mm and length of 800 mm produces equivalent pressure driving force to a tube geometry with a diameter of 127.0 mm and length of 1000 mm and a lower negative pressure driving force than a tube geometry with a diameter of 127.0 mm and length of 800 mm.

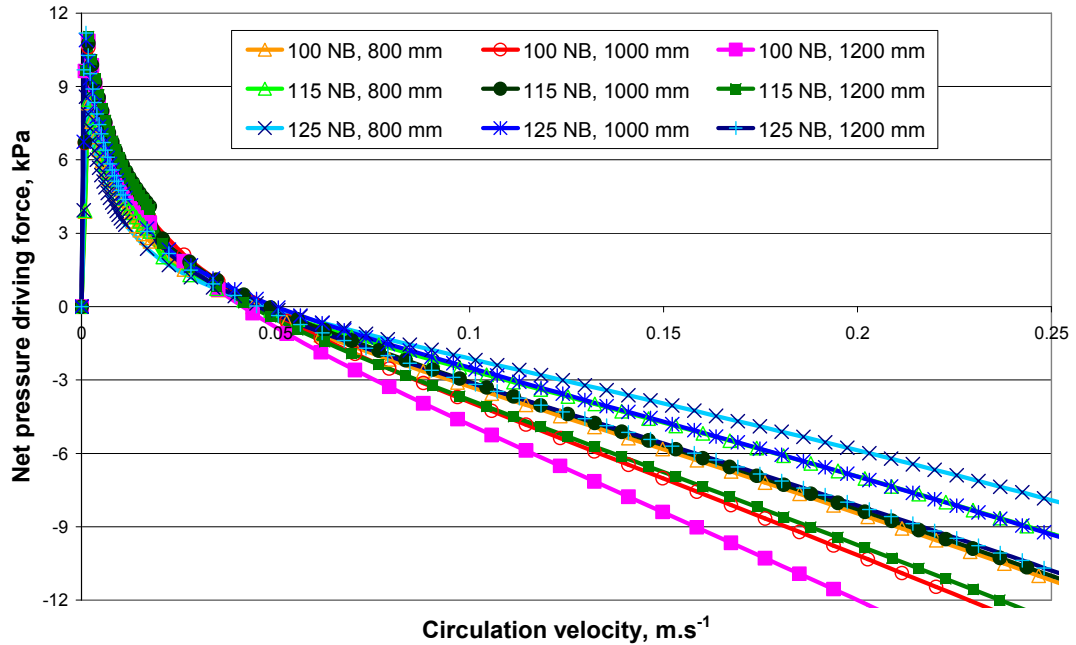


Figure 7-4 Performance curve showing the pressure driving force as a function of average circulation velocity through the calandria tube.

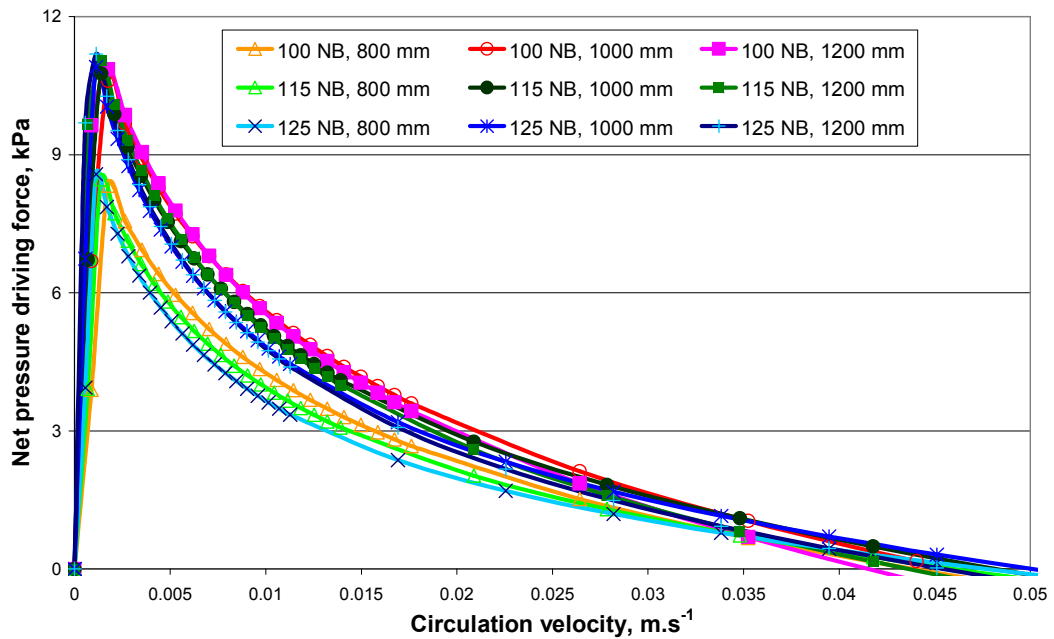


Figure 7-5 Performance curve showing a zoomed section of figure 7-4.

For a velocity of approximately 0.04 m.s^{-1} to 0.05 m.s^{-1} the net pressure driving force reduces to zero. For high-grade massecuite strikes the average circulation velocity is expected to be greater than 0.05 m.s^{-1} (see table 2-1).

Similar to the plots of pressure driving force against mass flow rate, at low circulation velocities ($<0.01 \text{ m.s}^{-1}$), greater net pressure driving force is produced by the longer length tubes. There is marginal difference in the 1000 mm and 1200 mm tubes for the various tube diameters, however in this case the largest net pressure driving force is predicted for the smallest tube diameter investigated (100 NB) as shown in figure 7-5.

The tube performance curves suggest that tubes of large diameter (125 NB) and a length of approximately 1000 mm will produce the greatest circulation (high net pressure driving force) and heat flux based on the mass flow rate through the tubes. However there are issues associated with increasing the tube diameter (Rein *et al.*, 2004). The specification of tube geometry is usually based on a compromise of factors. The arrangement of the tubes in the calandria is important in determining the footing volume and other design ratios. The fraction of volume occupied by the footing material compared to the total volume when the pan is full should be kept low for efficient and productive use of the available pan volume (Hugot, 1972). Normally in pan designs a preferred tube diameter and downtake diameter are selected first and the tube length is calculated to satisfy a determined number of design ratios such as heating surface area to massecuite volume ratio and footing volume fraction.

This can be illustrated by considering the Macknade No. 6 pan design that was investigated in the factory trials reported in chapter 3. The No. 6 pan has a diameter of 5.8 m, a downtake diameter of 2.5 m and the volume when the pan is full is 75 m^3 . In keeping a constant heat transfer area in the calandria of approximately 556 m^2 (includes the top and bottom tube plate area) and constant tube pitch spacing (distance between the outer walls of neighbouring tubes) the following geometries for the three main tube diameters used in industry were determined as follows;

- 1031 calandria tubes, 1285 mm long with an outside diameter of 127.0 mm,
- 1250 calandria tubes, 1180 mm long with an outside diameter of 114.3 mm, and
- 1541 calandria tubes, 1075 mm long with an outside diameter of 101.6 mm.

For the Macknade No. 6 pan design, 1250 tubes, 1180 mm long with an outside diameter of 114.3 mm were selected based on the footing volume provided.

Typically the sugar industry uses larger diameter tubes that are shorter in length for low-grade pan duties to overcome the increase in frictional resistance associated with the heavier, more viscous materials (Tippens, 1972). While high-grade pans typically utilise smaller diameter tubes that are longer (Rein *et al.*, 2004), in Australia pan designs normally employ tube diameters of 114.3 mm to 127.0 mm and tube lengths of approximately 990 mm to 1200 mm (Wright, 1966).

While it was stated that the tube performance curves can be used to determine an optimum tube geometry specification for a given set of operating conditions in the tubes, it should be noted that the numerical tube model by itself can not be used to determine the optimum tube geometry for the maximal operation and productivity of the vacuum pan. The frictional resistance to the flow in the vacuum pan external to the flow in the tubes, the energy losses associated with the vapour disengagement at the free surface and the pressure gain from buoyancy caused by thermal density changes also need to be evaluated as these factors will influence the circulation (and mass flow rate) through the calandria tubes. These factors may be determined by CFD models in future work. The one-dimensional numerical tube model allowed solutions to be obtained reasonably quickly, which is useful in the design process.

The average circulation velocity or mass flow rate in the calandria tubes is required to determine the operating point on the tube performance curve. The circulation in a vacuum pan is dependent on its geometry and heat transfer from the steam supply in the calandria and needs to be determined for each different pan design and duty. The use of tube performance curves (generated using the tube model) coupled with numerical modelling of the vacuum pan can be used to determine optimum tube geometries and operating conditions for pans of varying design and duty.

The evaluation of numerical tube models of circulation and heat transfer are relevant to the operation of the pilot scale rig but are only indicative of full-scale multi-calandria tube factory systems. Care should be taken in applying the numerical tube model to other conditions such as low-grade massecuite strikes and at mass flow rates outside the range investigated in the experimental trials. The trends produced by the numerical tube model modified in this research are indicative and should not be used unequivocally to design vacuum pans without some common knowledge and experience in pan design.

7.4 Summary

A one-dimensional tube model was modified to characterise and predict the operational behaviour of calandria tubes. The model was based on previous work conducted by Rouillard (1985) and Stephens (2001). Empirical correlations based on data obtained for a single calandria tube boiling rig were used to determine the heat transfer characteristics. The one-dimensional tube model was capable of providing reasonable predictions of important parameters such as heat flux and pressure driving forces when compared to the experimental data. The one-dimensional modelling approach has the benefit of simplicity (compared to CFD models), rapid execution times and accessibility is improved, using Microsoft Excel Visual Basic.

The numerical tube model was not able to predict the vapour volume fraction exiting the calandria tube to any degree of accuracy, partly due to the simplifying assumptions used in the model. The flow distribution parameter was unsuitable for predicting the vapour volume fraction because of the errors associated with calculating the bubble rise velocity. Improvements are required to enable the use of a flow distribution parameter to determine the effect of the non-uniform vapour distribution and improve the accuracy of the predictions of the numerical tube model.

An alternative method such as the slip ratio should be considered and correlated to experimental data to allow accurate predictions of the vapour volume fraction exiting the calandria tubes.

A modelling method has been outlined to determine the optimum tube geometry to ensure the performance and productivity of the pan is maximised. The method utilises tube performance curves generated using the one-dimensional tube model that can be coupled with CFD or numerical models of the vacuum pan external to the calandria.

8 CONCLUSIONS AND RECOMMENDATIONS

This chapter outlines the significant outcomes and summarises the conclusions of the research. Additional recommendations and suggestions are presented to improve the development of numerical models and experimental rig, which will provide greater understanding of the heat transfer and circulation behaviour of calandria tubes.

8.1 Conclusions

The crystallisation station is an important process in the production of raw sugar. Batch vacuum pans in particular comprise a large capital investment to sugar mills. For the Australian sugar industry to remain competitive, the need for more cost-effective designs and productivity improvements of vacuum pans are important. The design of vacuum pans has changed little over the past 30 years. Numerical and CFD modelling techniques are becoming a cost-effective and reliable way of developing vessel designs, especially when there are complex physics and geometries involved. Validation using factory measurements is required in order to obtain confidence in the CFD model predictions produced. Currently, however, there are no working numerical models of vacuum pans that can be confidently used to design pans with improved circulation and boiling.

Circulation is one of the key parameters in the performance of vacuum pans. The HTC can be used as a secondary quantitative measure, to gauge the performance of a pan. The heat transfer performance can be closely linked to circulation as the heat transfer produces vapour, which drives the development of circulation patterns within vacuum pans. Circulation measurements have been recorded in vacuum pans by a number of investigators, however, limited data exist on circulation within vacuum pans of modern design. A method for measuring circulation speeds in massecuite solutions and vacuum pans has been refined as part of this research. The method, which uses anemometer probes, has been effective in measuring velocity profiles within vacuum pans.

Circulation and heat transfer measurements were collected from factory trials on a typical modern vacuum pan. These data enabled the operating conditions for the single calandria tube boiling rig experimental trials to be determined.

Experimental trials were conducted on a single calandria tube boiling rig to determine circulation and heat transfer characteristics for boiling in calandria tubes with changing material properties and heat input conditions. The experimental rig was designed to simulate the conditions present in factory pans to allow detailed examination of the heat transfer process and to collect data on vapour volume fraction profiles. Experimental sugar solutions of varying fluid properties were prepared by combining various samples of materials found in factories. These samples were boiled under various operating conditions. Natural and forced circulation conditions were investigated in the experimental trials as both types of circulation are present in factory vacuum pans. The data gathered on the experimental rig were preliminary in nature as the rig did not adequately represent factory equipment.

The results achieved with the experimental rig show the applicability of a pilot scale rig to provide data that can be used to improve the understanding and modelling of flow and heat transfer in the calandria tubes of vacuum pans. The experimental trials also showed the difficulty in obtaining reliable data when boiling a highly viscous fluid in a single vertical tube as the boiling process is unsteady and difficult to characterise.

A one-dimensional tube model was modified to characterise and predict the operational behaviour of calandria tubes. The model was based on previous work conducted by Rouillard (1985) and Stephens (2001). Empirical correlations based on data obtained on a single calandria tube boiling rig were used to determine the heat transfer characteristics in the one-dimensional model. The one-dimensional modelling approach has the benefit of its simplicity (compared to CFD models), accessibility and rapid execution times.

The one-dimensional tube model was capable of providing reasonable predictions of important parameters such as heat flux and pressure driving forces when compared to the experimental data. The numerical tube model was not able to predict the vapour volume fraction exiting the calandria tube to any degree of accuracy, partly due to the simplifying assumptions used in the model. The flow distribution parameter was unsuitable for predicting the vapour volume fraction because of the errors associated with calculating the bubble rise velocity. Improvements are required to enable the use of a flow distribution parameter to determine the effect of the non-uniform vapour distribution and improve the accuracy of the predictions of the numerical tube model.

An alternative method such as the slip ratio should be considered and correlated to experimental data to allow accurate predictions of the vapour volume fraction exiting the calandria tubes.

To a certain extent, the numerical tube model which was used to generate tube performance curves, can be used to determine optimum tube geometry specifications for maximum performance and productivity of vacuum pans. Based on specific fluid conditions and operating parameters, the numerical tube model can be used in conjunction with CFD or numerical models of crystallisation vacuum pans to determine modifications or facilitate new designs of pans with improved circulation and boiling characteristics.

8.2 Recommendations

The two main avenues of future research involve improving the numerical tube model and the experimental rig. Improvements can be made in these areas to progress the understanding of the heat transfer and flow characteristics in calandria tubes and their effect on vacuum pan designs.

8.2.1 Modification of experimental rig

The experimental rig was designed and mostly constructed prior to the start of this study. Limited modifications were made to the experimental rig due to the financial constraints of the project. A number of improvements could be made to the experimental rig to enable better simulations of factory conditions. These include:

- Using steam to heat the calandria tube rather than electrical heating. Steam heating has the benefit of providing consistent heating over the entire tube length and also directly replicates the conditions in factory vessels. However, it can make it difficult to measure pressure, temperature and vapour volume fraction as the gamma rays have to pass through the calandria tube, steam annulus and insulation around the steam annulus. Realistically the pressure, temperature and vapour volume fraction need only to be measured at the outlet of the tube to determine outputs to validate and tune the tube model. There are also a number of safety issues that would need to be resolved in using steam heating;
- If electrical heating is used, current limiting switches should be installed on the active power transducers as an alternative to using PWM control through the function blocks in the ProcessACT software. The current limiting switches would allow smoother and more consistent heat flux to be applied over the entire length of the tube. Insulation should also be provided around the heating bands to reduce the heat losses to the atmosphere;

- Installing a viewing window in the header tank to allow observations to be made of the boiling level and vapour volume fraction exiting the calandria tube. Visual observations will provide additional information on the approximate bubble size and distribution of bubbles exiting the calandria tube;
- Installing a double mechanical seal on the internal gear pump to reduce the amount of air leaking into the rig during boiling under vacuum;
- Replacing the calandria tube with a pipe of constant wall thickness. Difficulties were encountered in this study due to the differences in tube wall thickness affecting the count rates measured by the radiation gauge;
- Linking the conductivity meter to the ProcessACT software. A control schematic could be designed to control a small water dosing pump at the inlet of the internal gear pump. This would enable the vapour that is humidified by the air leaking through the internal gear pump and removed from the rig to be replaced and ensure constant fluid conditions are maintained through the forced circulation boiling trials. This method would allow smooth and automatic control rather than the manual adjustments that were made in this study; and

Additional experimental work could also be conducted to allow further knowledge to be gained from the experimental rig. This should include:

- Conducting boiling trials on calandria tubes of various metals (*i.e.*, carbon steels, stainless steel, copper *etc.*) as well as varying tube wall thicknesses and diameters to determine the effect on the HTC and other operating parameters. These experiments may characterise the heat transfer occurring within the tube wall. Alternatively, teflon spacers could be installed between heating band sections to reduce the heat transfer that is transferred within the tube wall to the pipe work in adjacent sections of the experimental rig;
- Conducting boiling trials on a larger range of fluid properties that would include simulations of low grade massecuite. This would enable data to be gathered for all duties of vacuum pans in factories. The use of higher viscosity materials places importance on the method of mixing and transferring fluid to the experimental rig. This operation would be more ideally suited to experimental rig located in sugar factories where storage issues are less of a problem;
- Construction of a more detailed and representative calandria tube rig, such as a full sized multi-calandria tube system of approximately 20 tubes representing part of a continuous vacuum pan module with a full sized downtake and larger recirculation leg.

The rig should have an extended vapour space so that varying boiling levels could be simulated to represent both batch and continuous factory pan operation. The effects of multiple neighbouring calandria tubes on the flow in the upper pan region could also be investigated in this boiling rig. This rig should be located in a sugar factory to take advantage of the available factory materials and utilities.

8.2.2 Other experimentation

Further factory-based studies should be conducted to investigate certain aspects of the boiling process that have been questioned or suggested by this research. For example, the issue as to whether the boiling process in calandria tubes is an eruptive or steady state process has been called into question. Furthermore, issues related to heat transfer and wall temperature distribution in an industrial setting merits further study.

Additional factory-based investigations might include:

- Constructing a capacitance probe to measure the void fraction within the calandria tubes of industrial vacuum pans. The capacitance probe would need to be installed axially along the centreline within the tube and be able to take measurements along the length of the calandria tube. Ideally the probe would have a fast response to capture the dynamics of the boiling process and possibly the frequency of vapour production. The vapour produced in the tube significantly effects the conductivity measurement and measurements would determine if there was a cyclical or eruptive boiling process; and
- Installing a number of wall mounted temperature transmitters on the inside and outside of calandria tubes in a factory vessel. These temperature transmitters should be positioned at a number of positions along the tube length to determine if the wall temperature is uniform along the calandria tube length. These measurements will also allow an indication on the uniformity of heat transfer along the tube length.

An example of a number of capacitance and temperature measuring sensors including their distribution and positioning in a factory vessel is illustrated in figure 8-1 to show where the proposed additional factory measurements can be obtained. The capacitance sensors are illustrated along the centreline of the calandria tube in figure 8-1. The production of vapour is expected to initiate on the tube wall surface. The vapour bubbles will need to migrate to the centre of the tube before they will be measured by the sensors at this location. The sensors could be positioned by wrapping the sensors and their associated wiring (manufactured to withstand

the conditions within the vacuum pan) around a twisted stainless steel wire attached to both the internal vacuum pan roof and floor and passing through the middle of a calandria tube. This instrument configuration should be staged on a number of calandria tubes at varying radial locations within the vacuum pan.

Figure 8-1 also shows one of the capacitance sensors positioned above the exit of the calandria tube, as the boiling is sometimes suppressed within the calandria tube, due to the height of liquid above the calandria.

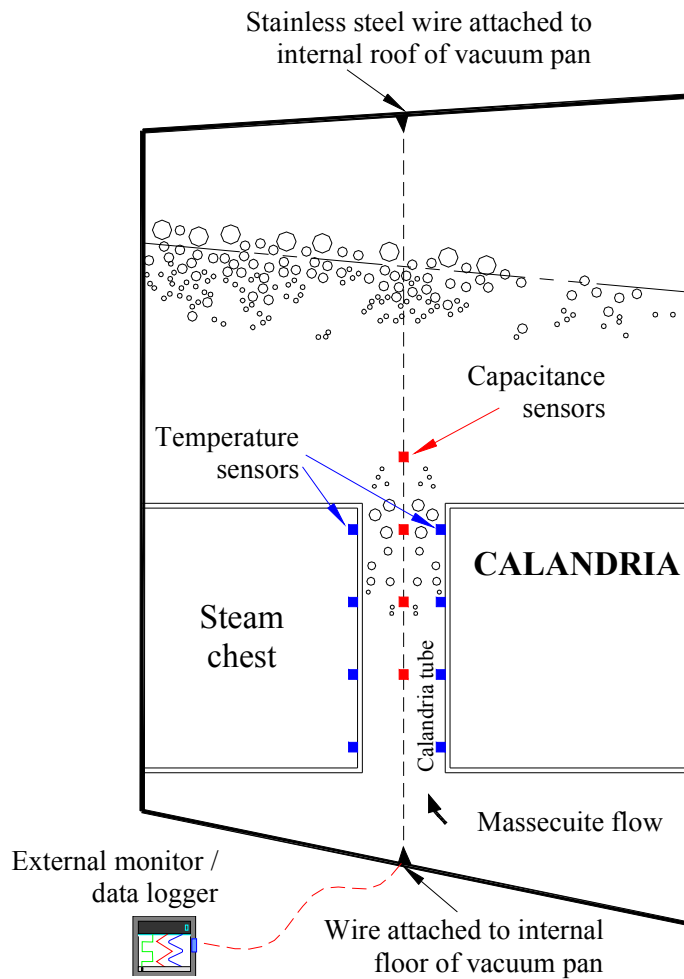


Figure 8-1 Suggested positioning of instrumentation for the additional factory-based trials in one calandria tube of a vacuum pan.

The hot film anemometer probes used in the factory trials were a fairly slow response instrument due to the metal film around the temperature detectors in the probe tip. This is suitable for measuring the slower changing flow patterns of viscous masseccite solutions. The

capacitance probes suggested to investigate the dynamics of the boiling process within the calandria tubes will require less lagging than the hot film anemometers to enable a more rapid response of the instrument. This may involve exposure of sensor wires which may then lead to problems with scale build up that will need to be resolved. Other issues to be considered include the connection of signal wires from the sensors to a data logger or monitoring device external to the vacuum pan and steam chest.

8.2.3 Numerical modelling

The numerical tube model modified in this project was unable to predict the vapour volume fraction exiting the calandria tube to a large degree of accuracy, partly due to the simplifying assumptions used in the model. Additional knowledge of the two-phase flow behaviour is desirable to improve the reliability of the numerical tube model to predict the vapour distribution along the tube length.

The prediction of the slip ratio through empirical correlations based on operating parameters in the experimental trials (*i.e.*, viscosity, operating pressure, velocity, surface tension and vapour volume fraction *etc.*) or improvements to the correlations of the flow distribution parameter is required for the numerical tube model to determine the effect of the non-uniform distribution of vapour on the vapour volume fraction exiting the calandria tube. These improvements will help to improve the accuracy of the predictions of the numerical tube model.

Alternative fundamental experimentation could be conducted to examine the bubble dynamics and drag information of vapour rising in viscous sugar solutions. This would enable more accurate predictions of vapour rise velocity to be calculated that would in turn improve the flow distribution data. More knowledge or determination of the wall superheat and bubble nuclei size at the onset of boiling is required to make accurate predictions of the point at which boiling is initiated as this will effect the overall production of vapour within the calandria tube.

Further improvements to the one-dimensional tube model can also be attained by the following;

- Incorporating varying fluid properties along the vertical length of the tube in the model as the temperature and static pressure change and the amount of vapour increases,
- Extending the model to include transient effects such as superheating. These effects maybe taken into account by the wall superheat required to initiate boiling, and

- Developing the model for the situation where a non-uniform or constant heat flux is applied along the length of the tube rather than an average tube wall temperature.

The use of tube performance curves coupled with numerical modelling of the vacuum pan can be used to determine optimum tube geometries and operating conditions for pans of varying design and duty. This will enable the selection of standard vacuum pan designs that can be used as a basis for the various massecuite duties in factories. The standard pan designs should satisfy most demands of factories with only minor modifications required to suit individual factory specifications.

BIBLIOGRAPHY

- Adkins, B.G. (1951). Notes on the viscosity of molasses and massecuites, Proc. Qld. Soc. Sugar Cane Technol., 18: 43-51.
- Allan, C.J. (1962). Some suggested revisions of pan circulation theory, Proc. Qld. Soc. Sugar Cane Technol., 29: 89-94.
- Allan, G.N. (1963). Steam consumption tests on vacuum pans, Proc. Sth. African Sugar Technol. Assoc., 7: 42-46.
- American Society of Mechanical Engineers (1967). *ASME Steam Tables*. (2nd edition), New York.
- Awang, M. and White, E.T. (1976). Effect of crystal on the viscosity of massecuites, Proc. Qld. Soc. Sugar Cane Technol., 43: 263-269.
- Austmeyer, K.E. and Schliephake, D. (1983). Solution flow and exchange and heat transfer in a heating tube of an evaporation-crystallizer, Int. Sugar Jnl., 85: 328-333.
- Austmeyer, K.E. (1986). Analysis of sugar boiling and its technical consequences – Part II. Heat transfer during sugar boiling, Int. Sugar Jnl., 88: 23-29.
- Batterham, R.J. and Norgate, T.E. (1975). Boiling point elevation and superheat in impure cane sugar solutions, Int. Sugar Jnl., 77: 359-364.
- Behne, E.R. (1938). Circulation in calandria vacuum pans, Int. Sugar Jnl., 40: 382-386.
- Berger, P.D. (1975). Surfactants and surface activity in sugar manufacturing, Sugar Technol. Review, 3, (4), 244.
- Black, B. and White, E.T. (1977). The effect of aeration on the viscosity of molasses, Proc. Qld. Soc Sugar Cane Technol., 44: 185-188.
- Bosworth, R.C.L. (1941). Jnl. Proc. of the Roy. Soc. of New South Wales. 81, 156-6.

- Bosworth, R.C.L. and Duloy, J.S.K. (1950). The measurement of pan circulation, Proc. Int. Soc. Sugar Cane Technol., 7: 644-654.
- Briody, P. (2001). *Australian Sugar Year Book 2000*. Rural Press (Qld) Pty Ltd.
- Broadfoot, R. and Steindl, R.J. (1974). Evaluation tests on a continuous vacuum pan element for low grade boiling, SRI Technical Report, 126.
- Broadfoot, R. (1980). 'A Modelling and optimal design of continuous sugar pans', Ph.D Thesis, University of Queensland, Brisbane.
- Broadfoot, R. and Steindl, R.J. (1980). Solubility-crystallization characteristics of Queensland molasses, Proc. Int. Soc. Sugar Cane Technol., 7: 2557-2580.
- Broadfoot, R. and Miller, K.F. (1990). Rheological studies of massecuites and molasses, Int. Sugar Jnl., 92: 107-112, 143-145.
- Broadfoot, R., Miller, K.F. and Davies, L.W. (1991). Continuous boiling of high-grade massecuite at Maryborough factory, Proc. Aust. Soc. Sugar Cane Technol., 13: 179-184.
- Broadfoot, R. (1992). Designing continuous pans for narrow size distributions and improved cost performance, Proc. Aust. Soc. Sugar Cane Technol., 14: 266-275.
- Broadfoot, R., Miller, K.F. and McLaughlin, R.L. (1998). Rheology of high-grade massecuites, Proc. Aust. Soc. Sugar Cane Technol., 20: 388-397.
- Broadfoot, R. (2001). Planning changes to Process sections of raw sugar factories for increased cogeneration, Proc. Aust. Soc. Sugar Cane Technol., 23: 395-402.
- Brown, D.J., Alexander, K. and Boysan, F. (1991). Crystal growth measurement and modelling of fluid flow in a crystallizer, Proc. Commission Int. Technique de Sucrierie, 19: 77-94.
- Bunton, J.J. (1981). 'Natural convection, two-phase flow, and crystallization in a vacuum pan sugar crystallizer', Ph.D thesis, Louisiana State University.

- Bureau of Sugar Experiment Stations (BSES), (1984). *The standard laboratory manual for Australian sugar mills, Vol. 1 – Principles and practices*. published by BSES.
- Bureau of Sugar Experiment Stations (BSES), (1991). *The standard laboratory manual for Australian sugar mills, Vol. 2 – Analytical methods and tables*. published by BSES.
- Butterworth, D. and Hewitt, G.F. (1977). *Two-phase flow and heat transfer*. Oxford University Press, London.
- Casey, M. and Wintergerste, T. (2000). Best practice guidelines, Special Interest Group on ‘Quality and Trust in Industrial CFD’, European Research Community on flow, turbulence and combustion.
- Collier, J.G. and Thome, J.R. (1996). *Convective boiling and condensation*. Clarendon, Oxford University Press.
- Devin, G. (2002). ‘Supervisory control and data acquisition for the chemical engineering bay’, Fourth year student thesis, Electrical Engineering, James Cook University, Townsville.
- Dhir, V.K. (1998). Boiling heat transfer, Annual Revision of Fluid Mechanics, 30: 365-401.
- Ditl, P., Beranek, L. and Rieger, F. (1990). Simulation of a stirred sugar boiling pan, Zuckerind., 115, (8): 667-676.
- Dittus, F.W. and Boelter, L.M.K. (1930). *Publications on Engineering*. Vol. 2, University of California, Berkely, 443.
- Garside, J. (1985). Industrial crystallization from solution, Chem. Eng. Science, 40, (1): 3-26.
- Giese, J. (2002). ‘Experimental viscous boiling rig – Process control’, Fourth year student thesis, Computer Systems Engineering, James Cook University, Townsville.
- Griffith, P. and Wallis, G.D. (1961). Two phase slug flow, Jnl. Heat Transfer, 83: 307-320.
- Grimsey, I.M. and Brown, D.J. (1994). Superheating effects during sucrose crystal growth in an evaporating crystallizer, Zuckerind., 119, (9): 769-775.

- Harris, J.A., Robinson, J.A. and Vigh, S. (1995). Mathematical modelling of flow and heat transfer in a vertical crystalliser, *Proc. Aust. Soc. Sugar Cane Technol.*, 17: 216-221.
- Helios Electroheat (2000). Flexible ceramic heating bands. <http://www.helios.com.au>
- Hill, J.W. (1969). Calandria pan studies, *Proc. Qld. Soc. Sugar Cane Technol.*, 36: 97-110.
- Honig, P. (1951). The technology of crystallizers, *The Sugar Jnl.*, October.
- Hsu, Y.Y. (1962). On the size range of active nucleation sites on a heating surface, *Jnl. Heat Transfer*, 84: 207-216.
- Hugot, E. (1972). *Handbook of cane sugar engineering*. (2nd edition), Elsevier, Amsterdam.
- ICUMSA (1994). *Specification and Standard SPS-5 Viscometry*. ICUMSA, Colney, England.
- Incropera, F.P. and DeWitt, D.P. (1996). *Fundamentals of heat and mass transfer*. (4th edition), John Wiley and Sons, Inc.
- Jenkins, G.H. (1958). Heating surface arrangement and circulation in vacuum pans, *Proc. Qld. Soc. Sugar Cane Technol.*, 25: 199-207.
- Janovskii, V.V. and Archangelskii, P.A. (1928). *Sachar. Prom.* 2, 614.
- King, L.V. (1914). On the convection of heat from small cylinders in a stream of fluid, *Philosophical Transactions of Royal Society, Series A*, Vol 214.
- Krishna, R., Urseanu, M.I., van Baten, J.M. and Ellenberger, J. (1999). Wall effects on the rise of single gas bubbles in liquids, *Int. Comm. Heat and Mass Transfer*, 26, (6): 781-790.
- Kroeger, P.G. and Zuber, N. (1968). An analysis of the effects of various parameters on the average void fractions in sub-cooled boiling, *Int. Jnl. Heat and Mass Transfer*, 11: 211-233.
- Liow, J.L. (2001). Personal communication. James Cook University, Townsville.

- Lockhart, R.W. and Martinelli, R.C. (1949). Proposed correlation of data for isothermal two-phase, two-component flow in pipes, *Chem. Eng. Progress*, 45: 39-48.
- Luo, M., Stanmore, B.R. and Dixon, T.F. (1997). Modelling combustion in corner-fired sugar mill boilers, *Proc. Aust. Soc. Sugar Cane Technol.*, 19: 466-472.
- Lyle, O. (1950). *Technology for sugar refinery workers*. Chapman and Hall, London.
- Malcomson, P.S. (2000). 'Steam distribution in a tube heat exchanger', Fourth year student thesis, Mechanical Engineering, James Cook University, Townsville.
- Mann, A.P., Pennisi, S.N., Dixon, T.F., Novozhilov, V., Kirkpatrick, M., Kent, J.H., Sazonov, V. and Zhang, L. (2001). Modelling of boiler tube erosion, *Proc. Aust. Soc. Sugar Cane Technol.*, 23: 369-375.
- Martinelli, R.C. and Nelson, D.B. (1948). Prediction of pressure drop during forced circulation boiling of water, *Trans. ASME*, 70: 695-702.
- Mavros, P. (2001). Flow visualization in stirred vessels – A review of experimental techniques, *Trans. Inst. Chem. Engineers*, 79, Part A, 113-127.
- Miller, K.F. and Pike, D.M. (1993). Surface active properties of cane molasses, *Proc. Aust. Soc. Sugar Cane Technol.*, 15: 208-213.
- Miller, K.F. and Muddle, C.P. (2000). The measurement of massecuite circulation in batch and continuous pans, (Poster Paper), *Proc. Aust. Soc. Sugar Cane Technol.*, 22: 529-530.
- Ness, J. (1984). Viscometry in cane sugar processing, *Proc. Aust. Soc. Sugar Cane Technol.*, 6: 271-277.
- Nicklin, J.H. and Beale, R.F. (1960). An investigation of impellor operation in vacuum pans, *Proc. Qld. Soc. Sugar Cane Technol.*, 27: 217-230.
- Nicklin, D.J., Wilkes, J.O. and Davidson, J.F. (1962). Two phase flow in vertical tubes, *Trans. Inst. Chem. Engineers*, 40: 61-68.

- Oliver, D.R. and Young Hoon, A. (1968). Two phase non-Newtonian flow. Part I Pressure drop and hold up. Part II Heat transfer, *Trans. Inst. Chem. Engineers*, 46: 106-125.
- Peacock, S. (1995). Predicting physical properties of factory juices and syrups, *Int. Sugar Jnl.*, 97: 571-577.
- Pennisi, S.N., Liow, J.L. and Schneider, P.A. (2004) CFD model development for a final effect evaporator, *Proc. Aust. Soc. Sugar Cane Technol.*, 26: CD-rom.
- Penny, D. (2001). 'Commissioning of an experimental viscous boiling rig', Fourth year student thesis, Mechatronic Engineering, James Cook University, Townsville.
- Queensland Sugar Corporation, (1997). *Sugar Notes*.
- Rackemann, D.W. and Stephens, D.W. (2002). Determining circulation velocities in vacuum pans, *Proc. Aust. Soc. Sugar Cane Technol.*, 24: 452-458.
- Rackemann, D.W. (2004). Circulation velocities and heat transfer data obtained on factory vacuum pans, SRI Consulting Research Report - SIRE, Project 5, Milestone 3.
- Rein, P.W., Echeverri, L.F. and Acharya, S. (2004). Circulation in vacuum pans, *Proc. Amer. Soc. Sugar Cane Technol.*, 24:1-17.
- Rouillard, E.E.A. and Koenig, M.F.S. (1980). The viscosity of molasses and massecuite, *Proc. Sth. African Sugar Technol. Assoc.*, 24: 89-92.
- Rouillard, E.E.A. (1983). A study of boiling parameters under conditions of laminar non-newtonian flow with particular reference to massecuite boiling, SMRI Technical Report No. 1375.
- Rouillard, E.E.A. (1984). Viscosity of factory products, SMRI Technical Report No. 1375.
- Rouillard, E.E.A. (1985). 'A study of boiling parameters under conditions of laminar non-newtonian flow with particular reference to massecuite boiling', Ph.D Thesis, University of Natal.

- Saska, M. (2002). Boiling point elevation of technical sugarcane solutions and its use in automatic pan boiling, *Int. Sugar Jnl.*, 104: 500-507.
- Sieder, E.N. and Tate, G.E. (1936). Heat transfer and pressure drop of liquids in tubes, *Ind. and Eng. Chem.*, 28: 1429-1434.
- Sima, M.A. and Harris, J.A. (1999). Numerical modelling of flow in a vertical cooling crystalliser, *Jnl. Fluids Eng.*, 121: 148-154.
- Skyring, A.G. (1965). Thoughts on future developments in vacuum pan design, *Proc. Qld. Soc. Sugar Cane Technol.*, 32: 231-236.
- Smythe, B.M. (1971). Sucrose crystal growth, *Sugar Tech. Review*, 1: 191-231.
- Steindl, R.J. (1981). Viscosity estimations for pan stage materials, *SRI Technical Circular*, No. 59, 65-70.
- Steindl, R.J. (1995). Optimum performance through CFD modeling of clarifier designs, *Proc. Aust. Soc. Sugar Cane Technol.*, 17: 207-215.
- Steindl, R.J., Fitzmaurice, A.L. and Alman, C.W. (1998). Recent developments in clarifier design, *Proc. Aust. Soc. Sugar Cane Technol.*, 20: 477-483.
- Steindl, R.J. and Ingram, G.D. (1999). Improved evaporator performance through circulation modelling, *SRI Syndicated Project Report 7/99*.
- Stephens, D.W. (2001). 'Studies on modelling circulation in sugar vacuum pans', Ph.D Thesis, James Cook University, Townsville.
- Tailby, S.R., Clutterbuck, E.K. and Bakshi, A.S. (1976). Heat transfer and pressure drop for vaporization of water in a vertical tube with particular reference to entrance effects, *Trans. Inst. Chem. Engineers*, 54: 84-88.
- Tait, P.J., Greig, C.R. and Abernethy, P.E. (1995). High-grade continuous pans: To stir or not to stir, *Proc. Aust. Soc. Sugar Cane Technol.*, 17: 244-249.

- Tippens, D.E. (1972). Modern calandria vacuum pan design criteria, Sugar Industry Technol. Paper, 349, 81-89.
- Thiele, H. and Langen, A. (1974). Viscosity and supersaturation of sugar solutions, Int. Sugar Jnl., 76: 136-140, 169-173.
- Tromp, L.A. (1966). Tube spacing in heating rig, Int. Sugar Jnl., 68: 163-165, 203-205.
- Turck (2001). Turck Data Sheet – Insertion Flow Sensors. Technical Reference Section.
- Unal, H.C. (1975). Determination of the initial point of net vapour generation in flow boiling systems, Int. Jnl. Heat and Mass Transfer, 18:1095-1099.
- Versteeg, H.K. and Malalasekera, W. (1995). *An introduction to computational fluid dynamics – The finite volume method*. Longman Scientific and Technical, England.
- Waddell, C.W. (1939). Circulation in vacuum pans, Int. Sugar Jnl., 41: 65-66.
- Watson, L.J., (1986). Heat transfer performance in evaporators – Part 1. Theory and mechanisms, SRI Technical Report No. 191.
- Webre, A.L. (1933). Experiments on the working of the calandria vacuum pan, Int. Sugar Jnl., 35: 184-187, 227-229.
- Webre, A.L. (1962). Mechanical circulation in vacuum pans, Sugar y Azucar, 57: 38-42.
- White, E.T. and Hertle, C.K. (1984). Mixing of high viscosity materials with thinning fluids, Proc. Aust. Soc. Sugar Cane Technol., 6: 263-270.
- Wood, M.G., Forsell, L., Smolski, B., Keller, J. and Dawson, M.W. (1997). Sugar mill effluent treatment in ponds, Proc. Aust. Soc. Sugar Cane Technol., 19: 402-409.
- Woodfield, P.L., Kent, J.H. and Dixon, T.F. (1998). Computational modelling of a bagasse fired furnace – effects of fuel moisture, Proc. Aust. Soc. Sugar Cane Technol., 20: 458-464.

- Wright, P.G. (1966). Circulation movements in sugar vacuum pans, Proc. Qld. Soc. Sugar Cane Technol., 33: 179-184.
- Wright, P.G. (1971). 'A model of industrial sugar crystallisation', Ph.D Thesis, University of Queensland, Brisbane.
- Wright, P.G. and White, E.T. (1974). A mathematical model of vacuum pan crystallisation, Proc. Int. Soc. Sugar Cane Technol., 29: 1547-1560.
- Zuber, N. (1964). On the dispersed two-phase flow in the laminar flow region, Chem. Eng. Science, 19: 897-917.
- Zuber, N. and Findlay, J.A. (1965). Average volumetric concentration in two phase flow systems, Jnl. Heat Transfer – Trans. ASME, 87: 453-468.

APPENDIX A – Glossary of terms

Bagasse: The residual fibrous material left after the extraction of juice from sugar cane in mills.

Brix: The brix of a solution is the concentration (in g solute per 100 g solution) of a solution of pure sucrose in water, having the same density as the solution at the same temperature. If the brix is measured optically using the refractive index of the material then the determined value is termed refractive brix.

Calandria: The term used to describe the heating element in evaporators and vacuum pans. The calandria consists of a series of vertical heating tubes held between two tube-plates with boiling liquid flowing through the inside of the tubes and condensing steam or vapour on the outside of the tubes, which is called the vapour or steam chest.

Centrifugal: A perforated basket, which spins inside a casing to separate sugar crystals from molasses.

Condensate: Water, which has been condensed, either from vapour liberated from boiling juice, or from steam.

Crystal content: The percentage by weight of sugar crystals present in the massecuite solution.

Dry substance: The weight of material remaining after drying the material under specific conditions. Dry substance is usually expressed as a percentage of the original weight. The determination of dry substance represents an attempt to measure the total solids, both soluble and insoluble, or, in the absence of insoluble solids, the total soluble solids.

Effect: An effect is the name given to an evaporator vessel.

Footing: The footing or footing volume refers to the initial volume or charge of syrup and seed drawn into the pan prior to the onset of a pan strike.

Headspace: The area of an evaporator vessel above the calandria where the vapour released from the boiling liquid is contained.

High-grade: The term used to describe the higher purity sugar streams (*i.e.*, 'A' and 'B' massecuite) or equipment processing high purity sugar materials (*i.e.*, high-grade crystallisation vacuum pans and centrifugals) that are used to produce the raw sugar from the factory available for export or consumption.

Impurities (soluble): The collective term for all substances other than sucrose present in the total soluble solids contained in a sample.

Juice: The term given to the liquid containing sucrose, impurities and water, that is squeezed out of the cane in the mills. The term juice is applied through the various stages of processing until it enters the evaporator station when it is called liquor.

Liquor: A concentrated sugar solution produced by evaporation of water from juice. The term syrup refers to the liquor leaving the final effect of the evaporator station.

Low-grade: The term used to describe the lower purity sugar streams (*i.e.*, 'C' massecuite) or equipment processing lower purity sugar materials (*i.e.*, low-grade crystallisation vacuum pans and centrifugals) that are not directly used to produce the raw sugar from the factory available for export or consumption.

Low-pressure (LP) steam: The steam discharged from turbo machinery that is slightly higher than atmospheric pressure and contains minimal superheat. LP steam is unsuitable for driving turbines, however, it still contains a large amount of latent heat energy suitable for other heating duties.

Magma: The mixture produced when sugar crystals (usually the lowest purity sugar) is mixed with a liquid such as syrup, juice or water.

Masseccuite: The mixture of sugar crystals and mother molasses liquor discharged from a vacuum pan. Masseccuites are usually classified according to descending purity as 'A', 'B' and 'C'.

Molasses: The mother liquid surrounding sugar crystals in massecuite, which is separated from the massecuite by centrifugal screens.

Polarisation (pol): An estimate of the sucrose content of sugar from optical polarization methods.

Purity: The percentage of sucrose by weight contained within the total solids of the solution measured in two forms, true purity or apparent purity:

$$\text{True purity} = \frac{\text{sucrose}}{\text{dry substance}}$$

or

$$\text{Apparent purity} = \frac{\text{pol}}{\text{brix}}$$

Seed: Fine sugar crystals, generally suspended in a liquid medium, in which case the mixture is known as seed slurry. Seed is used to provide the crystal surface for deposition of sugar.

Strike: The term given to each cycle of a batch vacuum pan. The term end of strike thus refers to the end of the batch boiling process.

Sucrose: The pure chemical composition with the formula $C_{12}H_{22}O_{11}$. Sucrose is also commonly referred to as pure cane sugar.

Sugar: The crystals of sucrose, together with any adhering molasses, as recovered from the massecuites in the centrifugals. The various grades of sugar found in a raw sugar factory are generally identified in terms of the grade of massecuite they originated from. (*i.e.*, 'A' sugar, 'B' sugar, or 'C' sugar). The term sugar can refer to both sucrose and sugar crystals.

Syrup: The concentrated sugar solution leaving the final evaporation stage.

APPENDIX B – Calibration constants for the anemometer probes.

The equations below detail the functional form of the calibration constants used for the four anemometer probes used in the factory trials.

Probe 1:

$$C_{1A} = -26.4 DS_{mass} + 120.1 P_{mass}$$

$$n1 = 0.003 DS_{mass} + 0.0015 P_{mass}$$

Probe 2:

$$C_{2A} = 22.2 DS_{mass} + 69.7 P_{mass}$$

$$n2 = 0.002 DS_{mass} + 0.003 P_{mass}$$

Probe 3:

$$C_{3A} = -9.8 DS_{mass} + 104.6 P_{mass}$$

$$n3 = 0.0026 DS_{mass} + 0.002 P_{mass}$$

Probe 4:

$$C_{4A} = 2.1 DS_{mass} + 88.6 P_{mass}$$

$$n4 = 0.002 DS_{mass} + 0.0025 P_{mass}$$

where DS_{mass} is the dry substance of the massecuite (%), and
 P_{mass} is the true purity of the massecuite (%).

APPENDIX C – MTL8000 I/O wiring information

MTL I/O Channel List and Wiring Guide							
MTL Slot #	Module	MTL Channel	Cable & UNAC Tag #	Tag Name	Description	Routing Info	
1	AI1	1	1	THC1	Calandria Tube THC #1	To THC & RTD Trans Box	
		2	2	THC2	Calandria Tube THC #2	To THC & RTD Trans Box	
		3	3	THC3	Calandria Tube THC #3	To THC & RTD Trans Box	
		4	4	THC4	Calandria Tube THC #4	To THC & RTD Trans Box	
		5	5	THC5	Calandria Tube THC #5	To THC & RTD Trans Box	
		6	6	THC6	Calandria Tube THC #6	To THC & RTD Trans Box	
		7	7	THC7	Calandria Tube THC #7	To THC & RTD Trans Box	
		8	8	THC8	Calandria Tube THC #8	To THC & RTD Trans Box	
2	AI2	1	9	THC9	Calandria Tube THC #9	To THC & RTD Trans Box	
		2	10	THC10	Calandria Tube THC #10	To THC & RTD Trans Box	
		3	11	THC11	Calandria Tube THC #11	To THC & RTD Trans Box	
		4	12	RTD1	Calandria Tube RTD #1	To THC & RTD Trans Box	
		5	13	RTD2	Calandria Tube RTD #2	To THC & RTD Trans Box	
		6	14	RTD3	Calandria Tube RTD #3	To THC & RTD Trans Box	
		7	15	RTD4	Calandria Tube RTD #4	To THC & RTD Trans Box	
		8	16	RTD5	Calandria Tube RTD #5	To THC & RTD Trans Box	
3	AI3	1	17	P1	Calandria Tube P #1	Direct to P1	
		2	18	P2	Calandria Tube P #2	Direct to P2	
		3	19	P3	Calandria Tube P #3	Direct to P3	
		4	20	P4	Calandria Tube P #4	Direct to P4	
		5	21	P5	Calandria Tube P #5	Direct to P6	
		6	22	P6	Header Tank P #6	Direct to P6	
		7	23	MF1	MF for Recirculation Pipe	To SI 6 then to MF1	
		8	24	MF2	MF for HX Cooling Water	To SI 7 then to MF2	
4	AI4	1	25	AWT1	AWT for HB #1	To HBPB (to SI 1 then to AWT1)	
		2	26	AWT2	AWT for HB #2	To HBPB (to SI 2 then to AWT2)	

Appendices

		3	27	AWT3	AWT for HB #3	To HBPB (to SI 3 then to AWT3)	
		4	28	AWT4	AWT for HB #4	To HBPB (to SI 4 then to AWT4)	
		5	29	AWT5	AWT for HB #5	To HBPB (to SI 5 then to AWT5)	
		6	30	DG	Density Gauge	To DG Controller (Via SI 8)	
		7	31	THX1	HX THC: Steam In	To THC & RTD Trans Box	
		8	32	THX2	HX THC: Condensate Return	To THC & RTD Trans Box	
5	AI5	1	33	THX3	HX THC: Condenser Water In	To THC & RTD Trans Box	
		2	34	THX4	HX THC: Condenser Water Out	To THC & RTD Trans Box	
		3	35	EMPTY			
		4	36	EMPTY			
		5	37	EMPTY			
		6	38	EMPTY			
		7	39	EMPTY			
		8	40	EMPTY			
6	DO1	1	41	HB1	Switch for HB #1	To HBPB Relay 1	
		2	42	HB2	Switch for HB #2	To HBPB Relay 2	
		3	43	HB3	Switch for HB #3	To HBPB Relay 3	
		4	44	HB4	Switch for HB #4	To HBPB Relay 4	
		5	45	HB5	Switch for HB #5	To HBPB Relay 5	
		6	46	LIGHT	Blue Strobe: Warning Light		
		7	47	MB	Carrier Movement Buzzer		
		8	48	WB	Fault Buzzer		Sew Connection
7	DO2	1	49	SEWI1	Sew Drive Input: /Controller Inhibit	To Sew Via Multicore (10): Pair # 1	1 W to X13.1 1 B to X13.7
		2	50	SEWI2	Sew Drive Input: Enable/Rapid Stop	To Sew Via Multicore (10): Pair # 2	2 W to X13.2 2 B to X13.7
		3	51	SEWI3	Sew Drive Input: Fault reset	To Sew Via Multicore (10): Pair # 3	3 W to X13.3 3 B to X13.7
		4	52	SEWI4	Sew Drive Input: IPOS Input (Handshake)	To Sew Via Multicore (10): Pair # 4	4 W to X22.1 4 B to X22.9
		5	53	SEWI5	Sew Drive Input: IPOS Input (Data)	To Sew Via Multicore (10): Pair # 5	5 W to X22.2 5 B to X22.9
		6	54	SEWI6	Sew Drive Input: IPOS Input (Data)	To Sew Via Dual Cable: Pair # 1	1 W to X22.3 1 B to X22.9
		7	55	SEWI7	Sew Drive Input: IPOS Input (Data)	To Sew Via Dual Cable: Pair # 2	2 W to X22.4 2 B to X22.9
		8	56	SEWI8	Sew Drive Input: IPOS Input (Heartbeat)	To Sew Via Single Pair Cable	Sew Connection
8	DI1	1	57	SEWO1	Sew Drive Output: /Brake	To Sew Via Multicore (10): Pair # 6	6 W to X10. 3 6 B: Free
		2	58	SEWO2	Sew Drive Output: Ready	To Sew Via Multicore (10): Pair # 7	7 W to X10.5 7 B: Free
		3	59	SEWO3	Sew Drive Output: /Fault	To Sew Via Multicore (10): Pair # 8	8 W to X10.7 8 B: Free

Appendices

	4	60	SEWO4	Sew Drive Output: IPOS In Position	To Sew Via Multicore (10): Pair # 9	9 W to X23.1	9 B: Free
	5	61	SEWO5	Sew Drive Output: IPOS Output (Shutdown)	To Sew Via Multicore (10): Pair # 10	10 W to X23.2	10 B: Free
	6	62	SEWO6	Sew Drive Output: IPOS Output (ACK)	To Sew Via Dual Cable: Pair # 1	1 W to X23.3	1 B: Free
	7	63	SEWO7	Sew Drive Output: IPOS Output (ACK)	To Sew Via Dual Cable: Pair # 2	2 W to X23.3	2 B: Free
	8	64	EMPTY				
	9	65	EMPTY				
	10	66	EMPTY				
	11	67	EMPTY				
	12	68	EMPTY				
	13	69	EMPTY				
	14	70	EMPTY				
	15	71	EMPTY				
	16	72	EMPTY				

Status of MTL8000

No of modules: 8
 No of free slots: 0
 Total No. of channels: 72
 No of used channels: 47
 No of free channels: 6 AI, 4 DO, 11 DI

Key

THC: Thermocouple	HB: Heating Band
RTD: Resistive Temperature Device	HBPB: Heating Band Power Box
P: Pressure Transducer	AWT: Active Power Transducer
SI: Signal Isolator	DG: Density Gauge
MF: Magnetic Flowmeter	HX: Heat Exchanger

APPENDIX D – ProcessACT schematics

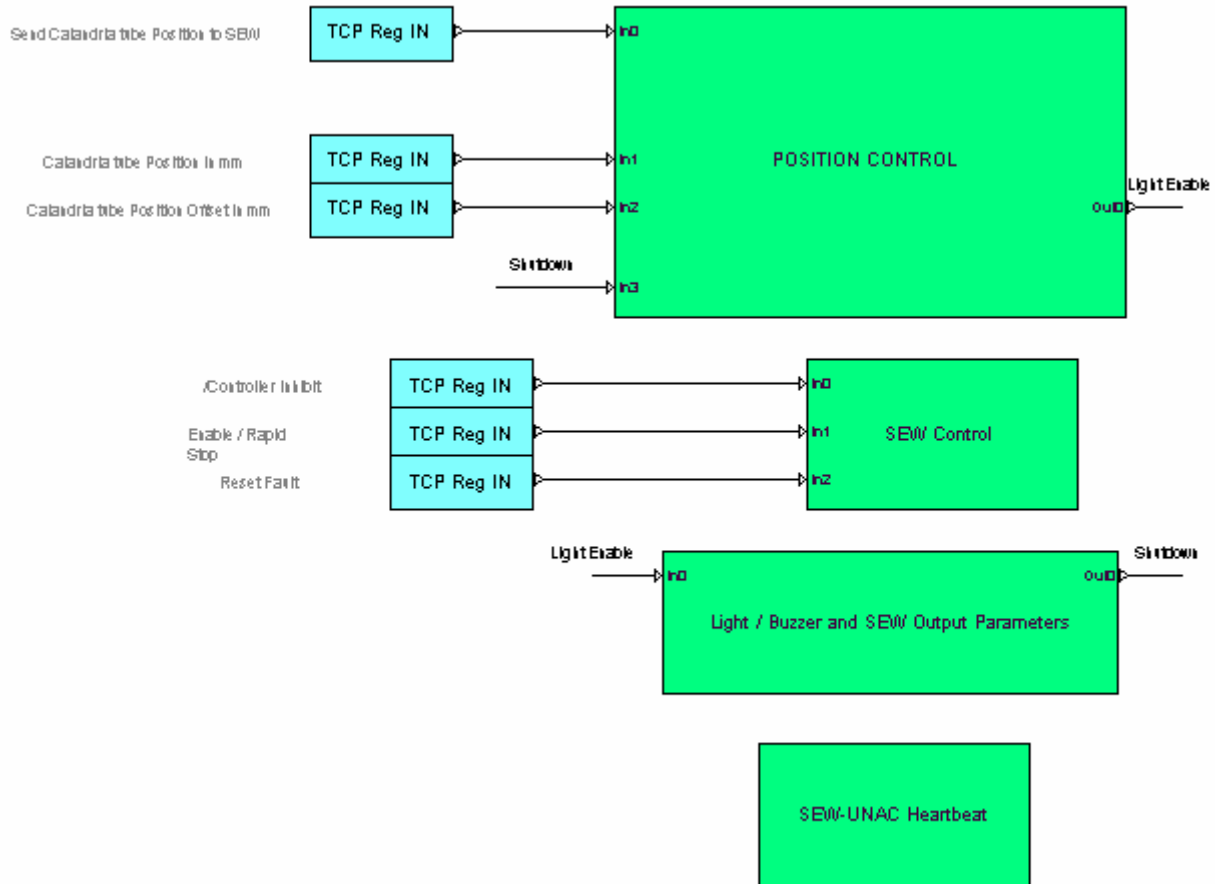


Figure D1: Schematic of densitometer positioning and SEW control super blocks.

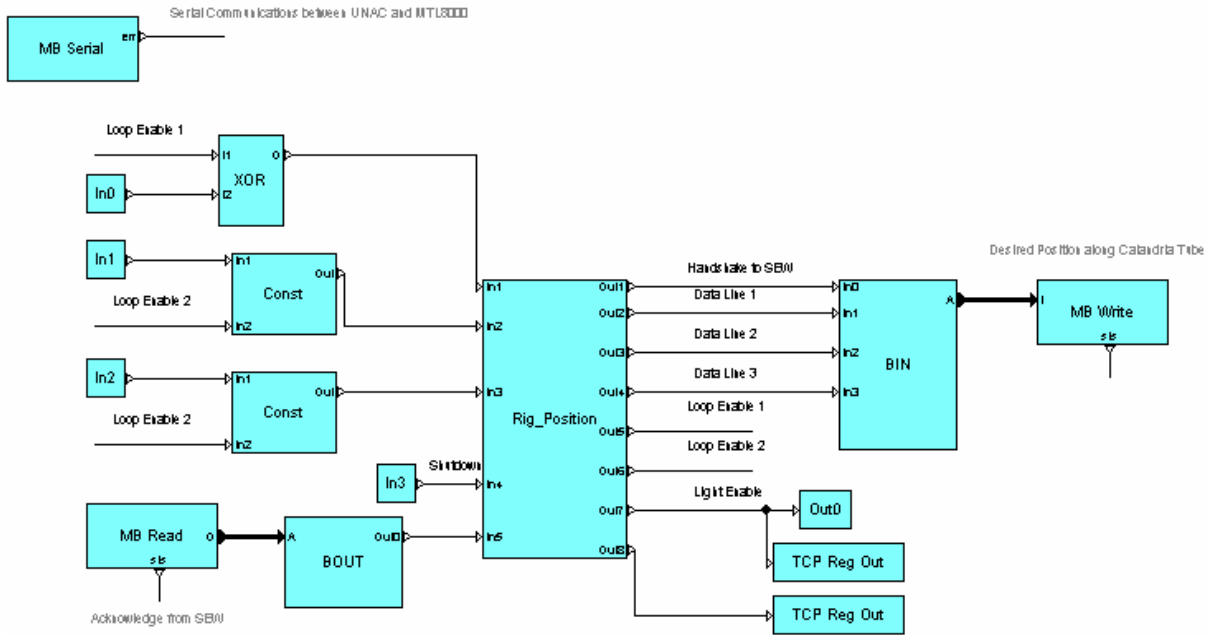


Figure D2: Radiation gauge positioning control schematic.

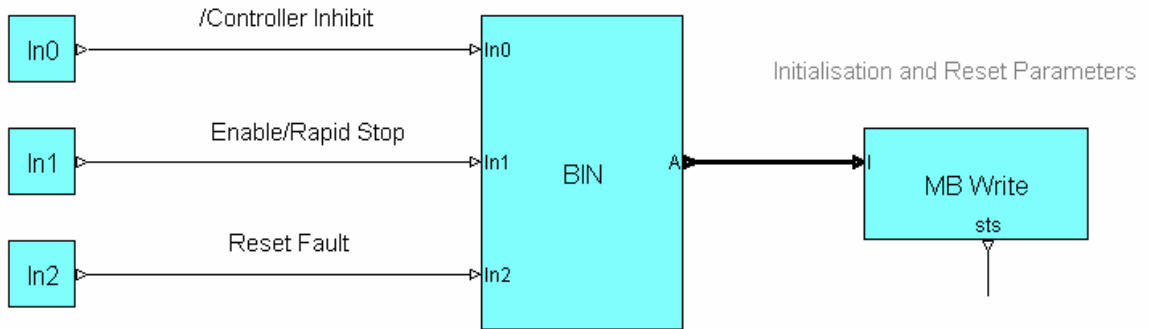


Figure D3: SEW MOVIDRIVE control schematic.

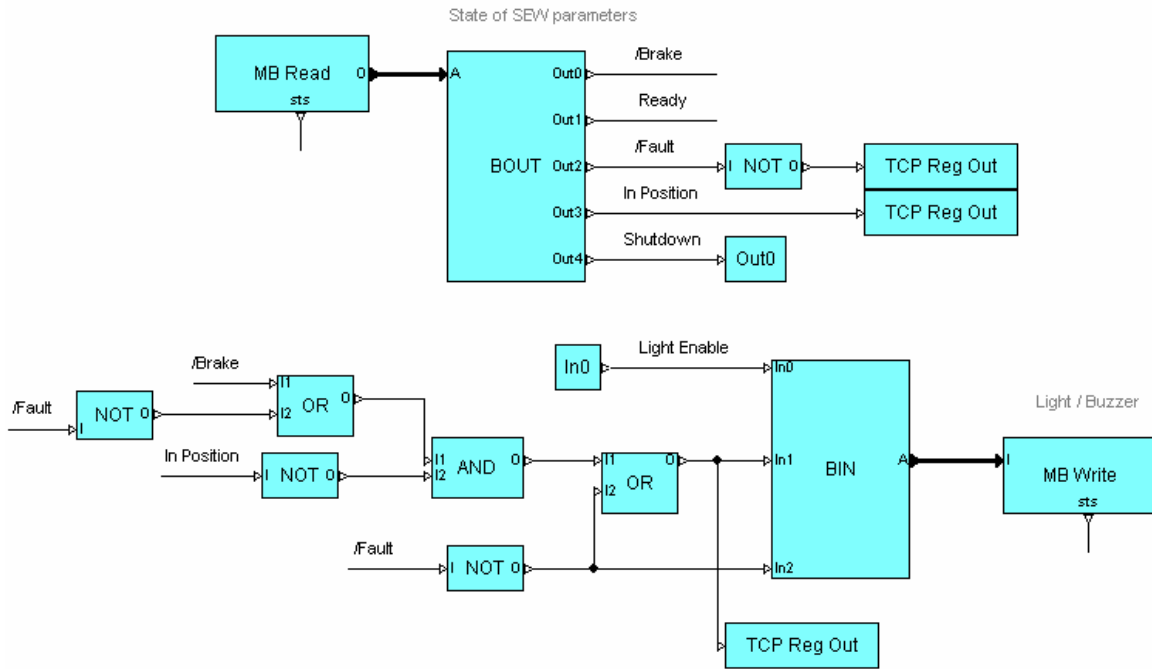


Figure D4: Light / buzzer and SEW output parameters schematic.

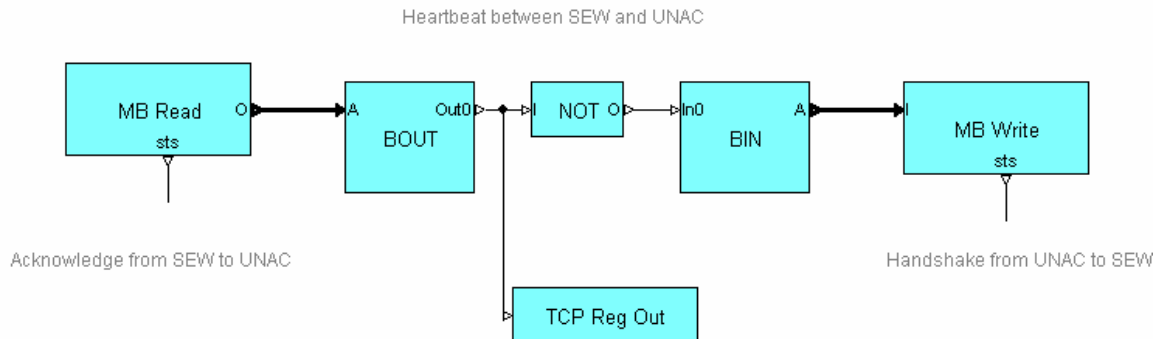


Figure D5: SEW – UNAC heartbeat schematic.

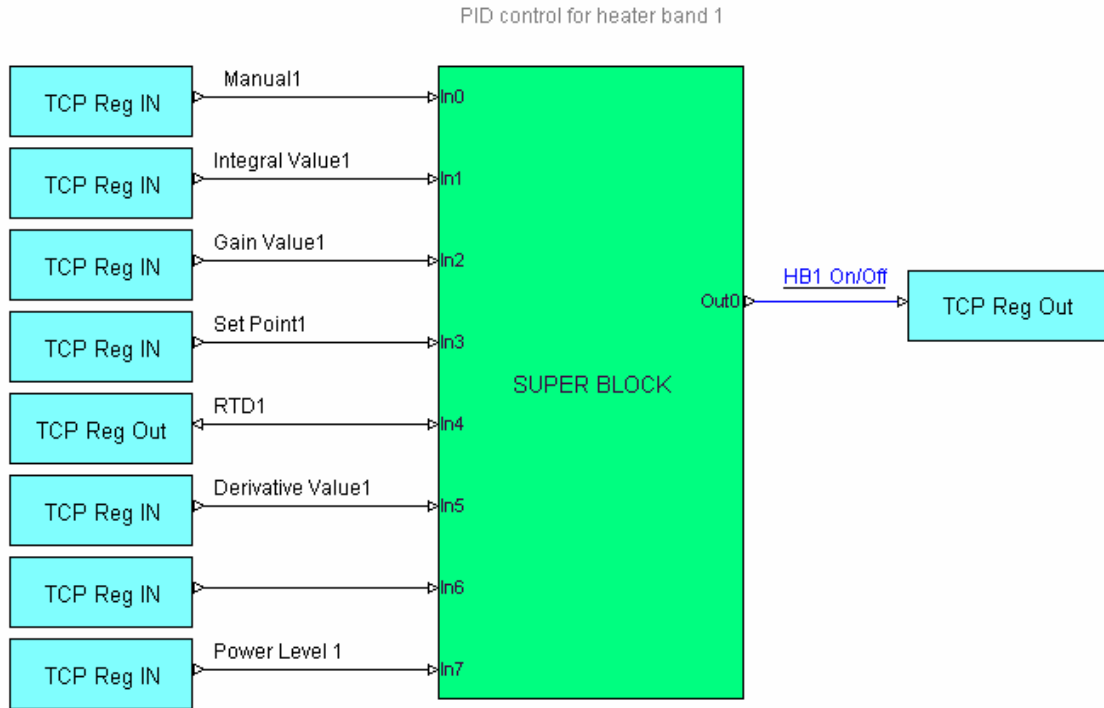


Figure D6: Schematic of heating band control super blocks.

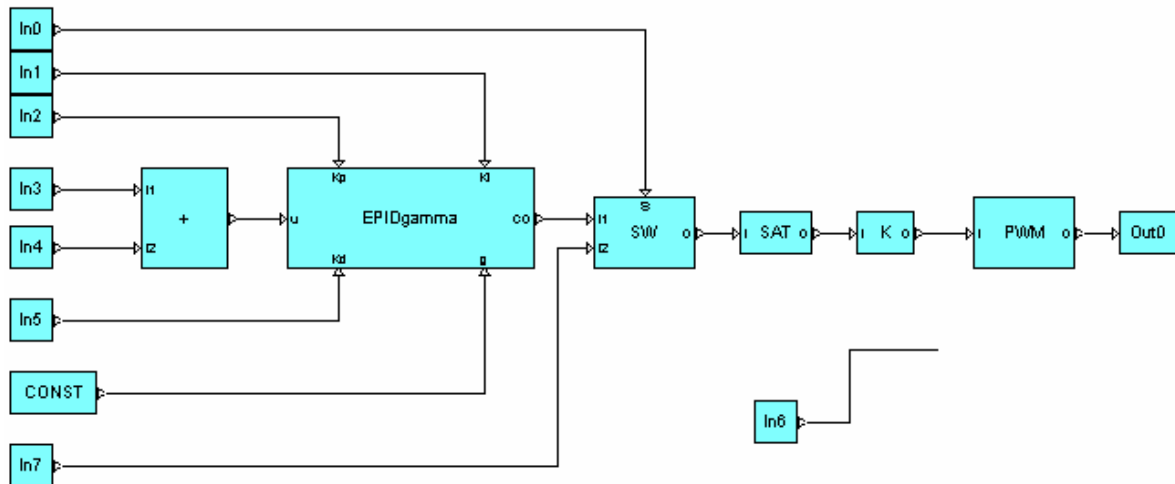


Figure D7: Heating band PID control schematic.

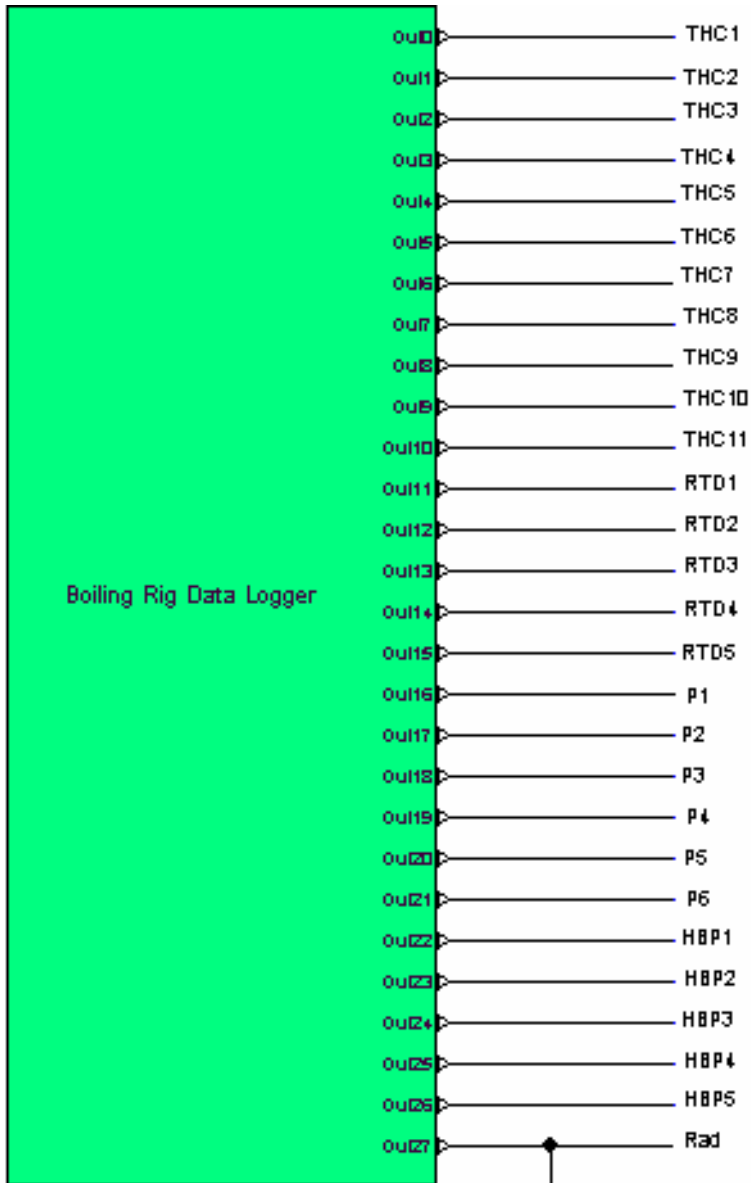


Figure D8: Schematic of data logger super block.

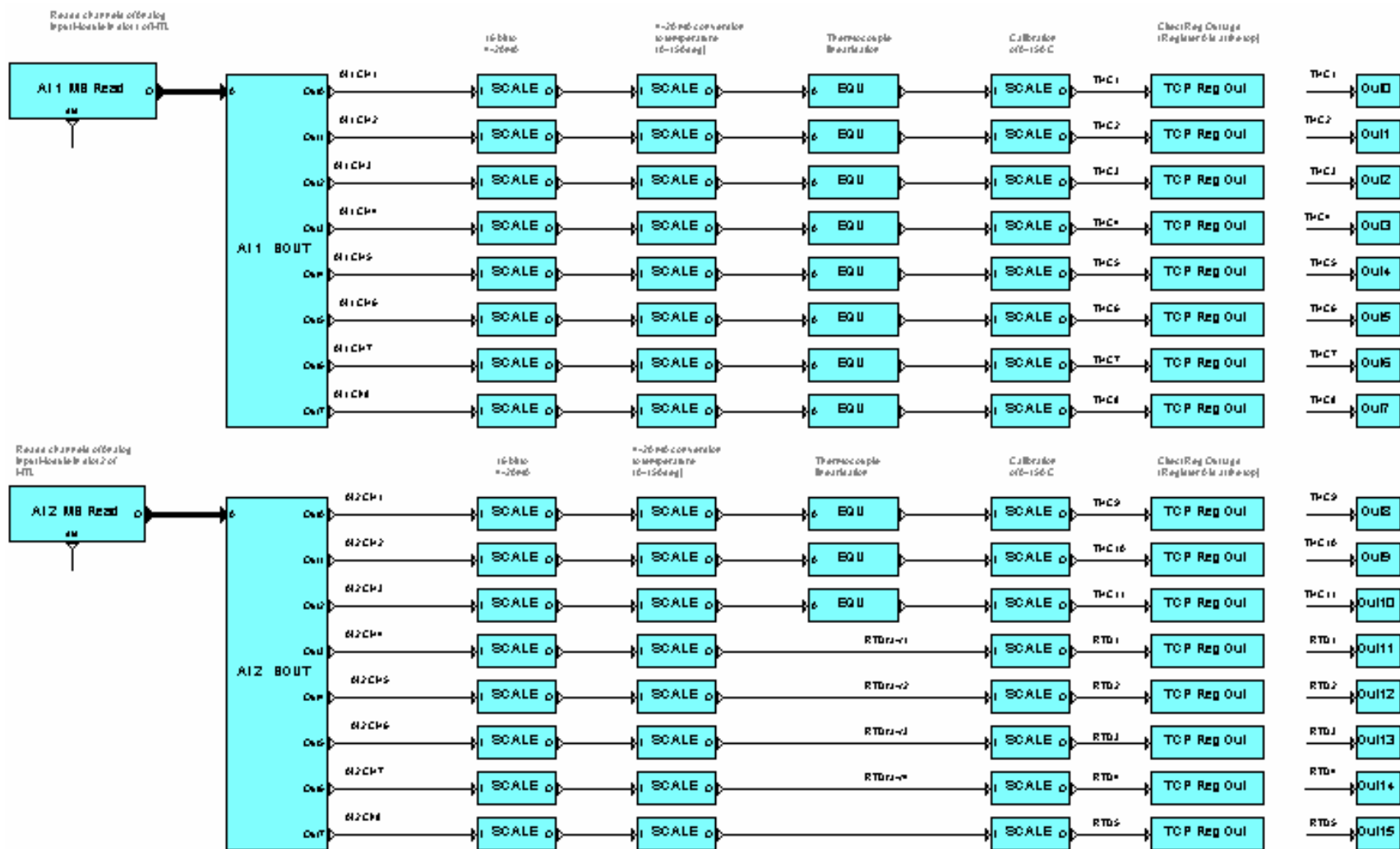


Figure D9: Example of data logger schematic.

APPENDIX E – Citect schematics

The interface pages necessary for controlling the boiling rig were divided up in a logical sequence to organise the data into manageable sections. The main pages necessary for control of the experimental rig are mapped out in Appendix D.

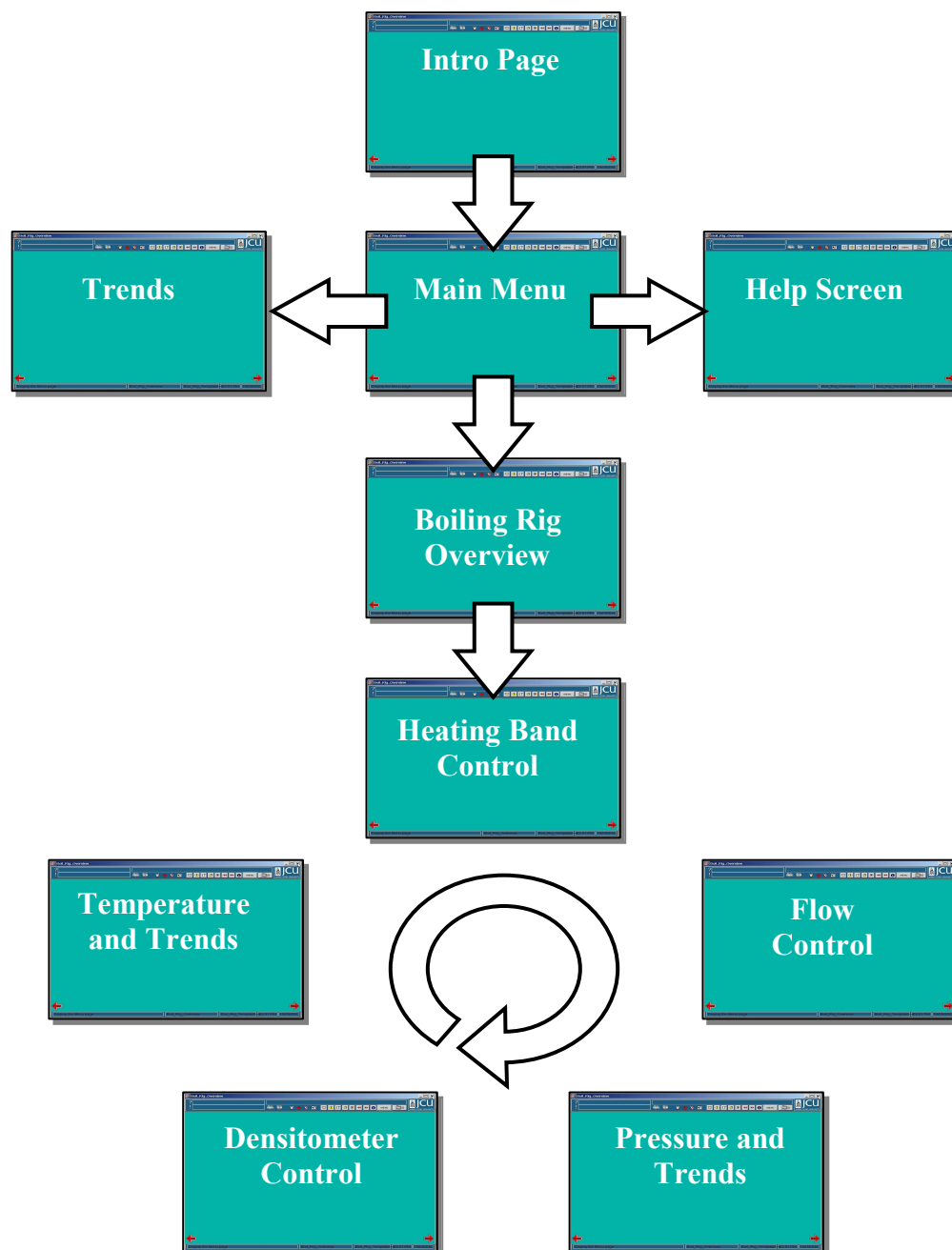


Figure E1: Summary of Citect interface schematics.
(N.B. The arrows show the navigation around the project)

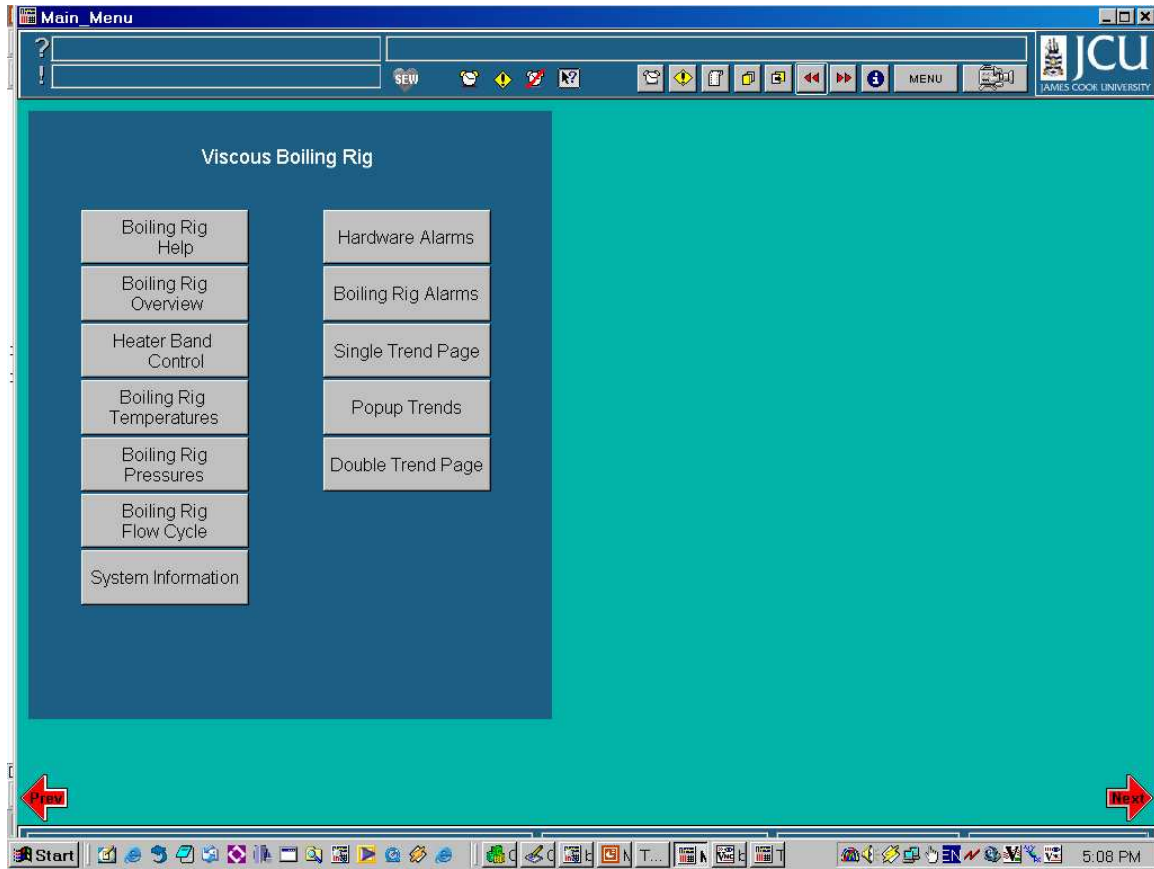


Figure E2: Main menu interface page.

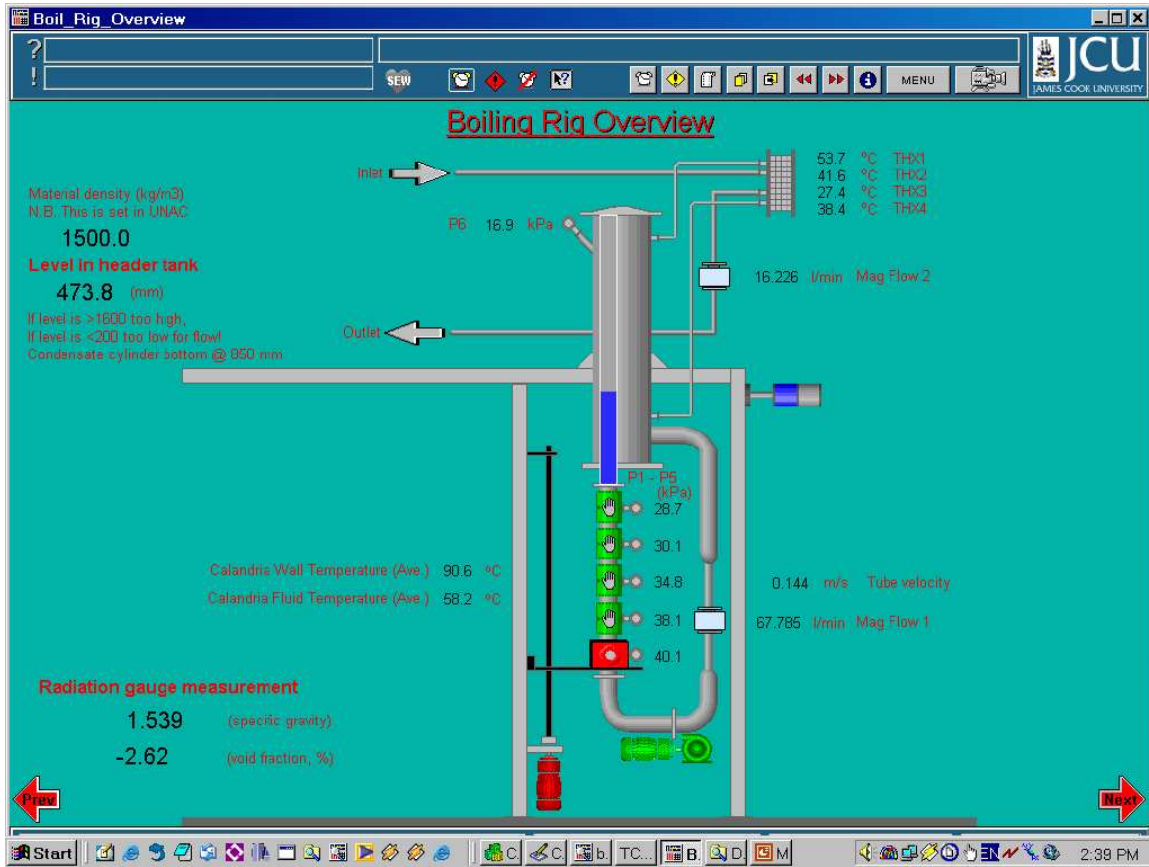


Figure E3: Boiling rig overview interface page.

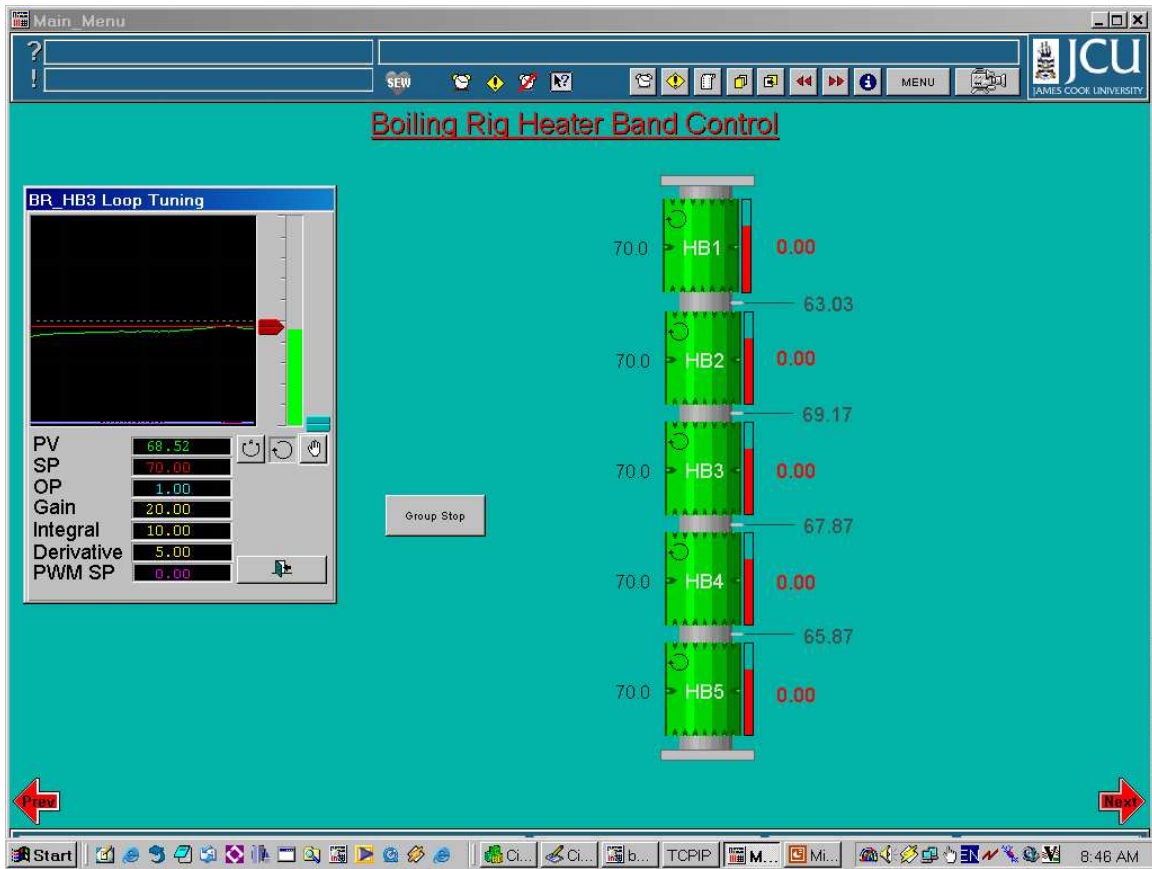


Figure E4: Heating band control interface page showing PID control.

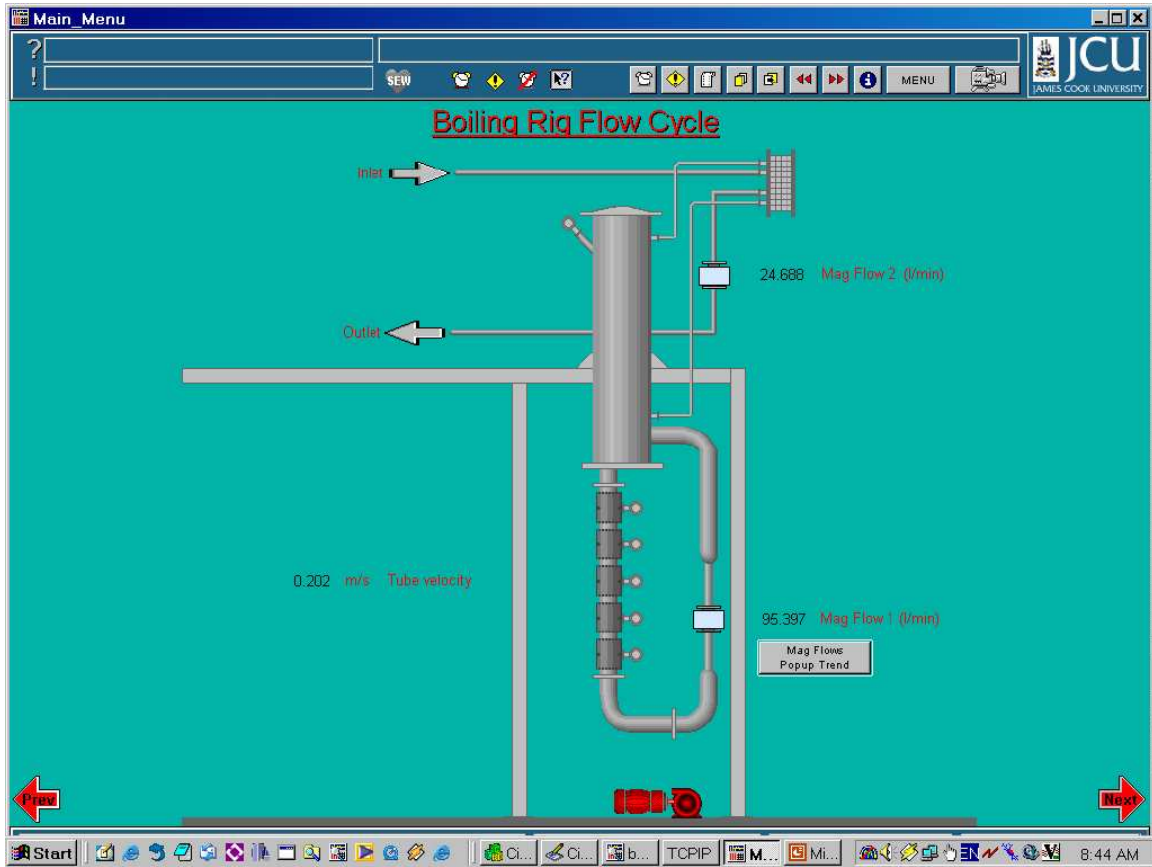


Figure E5: Flow control interface page.

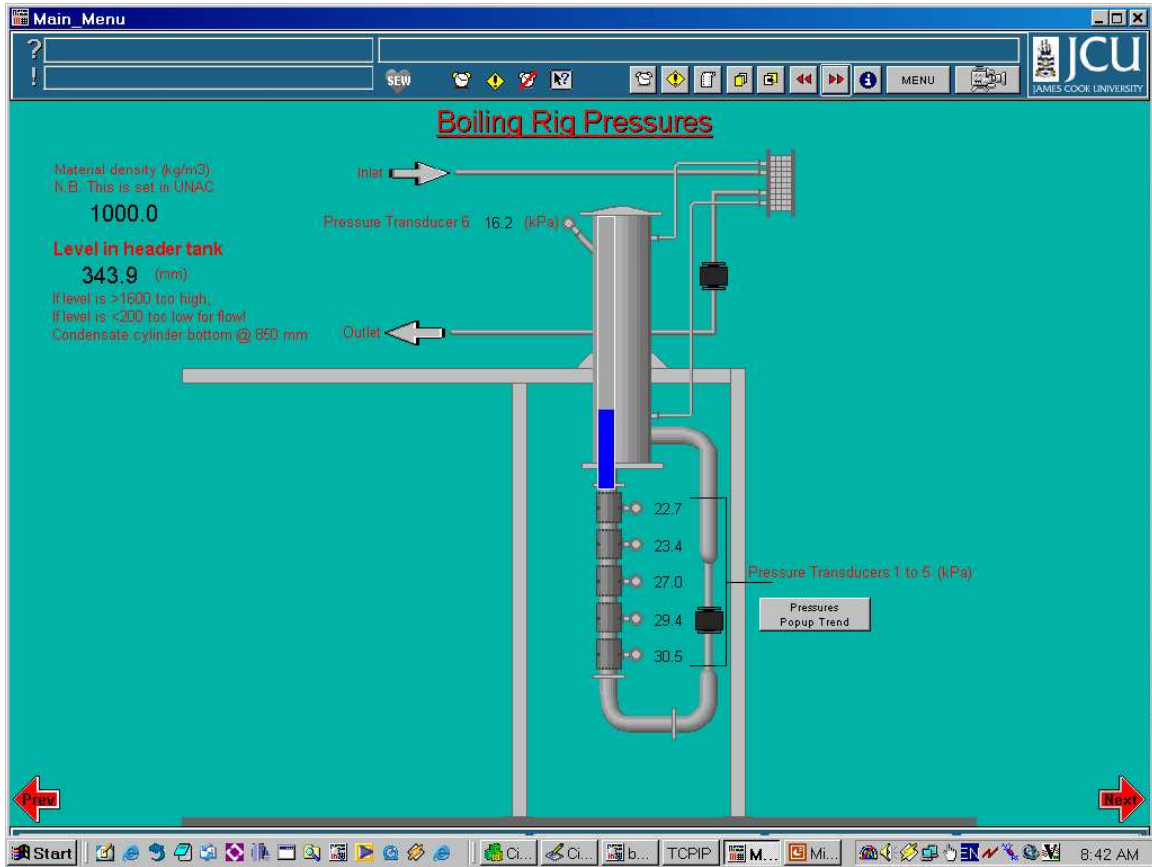


Figure E6: Pressure and trends interface page.

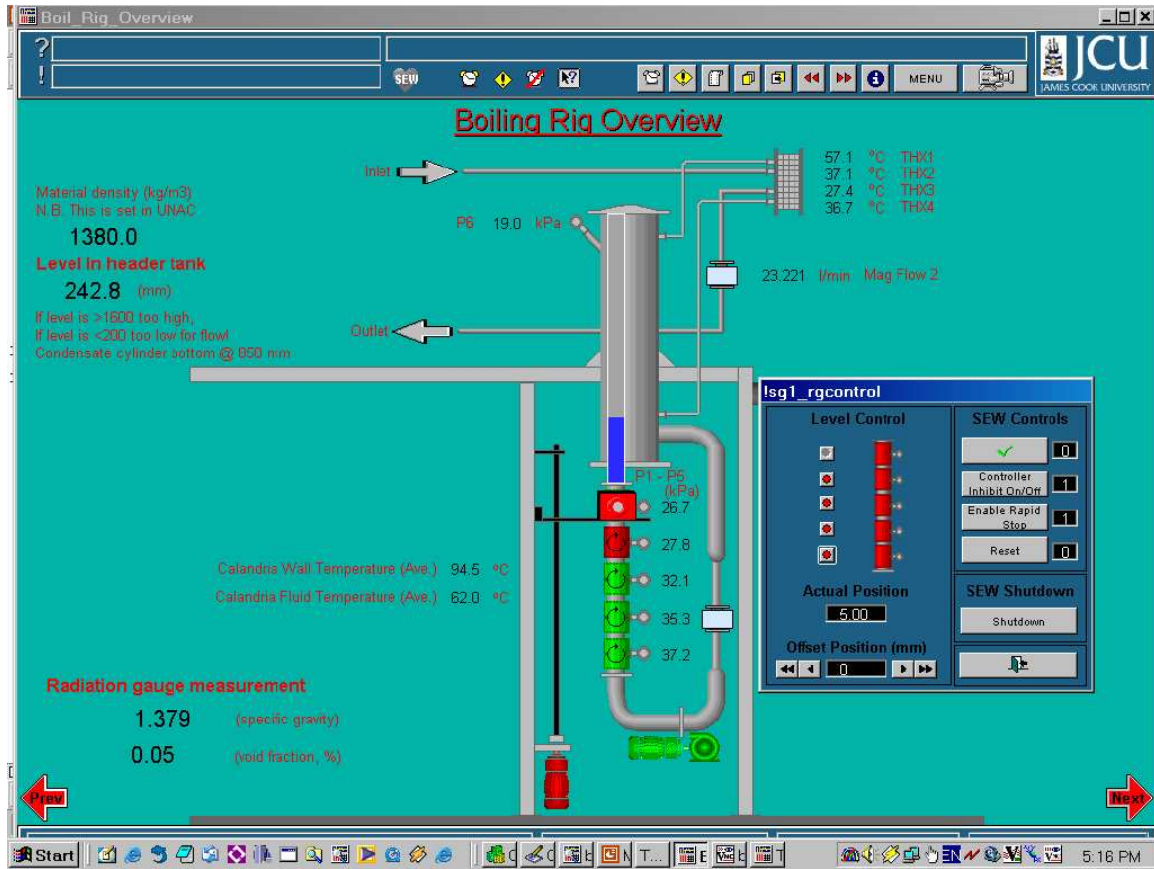


Figure E7: Boiling rig overview showing the densitometer control interface page.

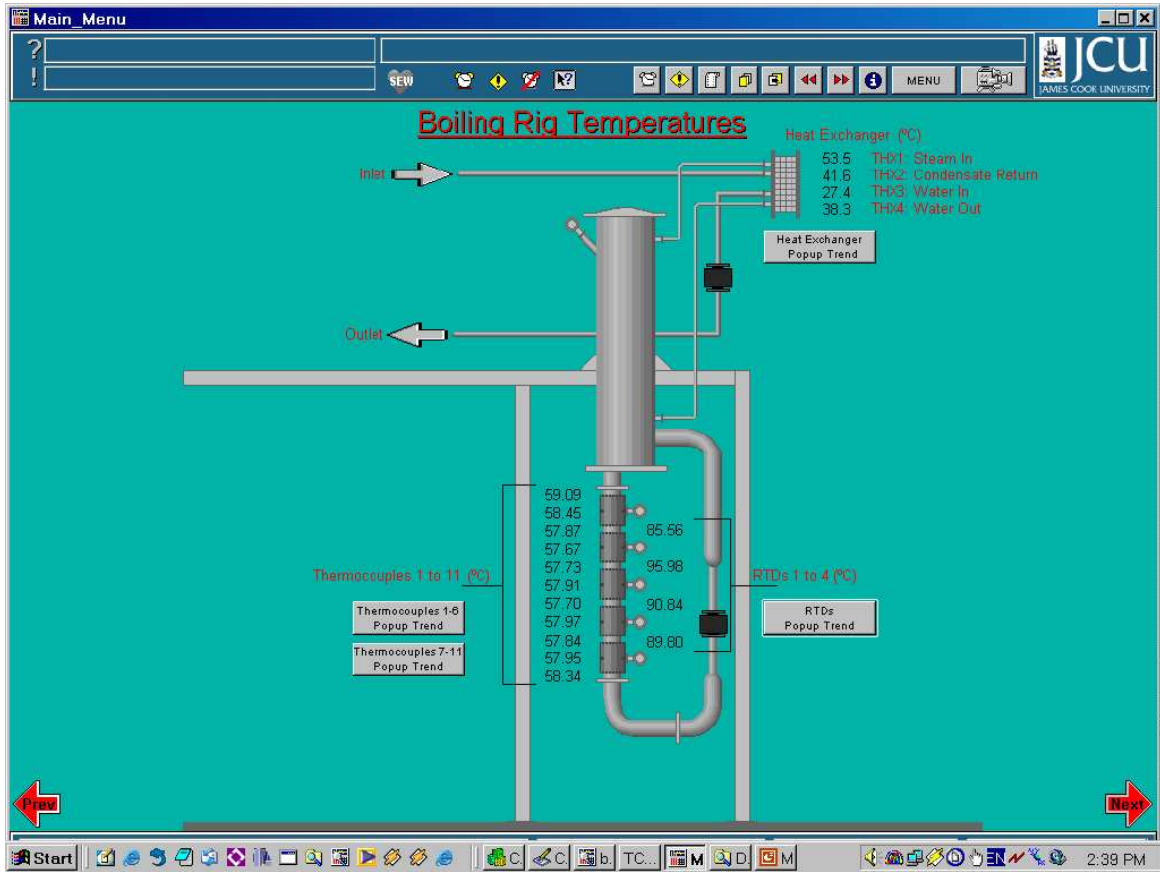


Figure E8: Temperature and trends interface page.

APPENDIX F – SEW Motor and Inverter wiring information

Wiring Connections for MoviDrive Drive Inverter - MDS Basic unit Size 1				
Term	Pin No.	Label	Description	Connection to be made
X1:	1/2/3	L1/L2/L3	Mains Connection	Connect to Mains 3 phase supply
X2:	4/5/6	U/V/W	Motor Cable	Connect to Motor Power Terminals
X3:	8/9	R+/R-	Braking Resistor Connection	Connect Brake Resistor Cables
X4:	1	+Vcd link	DC Link Connection	Not required
	2	-Vcd link		
X11:	1	REF1	+10 V (max 3mA)	Not required
	2	AI1	Setpoint input	
	3	AI12	Setpoint input	
	4	AGND	Reference potential for analog signals	
	5	REF2	-10 V (max 3mA)	
S11			Switch between V/I signals for X11	Leave as V
S12			Connect or disconnect terminating resistor for system bus	Leave as Disconnect
X12:	1	DGND	Reference potential for system bus	Not required
	2	SC11	System Bus High	
	3	SC12	System Bus Low	
X13:	1	DI00	Binary Input 1, Fixed assignment: /Controller inhibit	To MTL DO2: CH1 (SEWI1): 1W
	2	DI01	Binary Input 2, Set to Enable/rapid stop	To MTL DO2: CH2 (SEWI2): 2W
	3	DI02	Binary Input 3, Set to IPOS Input (Shutdown)	To MTL DO2: CH3 (SEWI3): 3W
	4	DI03	Binary Input 4, Set to /LIMIT SWITCH CCW	Connect to CCW Lim Switch
	5	DI04	Binary Input 5, Set to /LIMIT SWITCH CW	Connect to CW Lim Switch
	6	DI05	Binary Input 6, Set to No Function	Connect to reference cam
	7	DCOM	Reference for X13 Binary Inputs	Connect: 1B, 2B, 3B
	8	VO24	Auxiliary power supply output +24V for external command switches	Not required
	9	DGND	Reference potential for binary inputs	Not Required
	10	ST11	RS-485+	Not Required
	11	ST12	RS-485-	
X14:			Encoder Connection with option DPA11A/DIP11A	Not Required
X15:	1	Sin+ (S2)	Sine	Connect to Pin 5 Motor Terminal (MT3W)
	2	Cos+(S1)	Cosine	Connect to Pin 3 Motor Terminal (MT2W)
	3	Ref+(R1)	Reference	Connect to Pin 1 Motor Terminal (MT1W)
	4	N.C.	-	Not Connected
	5	DGND	Reference Potential DGND	Connect to Pin 10 Motor Terminal (MT4B)
	6	Sin-(S4)	Sine	Connect to Pin 6 Motor Terminal (MT3B)

Appendices

	7	Cos-(S3)	Cosine	Connect to Pin 4 Motor Terminal (MT2B)
	8	Ref-(R2)	Reference	Connect to Pin 2 Motor Terminal (MT1B)
	9	TF-/TH-	Thermal Motor Protection	Connect to Pin 9 Motor Terminal (MT4W)
X10:	1	TF1	TF-/TH connection.	Connect with X10.2
	2	DGND	Reference potential for binary inputs	Connect with X10.1
	3	DB00	Binary output 0, fixed assigned to: /Brake	To MTL DI1: CH1 -ve (SEWO1): 6W
	4	DO01-C	Binary Output 1, factory setting: Ready	Connect to X10.8
	5	DO01-NO	Binary Output 1, Normally Open Contact	To MTL DI1: CH2 -ve (SEWO2): 7W
	6	DO01-NC	Binary Output 1, Normally Closed Contact	Not Required
	7	DO02	Binary Output 2, Factory Setting: /Fault	To MTL DI1: CH3 -ve (SEWO3): 8W
	8	VO24	+24V auxiliary voltage output	Connect to X10.4, CCW and CW Limit Switch
	9	VI24	+24V external voltage supply	Not Required
	10	DGND	Reference potential for binary signals	Connect to 24VDC Power Supply BFP GND
Terminal			Slot for interface USS21A	Plug in USS21A interface
Option 1			Optional PCBs	DIO11A
X20	1	AI21	Analog differential input	Not Required
	2	AI22	Analog differential input	
	3	AGND	Reference Terminal	
X21	1	AOV1	Analog Outputs	Not Required
	2	AOC1		
	3	AGND		
	4	AOV2		
	5	AOC2		
	6	AGND		
X22	1	DI10	Binary Input, Set to IPOS Input (Handshake)	To MTL DO2: CH4 (SEWI4): 4W
	2	DI11	Binary Input, Set to IPOS Input (Data)	To MTL DO2: CH5 (SEWI5): 5W
	3	DI12	Binary Input, Set to IPOS Input (Data)	To MTL DO2: CH6
	4	DI13	Binary Input, Set to IPOS Input (Data)	To MTL DO2: CH7
	5	DI14	Binary Input, Set to IPOS Input (Heartbeat)	To MTL DO2: CH8
	6	DI15		
	7	DI16		
	8	DI17		
	9	DCOM	Reference Terminal: for Binary inputs	Connect: 4B, 5B
	10	DGND	Reference Terminal: for non-floating inputs	Not Required
X23	1	DO10	Binary Output, Set to IPOS Output (ACK)	To MTL DI1: CH4 -ve (SEWO4): 9W
	2	DO11	Binary Output, Set to IPOS In Position	To MTL DI1: CH5 -ve (SEWO5): 10W
	3	DO12	Binary Output, Set to IPOS Output (Heartbeat)	To MTL DI1: CH6 -ve
	4	DO13	Binary Output, Set to IPOS Output (Shutdown)	To MTL DI1: CH7 -ve
	5	DO14		

Appendices

6	DO15		
7	DO16		
8	DO17		
9	DGND	Reference Terminal: for Binary outputs	Connect to 24VDC Power Supply BFP GND
Option 2		Optional PCBs	Not Required

Motor Terminal Box			
1	R1	Reference	Connect to X15.3 MT1W
2	R2		Connect to X15.8 MT1B
3	S1	Cosine	Connect to X15.2 MT2W
4	S3		Connect to X15.7 MT2B
5	S2	Sine	Connect to X15.1 MT3W
6	S4		Connect to X15.6 MT3B
7	-	No Connection	Not Required
8	-	No Connection	Not Required
9	TH/TF	Thermal Motor Protection	Connect to X15.9 MT4W
10			Connect to X15.5 MT4B

Key	
x = Number	
xW = White wire no. x in multicore cable connecting SEW to MTL	
xB = Black wire no. x in multicore cable connection SEW to MTL	
CW = Clockwise hardware limit switch for upward travel	
CCW = Counterclockwise hardware limit switch for downward travel	
MTxB/W = Refers to multicore cable connecting motor terminal box to SEW: xB/W is black/white wire no. x	
BFP = Bus Field Power	
USS21A is the communications (RS232 and RS485) plug in terminal	

APPENDIX G – Summary of JCU experimental data

G1 – Natural circulation trials

Descriptor :				Descriptor :				Descriptor :			
Run1n				Run2n				Run3n			
Date:	29/04/2004			Date:	29/04/2004			Date:	29/04/2004		
Time:	10:10			Time:	11:00			Time:	11:40		
Brix	77.1 %			Brix	77.1 %			Brix	77.1 %		
Dry substance	75.51 %			Dry substance	75.51 %			Dry substance	75.51 %		
Purity	72.2 %			Purity	72.2 %			Purity	72.2 %		
Density	1357 kg/m ³			Density	1357 kg/m ³			Density	1357 kg/m ³		
Viscosity	0.24 Pa.s			Viscosity	0.24 Pa.s			Viscosity	0.24 Pa.s		
Tube inlet temperature	58.9 °C			Tube inlet temperature	62.8 °C			Tube inlet temperature	60.6 °C		
Vacuum (head space)	15.5 kPa.a			Vacuum (head space)	17.5 kPa.a			Vacuum (head space)	15.2 kPa.a		
Level in header tank	750 mm			Level in header tank	720 mm			Level in header tank	960 mm		
Circulation velocity	0.0376 m/s			Circulation velocity	0.0446 m/s			Circulation velocity	0.004 m/s		
Mass flow rate	0.419 kg/s			Mass flow rate	0.498 kg/s			Mass flow rate	0.046 kg/s		
Pressure drop (over tube)	13.62 kPa			Pressure drop (over tube)	13.82 kPa			Pressure drop (over tube)	10.36 kPa		
Void fraction at exit	3.38 %			Void fraction at exit	4.2 %			Void fraction at exit	4.1 %		
Heat flux (over tube - HBs)	15 kW			Heat flux (over tube - HBs)	18 kW			Heat flux (over tube - HBs)	14.4 kW		
Calculated heat flux (Heat exchanger)	14 kW			Calculated heat flux (Heat exchanger)	15.1 kW			Calculated heat flux (Heat exchanger)	12.88 kW		
Tube wall temperature	92.2 °C			Tube wall temperature	98.2 °C			Tube wall temperature	93.7 °C		
Vapour superheat	-0.7 °C			Vapour superheat	-0.5 °C			Vapour superheat	0.5 °C		
Position (mm)	Axial Temperature (°C)	Pressure (kPa)	Void fraction	Position (mm)	Axial Temperature (°C)	Pressure (kPa)	Void fraction	Position (mm)	Axial Temperature (°C)	Pressure (kPa)	Void fraction
0	58.90			0	62.78			0	60.58		
130	58.83	41.03	0.0552	130	62.77	42.59		130	60.40	40.09	
260	58.30		0.0277	260	62.17		0.0222	260	59.77		-0.0139
390	58.53	37.56	0.0493	390	62.50	39.03	0.0287	390	59.88	36.41	0.0270
520	58.16		0.0221	520	62.18		0.0155	520	59.32		0.0007
650	58.66	34.12	0.0487	650	62.77	35.58	0.0278	650	59.84	32.87	0.0276
780	60.65		0.0312	780	63.62		0.0241	780	61.08		0.0159
910	62.65	30.63	0.0475	910	65.41	32.03	0.0306	910	62.05	29.30	0.0247
1040	66.12		0.0388	1040	67.69		0.0288	1040	65.61		0.0198
1170	66.37	27.41	0.0500	1170	68.50	28.77	0.0343	1170	65.90	26.05	0.0310
1300	67.21		0.0338	1300	69.29		0.0419	1300	67.03		0.0406
Head space		15.53		Head space		17.49		Head space		15.21	

G1 – Natural circulation trials

Descriptor :				Run4n				Descriptor :				Run5n				Descriptor :				Run6n			
Date:				29/04/2004				Date:				29/04/2004				Date:				29/04/2004			
Time:				14:00				Time:				14:40				Time:				15:30			
Brix				82.1 %				Brix				82.1 %				Brix				82.1 %			
Dry substance				80.33 %				Dry substance				80.33 %				Dry substance				80.33 %			
Purity				72.8 %				Purity				72.8 %				Purity				72.8 %			
Density				1388 kg/m ³				Density				1388 kg/m ³				Density				1388 kg/m ³			
Viscosity				0.955 Pa.s				Viscosity				0.955 Pa.s				Viscosity				0.955 Pa.s			
Tube inlet temperature				59.8 °C				Tube inlet temperature				63.7 °C				Tube inlet temperature				71.7 °C			
Vacuum (head space)				14.7 kPa.a				Vacuum (head space)				16.9 kPa.a				Vacuum (head space)				22.7 kPa.a			
Level in header tank				590 mm				Level in header tank				585 mm				Level in header tank				620 mm			
Circulation velocity				0.0148 m/s				Circulation velocity				0.0285 m/s				Circulation velocity				0.0446 m/s			
Mass flow rate				0.169 kg/s				Mass flow rate				0.325 kg/s				Mass flow rate				0.503 kg/s			
Pressure drop (over tube)				14.05 kPa				Pressure drop (over tube)				14.13 kPa				Pressure drop (over tube)				14.46 kPa			
Void fraction at exit				4.6 %				Void fraction at exit				6.2 %				Void fraction at exit				7.4 %			
Heat flux (over tube - HBs)				15 kW				Heat flux (over tube - HBs)				18 kW				Heat flux (over tube - HBs)				18 kW			
Calculated heat flux (Heat exchanger)				12.5 kW				Calculated heat flux (Heat exchanger)				15.2 kW				Calculated heat flux (Heat exchanger)				15.3 kW			
Tube wall temperature				99.2 °C				Tube wall temperature				104.7 °C				Tube wall temperature				109.3 °C			
Vapour superheat				0 °C				Vapour superheat				0.3 °C				Vapour superheat				1.7 °C			
Position (mm)	Axial Temperature (°C)	Pressure (kPa)	Void fraction	Position (mm)	Axial Temperature (°C)	Pressure (kPa)	Void fraction	Position (mm)	Axial Temperature (°C)	Pressure (kPa)	Void fraction												
0	59.80			0	63.74			0	71.74														
130	59.70	38.58		130	63.43	40.74		130	71.31	46.98	-0.0119												
260	59.22			260	63.06			260	70.89		-0.0119												
390	59.61	35.00	0.0448	390	63.61	37.11	0.0392	390	71.64	43.21	0.0454												
520	59.19		0.0277	520	63.16		0.0204	520	71.20		0.0205												
650	59.73	31.44	0.0400	650	63.72	33.56	0.0397	650	71.65	39.63	0.0417												
780	60.87		0.0295	780	63.89		0.0309	780	71.67		0.0301												
910	61.06	27.84	0.0369	910	65.74	29.89	0.0397	910	73.05	35.81	0.0454												
1040	65.66		0.0316	1040	67.94		0.0388	1040	73.57		0.0421												
1170	66.01	24.53	0.0434	1170	68.63	26.61	0.0540	1170	75.26	32.52	0.0595												
1300	66.57		0.0458	1300	69.41		0.0616	1300	75.65		0.0744												
Head space		14.68		Head space		16.87		Head space		22.67													

G1 – Natural circulation trials

Descriptor : Run7n				Descriptor : Run8n				Descriptor : Run9n			
Date:	29/04/2004			Date:	29/04/2004			Date:	26/05/2004		
Time:	17:30			Time:	18:00			Time:	14:00		
Brix	86 %			Brix	86 %			Brix	82.1 %		
Dry substance	84.09 %			Dry substance	84.09 %			Dry substance	80.06 %		
Purity	72.4 %			Purity	72.4 %			Purity	76.2 %		
Density	1413 kg/m ³			Density	1413 kg/m ³			Density	1388 kg/m ³		
Viscosity	3.75 Pa.s			Viscosity	3.75 Pa.s			Viscosity	0.955 Pa.s		
Tube inlet temperature	67.5 °C			Tube inlet temperature	60.7 °C			Tube inlet temperature	57.2 °C		
Vacuum (head space)	16.6 kPa.a			Vacuum (head space)	13.2 kPa.a			Vacuum (head space)	15 kPa.a		
Level in header tank	370 mm			Level in header tank	360 mm			Level in header tank	1180 mm		
Circulation velocity	0.045 m/s			Circulation velocity	0.0199 m/s			Circulation velocity	0.0264 m/s		
Mass flow rate	0.52 kg/s			Mass flow rate	0.231 kg/s			Mass flow rate	0.301 kg/s		
Pressure drop (over tube)	14 kPa			Pressure drop (over tube)	9.9 kPa			Pressure drop (over tube)	10.22 kPa		
Void fraction at exit	53.1 %			Void fraction at exit	28.5 %			Void fraction at exit	7.6 %		
Heat flux (over tube - HBs)	18 kW			Heat flux (over tube - HBs)	12 kW			Heat flux (over tube - HBs)	12 kW		
Calculated heat flux (Heat exchanger)	14.98 kW			Calculated heat flux (Heat exchanger)	11.22 kW			Calculated heat flux (Heat exchanger)	11.3 kW		
Tube wall temperature	109.5 °C			Tube wall temperature	101.1 °C			Tube wall temperature	91.4 °C		
Vapour superheat	1.2 °C			Vapour superheat	2.5 °C			Vapour superheat	-1.4 °C		
Position (mm)	Axial Temperature (°C)	Pressure (kPa)	Void fraction	Position (mm)	Axial Temperature (°C)	Pressure (kPa)	Void fraction	Position (mm)	Axial Temperature (°C)	Pressure (kPa)	Void fraction
0	67.46			0	60.69			0	57.21		
130	67.16	37.94		130	60.57	34.43	-0.0256	130	57.00	43.46	
260	66.49			260	59.98		-0.0256	260	56.59		
390	67.34	33.99	0.0823	390	60.77	30.61	0.0343	390	59.75	39.99	0.0740
520	66.95		0.0379	520	60.54		0.0307	520	65.27		0.0677
650	68.15	30.47	0.1669	650	62.56	27.13	0.1612	650	65.48	36.61	0.0752
780	68.65		0.1844	780	63.02		0.1148	780	68.00		0.0729
910	69.37	26.90	0.2051	910	64.15	23.68	0.2677	910	68.18	33.24	0.0790
1040	69.73		0.3856	1040	64.82		0.3254	1040	69.40		0.0758
1170	70.79	23.94	0.3114	1170	65.96	20.71	0.3809	1170	70.22	30.04	0.0747
1300	71.41		0.5319	1300	66.44		0.2851	1300	69.94		0.0596
Head space		16.60		Head space		13.24		Head space		15.00	

G1 – Natural circulation trials

Descriptor :				Run10n				Descriptor :				Run11n				Descriptor :				Run12n			
Date:				26/05/2004				Date:				26/05/2004				Date:				27/05/2004			
Time:				15:00				Time:				16:00				Time:				8:40			
Brix				82.1 %				Brix				82.1 %				Brix				79.9 %			
Dry substance				80.06 %				Dry substance				80.06 %				Dry substance				77.65 %			
Purity				76.2 %				Purity				76.2 %				Purity				76.7 %			
Density				1388 kg/m ³				Density				1388 kg/m ³				Density				1371 kg/m ³			
Viscosity				0.955 Pa.s				Viscosity				0.955 Pa.s				Viscosity				0.4 Pa.s			
Tube inlet temperature				64.4 °C				Tube inlet temperature				62.85 °C				Tube inlet temperature				58.6 °C			
Vacuum (head space)				18.5 kPa.a				Vacuum (head space)				16.5 kPa.a				Vacuum (head space)				15.5 kPa.a			
Level in header tank				880 mm				Level in header tank				1050 mm				Level in header tank				810 mm			
Circulation velocity				0.053 m/s				Circulation velocity				0.032 m/s				Circulation velocity				0.032 m/s			
Mass flow rate				0.6 kg/s				Mass flow rate				0.366 kg/s				Mass flow rate				0.356 kg/s			
Pressure drop (over tube)				13.79 kPa				Pressure drop (over tube)				10.52 kPa				Pressure drop (over tube)				13.56 kPa			
Void fraction at exit				9.4 %				Void fraction at exit				13 %				Void fraction at exit				5.7 %			
Heat flux (over tube - HBs)				18 kW				Heat flux (over tube - HBs)				14.4 kW				Heat flux (over tube - HBs)				15 kW			
Calculated heat flux (Heat exchanger)				15.3 kW				Calculated heat flux (Heat exchanger)				12.97 kW				Calculated heat flux (Heat exchanger)				12.4 kW			
Tube wall temperature				97.4 °C				Tube wall temperature				103.4 °C				Tube wall temperature				91.2 °C			
Vapour superheat				0.5 °C				Vapour superheat				0.9 °C				Vapour superheat				-1.5 °C			
Position (mm)	Axial Temperature (°C)	Pressure (kPa)	Void fraction	Position (mm)	Axial Temperature (°C)	Pressure (kPa)	Void fraction	Position (mm)	Axial Temperature (°C)	Pressure (kPa)	Void fraction												
0	64.43			0	63.94			0	58.58														
130	64.26	46.42		130	63.65	43.19		130	58.40	42.14													
260	63.64		0.0413	260	62.85			260	58.57		0.0337												
390	64.47	42.80	0.0236	390	62.92	39.41		390	59.55	38.56	0.0348												
520	68.22		0.0475	520	64.56		0.0187	520	65.08		0.0327												
650	68.91	39.29	0.0483	650	65.41	35.82	0.0341	650	65.58	35.13	0.0366												
780	70.61		0.0556	780	70.48		0.0261	780	68.28		0.0355												
910	71.23	35.85	0.0526	910	70.46	32.23	0.0432	910	68.43	31.75	0.0386												
1040	72.19		0.0586	1040	70.69		0.0317	1040	69.78		0.0408												
1170	73.10	32.63	0.0721	1170	70.97	28.89	0.0698	1170	70.11	28.58	0.0224												
1300	73.45		0.0941	1300	69.98		0.1304	1300	69.82		0.0570												
Head space				18.50				Head space				16.50				Head space				15.50			

G1 – Natural circulation trials

Descriptor : Run13n				Descriptor : Run14n				Descriptor : Run15n			
Date:	27/05/2004			Date:	27/05/2004			Date:	27/05/2004		
Time:	9:20			Time:	11:30			Time:	12:20		
Brix	79.9 %			Brix	85.4 %			Brix	85.4 %		
Dry substance	77.65 %			Dry substance	82.23 %			Dry substance	82.23 %		
Purity	76.7 %			Purity	76.8 %			Purity	76.8 %		
Density	1371 kg/m ³			Density	1401 kg/m ³			Density	1401 kg/m ³		
Viscosity	0.4 Pa.s			Viscosity	1.71 Pa.s			Viscosity	1.71 Pa.s		
Tube inlet temperature	63.6 °C			Tube inlet temperature	62.97 °C			Tube inlet temperature	64.5 °C		
Vacuum (head space)	14 kPa.a			Vacuum (head space)	12 kPa.a			Vacuum (head space)	13 kPa.a		
Level in header tank	1050 mm			Level in header tank	930 mm			Level in header tank	900 mm		
Circulation velocity	0.048 m/s			Circulation velocity	0.013 m/s			Circulation velocity	0.011 m/s		
Mass flow rate	0.544 kg/s			Mass flow rate	0.15 kg/s			Mass flow rate	0.132 kg/s		
Pressure drop (over tube)	13.7 kPa			Pressure drop (over tube)	6.92 kPa			Pressure drop (over tube)	10.47 kPa		
Void fraction at exit	12.1 %			Void fraction at exit	11.2 %			Void fraction at exit	9.9 %		
Heat flux (over tube - HBs)	18 kW			Heat flux (over tube - HBs)	9 kW			Heat flux (over tube - HBs)	10.66 kW		
Calculated heat flux (Heat exchanger)	15.5 kW			Calculated heat flux (Heat exchanger)	9 kW			Calculated heat flux (Heat exchanger)	9.3 kW		
Tube wall temperature	100.2 °C			Tube wall temperature	105.7 °C			Tube wall temperature	106.3 °C		
Vapour superheat	5.1 °C			Vapour superheat	1.3 °C			Vapour superheat	-0.2 °C		
Position (mm)	Axial Temperature (°C)	Pressure (kPa)	Void fraction	Position (mm)	Axial Temperature (°C)	Pressure (kPa)	Void fraction	Position (mm)	Axial Temperature (°C)	Pressure (kPa)	Void fraction
0	63.60			0	59.52			0	58.33		
130	63.56	43.86		130	59.29	37.21		130	62.42	37.84	
260	63.05		0.0230	260	62.97			260	64.50		
390	63.83	40.15	0.0220	390	64.30	33.56		390	65.33	34.26	0.0525
520	67.61		0.0200	520	66.01		0.0524	520	64.82		0.0596
650	68.12	36.98	0.0228	650	66.72	30.04	0.0669	650	65.29	30.80	0.0515
780	70.95		0.0240	780	66.19		0.0572	780	64.54		0.0465
910	71.02	33.71	0.0324	910	65.47	26.65	0.1232	910	64.28	27.37	0.0658
1040	71.90		0.0313	1040	65.90		0.1120	1040	64.78		0.0488
1170	72.19	30.15	0.0692	1170	67.87	23.64	0.1838	1170	67.22	24.22	0.0685
1300	71.57		0.1207	1300	68.07		0.1018	1300	67.01		0.0988
Head space		14.00		Head space		12.00		Head space		13.00	

G2 – Forced circulation trials

Descriptor : Run1				Descriptor : Run2				Descriptor : Run3			
Date:		11/11/2003		Date:		11/11/2003		Date:		11/11/2003	
Time:		13:30		Time:		13:30		Time:		13:30	
Brix		72.8 %		Brix		72.8 %		Brix		72.8 %	
Dry substance		72.74 %		Dry substance		72.74 %		Dry substance		72.74 %	
Purity		79.2 %		Purity		79.2 %		Purity		79.2 %	
Density		1343 kg/m ³		Density		1343 kg/m ³		Density		1343 kg/m ³	
Viscosity		0.15 Pa.s		Viscosity		0.15 Pa.s		Viscosity		0.15 Pa.s	
Tube inlet temperature		°C		Tube inlet temperature		°C		Tube inlet temperature		°C	
Vacuum (head space)		17 kPa.a		Vacuum (head space)		16.8 kPa.a		Vacuum (head space)		16.9 kPa.a	
Level in header tank		580 mm		Level in header tank		585 mm		Level in header tank		585 mm	
Pump speed		150 rpm		Pump speed		300 rpm		Pump speed		600 rpm	
Circulation velocity		0.073 m/s		Circulation velocity		0.143 m/s		Circulation velocity		0.288 m/s	
Mass flow rate		0.8 kg/s		Mass flow rate		1.575 kg/s		Mass flow rate		3.18 kg/s	
Pressure drop (over tube)		10.8 kPa		Pressure drop (over tube)		11.04 kPa		Pressure drop (over tube)		11.24 kPa	
Void fraction at exit		4.1 %		Void fraction at exit		3.1 %		Void fraction at exit		2.5 %	
Heat flux (over tube - HBs)		15 kW		Heat flux (over tube - HBs)		15 kW		Heat flux (over tube - HBs)		15 kW	
Calculated heat flux (Heat exchanger)		12 kW		Calculated heat flux (Heat exchanger)		12.2 kW		Calculated heat flux (Heat exchanger)		12.7 kW	
Tube wall temperature		90 °C		Tube wall temperature		90.3 °C		Tube wall temperature		91.5 °C	
Vapour superheat		-2.9 °C		Vapour superheat		-2.9 °C		Vapour superheat		-2.7 °C	
Position (mm)	Axial Temperature (°C)	Pressure (kPa)	Void fraction	Position (mm)	Axial Temperature (°C)	Pressure (kPa)	Void fraction	Position (mm)	Axial Temperature (°C)	Pressure (kPa)	Void fraction
0				0				0			
130		40.02	0.0231	130		39.87	0.0168	130		40.06	0.0107
260			0.0075	260			-0.0084	260			-0.0153
390		36.69	0.0242	390		36.44	0.0197	390		36.60	0.0138
520			-0.0436	520			-0.0512	520			-0.0550
650	57.70	35.43	0.0340	650	57.81	35.11	0.0283	650	58.24	35.22	0.0231
780	57.56		0.0250	780	57.69		0.0188	780	58.10		0.0138
910	57.49	32.18	0.0315	910	57.63	31.79	0.0247	910	58.01	31.83	0.0215
1040	57.77		0.0327	1040	57.67		0.0273	1040	58.02		0.0261
1170	61.93	29.23	0.0396	1170	58.40	28.83	0.0318	1170	58.72	28.82	0.0246
1300	62.74		0.0408	1300	58.81		0.0310	1300	58.93		0.0251
Head space		16.96		Head space		16.77		Head space		16.95	

G2 – Forced circulation trials

Descriptor : Run4				Descriptor : Run5				Descriptor : Run6			
Date:		11/11/2003		Date:		11/11/2003		Date:		11/11/2003	
Time:		13:30		Time:		13:30		Time:		13:30	
Brix		72.8 %		Brix		72.8 %		Brix		72.8 %	
Dry substance		72.74 %		Dry substance		72.74 %		Dry substance		72.74 %	
Purity		79.2 %		Purity		79.2 %		Purity		79.2 %	
Density		1343 kg/m ³		Density		1343 kg/m ³		Density		1343 kg/m ³	
Viscosity		0.15 Pa.s		Viscosity		0.15 Pa.s		Viscosity		0.15 Pa.s	
Tube inlet temperature		°C		Tube inlet temperature		°C		Tube inlet temperature		°C	
Vacuum (head space)		18.6 kPa.a		Vacuum (head space)		18.7 kPa.a		Vacuum (head space)		19.1 kPa.a	
Level in header tank		550 mm		Level in header tank		530 mm		Level in header tank		490 mm	
Pump speed		600 rpm		Pump speed		300 rpm		Pump speed		150 rpm	
Circulation velocity		0.288 m/s		Circulation velocity		0.144 m/s		Circulation velocity		0.072 m/s	
Mass flow rate		3.18 kg/s		Mass flow rate		1.59 kg/s		Mass flow rate		0.791 kg/s	
Pressure drop (over tube)		11.23 kPa		Pressure drop (over tube)		11.04 kPa		Pressure drop (over tube)		10.93 kPa	
Void fraction at exit		2.4 %		Void fraction at exit		%		Void fraction at exit		6.2 %	
Heat flux (over tube - HBs)		18 kW		Heat flux (over tube - HBs)		18 kW		Heat flux (over tube - HBs)		18 kW	
Calculated heat flux (Heat exchanger)		14.5 kW		Calculated heat flux (Heat exchanger)		14.5 kW		Calculated heat flux (Heat exchanger)		14.25 kW	
Tube wall temperature		97.1 °C		Tube wall temperature		97.4 °C		Tube wall temperature		98.1 °C	
Vapour superheat		-1.55 °C		Vapour superheat		-1.4 °C		Vapour superheat		-1.4 °C	
Position (mm)	Axial Temperature (°C)	Pressure (kPa)	Void fraction	Position (mm)	Axial Temperature (°C)	Pressure (kPa)	Void fraction	Position (mm)	Axial Temperature (°C)	Pressure (kPa)	Void fraction
0				0				0			
130		41.28	0.0059	130		41.01		130		40.99	
260			0.0025	260				260			-0.01372
390		37.82	0.0092	390		37.64		390		37.59	
520			-0.0625	520				520			-0.06044
650	61.29	36.48	0.0190	650	61.99	36.34		650	66.68	36.32	
780	61.09		0.0068	780	61.84			780	66.41		0.013054
910	61.01	33.04	0.0169	910	61.89	32.94		910	66.87	32.95	
1040	61.06		0.0221	1040	62.12			1040	67.58		0.03405
1170	61.77	30.05	0.0269	1170	63.27	29.98		1170	69.07	30.06	
1300	62.12		0.0237	1300	64.00			1300	69.65		0.061504
Head space		18.62		Head space		18.68		Head space		19.10	

G2 – Forced circulation trials

Descriptor : Run7				Descriptor : Run8				Descriptor : Run9			
Date:		12/11/2003		Date:		12/11/2003		Date:		12/11/2003	
Time:		9:05		Time:		10:00		Time:			
Brix		74.6 %		Brix		74.6 %		Brix		74.6 %	
Dry substance		72.39 %		Dry substance		72.39 %		Dry substance		72.39 %	
Purity		78.5 %		Purity		78.5 %		Purity		78.5 %	
Density		1341 kg/m ³		Density		1341 kg/m ³		Density		1341 kg/m ³	
Viscosity		0.13 Pa.s		Viscosity		0.13 Pa.s		Viscosity		0.13 Pa.s	
Tube inlet temperature		61.5 °C		Tube inlet temperature		61.4 °C		Tube inlet temperature		62.4 °C	
Vacuum (head space)		18.2 kPa.a		Vacuum (head space)		18.4 kPa.a		Vacuum (head space)		19.1 kPa.a	
Level in header tank		560 mm		Level in header tank		560 mm		Level in header tank		575 mm	
Pump speed		150 rpm		Pump speed		300 rpm		Pump speed		600 rpm	
Circulation velocity		0.072 m/s		Circulation velocity		0.144 m/s		Circulation velocity		0.291 m/s	
Mass flow rate		0.79 kg/s		Mass flow rate		1.588 kg/s		Mass flow rate		3.2 kg/s	
Pressure drop (over tube)		7.8 kPa		Pressure drop (over tube)		7.8 kPa		Pressure drop (over tube)		7.9 kPa	
Void fraction at exit		2.3 %		Void fraction at exit		2.4 %		Void fraction at exit		1.6 %	
Heat flux (over tube - HBs)		14.4 kW		Heat flux (over tube - HBs)		14.4 kW		Heat flux (over tube - HBs)		14.4 kW	
Calculated heat flux (Heat exchanger)		12.3 kW		Calculated heat flux (Heat exchanger)		12.7 kW		Calculated heat flux (Heat exchanger)		12.5 kW	
Tube wall temperature		103.7 °C		Tube wall temperature		103.2 °C		Tube wall temperature		102.9 °C	
Vapour superheat		-2.95 °C		Vapour superheat		-2.2 °C		Vapour superheat		-2.5 °C	
Position (mm)	Axial Temperature (°C)	Pressure (kPa)	Void fraction	Position (mm)	Axial Temperature (°C)	Pressure (kPa)	Void fraction	Position (mm)	Axial Temperature (°C)	Pressure (kPa)	Void fraction
0	63.45			0	61.95			0	62.89		
130	62.85	40.98		130	60.73	41.18		130	61.71	42.02	
260	61.48		-0.036	260	61.37		-0.02897	260	62.36		-0.00756
390	61.30	37.31	0.006	390	60.99	37.58	0.00649	390	62.02	38.32	0.00497
520	60.07		-0.069	520	60.89		-0.06557	520	61.89		-0.06872
650	60.37	35.91	0.014	650	60.46	36.20	0.01411	650	61.45	36.92	0.01251
780	60.11		0.006	780	60.44		0.00372	780	61.46		0.00125
910	60.54	32.48	0.012	910	60.40	32.76	0.01267	910	61.41	33.43	0.00977
1040	60.63		0.016	1040	60.59			1040	61.49		0.01448
1170	61.01	29.51	0.029	1170	61.41	29.78	0.02395	1170	62.15	30.44	0.02105
1300	61.49		0.023	1300	62.09		-0.10522	1300	62.43		0.01592
Head space		18.24		Head space		18.42		Head space		19.07	

G2 – Forced circulation trials

Descriptor :				Run10				Descriptor :				Run11				Descriptor :				Run12			
Date:				12/11/2003				Date:				12/11/2003				Date:				12/11/2003			
Time:								Time:								Time:							
Brix				74.6 %				Brix				74.6 %				Brix				73.8 %			
Dry substance				72.39 %				Dry substance				72.39 %				Dry substance				73.91 %			
Purity				78.5 %				Purity				78.5 %				Purity				77.4 %			
Density				1341 kg/m ³				Density				1341 kg/m ³				Density				1365 kg/m ³			
Viscosity				0.13 Pa.s				Viscosity				0.13 Pa.s				Viscosity				0.95 Pa.s			
Tube inlet temperature				68.2 °C				Tube inlet temperature				67.9 °C				Tube inlet temperature				68.2 °C			
Vacuum (head space)				23.2 kPa.a				Vacuum (head space)				23.1 kPa.a				Vacuum (head space)				23.2 kPa.a			
Level in header tank				575 mm				Level in header tank				565 mm				Level in header tank				520 mm			
Pump speed				300 rpm				Pump speed				300 rpm				Pump speed				150 rpm			
Circulation velocity				0.289 m/s				Circulation velocity				0.143 m/s				Circulation velocity				0.072 m/s			
Mass flow rate				3.18 kg/s				Mass flow rate				1.58 kg/s				Mass flow rate				0.81 kg/s			
Pressure drop (over tube)				11.55 kPa				Pressure drop (over tube)				11.4 kPa				Pressure drop (over tube)				11.4 kPa			
Void fraction at exit				2.3 %				Void fraction at exit				2.2 %				Void fraction at exit				3.6 %			
Heat flux (over tube - HBs)				15 kW				Heat flux (over tube - HBs)				15 kW				Heat flux (over tube - HBs)				15 kW			
Calculated heat flux (Heat exchanger)				13 kW				Calculated heat flux (Heat exchanger)				12.9 kW				Calculated heat flux (Heat exchanger)				13 kW			
Tube wall temperature				102.4 °C				Tube wall temperature				101.9 °C				Tube wall temperature				102.3 °C			
Vapour superheat				-1.8 °C				Vapour superheat				-1.75 °C				Vapour superheat				-1.7 °C			
Position (mm)	Axial Temperature (°C)	Pressure (kPa)	Void fraction	Position (mm)	Axial Temperature (°C)	Pressure (kPa)	Void fraction	Position (mm)	Axial Temperature (°C)	Pressure (kPa)	Void fraction												
0	68.19			0	67.87			0	68.18														
130	67.57	46.19	0.002832	130	67.61	45.97	0.005749	130	67.49	45.81	0.005689												
260	67.67		-0.02383	260	67.57		-0.02403	260	67.68		-0.01875												
390	67.49	42.58	0.00904	390	67.45	42.43	0.00907	390	67.49	42.27	0.01107												
520	67.71		-0.06516	520	67.73		-0.06175	520	67.68		-0.06312												
650	67.31	41.22	0.01695	650	67.33	41.10	0.01761	650	67.22	40.92	0.01786												
780	67.44		0.00606	780	67.51		0.00830	780	69.59		0.00890												
910	67.38	37.67	0.01553	910	67.47	37.58	0.01551	910	72.06	37.40	0.01885												
1040	67.38		0.02094	1040	67.45		0.02170	1040	72.33		0.02406												
1170	68.03	34.64	0.02431	1170	68.20	34.55	0.02698	1170	73.22	34.41	0.03298												
1300	68.26		0.02327	1300	68.73		0.02191	1300	73.60		0.03656												
Head space		23.24		Head space		23.15		Head space		23.19													

G2 – Forced circulation trials

Descriptor : Run13				Descriptor : Run14				Descriptor : Run15			
Date:		12/11/2003		Date:		12/11/2003		Date:		12/11/2003	
Time:				Time:				Time:			
Brix		73.8	%	Brix		73.8	%	Brix		73.8	%
Dry substance		73.91	%	Dry substance		73.91	%	Dry substance		73.91	%
Purity		77.4	%	Purity		77.4	%	Purity		77.4	%
Density		1365	kg/m ³	Density		1365	kg/m ³	Density		1365	kg/m ³
Viscosity		0.95	Pa.s	Viscosity		0.95	Pa.s	Viscosity		0.95	Pa.s
Tube inlet temperature		69.3	°C	Tube inlet temperature		69.5	°C	Tube inlet temperature		69.9	°C
Vacuum (head space)		24.1	kPa.a	Vacuum (head space)		24.3	kPa.a	Vacuum (head space)		24.1	kPa.a
Level in header tank		500	mm	Level in header tank		525	mm	Level in header tank		535	mm
Pump speed		150	rpm	Pump speed		300	rpm	Pump speed		600	rpm
Circulation velocity		0.072	m/s	Circulation velocity		0.143	m/s	Circulation velocity		0.29	m/s
Mass flow rate		0.811	kg/s	Mass flow rate		1.6	kg/s	Mass flow rate		3.2	kg/s
Pressure drop (over tube)		11.4	kPa	Pressure drop (over tube)		11.3	kPa	Pressure drop (over tube)		11.44	kPa
Void fraction at exit		12.5	%	Void fraction at exit		3.1	%	Void fraction at exit		2.3	%
Heat flux (over tube - HBs)		18	kW	Heat flux (over tube - HBs)		18	kW	Heat flux (over tube - HBs)		18	kW
Calculated heat flux (Heat exchanger)		15.3	kW	Calculated heat flux (Heat exchanger)		15.6	kW	Calculated heat flux (Heat exchanger)		15.3	kW
Tube wall temperature		105	°C	Tube wall temperature		105.1	°C	Tube wall temperature		105	°C
Vapour superheat		-0.2	°C	Vapour superheat		0	°C	Vapour superheat		0	°C
Position (mm)	Axial Temperature (°C)	Pressure (kPa)	Void fraction	Position (mm)	Axial Temperature (°C)	Pressure (kPa)	Void fraction	Position (mm)	Axial Temperature (°C)	Pressure (kPa)	Void fraction
0	69.33			0	69.48			0	69.60		
130	73.22	46.45	0.162918	130	69.39	46.93	0.003856	130	69.07	46.95	0.001922
260	68.86		-0.00325	260	69.27		-0.02365	260	69.15		-0.02670
390	68.60	42.91	0.01082	390	69.10	43.42	0.00663	390	68.91	43.36	0.00940
520	68.87		-0.06026	520	69.46		-0.06700	520	69.18		-0.06296
650	68.96	41.57	0.02016	650	69.04	42.14	0.01678	650	68.75	42.05	0.01716
780	73.81		0.01038	780	69.24		0.00478	780	68.90		0.00274
910	73.71	38.01	0.02154	910	69.24	38.61	0.01644	910	68.84	38.48	0.01253
1040	74.34		0.02895	1040	69.38		0.01963	1040	68.83		0.01960
1170	75.22	35.05	0.05094	1170	71.34	35.66	0.03037	1170	69.57	35.51	0.02344
1300	75.40		0.12529	1300	72.38		0.03144	1300	69.96		0.02321
Head space		24.13		Head space		24.27		Head space		24.12	

G2 – Forced circulation trials

Descriptor : Run16				Descriptor : Run17				Descriptor : Run18			
Date:	12/11/2003			Date:	4/02/2004			Date:	4/02/2004		
Time:	17:45			Time:	10:15			Time:	11:10		
Brix	73.8 %			Brix	81.7 %			Brix	81.7 %		
Dry substance	73.91 %			Dry substance	79.6 %			Dry substance	79.6 %		
Purity	77.4 %			Purity	68.2 %			Purity	68.2 %		
Density	1365 kg/m ³			Density	1386 kg/m ³			Density	1386 kg/m ³		
Viscosity	0.95 Pa.s			Viscosity	1.1 Pa.s			Viscosity	1.1 Pa.s		
Tube inlet temperature	69.95 °C			Tube inlet temperature	60.0 °C			Tube inlet temperature	61.9 °C		
Vacuum (head space)	24.2 kPa.a			Vacuum (head space)	16.4 kPa.a			Vacuum (head space)	16.8 kPa.a		
Level in header tank	540 mm			Level in header tank	600 mm			Level in header tank	550 mm		
Pump speed	900 rpm			Pump speed	800 rpm			Pump speed	100 rpm		
Circulation velocity	0.43 m/s			Circulation velocity	0.39 m/s			Circulation velocity	0.09 m/s		
Mass flow rate	4.8 kg/s			Mass flow rate	4.41 kg/s			Mass flow rate	1.02 kg/s		
Pressure drop (over tube)	11.6 kPa			Pressure drop (over tube)	13.5 kPa			Pressure drop (over tube)	13.8 kPa		
Void fraction at exit	1.8 %			Void fraction at exit	%			Void fraction at exit	3.1 %		
Heat flux (over tube - HBs)	18 kW			Heat flux (over tube - HBs)	15 kW			Heat flux (over tube - HBs)	15 kW		
Calculated heat flux (Heat exchanger)	15.5 kW			Calculated heat flux (Heat exchanger)	12.2 kW			Calculated heat flux (Heat exchanger)	12.7 kW		
Tube wall temperature	105 °C			Tube wall temperature	96.9 °C			Tube wall temperature	102 °C		
Vapour superheat	0 °C			Vapour superheat	-2.6 °C			Vapour superheat	-2.7 °C		
Position (mm)	Axial Temperature (°C)	Pressure (kPa)	Void fraction	Position (mm)	Axial Temperature (°C)	Pressure (kPa)	Void fraction (%)	Position (mm)	Axial Temperature (°C)	Pressure (kPa)	Void fraction (%)
0	69.95			0	59.95			0	61.88		
130	69.31	47.09	-0.00031	130	59.50	40.40	0.1356	130	61.43	40.15	
260	69.40		-0.00662	260	59.32		-0.1873	260	61.35		0.0049
390	69.15	43.45	0.00321	390	59.38	37.03	0.0839	390	61.33	36.48	0.0110
520	69.41		-0.06382	520	59.06		-0.1178	520	61.10		0.0052
650	69.00	42.09	0.01223	650	59.42	33.68	0.0546	650	61.66	33.14	0.0203
780	69.12		0.00246	780	59.18		-0.0440	780	65.34		0.0030
910	69.05	38.46	0.01303	910	59.17	30.06	0.0339	910	65.04	29.49	0.0248
1040	69.04		0.02116	1040	59.28		-0.1292	1040	66.31		0.0085
1170	69.74	35.45	0.02375	1170	59.79	26.90	0.0135	1170	67.00	26.31	0.0306
1300	70.07		0.01842	1300	59.97		-0.0085	1300	66.98		
Head space		24.19		Head space		16.36		Head space		16.82	

G2 – Forced circulation trials

Descriptor : Run19				Descriptor : Run20				Descriptor : Run21			
Date:	4/02/2004			Date:	4/02/2004			Date:	4/02/2004		
Time:	11:55			Time:	12:40			Time:	13:25		
Brix	81.7 %			Brix	81.7 %			Brix	81.7 %		
Dry substance	79.6 %			Dry substance	79.6 %			Dry substance	79.6 %		
Purity	68.2 %			Purity	68.2 %			Purity	68.2 %		
Density	1386 kg/m ³			Density	1386 kg/m ³			Density	1386 kg/m ³		
Viscosity	1.1 Pa.s			Viscosity	1.1 Pa.s			Viscosity	1.1 Pa.s		
Tube inlet temperature	62.8 °C			Tube inlet temperature	62.2 °C			Tube inlet temperature	65.1 °C		
Vacuum (head space)	14.5 kPa.a			Vacuum (head space)	16.9 kPa.a			Vacuum (head space)	18.8 kPa.a		
Level in header tank	550 mm			Level in header tank	540 mm			Level in header tank	525 mm		
Pump speed	400 rpm			Pump speed	200 rpm			Pump speed	200 rpm		
Circulation velocity	0.19 m/s			Circulation velocity	0.096 m/s			Circulation velocity	0.096 m/s		
Mass flow rate	2.21 kg/s			Mass flow rate	1.1 kg/s			Mass flow rate	1.1 kg/s		
Pressure drop (over tube)	14.1 kPa			Pressure drop (over tube)	13.9 kPa			Pressure drop (over tube)	13.9 kPa		
Void fraction at exit	1.8 %			Void fraction at exit	3.4 %			Void fraction at exit	7.5 %		
Heat flux (over tube - HBs)	15 kW			Heat flux (over tube - HBs)	15 kW			Heat flux (over tube - HBs)	18 kW		
Calculated heat flux (Heat exchanger)	12.98 kW			Calculated heat flux (Heat exchanger)	12.9 kW			Calculated heat flux (Heat exchanger)	14.96 kW		
Tube wall temperature	104.1 °C			Tube wall temperature	103.8 °C			Tube wall temperature	108.4 °C		
Vapour superheat	-1.65 °C			Vapour superheat	-1.7 °C			Vapour superheat	-1.4 °C		
Position (mm)	Axial Temperature (°C)	Pressure (kPa)	Void fraction (%)	Position (mm)	Axial Temperature (°C)	Pressure (kPa)	Void fraction (%)	Position (mm)	Axial Temperature (°C)	Pressure (kPa)	Void fraction (%)
0	62.85			0	62.23			0	65.11		
130	62.53	40.43	-0.0060	130	61.85	40.15	0.0018	130	64.65	41.80	0.0019
260	62.34		-0.0123	260	61.60		-0.0186	260	64.43		-0.0161
390	62.42	36.67	-0.0039	390	61.78	36.47	0.0037	390	64.73	38.09	0.0007
520	62.05		-0.0112	520	61.40		-0.0046	520	64.32		0.0010
650	62.43	33.27	-0.0035	650	61.76	33.12	0.0064	650	64.91	34.75	0.0108
780	62.27		-0.0119	780	61.66		-0.0039	780	65.81		0.0047
910	62.32	29.53	-0.0029	910	61.91	29.44	0.0154	910	67.50	31.02	0.0224
1040	62.45		0.0026	1040	62.64		0.0100	1040	68.54		0.0237
1170	63.13	26.31	-0.0013	1170	64.55	26.26	0.0209	1170	69.76	27.90	0.0614
1300	63.89		0.0183	1300	66.66		0.0339	1300	70.24		0.0750
Head space		17.00		Head space		16.93		Head space		18.77	

G2 – Forced circulation trials

Descriptor : Run22				Descriptor : Run23				Descriptor : Run24			
Date:	4/02/2004			Date:	4/02/2004			Date:	4/02/2004		
Time:	14:10			Time:	15:00			Time:	17:00		
Brix	81.7 %			Brix	81.7 %			Brix	81.7 %		
Dry substance	79.6 %			Dry substance	79.6 %			Dry substance	79.6 %		
Purity	68.2 %			Purity	68.2 %			Purity	68.2 %		
Density	1386 kg/m ³			Density	1386 kg/m ³			Density	1386 kg/m ³		
Viscosity	1.1 Pa.s			Viscosity	1.1 Pa.s			Viscosity	1.1 Pa.s		
Tube inlet temperature	66.0 °C			Tube inlet temperature	66.7 °C			Tube inlet temperature	60.4 °C		
Vacuum (head space)	19.2 kPa.a			Vacuum (head space)	19.2 kPa.a			Vacuum (head space)	15.7 kPa.a		
Level in header tank	550 mm			Level in header tank	620 mm			Level in header tank	820 mm		
Pump speed	400 rpm			Pump speed	800 rpm			Pump speed	400 rpm		
Circulation velocity	0.19 m/s			Circulation velocity	0.388 m/s			Circulation velocity	0.196 m/s		
Mass flow rate	2.2 kg/s			Mass flow rate	4.42 kg/s			Mass flow rate	2.23 kg/s		
Pressure drop (over tube)	14.1 kPa			Pressure drop (over tube)	14.7 kPa			Pressure drop (over tube)	10.6 kPa		
Void fraction at exit	4.9 %			Void fraction at exit	1.6 %			Void fraction at exit	1.33 %		
Heat flux (over tube - HBs)	18 kW			Heat flux (over tube - HBs)	18 kW			Heat flux (over tube - HBs)	12 kW		
Calculated heat flux (Heat exchanger)	15.3 kW			Calculated heat flux (Heat exchanger)	15.2 kW			Calculated heat flux (Heat exchanger)	10.9 kW		
Tube wall temperature	110.2 °C			Tube wall temperature	97.2 °C			Tube wall temperature	101.2 °C		
Vapour superheat	-1.1 °C			Vapour superheat	-1 °C			Vapour superheat	-2.3 °C		
Position (mm)	Axial Temperature (°C)	Pressure (kPa)	Void fraction (%)	Position (mm)	Axial Temperature (°C)	Pressure (kPa)	Void fraction (%)	Position (mm)	Axial Temperature (°C)	Pressure (kPa)	Void fraction (%)
0	65.95			0	66.75			0	60.44		
130	65.08	42.55	-0.0007	130	66.22	43.56	-0.0039	130	60.03	39.29	0.0134
260	64.65		-0.0158	260	65.47		-0.0328	260	59.73		-0.0007
390	65.54	38.78	-0.0019	390	66.67	39.66	-0.0213	390	59.78	35.66	0.0125
520	65.14		-0.0149	520	66.07		-0.0288	520	59.33		0.0075
650	65.56	35.44	0.0016	650	66.60	36.19	-0.0088	650	59.74	32.32	0.0231
780	65.45		-0.0172	780	66.46		-0.0212	780	59.63		0.0105
910	65.58	31.60	0.0116	910	66.56	32.14	-0.0085	910	59.76	28.67	0.0260
1040	65.75		0.0062	1040	66.41		0.0024	1040	59.93		0.0133
1170	66.65	28.45	0.0182	1170	67.23	28.89	0.0157	1170	61.30	25.45	0.0169
1300	67.90		0.0494	1300	67.63		0.0156	1300	61.84		0.0200
Head space		19.19		Head space		19.23		Head space		15.75	

G2 – Forced circulation trials

Descriptor : Run25				Descriptor : Run26				Descriptor : Run27			
Date:	4/02/2004			Date:	4/02/2004			Date:	4/02/2004		
Time:	17:30			Time:	19:00			Time:	19:45		
Brix	81.7 %			Brix	81.7 %			Brix	81.7 %		
Dry substance	79.6 %			Dry substance	79.6 %			Dry substance	79.6 %		
Purity	68.2 %			Purity	68.2 %			Purity	68.2 %		
Density	1386 kg/m ³			Density	1386 kg/m ³			Density	1386 kg/m ³		
Viscosity	1.1 Pa.s			Viscosity	1.1 Pa.s			Viscosity	1.1 Pa.s		
Tube inlet temperature	60.1 °C			Tube inlet temperature	59.9 °C			Tube inlet temperature	59.7 °C		
Vacuum (head space)	15.6 kPa.a			Vacuum (head space)	15.5 kPa.a			Vacuum (head space)	15.4 kPa.a		
Level in header tank	790 mm			Level in header tank	550 mm			Level in header tank	580 mm		
Pump speed	200 rpm			Pump speed	200 rpm			Pump speed	400 rpm		
Circulation velocity	0.096 m/s			Circulation velocity	0.096 m/s			Circulation velocity	0.195 m/s		
Mass flow rate	1.1 kg/s			Mass flow rate	1.1 kg/s			Mass flow rate	2.22 kg/s		
Pressure drop (over tube)	10.4 kPa			Pressure drop (over tube)	10.2 kPa			Pressure drop (over tube)	10.4 kPa		
Void fraction at exit	2.7 %			Void fraction at exit	2.6 %			Void fraction at exit	2.1 %		
Heat flux (over tube - HBs)	12 kW			Heat flux (over tube - HBs)	12 kW			Heat flux (over tube - HBs)	12 kW		
Calculated heat flux (Heat exchanger)	10.6 kW			Calculated heat flux (Heat exchanger)	10.6 kW			Calculated heat flux (Heat exchanger)	10.6 kW		
Tube wall temperature	103.9 °C			Tube wall temperature	101.3 °C			Tube wall temperature	100.5 °C		
Vapour superheat	-1.85 °C			Vapour superheat	-2.5 °C			Vapour superheat	-2.15 °C		
Position (mm)	Axial Temperature (°C)	Pressure (kPa)	Void fraction (%)	Position (mm)	Axial Temperature (°C)	Pressure (kPa)	Void fraction (%)	Position (mm)	Axial Temperature (°C)	Pressure (kPa)	Void fraction (%)
0	60.12			0	60.78			0	60.63		
130	59.69	38.69	0.0392	130	60.28	38.76		130	60.12	39.15	
260	59.34		0.0281	260	59.86		0.0011	260	59.71		0.0061
390	59.62	35.09	0.0338	390	59.56	34.91	0.0192	390	59.40	35.22	0.0131
520	58.96		0.0126	520	58.78		0.0152	520	58.73		0.0049
650	59.63	31.82	0.0180	650	59.43	31.51	0.0181	650	59.30	31.77	0.0121
780	59.79		0.0217	780	59.29		0.0045	780	59.17		0.0084
910	60.36	28.26	0.0190	910	59.35	27.88	0.0165	910	59.18	28.07	0.0184
1040	61.11		0.0271	1040	59.48		0.0107	1040	59.17		0.0225
1170	62.93	25.13	0.0216	1170	60.64	24.71	0.0204	1170	59.81	24.85	0.0134
1300	63.41		0.0490	1300	63.43		0.0263	1300	60.17		0.0209
Head space		15.58		Head space		15.46		Head space		15.43	

G2 – Forced circulation trials

Descriptor : Run28				Descriptor : Run29				Descriptor : Run30			
Date:	5/02/2004			Date:	5/02/2004			Date:	5/02/2004		
Time:	14:50			Time:	15:40			Time:	16:30		
Brix	79.9 %			Brix	79.9 %			Brix	79.9 %		
Dry substance	86.2 %			Dry substance	86.2 %			Dry substance	86.2 %		
Purity	77.3 %			Purity	77.3 %			Purity	77.3 %		
Density	1430 kg/m ³			Density	1430 kg/m ³			Density	1430 kg/m ³		
Viscosity	16.9 Pa.s			Viscosity	16.9 Pa.s			Viscosity	16.9 Pa.s		
Tube inlet temperature	64.8 °C			Tube inlet temperature	65 °C			Tube inlet temperature	64.9 °C		
Vacuum (head space)	15.5 kPa.a			Vacuum (head space)	15.3 kPa.a			Vacuum (head space)	15.2 kPa.a		
Level in header tank	500 mm			Level in header tank	560 mm			Level in header tank	320 mm		
Pump speed	200 rpm			Pump speed	400 rpm			Pump speed	100 rpm		
Circulation velocity	0.096 m/s			Circulation velocity	0.195 m/s			Circulation velocity	0.051 m/s		
Mass flow rate	1.13 kg/s			Mass flow rate	2.29 kg/s			Mass flow rate	0.6 kg/s		
Pressure drop (over tube)	14.1 kPa			Pressure drop (over tube)	14.6 kPa			Pressure drop (over tube)	13.3 kPa		
Void fraction at exit	26 %			Void fraction at exit	33.3 %			Void fraction at exit	53.4 %		
Heat flux (over tube - HBs)	15 kW			Heat flux (over tube - HBs)	15 kW			Heat flux (over tube - HBs)	15 kW		
Calculated heat flux (Heat exchanger)	12.5 kW			Calculated heat flux (Heat exchanger)	12.1 kW			Calculated heat flux (Heat exchanger)	12.1 kW		
Tube wall temperature	105.9 °C			Tube wall temperature	106.4 °C			Tube wall temperature	115.2 °C		
Vapour superheat	0.5 °C			Vapour superheat	0.25 °C			Vapour superheat	0 °C		
Position (mm)	Axial Temperature (°C)	Pressure (kPa)	Void fraction (%)	Position (mm)	Axial Temperature (°C)	Pressure (kPa)	Void fraction (%)	Position (mm)	Axial Temperature (°C)	Pressure (kPa)	Void fraction (%)
0	64.76			0	64.96			0	64.86		
130	64.08	38.89	0.0527	130	64.24	39.54	0.0370	130	64.40	36.12	0.0555
260	64.19		0.0196	260	64.03		0.0012	260	64.09		0.0065
390	64.46	35.15	0.0449	390	64.50	35.47	0.0556	390	64.65	32.35	0.0469
520	64.07		0.0252	520	63.98		0.0225	520	64.46		0.0349
650	64.76	31.78	0.0455	650	64.43	31.89	0.0381	650	66.17	29.05	0.1059
780	65.03		0.0300	780	64.37		0.0327	780	66.87		0.2489
910	66.14	28.17	0.1307	910	64.64	28.09	0.0322	910	67.90	25.60	0.1649
1040	66.87		0.0421	1040	65.11		0.2143	1040	68.45		0.4090
1170	68.21	25.13	0.0886	1170	65.89	24.95	0.0600	1170	69.26	22.82	0.3217
1300	68.48		0.2595	1300	66.39		0.3327	1300	69.51		0.5338
Head space		15.51		Head space		15.30		Head space		15.23	

G2 – Forced circulation trials

Descriptor : Run31				Descriptor : Run32				Descriptor : Run33			
Date:	5/02/2004			Date:	5/02/2004			Date:	17/02/2004		
Time:	17:15			Time:	19:40			Time:	11:00		
Brix	79.9 %			Brix	79.9 %			Brix	73 %		
Dry substance	86.2 %			Dry substance	86.2 %			Dry substance	71.08 %		
Purity	77.3 %			Purity	77.3 %			Purity	73.7 %		
Density	1430 kg/m ³			Density	1430 kg/m ³			Density	1332 kg/m ³		
Viscosity	16.9 Pa.s			Viscosity	16.9 Pa.s			Viscosity	0.11 Pa.s		
Tube inlet temperature	66.8 °C			Tube inlet temperature	65.2 °C			Tube inlet temperature	58.1 °C		
Vacuum (head space)	16.2 kPa.a			Vacuum (head space)	17.3 kPa.a			Vacuum (head space)	15.2 kPa.a		
Level in header tank	1050 mm			Level in header tank	580 mm			Level in header tank	610 mm		
Pump speed	800 rpm			Pump speed	400 rpm			Pump speed	300 rpm		
Circulation velocity	0.35 m/s			Circulation velocity	0.194 m/s			Circulation velocity	0.15 m/s		
Mass flow rate	4.13 kg/s			Mass flow rate	2.28 kg/s			Mass flow rate	1.64 kg/s		
Pressure drop (over tube)	18.9 kPa			Pressure drop (over tube)	14.4 kPa			Pressure drop (over tube)	13.5 kPa		
Void fraction at exit	27.5 %			Void fraction at exit	6.7 %			Void fraction at exit	0.2 %		
Heat flux (over tube - HBs)	15 kW			Heat flux (over tube - HBs)	17 kW			Heat flux (over tube - HBs)	15.1 kW		
Calculated heat flux (Heat exchanger)	13.2 kW			Calculated heat flux (Heat exchanger)	13.5 kW			Calculated heat flux (Heat exchanger)	kW		
Tube wall temperature	107.2 °C			Tube wall temperature	105.4 °C			Tube wall temperature	92.1 °C		
Vapour superheat	0.15 °C			Vapour superheat	-0.15 °C			Vapour superheat	-0.5 °C		
Position (mm)	Axial Temperature (°C)	Pressure (kPa)	Void fraction (%)	Position (mm)	Axial Temperature (°C)	Pressure (kPa)	Void fraction (%)	Position (mm)	Axial Temperature (°C)	Pressure (kPa)	Void fraction
0	66.85			0	65.16			0	58.14		
130	66.35	47.25	0.0235	130	64.68	41.78	0.0773	130	56.91	38.35	
260	65.91		-0.0353	260	64.30		0.0089	260	57.90		-0.0289
390	66.18	41.84	0.0389	390	65.25	37.92	0.0225	390	57.98	34.89	-0.0055
520	65.46		0.0239	520	64.43		0.0280	520	57.73		-0.0135
650	66.09	37.13	0.0423	650	65.25	34.36	0.0260	650	58.09	31.52	-0.0021
780	65.88		0.0264	780	65.01		0.0040	780	58.00		-0.0121
910	66.09	32.51	0.0219	910	65.23	30.72	0.0271	910	58.09	28.13	-0.0016
1040	66.01		0.0762	1040	65.48		0.0202	1040	58.18		0.0006
1170	66.60	28.36	0.0608	1170	66.17	27.36	0.0406	1170	58.76	24.81	-0.0003
1300	66.87		0.2747	1300	67.08		0.0673	1300	59.60		0.0024
Head space		16.21		Head space		17.31		Head space		15.17	

G2 – Forced circulation trials

Descriptor : Run34				Descriptor : Run35				Descriptor : Run36			
Date:	17/02/2004			Date:	17/02/2004			Date:	17/02/2004		
Time:	11:45			Time:	12:30			Time:	13:15		
Brix	73 %			Brix	73 %			Brix	73 %		
Dry substance	71.08 %			Dry substance	71.08 %			Dry substance	71.08 %		
Purity	73.7 %			Purity	73.7 %			Purity	73.7 %		
Density	1332 kg/m ³			Density	1332 kg/m ³			Density	1332 kg/m ³		
Viscosity	0.11 Pa.s			Viscosity	0.11 Pa.s			Viscosity	0.11 Pa.s		
Tube inlet temperature	58.3 °C			Tube inlet temperature	60.7 °C			Tube inlet temperature	60.8 °C		
Vacuum (head space)	15.4 kPa.a			Vacuum (head space)	16.7 kPa.a			Vacuum (head space)	16.6 kPa.a		
Level in header tank	620 mm			Level in header tank	620 mm			Level in header tank	590 mm		
Pump speed	600 rpm			Pump speed	600 rpm			Pump speed	300 rpm		
Circulation velocity	0.3 m/s			Circulation velocity	0.3 m/s			Circulation velocity	0.15 m/s		
Mass flow rate	3.28 kg/s			Mass flow rate	3.28 kg/s			Mass flow rate	1.64 kg/s		
Pressure drop (over tube)	13.7 kPa			Pressure drop (over tube)	13.75 kPa			Pressure drop (over tube)	13.6 kPa		
Void fraction at exit	0 %			Void fraction at exit	0.5 %			Void fraction at exit	0 %		
Heat flux (over tube - HBs)	15.1 kW			Heat flux (over tube - HBs)	18 kW			Heat flux (over tube - HBs)	18 kW		
Calculated heat flux (Heat exchanger)	kW			Calculated heat flux (Heat exchanger)	kW			Calculated heat flux (Heat exchanger)	kW		
Tube wall temperature	91.9 °C			Tube wall temperature	97.8 °C			Tube wall temperature	98.8 °C		
Vapour superheat	-0.3 °C			Vapour superheat	-0.3 °C			Vapour superheat	-0.2 °C		
Position (mm)	Axial Temperature (°C)	Pressure (kPa)	Void fraction	Position (mm)	Axial Temperature (°C)	Pressure (kPa)	Void fraction	Position (mm)	Axial Temperature (°C)	Pressure (kPa)	Void fraction
0	58.30			0	60.66			0	60.84		
130	58.06	38.77	-0.0059	130	60.43	39.98		130	60.62	39.52	-0.0148
260	57.90			260	60.15		-0.0427	260	60.51		
390	57.99	35.27	-0.0034	390	60.29	36.45	-0.0099	390	60.59	36.06	-0.0131
520	57.68		-0.0124	520	59.91		-0.0072	520	60.17		-0.0192
650	58.04	31.88	0.0051	650	60.29	33.01	-0.0052	650	60.54	32.68	-0.0022
780	57.96		-0.0115	780	60.09		-0.0148	780	60.48		-0.0203
910	58.03	28.45	0.0062	910	60.13	29.50	-0.0062	910	60.75	29.21	0.0009
1040	57.98		-0.0059	1040	60.18		0.0015	1040	61.08		-0.0179
1170	58.46	25.11	0.0109	1170	60.94	26.22	-0.0018	1170	62.57	25.96	0.0049
1300	58.60		-0.0016	1300	61.33		0.0048	1300	63.82		-0.0032
Head space		15.36		Head space		16.65		Head space		16.57	

G2 – Forced circulation trials

Descriptor : Run37				Descriptor : Run38				Descriptor : Run39			
Date:	17/02/2004			Date:	17/02/2004			Date:	17/02/2004		
Time:	14:30			Time:	15:30			Time:	16:20		
Brix	73 %			Brix	73 %			Brix	73 %		
Dry substance	71.08 %			Dry substance	71.08 %			Dry substance	71.08 %		
Purity	73.7 %			Purity	73.7 %			Purity	73.7 %		
Density	1332 kg/m ³			Density	1332 kg/m ³			Density	1332 kg/m ³		
Viscosity	0.11 Pa.s			Viscosity	0.11 Pa.s			Viscosity	0.11 Pa.s		
Tube inlet temperature	56.8 °C			Tube inlet temperature	56.3 °C			Tube inlet temperature	52.1 °C		
Vacuum (head space)	14.5 kPa.a			Vacuum (head space)	14.1 kPa.a			Vacuum (head space)	12.2 kPa.a		
Level in header tank	610 mm			Level in header tank	630 mm			Level in header tank	630 mm		
Pump speed	300 rpm			Pump speed	600 rpm			Pump speed	600 rpm		
Circulation velocity	0.15 m/s			Circulation velocity	0.3 m/s			Circulation velocity	0.3 m/s		
Mass flow rate	1.64 kg/s			Mass flow rate	3.28 kg/s			Mass flow rate	3.28 kg/s		
Pressure drop (over tube)	10.2 kPa			Pressure drop (over tube)	10.3 kPa			Pressure drop (over tube)	6.8 kPa		
Void fraction at exit	0 %			Void fraction at exit	0 %			Void fraction at exit	0 %		
Heat flux (over tube - HBs)	14.4 kW			Heat flux (over tube - HBs)	14.4 kW			Heat flux (over tube - HBs)	10.8 kW		
Calculated heat flux (Heat exchanger)	kW			Calculated heat flux (Heat exchanger)	kW			Calculated heat flux (Heat exchanger)	kW		
Tube wall temperature	97.5 °C			Tube wall temperature	94.7 °C			Tube wall temperature	92.2 °C		
Vapour superheat	-0.25 °C			Vapour superheat	-0.1 °C			Vapour superheat	-0.1 °C		
Position (mm)	Axial Temperature (°C)	Pressure (kPa)	Void fraction	Position (mm)	Axial Temperature (°C)	Pressure (kPa)	Void fraction	Position (mm)	Axial Temperature (°C)	Pressure (kPa)	Void fraction
0	57.74			0	57.13			0	53.03		
130	57.39	37.70		130	56.75	37.54		130	52.68	35.73	
260	56.84		-0.0495	260	56.31		-0.0328	260	52.70		
390	56.71	34.13	-0.0071	390	56.18	33.90	-0.0095	390	52.50	32.25	
520	56.26		-0.0153	520	55.80		-0.0189	520	52.06		-0.0159
650	56.60	30.69	-0.0034	650	56.07	30.41	-0.0020	650	51.99	28.66	-0.0010
780	56.38		-0.0091	780	55.83		-0.0202	780	51.70		-0.0115
910	56.41	27.22	-0.0025	910	55.85	26.95	-0.0160	910	51.73	25.20	0.0000
1040	56.45		-0.0062	1040	55.92		-0.0135	1040	51.82		-0.0078
1170	57.38	23.94	-0.0025	1170	56.52	23.61	0.0017	1170	52.43	21.86	0.0003
1300	58.09		-0.0011	1300	56.68			1300	52.56		
Head space		14.49		Head space		14.07		Head space		12.19	

G2 – Forced circulation trials

Descriptor : Run40				Descriptor : Run41				Descriptor : Run42			
Date:	17/02/2004			Date:	17/02/2004			Date:	17/02/2004		
Time:	19:15			Time:	19:15			Time:	19:55		
Brix	73 %			Brix	78.2 %			Brix	78.2 %		
Dry substance	71.08 %			Dry substance	75.76 %			Dry substance	75.76 %		
Purity	73.7 %			Purity	73.5 %			Purity	73.5 %		
Density	1332 kg/m ³			Density	1362 kg/m ³			Density	1362 kg/m ³		
Viscosity	0.11 Pa.s			Viscosity	0.33 Pa.s			Viscosity	0.33 Pa.s		
Tube inlet temperature	51.5 °C			Tube inlet temperature	59.1 °C			Tube inlet temperature	59.2 °C		
Vacuum (head space)	12.1 kPa.a			Vacuum (head space)	15.1 kPa.a			Vacuum (head space)	14.9 kPa.a		
Level in header tank	630 mm			Level in header tank	520 mm			Level in header tank	510 mm		
Pump speed	300 rpm			Pump speed	300 rpm			Pump speed	600 rpm		
Circulation velocity	0.15 m/s			Circulation velocity	0.15 m/s			Circulation velocity	0.3 m/s		
Mass flow rate	1.64 kg/s			Mass flow rate	1.68 kg/s			Mass flow rate	3.36 kg/s		
Pressure drop (over tube)	6.7 kPa			Pressure drop (over tube)	13.5 kPa			Pressure drop (over tube)	13.5 kPa		
Void fraction at exit	0 %			Void fraction at exit	2 %			Void fraction at exit	1.6 %		
Heat flux (over tube - HBs)	10.6 kW			Heat flux (over tube - HBs)	15 kW			Heat flux (over tube - HBs)	15 kW		
Calculated heat flux (Heat exchanger)	kW			Calculated heat flux (Heat exchanger)	kW			Calculated heat flux (Heat exchanger)	kW		
Tube wall temperature	93.1 °C			Tube wall temperature	98.4 °C			Tube wall temperature	97.6 °C		
Vapour superheat	-0.15 °C			Vapour superheat	0.8 °C			Vapour superheat	0.25 °C		
Position (mm)	Axial Temperature (°C)	Pressure (kPa)	Void fraction	Position (mm)	Axial Temperature (°C)	Pressure (kPa)	Void fraction	Position (mm)	Axial Temperature (°C)	Pressure (kPa)	Void fraction
0	52.60			0	59.15			0	59.23		
130	52.22	35.61		130	58.92	37.65	0.0036	130	59.02	37.23	0.0011
260	52.25			260	58.73			260	58.80		
390	51.99	32.17		390	58.78	34.19	0.0044	390	59.01	33.96	-0.0040
520	51.50		-0.0046	520	58.34		-0.1109	520	58.57		-0.1182
650	51.45	28.61	0.0093	650	58.72	30.81	0.0144	650	58.94	30.55	0.0016
780	51.13		-0.0056	780	58.59		-0.0001	780	58.71		-0.0074
910	51.14	25.18	0.0103	910	58.79	27.39	0.0094	910	58.71	27.07	-0.0026
1040	51.25		-0.0005	1040	59.13		0.0106	1040	58.79		0.0140
1170	51.88	21.89	0.0119	1170	60.22	24.10	0.0149	1170	59.53	23.77	0.0061
1300	52.06		0.0012	1300	61.27		0.0197	1300	59.97		0.0163
Head space		12.09		Head space		15.09		Head space		14.86	

G2 – Forced circulation trials

Descriptor : Run43				Descriptor : Run44				Descriptor : Run45			
Date:	18/02/2004			Date:	18/02/2004			Date:	18/02/2004		
Time:	9:35			Time:	10:10			Time:	11:00		
Brix	80.7 %			Brix	80.7 %			Brix	80.7 %		
Dry substance	79.73 %			Dry substance	79.73 %			Dry substance	79.73 %		
Purity	80.4 %			Purity	80.4 %			Purity	80.4 %		
Density	1389 kg/m ³			Density	1389 kg/m ³			Density	1389 kg/m ³		
Viscosity	1.14 Pa.s			Viscosity	1.14 Pa.s			Viscosity	1.14 Pa.s		
Tube inlet temperature	63.6 °C			Tube inlet temperature	58.8 °C			Tube inlet temperature	57.2 °C		
Vacuum (head space)	16.8 kPa.a			Vacuum (head space)	16.8 kPa.a			Vacuum (head space)	16.8 kPa.a		
Level in header tank	390 mm			Level in header tank	360 mm			Level in header tank	330 mm		
Pump speed	600 rpm			Pump speed	400 rpm			Pump speed	200 rpm		
Circulation velocity	0.3 m/s			Circulation velocity	0.2 m/s			Circulation velocity	0.1 m/s		
Mass flow rate	3.42 kg/s			Mass flow rate	2.28 kg/s			Mass flow rate	1.14 kg/s		
Pressure drop (over tube)	14.4 kPa			Pressure drop (over tube)	14.15 kPa			Pressure drop (over tube)	13.9 kPa		
Void fraction at exit	5.9 %			Void fraction at exit	19.5 %			Void fraction at exit	16.7 %		
Heat flux (over tube - HBs)	18 kW			Heat flux (over tube - HBs)	18 kW			Heat flux (over tube - HBs)	18 kW		
Calculated heat flux (Heat exchanger)	kW			Calculated heat flux (Heat exchanger)	kW			Calculated heat flux (Heat exchanger)	kW		
Tube wall temperature	102.1 °C			Tube wall temperature	103.4 °C			Tube wall temperature	103.4 °C		
Vapour superheat	0.05 °C			Vapour superheat	0.1 °C			Vapour superheat	0.1 °C		
Position (mm)	Axial Temperature (°C)	Pressure (kPa)	Void fraction	Position (mm)	Axial Temperature (°C)	Pressure (kPa)	Void fraction	Position (mm)	Axial Temperature (°C)	Pressure (kPa)	Void fraction
0	63.59			0	58.78			0	57.16		
130	63.07	37.97	-0.0123	130	58.36	37.66	-0.0172	130	56.73	37.23	
260	63.08		0.0236	260	58.33			260	56.73		-0.0253
390	63.46	34.28	-0.0183	390	63.46	34.02	-0.0166	390	63.16	33.66	-0.0052
520	63.08		-0.0353	520	63.11		-0.0315	520	62.82		-0.0041
650	63.51	30.68	-0.0104	650	63.54	30.48	-0.0048	650	63.85	30.19	0.0038
780	63.24		-0.0290	780	63.41		-0.0192	780	66.03		0.0035
910	63.29	26.99	-0.0071	910	63.64	26.84	0.0053	910	66.91	26.60	0.0289
1040	63.55		-0.0080	1040	64.36		0.0072	1040	67.35		0.0280
1170	64.41	23.59	0.0162	1170	65.91	23.51	0.0524	1170	68.40	23.33	0.2049
1300	65.21		0.0588	1300	66.64		0.1950	1300	68.35		0.1670
Head space		16.77		Head space		16.79		Head space		16.77	

G2 – Forced circulation trials

Descriptor : Run46				Descriptor : Run47				Descriptor : Run48			
Date:	18/02/2004			Date:	18/02/2004			Date:	18/02/2004		
Time:	12:00			Time:	12:45			Time:	14:25		
Brix	80.7 %			Brix	80.7 %			Brix	80.7 %		
Dry substance	79.73 %			Dry substance	79.73 %			Dry substance	79.73 %		
Purity	80.4 %			Purity	80.4 %			Purity	80.4 %		
Density	1389 kg/m ³			Density	1389 kg/m ³			Density	1389 kg/m ³		
Viscosity	1.14 Pa.s			Viscosity	1.14 Pa.s			Viscosity	1.14 Pa.s		
Tube inlet temperature	56.7 °C			Tube inlet temperature	59.4 °C			Tube inlet temperature	61.1 °C		
Vacuum (head space)	14.7 kPa.a			Vacuum (head space)	15 kPa.a			Vacuum (head space)	14.8 kPa.a		
Level in header tank	370 mm			Level in header tank	450 mm			Level in header tank	350 mm		
Pump speed	200 rpm			Pump speed	400 rpm			Pump speed	400 rpm		
Circulation velocity	0.1 m/s			Circulation velocity	0.2 m/s			Circulation velocity	0.2 m/s		
Mass flow rate	1.14 kg/s			Mass flow rate	2.28 kg/s			Mass flow rate	2.28 kg/s		
Pressure drop (over tube)	10.46 kPa			Pressure drop (over tube)	10.6 kPa			Pressure drop (over tube)	14.2 kPa		
Void fraction at exit	16.7 %			Void fraction at exit	4.7 %			Void fraction at exit	4.5 %		
Heat flux (over tube - HBs)	14.4 kW			Heat flux (over tube - HBs)	14.4 kW			Heat flux (over tube - HBs)	15 kW		
Calculated heat flux (Heat exchanger)	kW			Calculated heat flux (Heat exchanger)	kW			Calculated heat flux (Heat exchanger)	kW		
Tube wall temperature	100.7 °C			Tube wall temperature	97 °C			Tube wall temperature	99.7 °C		
Vapour superheat	0 °C			Vapour superheat	-0.25 °C			Vapour superheat	0.3 °C		
Position (mm)	Axial Temperature (°C)	Pressure (kPa)	Void fraction	Position (mm)	Axial Temperature (°C)	Pressure (kPa)	Void fraction	Position (mm)	Axial Temperature (°C)	Pressure (kPa)	Void fraction
0	57.33			0	60.55			0	61.15		
130	56.94	35.59		130	60.12	37.07		130	60.76	35.50	
260	56.71			260	59.42			260	60.53		-0.0468
390	60.05	31.83	-0.0146	390	59.44	33.25	-0.0021	390	60.94	31.86	-0.0194
520	59.62		-0.0176	520	59.01		-0.0097	520	60.56		-0.0182
650	60.04	28.28	0.0007	650	59.42	29.68	0.0004	650	60.90	28.29	-0.0160
780	60.18		-0.0077	780	59.22		-0.0041	780	60.75		-0.0146
910	62.32	24.68	0.0112	910	59.28	26.04	0.0118	910	60.87	24.70	-0.0138
1040	63.10		0.0230	1040	59.28		0.0167	1040	61.23		0.0133
1170	64.34	21.37	0.0580	1170	60.18	22.66	0.0388	1170	62.30	21.32	0.0258
1300	64.30		0.1665	1300	61.16		0.0468	1300	63.15		0.0451
Head space		14.67		Head space		15.02		Head space		14.81	

G2 – Forced circulation trials

Descriptor : Run49				Descriptor : Run50				Descriptor : Run51			
Date:	18/02/2004			Date:	18/02/2004			Date:	19/02/2004		
Time:	15:00			Time:	16:00			Time:	18:55		
Brix	80.7 %			Brix	80.7 %			Brix	73.6 %		
Dry substance	79.73 %			Dry substance	79.73 %			Dry substance	71.71 %		
Purity	80.4 %			Purity	80.4 %			Purity	66.2 %		
Density	1389 kg/m ³			Density	1389 kg/m ³			Density	1336 kg/m ³		
Viscosity	1.14 Pa.s			Viscosity	1.14 Pa.s			Viscosity	0.14 Pa.s		
Tube inlet temperature	60.9 °C			Tube inlet temperature	61 °C			Tube inlet temperature	58.8 °C		
Vacuum (head space)	14.6 kPa.a			Vacuum (head space)	14.9 kPa.a			Vacuum (head space)	15.3 kPa.a		
Level in header tank	290 mm			Level in header tank	380 mm			Level in header tank	640 mm		
Pump speed	200 rpm			Pump speed	600 rpm			Pump speed	200 rpm		
Circulation velocity	0.1 m/s			Circulation velocity	0.3 m/s			Circulation velocity	0.1 m/s		
Mass flow rate	1.14 kg/s			Mass flow rate	3.43 kg/s			Mass flow rate	1.098 kg/s		
Pressure drop (over tube)	13.9 kPa			Pressure drop (over tube)	14.4 kPa			Pressure drop (over tube)	13.5 kPa		
Void fraction at exit	28 %			Void fraction at exit	2.8 %			Void fraction at exit	%		
Heat flux (over tube - HBs)	15 kW			Heat flux (over tube - HBs)	15 kW			Heat flux (over tube - HBs)	15 kW		
Calculated heat flux (Heat exchanger)	kW			Calculated heat flux (Heat exchanger)	kW			Calculated heat flux (Heat exchanger)	kW		
Tube wall temperature	98.3 °C			Tube wall temperature	99.5 °C			Tube wall temperature	96.9 °C		
Vapour superheat	0.4 °C			Vapour superheat	0.5 °C			Vapour superheat	0.3 °C		
Position (mm)	Axial Temperature (°C)	Pressure (kPa)	Void fraction	Position (mm)	Axial Temperature (°C)	Pressure (kPa)	Void fraction	Position (mm)	Axial Temperature (°C)	Pressure (kPa)	Void fraction
0	60.91			0	61.01			0	58.82		
130	60.36	34.48	-0.0180	130	60.53	35.95		130	58.48	39.02	
260	60.32			260	60.45		-0.0254	260	58.32		-0.0384
390	60.75	30.92	-0.0165	390	60.91	32.27	-0.0193	390	58.37	35.58	-0.0113
520	60.41		-0.0304	520	60.50		-0.0231	520	57.99		-0.0087
650	60.78	27.41	-0.0104	650	60.86	28.63	-0.0169	650	58.32	32.22	-0.0125
780	61.37		-0.0172	780	60.70		-0.0112	780	58.27		-0.1101
910	63.05	23.89	0.0027	910	60.75	24.97	-0.0193	910	58.51	28.81	-0.0086
1040	63.92		0.0164	1040	60.79		0.0050	1040	59.38		0.0008
1170	64.95	20.59	0.0534	1170	61.61	21.53	0.0107	1170	61.61	25.51	0.0016
1300	64.92		0.2800	1300	62.09		0.0276	1300	62.67		-0.2860
Head space		14.56		Head space		14.91		Head space		15.29	

G2 – Forced circulation trials

Descriptor : Run52				Descriptor : Run53				Descriptor : Run54			
Date:	19/02/2004			Date:	24/02/2004			Date:	24/02/2004		
Time:	19:50			Time:	17:25			Time:	18:10		
Brix	73.6 %			Brix	75.8 %			Brix	75.8 %		
Dry substance	71.71 %			Dry substance	73.9 %			Dry substance	73.9 %		
Purity	66.2 %			Purity	66.8 %			Purity	66.8 %		
Density	1336 kg/m ³			Density	1350 kg/m ³			Density	1350 kg/m ³		
Viscosity	0.14 Pa.s			Viscosity	0.23 Pa.s			Viscosity	0.23 Pa.s		
Tube inlet temperature	59.1 °C			Tube inlet temperature	58.4 °C			Tube inlet temperature	58.3 °C		
Vacuum (head space)	15.5 kPa.a			Vacuum (head space)	14.2 kPa.a			Vacuum (head space)	14.4 kPa.a		
Level in header tank	745 mm			Level in header tank	550 mm			Level in header tank	540 mm		
Pump speed	400 rpm			Pump speed	400 rpm			Pump speed	200 rpm		
Circulation velocity	0.2 m/s			Circulation velocity	0.2 m/s			Circulation velocity	0.1 m/s		
Mass flow rate	2.2 kg/s			Mass flow rate	2.22 kg/s			Mass flow rate	1.11 kg/s		
Pressure drop (over tube)	13.7 kPa			Pressure drop (over tube)	13.7 kPa			Pressure drop (over tube)	13.5 kPa		
Void fraction at exit	%			Void fraction at exit	0.1 %			Void fraction at exit	1.2 %		
Heat flux (over tube - HBs)	15 kW			Heat flux (over tube - HBs)	15 kW			Heat flux (over tube - HBs)	15 kW		
Calculated heat flux (Heat exchanger)	kW			Calculated heat flux (Heat exchanger)	kW			Calculated heat flux (Heat exchanger)	kW		
Tube wall temperature	96.7 °C			Tube wall temperature	99.8 °C			Tube wall temperature	99.1 °C		
Vapour superheat	0.35 °C			Vapour superheat	-0.4 °C			Vapour superheat	-0.3 °C		
Position (mm)	Axial Temperature (°C)	Pressure (kPa)	Void fraction	Position (mm)	Axial Temperature (°C)	Pressure (kPa)	Void fraction	Position (mm)	Axial Temperature (°C)	Pressure (kPa)	Void fraction
0	59.02			0	58.38			0	58.35		
130	58.89	40.53		130	58.28	36.90	-0.0215	130	58.20	37.02	
260	58.68		-0.0325	260	57.99			260	57.93		-0.0321
390	58.81	37.03	-0.0054	390	58.13	33.45	-0.0191	390	58.11	33.61	-0.0122
520	58.41		-0.0092	520	57.71		-0.0241	520	57.77		-0.0195
650	58.77	33.60	-0.0016	650	58.00	29.98	-0.0179	650	58.10	30.20	-0.0080
780	58.55		-0.0074	780	57.87		-0.0251	780	58.61		-0.0129
910	58.55	30.11	0.0005	910	58.03	26.50	-0.0156	910	58.99	26.77	-0.0077
1040	58.64		0.0041	1040	58.41		-0.0103	1040	59.99		-0.0095
1170	59.29	26.84	0.0050	1170	59.45	23.19	-0.0104	1170	62.39	23.51	0.0021
1300	59.56		-0.0029	1300	60.48		0.0015	1300	63.16		0.0117
Head space		15.47		Head space		14.19		Head space		14.42	

G2 – Forced circulation trials

Descriptor : Run55				Descriptor : Run56				Descriptor : Run57			
Date:	24/02/2004			Date:	25-Feb-04			Date:	25/02/2004		
Time:	19:20			Time:	8:35am			Time:	9:20		
Brix	75.8 %			Brix	81.6 %			Brix	81.6 %		
Dry substance	73.9 %			Dry substance	79.47 %			Dry substance	79.47 %		
Purity	66.8 %			Purity	66.6 %			Purity	66.6 %		
Density	1350 kg/m ³			Density	1386 kg/m ³			Density	1386 kg/m ³		
Viscosity	0.23 Pa.s			Viscosity	1.1 Pa.s			Viscosity	1.1 Pa.s		
Tube inlet temperature	58.1 °C			Tube inlet temperature	61.1 °C			Tube inlet temperature	61.7 °C		
Vacuum (head space)	14.6 kPa.a			Vacuum (head space)	15.9 kPa.a			Vacuum (head space)	15.9 kPa.a		
Level in header tank	560 mm			Level in header tank	500 mm			Level in header tank	510 mm		
Pump speed	600 rpm			Pump speed	200 rpm			Pump speed	600 rpm		
Circulation velocity	0.3 m/s			Circulation velocity	0.1 m/s			Circulation velocity	0.3 m/s		
Mass flow rate	3.33 kg/s			Mass flow rate	1.14 kg/s			Mass flow rate	3.42 kg/s		
Pressure drop (over tube)	13.4 kPa			Pressure drop (over tube)	12.7 kPa			Pressure drop (over tube)	12.9 kPa		
Void fraction at exit	0.9 %			Void fraction at exit	%			Void fraction at exit	%		
Heat flux (over tube - HBs)	15 kW			Heat flux (over tube - HBs)	15.8 kW			Heat flux (over tube - HBs)	15.5 kW		
Calculated heat flux (Heat exchanger)	kW			Calculated heat flux (Heat exchanger)	kW			Calculated heat flux (Heat exchanger)	kW		
Tube wall temperature	97 °C			Tube wall temperature	102 °C			Tube wall temperature	101.8 °C		
Vapour superheat	-0.55 °C			Vapour superheat	0 °C			Vapour superheat	0 °C		
Position (mm)	Axial Temperature (°C)	Pressure (kPa)	Void fraction	Position (mm)	Axial Temperature (°C)	Pressure (kPa)	Void fraction	Position (mm)	Axial Temperature (°C)	Pressure (kPa)	Void fraction
0	58.10			0	61.08			0	61.74		
130	57.92	37.45		130	59.36	38.59		130	60.70	38.77	
260	57.61		-0.0051	260	60.72		-0.0411	260	61.34		-0.0438
390	57.87	34.21	-0.0090	390	61.04	35.34	-0.0236	390	61.69	35.51	-0.0255
520	57.51		-0.0113	520	60.68		-0.0352	520	61.36		-0.0466
650	57.82	30.81	-0.0060	650	61.32	32.21	-0.0172	650	61.74	32.29	-0.0262
780	57.69		-0.0110	780	61.63		-0.0257	780	61.64		-0.0311
910	57.74	27.34	-0.0034	910	62.24	28.93	-0.0114	910	61.73	28.91	-0.0308
1040	57.71		-0.0073	1040	63.00		-0.0102	1040	61.66		-0.0202
1170	58.44	24.07	0.0028	1170	65.63	25.90	0.0081	1170	62.25	25.84	-0.0207
1300	58.85		0.0089	1300	66.16		-0.0381	1300	62.73		-0.0073
Head space		14.56		Head space		15.92		Head space		15.92	

G2 – Forced circulation trials

Descriptor : Run58				Descriptor : Run59				Descriptor : Run60			
Date:	25/02/2004			Date:	25/02/2004			Date:	25/02/2004		
Time:	10:20			Time:	11:30			Time:	13:50		
Brix	81.6 %			Brix	81.6 %			Brix	81.2 %		
Dry substance	79.47 %			Dry substance	79.47 %			Dry substance	79.1 %		
Purity	66.6 %			Purity	66.6 %			Purity	66.3 %		
Density	1386 kg/m ³			Density	1386 kg/m ³			Density	1382 kg/m ³		
Viscosity	1.1 Pa.s			Viscosity	1.1 Pa.s			Viscosity	0.99 Pa.s		
Tube inlet temperature	61.6 °C			Tube inlet temperature	63.7 °C			Tube inlet temperature	63.1 °C		
Vacuum (head space)	15.6 kPa.a			Vacuum (head space)	16 kPa.a			Vacuum (head space)	16.3 kPa.a		
Level in header tank	480 mm			Level in header tank	450 mm			Level in header tank	480 mm		
Pump speed	400 rpm			Pump speed	400 rpm			Pump speed	400 rpm		
Circulation velocity	0.2 m/s			Circulation velocity	0.2 m/s			Circulation velocity	0.2 m/s		
Mass flow rate	2.28 kg/s			Mass flow rate	2.28 kg/s			Mass flow rate	2.27 kg/s		
Pressure drop (over tube)	12.8 kPa			Pressure drop (over tube)	12.8 kPa			Pressure drop (over tube)	12.9 kPa		
Void fraction at exit	4.9 %			Void fraction at exit	12.05 %			Void fraction at exit	7.2 %		
Heat flux (over tube - HBs)	14.7 kW			Heat flux (over tube - HBs)	15.2 kW			Heat flux (over tube - HBs)	18 kW		
Calculated heat flux (Heat exchanger)	kW			Calculated heat flux (Heat exchanger)	kW			Calculated heat flux (Heat exchanger)	kW		
Tube wall temperature	101.4 °C			Tube wall temperature	105 °C			Tube wall temperature	107.7 °C		
Vapour superheat	0 °C			Vapour superheat	0 °C			Vapour superheat	0.15 °C		
Position (mm)	Axial Temperature (°C)	Pressure (kPa)	Void fraction	Position (mm)	Axial Temperature (°C)	Pressure (kPa)	Void fraction	Position (mm)	Axial Temperature (°C)	Pressure (kPa)	Void fraction
0	61.6			0	63.68			0	63.05		
130	61.3	38.02		130	63.12	38.00		130	62.63	38.58	
260	61.3		0.0601	260	62.62		-0.0212	260	61.94		-0.0007
390	61.6	34.71	0.0075	390	63.45	34.64	0.0029	390	63.23	35.54	0.0347
520	61.3		0.0044	520	63.00		-0.0173	520	62.79		0.0119
650	61.6	31.54	0.0037	650	63.42	31.48	-0.0175	650	63.17	32.07	0.0256
780	61.7		-0.0155	780	63.56		0.0499	780	63.09		0.0077
910	61.9	28.22	0.0114	910	64.01	28.15	-0.0202	910	63.39	28.53	0.0155
1040	61.9		0.0096	1040	64.11		0.0118	1040	63.68		0.0240
1170	62.7	25.23	0.0142	1170	65.00	25.19	0.0374	1170	64.85	25.66	0.0628
1300	63.6		0.0492	1300	65.74		0.1205	1300	65.63		0.0720
Head space		15.61		Head space		16.01		Head space		16.27	

G2 – Forced circulation trials

Descriptor : Run61				Descriptor : Run62				Descriptor : Run63			
Date:	25/02/2004			Date:	25/02/2004			Date:	25/02/2004		
Time:	14:30			Time:	15:40			Time:	16:10		
Brix	81.2 %			Brix	81.2 %			Brix	81.2 %		
Dry substance	79.1 %			Dry substance	79.1 %			Dry substance	79.1 %		
Purity	66.3 %			Purity	66.3 %			Purity	66.3 %		
Density	1382 kg/m ³			Density	1382 kg/m ³			Density	1382 kg/m ³		
Viscosity	0.99 Pa.s			Viscosity	0.99 Pa.s			Viscosity	0.99 Pa.s		
Tube inlet temperature	63.4 °C			Tube inlet temperature	59.6 °C			Tube inlet temperature	59.1 °C		
Vacuum (head space)	16.6 kPa.a			Vacuum (head space)	14.5 kPa.a			Vacuum (head space)	14.3 kPa.a		
Level in header tank	500 mm			Level in header tank	550 mm			Level in header tank	535 mm		
Pump speed	600 rpm			Pump speed	600 rpm			Pump speed	400 rpm		
Circulation velocity	0.3 m/s			Circulation velocity	0.3 m/s			Circulation velocity	0.2 m/s		
Mass flow rate	3.41 kg/s			Mass flow rate	3.41 kg/s			Mass flow rate	2.27 kg/s		
Pressure drop (over tube)	13.2 kPa			Pressure drop (over tube)	10.3 kPa			Pressure drop (over tube)	10.2 kPa		
Void fraction at exit	6 %			Void fraction at exit	1.6 %			Void fraction at exit	1.8 %		
Heat flux (over tube - HBs)	18 kW			Heat flux (over tube - HBs)	14.4 kW			Heat flux (over tube - HBs)	14.4 kW		
Calculated heat flux (Heat exchanger)	kW			Calculated heat flux (Heat exchanger)	kW			Calculated heat flux (Heat exchanger)	kW		
Tube wall temperature	108.8 °C			Tube wall temperature	104.2 °C			Tube wall temperature	103.9 °C		
Vapour superheat	0.05 °C			Vapour superheat	0.1 °C			Vapour superheat	0.3 °C		
Position (mm)	Axial Temperature (°C)	Pressure (kPa)	Void fraction	Position (mm)	Axial Temperature (°C)	Pressure (kPa)	Void fraction	Position (mm)	Axial Temperature (°C)	Pressure (kPa)	Void fraction
0	63.37			0	60.76			0	59.99		
130	63.10	39.21		130	60.41	37.77		130	59.69	37.37	
260	62.31		-0.0119	260	59.63			260	59.10		
390	63.68	36.13	0.0303	390	59.63	34.46	0.0107	390	58.90	34.20	0.0124
520	63.22		0.0064	520	59.13		0.0014	520	58.41		0.0086
650	63.61	32.59	0.0232	650	59.50	30.79	0.0157	650	58.75	30.56	0.0226
780	63.43		-0.0013	780	59.31		0.0050	780	58.56		0.0136
910	63.58	28.96	0.0085	910	59.46	27.14	0.0103	910	58.69	26.96	0.0224
1040	63.54		0.0114	1040	59.31		0.0031	1040	58.60		0.0090
1170	64.49	26.06	0.0209	1170	60.17	24.16	0.0058	1170	59.55	24.05	0.0177
1300	65.12		0.0601	1300	60.64		0.0162	1300	60.35		
Head space		16.56		Head space		14.50		Head space		14.28	

G2 – Forced circulation trials

Descriptor : Run64				Descriptor : Run65				Descriptor : Run66			
Date:	25/02/2004			Date:	26/02/2004			Date:	26/02/2004		
Time:	17:00			Time:	8:40			Time:	9:25		
Brix	81.2 %			Brix	79.9 %			Brix	79.9 %		
Dry substance	79.1 %			Dry substance	77.42 %			Dry substance	77.42 %		
Purity	66.3 %			Purity	71.9 %			Purity	71.9 %		
Density	1382 kg/m ³			Density	1372.5 kg/m ³			Density	1372.5 kg/m ³		
Viscosity	0.99 Pa.s			Viscosity	0.53 Pa.s			Viscosity	0.53 Pa.s		
Tube inlet temperature	55.9 °C			Tube inlet temperature	59.8 °C			Tube inlet temperature	60 °C		
Vacuum (head space)	12.6 kPa.a			Vacuum (head space)	14.8 kPa.a			Vacuum (head space)	14.8 kPa.a		
Level in header tank	540 mm			Level in header tank	500 mm			Level in header tank	515 mm		
Pump speed	400 rpm			Pump speed	400 rpm			Pump speed	600 rpm		
Circulation velocity	0.2 m/s			Circulation velocity	0.2 m/s			Circulation velocity	0.3 m/s		
Mass flow rate	2.27 kg/s			Mass flow rate	2.26 kg/s			Mass flow rate	3.38 kg/s		
Pressure drop (over tube)	6.54 kPa			Pressure drop (over tube)	12.8 kPa			Pressure drop (over tube)	12.74 kPa		
Void fraction at exit	%			Void fraction at exit	1.3 %			Void fraction at exit	0.9 %		
Heat flux (over tube - HBs)	10.8 kW			Heat flux (over tube - HBs)	15 kW			Heat flux (over tube - HBs)	15 kW		
Calculated heat flux (Heat exchanger)	kW			Calculated heat flux (Heat exchanger)	kW			Calculated heat flux (Heat exchanger)	kW		
Tube wall temperature	101.8 °C			Tube wall temperature	100.0 °C			Tube wall temperature	99.9 °C		
Vapour superheat	0.6 °C			Vapour superheat	1.3 °C			Vapour superheat	0.65 °C		
Position (mm)	Axial Temperature (°C)	Pressure (kPa)	Void fraction	Position (mm)	Axial Temperature (°C)	Pressure (kPa)	Void fraction	Position (mm)	Axial Temperature (°C)	Pressure (kPa)	Void fraction
0	57.09			0	59.84			0	60.02		
130	56.75	35.68		130	59.65	37.30		130	59.77	37.49	
260	56.75			260	59.44		-0.0039	260	59.59		-0.0086
390	56.54	32.58		390	59.66	34.19	0.0047	390	59.75	34.47	0.0052
520	55.89			520	59.33		-0.0003	520	59.36		-0.0062
650	55.73	28.72	0.0157	650	59.70	30.92	0.0095	650	59.71	31.19	0.0058
780	55.52		0.0146	780	59.43		0.0001	780	59.47		-0.0032
910	55.64	25.13	0.0202	910	59.51	27.65	0.0122	910	59.54	27.90	0.0183
1040	55.58		0.0112	1040	59.62		0.0047	1040	59.56		0.0024
1170	56.45	22.19	0.0089	1170	60.30	24.50	0.0061	1170	60.27	24.75	0.0121
1300	57.02			1300	61.06		0.0129	1300	60.63		0.0092
Head space		12.57		Head space		14.81		Head space		14.84	

G2 – Forced circulation trials

Descriptor : Run67				Descriptor : Run68				Descriptor : Run69			
Date:	26/02/2004			Date:	26/02/2004			Date:	26/02/2004		
Time:	10:15			Time:	11:45			Time:	12:30		
Brix	79.9 %			Brix	79.9 %			Brix	79.9 %		
Dry substance	77.42 %			Dry substance	77.42 %			Dry substance	77.42 %		
Purity	71.9 %			Purity	71.9 %			Purity	71.9 %		
Density	1372.5 kg/m ³			Density	1372.5 kg/m ³			Density	1372.5 kg/m ³		
Viscosity	0.53 Pa.s			Viscosity	0.53 Pa.s			Viscosity	0.53 Pa.s		
Tube inlet temperature	59.4 °C			Tube inlet temperature	61.8 °C			Tube inlet temperature	62.4 °C		
Vacuum (head space)	14.7 kPa.a			Vacuum (head space)	16.2 kPa.a			Vacuum (head space)	16.6 kPa.a		
Level in header tank	495 mm			Level in header tank	480 mm			Level in header tank	490 mm		
Pump speed	200 rpm			Pump speed	400 rpm			Pump speed	600 rpm		
Circulation velocity	0.1 m/s			Circulation velocity	0.1 m/s			Circulation velocity	0.3 m/s		
Mass flow rate	1.13 kg/s			Mass flow rate	2.26 kg/s			Mass flow rate	3.38 kg/s		
Pressure drop (over tube)	12.6 kPa			Pressure drop (over tube)	12.64 kPa			Pressure drop (over tube)	12.7 kPa		
Void fraction at exit	3.4 %			Void fraction at exit	3.5 %			Void fraction at exit	4.1 %		
Heat flux (over tube - HBs)	15 kW			Heat flux (over tube - HBs)	18 kW			Heat flux (over tube - HBs)	18 kW		
Calculated heat flux (Heat exchanger)	kW			Calculated heat flux (Heat exchanger)	kW			Calculated heat flux (Heat exchanger)	kW		
Tube wall temperature	100.6 °C			Tube wall temperature	105.5 °C			Tube wall temperature	105.0 °C		
Vapour superheat	0.45 °C			Vapour superheat	0.1 °C			Vapour superheat	-0.2 °C		
Position (mm)	Axial Temperature (°C)	Pressure (kPa)	Void fraction	Position (mm)	Axial Temperature (°C)	Pressure (kPa)	Void fraction	Position (mm)	Axial Temperature (°C)	Pressure (kPa)	Void fraction
0	59.44			0	61.84			0	62.37		
130	59.26	37.10		130	61.61	38.44		130	62.10	38.86	0.0029
260	59.01		-0.0162	260	61.25		-0.0226	260	61.85		
390	59.22	34.07	0.0105	390	61.48	35.39	0.0053	390	62.11	35.87	0.0021
520	58.83		-0.0068	520	61.02		-0.0083	520	61.70		0.1492
650	59.17	30.84	0.0144	650	61.39	32.14	0.0071	650	62.04	32.61	0.0059
780	58.99		0.0013	780	61.23		0.0016	780	61.85		0.0763
910	59.46	27.61	0.0216	910	61.45	28.89	0.0118	910	61.97	29.29	0.0142
1040	60.70		0.0147	1040	61.69		0.0158	1040	61.91		0.1507
1170	62.50	24.52	0.0253	1170	62.86	25.81	0.0140	1170	62.77	26.16	0.0176
1300	63.83		0.0339	1300	63.99		0.0347	1300	63.34		0.0410
Head space		14.70		Head space		16.22		Head space		16.56	

G2 – Forced circulation trials

Descriptor : Run70				Descriptor : Run71				Descriptor : Run72			
Date:	26/02/2004			Date:	26/02/2004			Date:	26/02/2004		
Time:	13:20			Time:	14:00			Time:	15:45		
Brix	83.2 %			Brix	83.2 %			Brix	83.2 %		
Dry substance	84.07 %			Dry substance	84.07 %			Dry substance	84.07 %		
Purity	76.3 %			Purity	76.3 %			Purity	76.3 %		
Density	1414 kg/m ³			Density	1414 kg/m ³			Density	1414 kg/m ³		
Viscosity	4.06 Pa.s			Viscosity	4.06 Pa.s			Viscosity	4.06 Pa.s		
Tube inlet temperature	63.9 °C			Tube inlet temperature	64.3 °C			Tube inlet temperature	61.4 °C		
Vacuum (head space)	16.8 kPa.a			Vacuum (head space)	16.6 kPa.a			Vacuum (head space)	14.7 kPa.a		
Level in header tank	580 mm			Level in header tank	540 mm			Level in header tank	530 mm		
Pump speed	600 rpm			Pump speed	400 rpm			Pump speed	400 rpm		
Circulation velocity	0.3 m/s			Circulation velocity	0.2 m/s			Circulation velocity	0.2 m/s		
Mass flow rate	3.49 kg/s			Mass flow rate	2.32 kg/s			Mass flow rate	2.32 kg/s		
Pressure drop (over tube)	13.4 kPa			Pressure drop (over tube)	13.1 kPa			Pressure drop (over tube)	13.2 kPa		
Void fraction at exit	7.6 %			Void fraction at exit	5.3 %			Void fraction at exit	3.2 %		
Heat flux (over tube - HBs)	18 kW			Heat flux (over tube - HBs)	18 kW			Heat flux (over tube - HBs)	15 kW		
Calculated heat flux (Heat exchanger)	kW			Calculated heat flux (Heat exchanger)	kW			Calculated heat flux (Heat exchanger)	kW		
Tube wall temperature	104.7 °C			Tube wall temperature	105.1 °C			Tube wall temperature	101.3 °C		
Vapour superheat	2.5 °C			Vapour superheat	2.1 °C			Vapour superheat	1 °C		
Position (mm)	Axial Temperature (°C)	Pressure (kPa)	Void fraction	Position (mm)	Axial Temperature (°C)	Pressure (kPa)	Void fraction	Position (mm)	Axial Temperature (°C)	Pressure (kPa)	Void fraction
0	63.95			0	64.25			0	61.44		
130	63.52	41.03	0.0064	130	63.67	40.32	0.0107	130	61.17	38.20	
260	63.57			260	63.68			260	60.74		-0.0112
390	64.07	37.71	0.0170	390	64.23	37.06	0.0219	390	61.00	34.94	0.0033
520	63.64		-0.0051	520	63.76		0.0021	520	60.56		-0.0050
650	64.02	34.29	0.0208	650	64.18	33.73	0.0146	650	60.94	31.54	0.0048
780	63.83		-0.0042	780	64.05		-0.0004	780	60.75		-0.0083
910	64.00	30.80	0.0195	910	64.36	30.35	0.0233	910	61.01	28.16	0.0090
1040	63.93		0.0167	1040	64.70		0.0224	1040	61.13		0.0122
1170	64.86	27.60	0.0261	1170	65.81	27.26	0.0758	1170	62.19	24.98	0.0318
1300	65.54		0.0760	1300	66.93		0.0527	1300	63.14		0.0325
Head space		16.75		Head space		16.62		Head space		14.68	

G2 – Forced circulation trials

Descriptor : Run73				Descriptor : Run74				Descriptor : Run75			
Date:	26/02/2004			Date:	26/02/2004			Date:	26/02/2004		
Time:	16:20			Time:	17:00			Time:	17:50		
Brix	83.2 %			Brix	83.2 %			Brix	83.2 %		
Dry substance	84.07 %			Dry substance	84.07 %			Dry substance	84.07 %		
Purity	76.3 %			Purity	76.3 %			Purity	76.3 %		
Density	1414 kg/m ³			Density	1414 kg/m ³			Density	1414 kg/m ³		
Viscosity	4.06 Pa.s			Viscosity	4.06 Pa.s			Viscosity	4.06 Pa.s		
Tube inlet temperature	61.1 °C			Tube inlet temperature	58.8 °C			Tube inlet temperature	57.8 °C		
Vacuum (head space)	14.9 kPa.a			Vacuum (head space)	13.4 kPa.a			Vacuum (head space)	13.1 kPa.a		
Level in header tank	560 mm			Level in header tank	840 mm			Level in header tank	805 mm		
Pump speed	600 rpm			Pump speed	600 rpm			Pump speed	400 rpm		
Circulation velocity	0.3 m/s			Circulation velocity	0.3 m/s			Circulation velocity	0.2 m/s		
Mass flow rate	3.49 kg/s			Mass flow rate	3.49 kg/s			Mass flow rate	2.32 kg/s		
Pressure drop (over tube)	13.4 kPa			Pressure drop (over tube)	10.2 kPa			Pressure drop (over tube)	9.85 kPa		
Void fraction at exit	3.1 %			Void fraction at exit	1.7 %			Void fraction at exit	1.4 %		
Heat flux (over tube - HBs)	15 kW			Heat flux (over tube - HBs)	12 kW			Heat flux (over tube - HBs)	12 kW		
Calculated heat flux (Heat exchanger)	kW			Calculated heat flux (Heat exchanger)	kW			Calculated heat flux (Heat exchanger)	kW		
Tube wall temperature	101.5 °C			Tube wall temperature	102.8 °C			Tube wall temperature	103.0 °C		
Vapour superheat	0.95 °C			Vapour superheat	1.2 °C			Vapour superheat	1.65 °C		
Position (mm)	Axial Temperature (°C)	Pressure (kPa)	Void fraction	Position (mm)	Axial Temperature (°C)	Pressure (kPa)	Void fraction	Position (mm)	Axial Temperature (°C)	Pressure (kPa)	Void fraction
0	61.05			0	58.81			0	57.84		
130	60.88	38.88		130	58.59	37.66		130	57.55	36.87	
260	60.41		-0.0215	260	58.12		-0.0014	260	57.05		0.0095
390	60.77	35.63	0.0111	390	58.48	34.39	-0.0082	390	57.46	33.70	0.0116
520	60.35		-0.0061	520	58.04		-0.0027	520	57.01		-0.0021
650	60.70	32.20	0.0120	650	58.38	30.94	0.0085	650	57.37	30.35	0.0160
780	60.49		-0.0037	780	58.14		-0.0042	780	57.13		0.0018
910	60.69	28.76	0.0159	910	58.35	27.48	0.0102	910	57.36	27.01	0.0166
1040	60.50		0.0124	1040	58.33		0.0173	1040	57.45		0.0140
1170	61.36	25.51	0.0211	1170	59.40	24.16	0.0091	1170	58.66	23.81	0.0175
1300	61.86		0.0312	1300	59.63		0.0203	1300	59.07		0.0193
Head space		14.91		Head space		13.42		Head space		13.08	

APPENDIX H – One dimensional Visual Basic tube model

```
' Program to solve for boiling in a single calandria tube
'*****
'***** Declarations *****
Const m As Double = 100 'Number of increments along tube length

Dim z(m + 1) As Double, p(m + 1) As Double, ts(m + 1) As Double
Dim dts(m + 1) As Double, x(m + 1) As Double, alpha(m + 1) As Double
Dim fg(m + 1) As Double, ff(m + 1) As Double, fa(m + 1) As Double
Dim tw(m + 1) As Double, deltat(m + 1) As Double, dpg(m) As Double
Dim dpf(m) As Double, dpa(m) As Double, pnew(m + 1) As Double
Dim u(m + 1) As Double, tsnew(m + 1) As Double, length As Double
Dim pg(m + 1) As Double, p2(m + 1) As Double, q_sen(m + 1) As Double
Dim q(m + 1) As Double, hr(m + 1) As Double, ha(m + 1) As Double
Dim qin(m + 1) As Double, gf(m + 1) As Double, gg(m + 1) As Double
Dim Velf(m + 1) As Double, Velg(m + 1) As Double, reynf(m + 1) As Double
Dim reff(m + 1) As Double, refg(m + 1) As Double
Dim mdot As Double, drys As Double, temp As Double, brix As Double, _
  pty As Double, k As Double, n As Double, dia As Double, vis As Double, _
  tsteam As Double, kt As Double, rhog As Double, temp1 As Double, _
  temp2 As Double, temp3 As Double, rhof As Double, visg As Double, _
  qtotal As Double, bp As Double, cp As Double, level As Double
Dim qflux(m + 1) As Double, t(m + 1) As Double, tnew(m + 1) As Double

'***** Variables obtained from 'Inputs' sheet *****
mdot = CDBl(Range("mdot")) 'Mass flowrate (kg/s)
rincr = CDBl(Range("rincr")) 'Mass flowrate increment
For jj = 1 To CDBl(Range("Niter")) 'No. of mass flowrate increments
'***** Iteration control *****
ptol = CDBl(Range("ptol")) 'Tolerance on pressure change (Pa)
tstol = CDBl(Range("tstol")) 'Tolerance on saturation temperature change (deg. C)
itmax = CDBl(Range("itmax")) 'Maximum number of iterations on pressure
itsmax = CDBl(Range("itsmax")) 'Maximum number of iterations on saturation
temperature
'*****
'***** Tube geometry *****
d = CDBl(Range("d")) 'Tube external diameter (m)
length = CDBl(Range("length")) 'Tube length (m)
kt = CDBl(Range("kt")) 'Tube thermal conductivity (W/m)
'*****
'***** Fluid properties*****
drys = CDBl(Range("drys")) 'Dry substance
pty = CDBl(Range("pty")) 'Purity
brix = CDBl(Range("brix")) 'Brix
```

```

rhog = CDbI(Range("rhog"))      'Vapour density (kg/m^3)
visg = CDbI(Range("visg"))      'Dynamic viscosity of vapour (Pa.s)
visf = CDbI(Range("visf"))      'Dynamic viscosity of liquid (Pa.s)
rhof = CDbI(Range("rhof"))      'Density of liquid (kg/m^3)
sigma = CDbI(Range("sigma"))    'Surface tension of liquid (
cp = CDbI(Range("cp"))          'Fluid heat capacity (J/kg.K)
k = CDbI(Range("k"))            'Thermal conductivity of fluid (W/m)
hfg = CDbI(Range("hfg"))        'Latent heat of vapourization (J/kg)
*****
***** Crystal properties *****
vol = CDbI(Range("Vol"))        'Volume ratio of crystals to molasses
L = CDbI(Range("L"))            'Mean crystal size in mm
factor = CDbI(Range("factor"))  'Crystal viscosity modification factor
*****
***** Operating conditions *****
tsteam = CDbI(Range("tsteam")) + 273.15 'Steam temperature (K)
level = CDbI(Range("level"))      'Boiling level above calandria (m)
pvac = CDbI(Range("pvac")) * 1000 + rhof * level * 9.81
      'Absolute pressure at tube outlet (Pa)
t(1) = CDbI(Range("inletT")) + 273.15 'Tube inlet temperature (K)
*****
***** Define constants *****
Co = CDbI(Range("Co"))           'Distribution parameter
Pi = Application.Pi
g = 9.81                         'Gravitational acceleration (m/s^2)
*****
***** Calculated parameters *****
area = Pi * d ^ 2 / 4            'Cross-sectional area (m^2)
gmass = mdot / area             'Mass velocity (kg/m^2.s)
q1 = (mdot / rhof)
Velf(1) = mdot / (rhof * area)
*****
***** Define uniform grid spacing *****
For i = 1 To m + 1
    dz = (length / (1 * m))
    z(i) = (i - 1) * dz
Next
*****
' Initial guess for pressure distribution (hydrostatic)
' Initial temperature equal inlet temperature
For i = 1 To m + 1
    x(i) = 0
    alpha(i) = 0
    t(i) = t(1)
    tw(i) = tsteam

```

```

p(i) = pvac + (length - z(i)) * rhof * g
pg(i) = p(i)
p2(i) = p(i)
bp = bpe(drys, pty, tsat(pvac))
ts(i) = tsat(p(i)) + bp
dts(i) = ts(i) - T(i)
Velf(i) = Velf(1)
Next
*****
' Begin global iteration loop
1  itser = 0
   itser = itser + 1
' Begin outer iteration loop
   iter = 0
2  iter = iter + 1
   *****
' Steam temperature option
' Calculation of heat transfer parameters
   For i = 1 To m + 1
       deltat(i) = tw(i) - t(i)
       Pr = cp * k / viscf
       reynf(i) = Re(d, mvis, Velf(i), rhof) 'Reynolds no. for HTC
       hr(i) = (4404.2 * reynf(i) ^ (0.018)) * (Pr ^ -0.0126) * (rhof / rhog) ^ (-0.203) *
               k / d * (d / length) ^ 0.56
       Pe = Velf(i) * d * rhof * cp / k
       xstar = (length / d) / Pe
       ha(i) = (1.077 * xstar ^ (-1 / 3) - 0.7) * k / d           'Based on Stephens (2001)
       If (hr(i) <= ha(i)) Then
           hr(i) = ha(i)
       End If
   Next
   *****
   dtb = 0.00052 * mdot ^ 4 - 0.0178 * mdot ^ 3 + 0.25088 * mdot ^ 2 - 2.19285 * mdot +
         11.75543
   For i = 1 To m
       If (dts(i) > dtb) Then
           q(i) = ha(i) * deltat(i) * dz * Pi * d
           q_sen(i) = q(i)
           iflag2 = 0
           xb = (q(i) - q_sen(i)) / (mdot * hfg)
           x(i + 1) = x(i) + xb
           q3 = q1 * x(i + 1) * (rhof / rhog)
           q4 = q1 * (1 - x(i + 1))
           q6 = (q3 + q4) / area
           fl = 1.53 * ((sigma * g * (rhof - rhog)) / (rhof ^ 2) ^ (0.25)

```

```

    alpha(i + 1) = q3 / (area * (Co * q6 + f1))
    Else
    End If
    iflag2 = 0    'Sub-cooled regime

ElseIf (dts(i) > 0) Then
    q(i) = hr(i) * deltat(i) * dz * Pi * d
    q_sen(i) = ha(i) * deltat(i) * dz * Pi * d
    xb = (q(i) - q_sen(i)) / (mdot * hfg)
    x(i + 1) = x(i) + xb
    q3 = q1 * x(i + 1) * (rhof / rhog)
    q4 = q1 * (1 - x(i + 1))
    q6 = (q3 + q4) / area
    f1 = 1.53 * ((sigma * g * (rhof - rhog)) / (rhof ^ 2) ^ (0.25))
    alpha(i + 1) = q3 / (area * (Co * q6 + f1))
    Else
    End If
    iflag2 = 1    'Saturated regime
End If

t(i + 1) = t(i) + q_sen(i) / (mdot * cp) - g * dz / cp

If (t(i + 1) >= ts(i + 1)) Then
    t(i + 1) = ts(i + 1)
    q_sen(i) = 0
    q(i) = hr(i) * deltat(i) * dz * Pi * d
    x(i + 1) = (q(i) + mdot * cp * (ts(i) - ts(i + 1))) / hfg + x(i)
    q3 = q1 * x(i + 1) * (rhof / rhog)
    q4 = q1 * (1 - x(i + 1))
    q6 = (q3 + q4) / area
    f1 = 1.53 * ((sigma * g * (rhof - rhog)) / (rhof ^ 2) ^ (0.25))
    alpha(i + 1) = q3 / (area * (Co * q6 + f1))
    Else
    End If
    iflag2 = 2    'Superheated regime
End If
Next

qsum = 0
qsum2 = 0

For i = 1 To m
    qsum = qsum + q(i)
    qsum2 = qsum2 + q_sen(i)
Next
*****

```

```

' Compute contributions to pressure derivative
For i = 1 To m + 1
  'Gravitational pressure contribution (based on alpha not quality)
  fg(i) = -g * (alpha(i) * rhog + (1 - alpha(i)) * rhof)

  'Frictional pressure contribution
  'Liquid component of friction
  Velf(i) = q1 * (1 - x(i)) / (area * (1 - alpha(i)))
  gf(i) = (1 - x(i)) * gmass / (1 - alpha(i))
  reff(i) = Re(d, visf, Velf(i), rhof)

  If (reff(i) = 0) Then
    frictf = 0
  Else
    frictf = 16 / reff(i)
  End If
  fff = -2 * frictf * rhof * Velf(i) ^ 2 / d

  If (alpha(i) = 0) Then
    ffg = 0
    Velg(i) = 0
    gg(i) = 0
  Else
    'Vapour component of friction
    Velg(i) = x(i) * mdot / (rhog * area * alpha(i))
    gg(i) = x(i) * gmass / alpha(i)
    refg(i) = Re(d, visg, Velg(i), rhog)

    If (refg(i) <= 2000) Then
      frictg = 16 / refg(i)

    Else
      frictg = 1
    End If
    ffg = (-2 * frictg * rhog * Velg(i) ^ 2) / d
  End If

  'Combine liquid and vapour components
  ff(i) = alpha(i) * ffg + (1 - alpha(i)) * fff
  'Can change weighted frictional factor approach [area weighted]

  'Acceleration pressure contribution
  'Eqn 3.25 -> Butterworth and Hewitt, 1977 "Two-phase flow and heat transfer"
  If (alpha(i) = 0) Then
    dtempdz = 0

```

```

Else
  If (i = 1) Then
    temp3 = alpha(3) * gg(3) * Velg(3) + (1 - alpha(3)) * gf(3) * Velf(3)
    temp2 = alpha(2) * gg(2) * Velg(2) + (1 - alpha(2)) * gf(2) * Velf(2)
    temp1 = alpha(1) * gg(1) * Velg(1) + (1 - alpha(1)) * gf(1) * Velf(1)
    dtempdz = (-3 * temp1 + 4 * temp2 - temp3) / (2 * dz)
  ElseIf (i = m + 1) Then
    temp3 = alpha(m + 1) * gg(m + 1) * Velg(m + 1) + (1 - alpha(m + 1)) * gf(m + 1)
      * Velf(m + 1)
    temp2 = alpha(m) * gg(m) * Velg(m) + (1 - alpha(m)) * gf(m) * Velf(m)
    temp1 = alpha(m - 1) * gg(m - 1) * Velg(m - 1) + (1 - alpha(m - 1)) * gf(m - 1)
      * Velg(m - 1)
    dtempdz = (3 * temp3 - 4 * temp2 + temp1) / (2 * dz)
  Else
    temp2 = alpha(i + 1) * gg(i + 1) * Velg(i + 1) + (1 - alpha(i + 1)) * gf(i + 1) *
      Velf(i + 1)
    temp1 = alpha(i - 1) * gg(i - 1) * Velg(i - 1) + (1 - alpha(i - 1)) * gf(i - 1) *
      Velf(i - 1)
    dtempdz = (temp2 - temp1) / (z(i + 1) - z(i - 1))
  End If
End If
fa(i) = -dtempdz      'Acceleration part
Next

' Compute change in pressure over a cell using trapezoidal rule
For i = 1 To m
  dpg(i) = (fg(i) + fg(i + 1)) / 2 * (z(i + 1) - z(i))
  dpf(i) = (ff(i) + ff(i + 1)) / 2 * (z(i + 1) - z(i))
  dpa(i) = (fa(i) + fa(i + 1)) / 2 * (z(i + 1) - z(i))
Next

' Calculate new pressure distribution
pnew(m + 1) = pvac      'Pressure at top of tube is fixed
For i = m To 1 Step -1
  pnew(i) = pnew(i + 1) - dpg(i) - dpf(i) - dpa(i)
Next

' Compute rms change in pressure distribution from previous iteration
perr = 0
For i = 1 To m + 1
  perr = perr + (pnew(i) - p(i)) ^ 2
Next

perr = (perr / (m + 1)) ^ 0.5      'rms change in pressure (Pa)

```

```

' Update pressure distribution
  For i = 1 To m + 1
    p(i) = pnew(i)
  Next

' If not converged go back and iterate on the pressure
  If ((perr > ptol) And (iter <= itmax)) Then
    GoTo 2
  End If

' Calculate saturation temperature distribution
  For i = 1 To m + 1
    tsnew(i) = tsat(p(i)) + bp
  Next

' Compute rms change in saturation temperature distribution from previous iteration
  tserr = 0
  For i = 1 To m + 1
    tserr = tserr + (tsnew(i) - ts(i)) ^ 2
  Next

  tserr = (tserr / (m + 1)) ^ 0.5 ' rms change in saturation temperature (deg. C)
  For i = 1 To m + 1
    ts(i) = tsnew(i) 'Update saturation temperature distribution
  Next

' If not converged go back and iterate on the pressure
  If ((tserr > tstol) And (itser <= itsmax)) Then
    GoTo 1
  End If

  phyd = pvac + length * rhof * g
  dptp = (phyd - p(1)) / 1000

  Dim currentRow As Integer
  currentRow = jj + 5

  With Sheets("Outputs")
    .Range("A" & currentRow) = jj
    .Range("B" & currentRow) = mdot
    .Range("C" & currentRow) = dptp
    .Range("D" & currentRow) = x(m + 1) * mdot
    .Range("E" & currentRow) = qsum
    .Range("F" & currentRow) = qsum2
    .Range("G" & currentRow) = ts(m + 1)
  End With

```

```
.Range("H" & currentRow) = T(m + 1)
.Range("I" & currentRow) = dtb
.Range("J" & currentRow) = iflag2
.Range("K" & currentRow) = x(m + 1)
.Range("L" & currentRow) = alpha(m + 1)
End With
End Sub
```